Vol. 109 No. 2 September 1, 1979
Completing Vol. 109

ISSN 0003-2670

ANALYTICA CHIMICA ACTA

International journal devoted to all branches of analytical chemistry

EDITORS

A. M. G. MACDONALD (Birmingham, Great Britain)
D. M. W. ANDERSON (Edinburgh, Great Britain)

Editorial Advisers

F. C. Adams, Antwerp
R. P. Buck, Chapel Hill, N.C.
E. A. M. F. Dahmen, Enschede
G. den Boef, Amsterdam
G. Duyckaerts, Liège
D. Dyrssen, Göteborg
W. Haerdi, Geneva
G. M. Hieftje, Bloomington, Ind.
J. Hoste, Ghent
A. Hulanicki, Warsaw
E. Jackwerth, Bochum
G. Johansson, Lund
D. C. Johnson, Ames, Iowa
J. H. Knox, Edinburgh
P. D. LaFleur, Washington, D.C.
D. E. Leyden, Denver, Colo.
H. Malissa, Vienna
A. Mizuike, Nagoya
G. H. Morrison, Ithaca, N.Y.
E. Pungor, Budapest
J. P. Riley, Liverpool
J. W. Robinson, Baton Rouge, La.
J. Růžička, Copenhagen
D. E. Ryan, Halifax, N.S.
W. Simon, Zürich
R. K. Skogerboe, Fort Collins, Colo.
W. I. Stephen, Birmingham
G. Tölg, Schwäbisch Gmünd, B.R.D.
A. Townshend, Birmingham
B. Trémillon, Paris
A. Walsh, Melbourne
H. Weisz, Freiburg i Br.
P. W. West, Baton Rouge, La.
T. S. West, Aberdeen
J. B. Willis, Melbourne
Yu. A. Zolotov, Moscow
P. Zuman, Potsdam, N.Y.

ELSEVIER SCIENTIFIC PUBLISHING COMPANY

ANALYTICA CHIMICA ACTA

International journal devoted to all branches of analytical chemistry
Revue internationale consacrée à tous les domaines de la chimie analytique
Internationale Zeitschrift für alle Gebiete der analytischen Chemie

PUBLICATION SCHEDULE FOR 1979 (incorporating the section on Computer Techniques and Optimization).

	J	F	M	A	M	J	J	A	S	O	N	D
Analytica Chimica Acta	104/1	104/2	105	106/1	106/2	107	108	109/1	109/2	110/1	110/2	111
Section on Computer Techniques and Optimization			112/1			112/2			112/3			112/4

Scope. *Analytica Chimica Acta* publishes original papers, short communications, and reviews dealing with every aspect of modern chemical analysis, both fundamental and applied. The section on *Computer Techniques and Optimization* is devoted to new developments in chemical analysis by the application of computer techniques and by interdisciplinary approaches, including statistics, systems theory and operation research. The section deals with the following topics: Computerized acquisition, processing and evaluation of data. Computerized methods for the interpretation of analytical data including chemometrics, cluster analysis, and pattern recognition. Storage and retrieval systems. Optimization procedures and their application. Automated analysis for industrial processes and quality control. Organizational problems.

Submission of Papers. Manuscripts (three copies) should be submitted to:
for *Analytica Chimica Acta:* Dr. A. M. G. Macdonald, Department of Chemistry, The University, P.O. Box 363, Birmingham B15 2TT, England;
for the section on *Computer Techniques and Optimization:* Dr. J. T. Clerc, Universität Bern, Pharmazeutisches Institut, Sahlistrasse 10, CH-3012 Bern, Switzerland.

Information for Authors. Papers in English, French and German are published. There are no page charges. Manuscripts should conform in layout and style to the papers published in this Volume. Authors should consult Vol. 102, p. 253 for detailed information. Reprints of this information are available from the Editors or from: Elsevier Editorial Services Ltd., Mayfield House, 256 Banbury Road, Oxford OX2 7DE (Great Britain).

Reprints. Fifty reprints will be supplied free of charge. Additional reprints (minimum 100) can be ordered. An order form containing price quotations will be sent to the authors together with the proofs of their article.

Advertisements. Advertisement rates are available from the publisher.

Subscriptions. Subscriptions should be sent to: Elsevier Scientific Publishing Company, P.O. Box 211, 1000 AE Amsterdam, The Netherlands. The section on *Computer Techniques and Optimization* can be subscribed to separately.

Publication. *Analytica Chimica Acta* (including the section on *Computer Techniques and Optimization*) appears in 9 volumes in 1979. The subscription for 1979 (Vols. 104–112) is Dfl. 1179.00 plus Dfl. 135.00 (postage) (total approx. U.S. $641.00). The subscription for the *Computer Techniques and Optimization* section only (Vol. 112) is Dfl. 131.00 plus Dfl. 15.00 (postage) (total approx. U.S. $71.00). Journals are sent automatically by air mail to the U.S.A. and Canada at no extra cost and to Japan, Australia and New Zealand for a small additional postal charge. All earlier volumes (Vols. 1–95) except Vols. 23 and 28 are available at Dfl. 144.00 (U.S. $70.00), plus Dfl. 10.00 (U.S. $5.00) postage and handling, per volume.

Claims for issues not received should be made within three months of publication of the issue, otherwise they cannot be honoured free of charge.

Customers in the U.S.A. and Canada who wish to obtain additional bibliographic information on this and other Elsevier journals should contact Elsevier/North Holland Inc., Journal Information Center, 52 Vanderbilt Avenue, New York, NY 10017. Tel: (212) 867-9040.

Chromatographie liquide à hautes performances

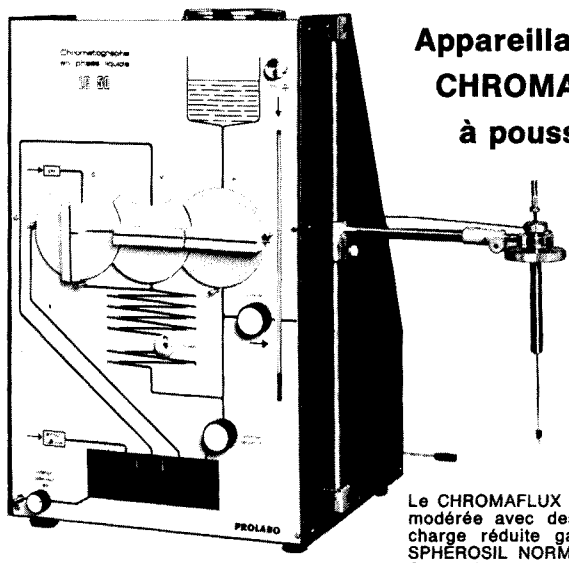

Appareillage PROLABO CHROMAFLUX LC 50 à poussée de gaz

Le CHROMAFLUX fonctionne sous pression modérée avec des colonnes à perte de charge réduite garnies par exemple de SPHÉROSIL NORMATOM XOA 600 ou 800. Ses performances sont de tout premier plan.

Emploi facile :
- Mise au courant immédiate d'une personne non initiée.
- Manipulations simples, sans aucun "tour de main" spécial.
- Ensemble cohérent, mis en œuvre en quelques minutes, raccordable à tout détecteur.

Entretien simplifié :
- Colonnes sans raccords spéciaux en bout, se démontant sans outil.
- Circuit en tubes normalisés de 1,6 mm (1/16"). Colonnes de Ø 6,3 mm (1/4").
- Volumes morts très réduits par construction.
- Flancs démontables pour un accès facile aux organes internes.

Sécurité :
- Pression modérée, ne dépassant pas 25 bar.
- Sécurité positive au niveau des vannes, liées mécaniquement pour empêcher toute fausse manœuvre.
- Réservoir récupérateur de solvant avec tube de respiration.

Commodité :
- Visualisation des circuits en façade.
- Niveau de solvant, réservoir de récupération et débitmètre.
- Réservoir de solvant suffisant pour 1 jour de travail.
- Aiguille d'injection guidée pour injecter dans des conditions bien reproductibles.

Economie :
- Prix modéré de l'installation.
- Entretien peu coûteux.
- Faible consommation de solvant.
- Faible consommation de gaz, juste ce qu'il faut pour dégazer lors des remplissages.

SPHÉROSIL NORMATOM®

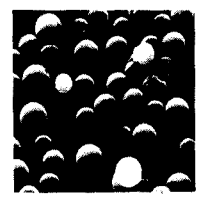

Matériaux de remplissage de colonnes constitués de microbilles de silice calibrées, à surface spécifique élevée (600 m^2/g pour le SPHEROSIL NORMATOM ® XOA 600 et 800 m^2/g pour le XOA 800).

En garnissant de SPHEROSIL NORMATOM ® les colonnes de tout appareil de chromatographie liquide, on obtient des performances exceptionnelles, moyennant une pression motrice modérée.

PROLABO

12, rue Pelée - 75011 PARIS
Téléphone : (1) 355.44.88
Télex : PRLAB X 680 566 F

rhône-poulenc

Lasers in Chemistry

Proceedings of the Conference held at the Royal Institution, London, 31 May - 2 June 1977

edited by MICHAEL A. WEST, *The Royal Institution, London.*

As lasers and associated electro-optics have been developed in the past few years, chemists have rapidly adapted and used these new light sources in many diverse ways. This conference was held in order to review and discuss the present state-of-the-art in this fast-growing field and the proceedings contain 79 papers organized into seven sections. Each section, except one, contains a review paper by an invited speaker and a set of contributed papers which, taken together, indicate the overall scope of current research and point to likely future advances in a particular area. This volume will be of value to academic, government and industrial scientists as well as to technologists in chemistry, physics and electro-optics.

In the contents listed below, the main topics of the conference are given with the total number of papers in each section noted in parentheses. Limitation of space allows titles of only a few randomly selected papers to be mentioned.

Sept. 1977 xii + 438 pages US $69.50/Dfl. 170.00 ISBN 0-444-41630-7

ELSEVIER

P.O. Box 211, Amsterdam
The Netherlands
52 Vanderbilt Ave
New York, N.Y. 10017

The Dutch guilder price is definitive. US $ prices are subject to exchange rate fluctuations.

7057

ffinity hromatography

DSLAVA TURKOVA, *Czechoslovak lemy of Sciences, Prague.*

RNAL OF CHROMATOGRAPHY ARY - Volume 12

book reviews the application of ity chromatography for the isolation rious biologically active substances. reviewing table comprises almost) references and is completed by data se of solid supports and spacers. t attention is given to the review of most commonly used solid supports to the method of attachment, together the methods of characterization of the carriers and the immobilized ity ligands.

extensive and up-to-date review is nded mainly for biochemists and ogists. It will be particularly useful linicians engaged in human or veter- y medicine, as well as to those dealing chromatography and industrial chem- .

NTENTS: Chapters: 1. Introduction. 2. The ciple, history and use of affinity chro- ography. 3. Theory of affinity chromato- hy. 4. Application of affinity chroma- aphy to the quantitative evaluation of ific complexes. 5. General considerations affinant—sorbent bonding. 6. Choice of ity ligands for attachment. 7. Hydrophobic matography, covalent affinity chro- ography, affinity elution and related hods. 8. Solid matrix supports and the t used methods of binding. 9. Charac- ation of supports and immobilized affinity nds. 10. General considerations on sorption, ion and non-specific binding. 11. Exam- of the use of affinity chromatography. mmobilized enzymes. Subject Index.

ch 1978 x + 406 pages
$69.75/Dfl. 167.00 0-444-41605-6

ELSEVIER

Box 211, Amsterdam 52 Vanderbilt Ave
Netherlands New York, N.Y. 10017

utch guilder price is definitive. US $ prices are subject hange rate fluctuations.

7086

K. Cammann

Working with Ion-selective Electrodes

Chemical Laboratory Practice
Translated from the German by A.H. Schroeder

1979. 65 figures. Approx. 240 pages
Cloth DM 76,–; US $ 41.80
ISBN 3-540-09320-6
Prices are subject to change without notice

Contents:
Fundamentals of Potentiometry.– Electrode Potential Measurements.– Ion-Selective Electrodes.– Measuring Techniques with Ion-Selective Electrodes.– Analysis Techniques Using Ion-Selective Electrodes.– Applications of Ion-Selective Electrodes.– Appendix.

The field of ion-selective electrodes has grown enormously since the publication of the first edition of this work. The Second Edition, now in English, considers new developments which have since taken place in gas sensors, enzyme electrodes and industrial applications of ion-selective electrodes.
Lucidly written and containing a helpful index, the book uses a new theoretical approach to explain the behavior of electrodes in a way comprehensible to a new-comer in the field. Various electrode types available are described as well as "do-it-yourself" electrodes, microelectrodes, industrial flow-thru assemblies, and pollution control monitors.
The accent of the book is on simple procedures. The user therefore learns to avoid errors resulting from an unfamiliarity with electrochemical measurements of single ion activities. The bibliography of the New Edition has been expanded considerable to include important new publications.
Already regarded as a standard among the literature in West Germany, this new English Edition now offers analytical scientists worldwide a systematic and inviting introduction to the field of ion-selective electrodes.

5545/5/2hg

Springer-Verlag
Berlin Heidelberg New York

Reagents

MERCK

Liquid Chromatography under Pressure – HPLC

LiChrosorb®

Separation example:
Chlorinated hydrocarbons
LiChrosorb Si 60
7 µm
Available:
Si 60, Si 100,
Alox T

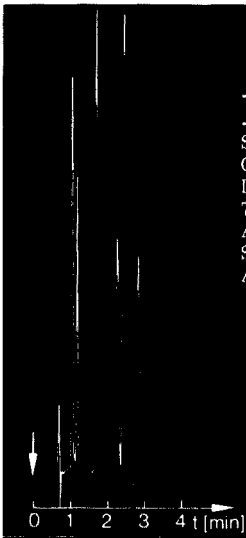

LiChrospher®

Separation example:
Oligophenylenes
LiChrospher Si 500
10 µm
Available:
Si 100, Si 300,
Si 500, Si 1000,
Si 4000

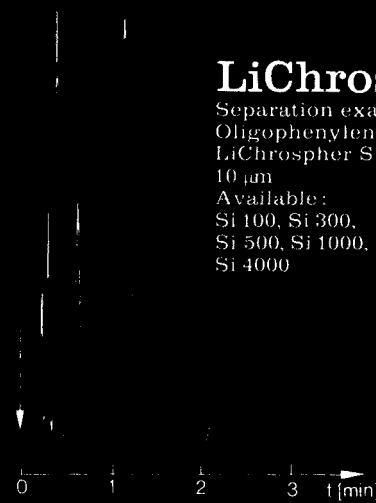

Chemically modified

LiChrosorb®

Separation example:
Aromatic compounds
LiChrosorb RP-8
10 µm
Available:
RP-2, RP-8,
RP-18,
NH_2, DIOL,
KAT, AN

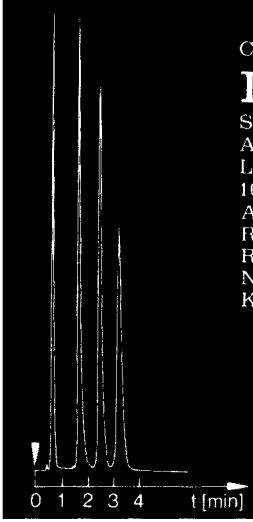

Perisorb®

Separation example:
Phthalic acid esters
Perisorb A
30–40 µm
Available:
A (silica gel)
Chemically modified:
RP-2, RP-8,
RP-18,
KAT, AN,
PA 6

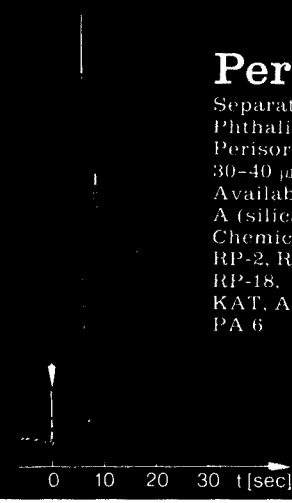

LiChrosorb® totally porous, irregularly shaped particles:
(1) about 30 µm, for dry filling;
(2) microparticles (5, 7, 10 µm), to be filled into the column by a slurry method.

LiChrospher® spherical particles, totally porous.
Perisorb® superficially porous supports with an about 1–2 µm chromatographically active layer around a glass core, spherical (30–40 µm).

397g-EU

Please send for Data sheets and Series of application examples.

E. Merck, Darmstadt, Federal Republic of Germany

Analytica Chimica Acta, 109 (1979) 209—228
© Elsevier Scientific Publishing Company, Amsterdam — Printed in The Netherlands

STANDARDIZATION OF METHODS FOR THE DETERMINATION OF TRACES OF MERCURY
Part 5. Determination of Total Mercury in Water

A REPORT PREPARED BY THE MERCURY ANALYSIS WORKING PARTY OF THE BUREAU INTERNATIONAL TECHNIQUE DU CHLORE*

BITC, 250 Avenue Louise, Bte 72, B-1050 Bruxelles (Belgium)

(Received 8th March 1979)

SUMMARY

For the determination of total mercury in water, two procedures based on cold-vapour atomic absorption spectrometry are given, each with and without a concentration step. These procedures have been accepted as reference methods by the member companies of the Bureau International Technique du Chlore. The methods give reliable results down to a concentration of 0.2 μg of mercury per litre of water. Results of an interlaboratory test involving 22 laboratories are reported. At the 0.75 μg Hg l^{-1} level the results did not differ significantly; the coefficient of variation for repeatability was 3.8—10.9% and the coefficient of variation for reproducibility 7.2—29.4% for the different methods.

ZUSAMMENFASSUNG

Für die Bestimmung des Gesamtquecksilbers in Wasser werden zwei Verfahren beschrieben, jeder mit und ohne Anreicherung. Die beiden Methoden würden als Standardverfahren von den Mitgliedsfirmen des Bureau International Technique du Chlore anerkannt. Bis zu einer Konzentration von 0,2 μg Hg l^{-1} ergeben die Verfahren zuverlässige Resultate. Es werden die Ergebnisse eines Ringversuches angeführt, an dem sich 22 Laboratorien beteiligten. Bei einem Niveau von 0,75 μg Hg l^{-1} Wasser konnten keine signifikanten Unterschiede festgestellt werden. Die Variationskoeffizienten der Wiederholbarkeit lagen zwischen 3,8 und 10,9% und die der Vergleichbarkeit zwischen 7,2 und 29,4%.

RÉSUMÉ

On décrit deux méthodes de dosage du mercure total dans les eaux ainsi que, pour chacune d'elles, une étape de concentration. Ces méthodes ont été retenues à titre de méthodes de référence par les Sociétés membres du Bureau International Technique du Chlore. Il a été vérifié qu'elles donnent des résultats fiables jusqu'à des concentrations aussi faibles que 0,2 μg de mercure par litre d'eau. Des résultats d'un essai interlaboratoire groupant 22 participants sont présentés. Au niveau de 0,75 μg Hg l^{-1}, les écarts entre les résultats n'étaient pas significatifs: la répétabilité et la reproductibilité des diverses méthodes étaient respectivement comprises entre 3,8—10,9% et 7,2—29,4%.

*The members of the Working Party responsible for the preparation of this report were J. A. Aliseda, R. Ankersmit, G. W. Ashley, J. Barjhoux, R. Bult, W. T. Carter, W. Dürr, J. Garbayo, M. Garcia, Ch. Killens, L. Mariani, S. A. Norberg, F. Nouyrigat, M. Olivier and H. Romeis. This report has been approved by the General Technical Committee of the BITC, which also authorized its publication.

As part of its programme to evaluate methods of analysis for mercury in a wide variety of process intermediates and products of the chlor-alkali industry and in other materials of environmental interest, the Mercury Analysis Working Group of the Bureau International Technique du Chlore has investigated the determination of mercury in water. This is a task with a very wide scope since not only does the level of mercury, which is of interest in considering a given effect, vary over a very wide range, but the levels of organic contamination and salinity may also vary widely. For example, the upper level of total mercury set by the EEC for candidate drinking water is 1 μg Hg l^{-1} [1] and to ensure reliable monitoring at this level it is necessary to have an analytical procedure with a limit of detection of ca. 0.2 μg Hg l^{-1}. In studies of the effect of mercury on marine and freshwater aquatic systems, much lower levels of soluble mercury are considered significant, e.g., 0.05—100 ng Hg l^{-1} [2, 3]. Working at these levels is extremely difficult because the procedures chosen must include only reagents with mercury levels of the same order as the samples; also because the mercury levels are metastable and may change with time, sample storage is impossible and measurements have to be done at the point of sampling. Group studies of such procedures are very difficult to organize.

At the other end of the spectrum in the vicinity of large users of mercury and in areas where mercury deposits occur naturally, concentrations of mercury higher than 1 μg Hg l^{-1} may be encountered. In some respects, this reduces the problems of analysis, but as the levels of organic contamination and salinity increase, greater quantities of reagents are needed to preserve the samples for transport and storage and to oxidize them before analysis. Under these circumstances, it becomes necessary to accept higher limits of detection as the standard deviations of the blanks from increased reagent additions become higher. When the reagent additions become unacceptably high, it is necessary to sacrifice sensitivity of the mercury measurement and use a reduced sample volume together with a wet digestion procedure as described in the Working Groups document on the determination of mercury in organic materials [2].

Finally, the mercury may be present in suspension or solution and in inorganic or organic combinations, because while chlor-alkali plants do not emit mercury in the organic form, organomercury compounds are still used widely for other purposes. With these considerations in mind, it was decided to investigate a variety of procedures with a view to recommending a combination which would allow the determination of total mercury down to a determination limit of 0.2 μg Hg l^{-1} with equipment and reagents which are readily available, and including recommendations for the strict control of blanks, which is necessary to obtain meaningful results at this level of concentration.

As a result of a literature survey combined with the experience of members of the Working Group, it was decided to standardize the method of sampling and sample preservation and to select two oxidation procedures, one based on the work of Kopp et al. [4] (on which the method of the U.S. Environ-

mental Protection Agency [5] is also based) who used nitric acid—sulphuric acid—potassium permanganate—potassium persulphate, and the other on the work of Frimmel and Winkler [6] who used u.v. irradiation in the presence of sulphuric acid—potassium dichromate. These two procedures are complementary in that the former has a high tolerance to organic contamination and salinity but also has a high reagent blank because of the use of potassium permanganate, while the latter has a lower and less completely understood tolerance to organic contamination, but has very low reagent blanks and is very easy as it involves a minimal number of manipulations. Both these procedures use 100 ml of sample so that working in the desired range of 0.2—1 μg Hg l^{-1} implies an instrument calibration of 0.02—0.1 μg Hg. Great care is necessary to minimize background contamination and its effect on the accuracy of the method in this range. For this reason optional procedures have been included in which the two oxidation procedures are combined with a concentration technique based on the work carried out by Topping and Pirie [7] and by Harsányi et al. [8].

The factors governing the choice of these procedures are further discussed below and the detailed procedures are given in subsequent sections.

FACTORS GOVERNING CHOICE OF PROCEDURES

Sample preservation

It is generally recognised that there are problems associated with collecting and storing samples of water intended for cation analysis, because of precipitation and adsorption of cations on the walls of containers, and it is normally recommended that such samples be acidified to pH 1 or less on collection. The ease with which ionic mercury is reduced to the metallic state and volatilized creates an additional problem in samples intended for low-level mercury analysis; to prevent possible losses of mercury by this route the addition of an oxidizing agent is also recommended [9]. Some types of sample containers have also been found by some workers to cause loss of trace metals during storage.

It was decided to select the sampling procedure most appropriate to the needs of the Working Group and then carry out sufficient storage tests to prove that it was reliable.

For acidification, nitric, sulphuric and hydrochloric acids have all been recommended. Hydrochloric acid forms few insoluble salts but has the disadvantage in mercury analysis of reacting with oxidizing agents such as permanganate and dichromate thereby reducing their effectiveness. Sulphuric acid will precipitate calcium if present in sufficient amount but, apart from this, sulphuric and nitric acids are equally acceptable. The choice of oxidizing agents is usually between potassium permanganate and potassium dichromate. The former precipitates manganese dioxide on storage and since this adsorbs mercury very strongly it is essential that it be redissolved before any sample is removed from the bottle for analysis. Potassium dichromate does not suffer from this limitation.

The choice of sample bottle materials is essentially between glass and plastic; of the latter, polyethylene is preferred on the grounds of cost and availability. In addition, polyethylene bottles are much more suitable for field use than glass ones and it would be advantageous to be able to use them with confidence. However, the information available in the literature on losses from mercury solutions stored in polyethylene is conflicting, and it is possible that the losses reported by some authors are due to variations in the anti-oxidants, lubricants, etc., used to make the bottles.

From these considerations it was decided to evaluate sampling procedures with potassium dichromate as the oxidizing agent and either sulphuric acid or nitric acid for acidification in either glass or polyethylene sample bottles. Two laboratories in the Working Group examined this problem and their findings are given later in this paper. The effectiveness of the proposed chemical pretreatment was confirmed and no difference could be found between storage in polyethylene and glass containers. It is concluded that either may be used but that if polyethylene bottles are used they should be checked for storage losses before use. A rather unusual source of contamination when polyethylene bottles are used has been reported [10]; mercury diffused through the bottle walls from a mercury-contaminated storage environment. Care should be taken to avoid this problem.

The presence of suspended matter in samples also creates problems because a high proportion of the mercury present is likely to be associated with it. The addition of preservatives to the sample will solubilize some if not all of this mercury, but this may be undesirable if it is necessary to differentiate between soluble and insoluble mercury. Under these circumstances, it is necessary to filter the sample before the addition of the preservative. A second problem is that the preservative may slowly oxidize any organo-mercury compounds to ionic mercury but this can be ignored in the determination of total mercury.

Oxidation with nitric acid—sulphuric acid—potassium permanganate—potassium persulphate

This procedure [4, 5] has been widely investigated and has also been the subject of an interlaboratory trial carried out jointly by the ASTM and the EPA [11]. It uses only readily available equipment and reagents, and since it requires high oxidizing-reagent additions it has a high tolerance to organic pollutants and chloride. However, the high reagent additions lead to high blanks which reduce the sensitivity of the method, and strict control of blanks is necessary for use at concentrations of 1 μg Hg l^{-1} and below.

Ultraviolet irradiation

The use of u.v. irradiation was proposed by Armstrong et al. [12] as a means of oxidizing organic matter in sea water prior to the determination of total phosphorus. It has been used for the destruction of organo-mercury compounds by Goulden and Afghan [13], by Winkler and co-workers [6, 14,

15] and by Kiemeneij and Kloosterboer [16]. Winkler and co-workers obtained complete destruction of a range of organo-mercury compounds in less than 10 min with either a 150-W medium-pressure or a 15-W low-pressure u.v. source. The low-pressure lamp has the advantage of low heat generation which eliminates the need for cooling during irradiation. Kiemeneij and Kloosterboer obtained only 60% destruction of methylmercury chloride in 20 min, using a pure mercury lamp but 100% in 10 min with a zinc/cadmium/mercury lamp.

Some work on the efficiency of u.v. irradiation done by participating laboratories in the Working Group (see below) has established that a range of organo-mercury compounds can be completely oxidized to the ionic state by u.v. irradiation in 15 min or less and that sample volumes up to 2000 ml can be treated by using efficient stirring with no increase in irradiation time. Some work has also been done on the effect of organic compounds on the efficiency of destruction of organo-mercury compounds by u.v. irradiation. This work is not exhaustive and was done only as a result of the accidental discovery that isopropanol which was being used as a solvent for methylmercury chloride seriously reduced the rate at which the mercury compound was destroyed. Some results showing the effect of alcohols on the irradiation process are quoted below in the section entitled "Testing the Methods". Because of this effect and the possibility that other compounds may also produce it, it is considered advisable to restrict the u.v. irradiation method to drinking water and candidate drinking water. Problems may also arise during experimental work if alcohols are used to prepare standard solutions of organomercurial compounds which are not water-soluble for irradiation experiments.

Concentration of mercury after oxidation or irradiation

The procedures of Kopp et al. and Winkler et al. involve, in their original versions, 100 ml of sample, which implies that in order to achieve a working range of 0.1—1.0 $\mu g\ Hg\ l^{-1}$ it is necessary to calibrate the method in the range 0.01—0.1 μg Hg. It was anticipated that there would be difficulty in working in this range because of background contamination and it was decided to investigate the use of a concentration technique such as that described by Harsányi et al. [8]. The application of this procedure to the nitric acid—sulphuric acid—potassium permanganate—potassium persulphate procedure involves a simple scale up of the sample and reagent volumes by a factor of six. Inevitably, however, the blank is also scaled up by the same amount. To apply it to the u.v. irradiation procedure involves the provision of a well-stirred irradiation vessel large enough to take a 600-ml sample. The blank from reagents is also increased by a factor of six in this procedure but the contribution of the reagents to the blank is smaller than in the oxidation method.

Interference from water vapour during mercury measurement

Two effects of water vapour must be guarded against. The first is the condensation of water in the measuring cell of the instrument. This can be avoided by heating the cell above ambient temperature with a short coil of nichrome

wire, or by cooling the sample solutions to a temperature below ambient before aeration, or by using a drying tube on the inlet to the optical cell. The desiccant may be magnesium perchlorate, calcium chloride or silica gel, and should be checked to ensure that its use does not cause loss of mercury from the air stream; it should be changed regularly.

The second effect of water vapour is a baseline drift with some instruments at high sensitivities; this arises from variations in water vapour pressure when sample and standard solutions are aerated at different temperatures. The effect can be eliminated by the use of a drying tube as described above or by adjusting the temperature of all sample and standard solutions to 20 ± 0.5°C before aeration.

*Method descriptions**

The chemical method and the u.v. method are described separately, except for the paragraphs *Sampling and sample preparation*, *Determination of mercury content*, *Calculation*, *Blank control* and *Notes*. For each method, two procedures are given: one without and one with a concentration step.

SAMPLING AND SAMPLE PREPARATION

Before taking a sample, clean all the bottles with a cleaning solution (see Note 3). If polyethylene bottles are used, confirm by storage experiments that mercury losses do not occur during storage.

In many natural waters, most of the mercury is associated with the suspended matter. To obtain representative samples, they should be taken from points of the highest possible turbulence (e.g. a weir) and vigorously shaken before any subsampling is done. It may in some cases be necessary to confirm that the preservative has dissolved all the mercury out of the suspended matter by filtering it off and analysing it for mercury by one of the procedures already described [2].

Collect samples in 1- or 2-l glass or polyethylene bottles containing 50 ml of the preservative reagent (see below) per litre of sample. If the sample contains free alkali, sufficient acid should be added to neutralize this.

The sample may be so contaminated with suspended matter or dissolved pollutants that the preservative is destroyed as quickly as it is added. In this case the best solution is to sample 50 ml directly into the reaction flask for the wet digestion procedure [2] and complete the analysis in this way. The loss in sensitivity which this implies is usually acceptable, because samples of this purity will never be candidate water supplies and will rarely need to be analysed to low limits of detection.

*For technical reasons, the text of the original methods has been modified and shortened in certain places; those interested in the original text can obtain it in French, German or English on application to the BITC.

OXIDATION WITH NITRIC ACID–SULPHURIC ACID–POTASSIUM PERMANGANATE–POTASSIUM PERSULPHATE (CHEMICAL METHOD) [4]

Scope, field of application and principle

This method is suitable for the determination of total mercury in drinking, surface and saline water, domestic and industrial wastes. The lower limit of determination is ca. 0.2 μg Hg l^{-1} (see below).

All forms of mercury, including organic compounds, are pre-oxidized to ionic mercury by acidic potassium permanganate. The final and complete oxidation is achieved by adding potassium persulphate and heating to about 100°C for 2 h. After cooling, the mercury is either determined directly or concentrated into a smaller volume and then determined by cold-vapour atomic absorption spectrometry.

Apparatus

An atomic absorption spectrophotometer and accessories as described previously [17] are required. Also, 1-l and 250-ml glass bottles fitted with ground-glass stoppers are required; the type of stopper with an overhanging rim, which protects the bottle neck from dust, is preferred. The 250-ml bottles can be used for the aeration step (see Notes 3, 6) or the solution may be transferred to a 250-ml wash bottle fitted with a sintered-glass gas distributor, which is reserved exclusively for use as an aeration flask.

For the method with concentration step, the concentration apparatus consists of: an air supply metered by a flow meter (0—100 l h^{-1}); a 125-ml wash bottle containing acidic permanganate solution (to remove traces of mercury from the air used); a 1-l wash bottle fitted with a sintered-glass gas distributor (to achieve rapid mercury removal, this bottle should be tall and narrow); and 125-ml wash bottles fitted with a sintered-glass gas distributor (these are used as the absorber in the concentration and as the aeration flask in the measurement step, see Note 6).

Reagents

All reagents must be of analytical-reagent grade and must contain only very low amounts of mercury; E. Merck, Darmstadt, Germany, for example, markets reagents with guaranteed low mercury contents (see also Note 4). All references to water imply distilled water or water of equivalent purity (see Note 5). A blank determination must always be done. Common reagents are not listed here.

Preservative reagent. Dissolve 4 g of potassium dichromate in 500 ml of water and carefully add 500 ml of concentrated sulphuric acid (ca. 18 M) or concentrated nitric acid (ca. 14 M). Use the nitric acid if there is any danger of precipitation of calcium sulphate (see Note 4).

Mixed acids solution. Carefully add 250 ml of nitric acid (ca. 14 M) to 500 ml of sulphuric acid (ca. 18 M). Dilute to 1 l with water and mix. Store in an amber glass bottle.

Reducing solution. Transfer 25 g of tin(II) chloride dihydrate to a 250-ml standard flask. Add 50 ml of warm, concentrated hydrochloric acid (ca. 12 M). Swirl to dissolve, add 1—2 g of tin metal, dilute to volume with water and mix. Pass a slow stream of nitrogen through the solution for 30 min to remove traces of mercury. Discard the solution if a turbidity appears (see Note 2).

Standard mercury solutions. (1 g Hg l^{-1}, 10 mg Hg l^{-1}, 0.1 mg Hg l^{-1}). Introduce 1.354 g of mercury(II) chloride into a 1-l standard flask. Add 25 ml of concentrated hydrochloric acid (ca. 12 M) and swirl to dissolve. Dilute to volume with distilled water and mix. This solution contains 1 g Hg l^{-1}. From this solution, prepare the other standard mercury solutions by dilution with hydrochloric acid (ca. 0.3 M) (see Note 1).

Sample preparation without concentration step

Transfer 100 ml of the well shaken sample to a 250-ml glass bottle and add 15 ml of potassium permanganate solution (50 g l^{-1}) followed by 10 ml of the mixed acids solution (see Note 7). Stopper the bottle, swirl to mix and allow to stand for at least 15 min. Add 10 ml of potassium persulphate solution (40 g l^{-1}), mix and heat for 2 h on a water bath maintained at 95°C with the stopper loosely inserted. Cool the sample to 20°C, and just prior to the aeration add 5 ml of hydroxylammonium chloride solution (150 g l^{-1}) to reduce excess of oxidants and to redissolve any precipitated manganese dioxide. When the solution is completely decolourized, immediately measure the mercury content by the procedure given under *Determination of mercury content.*

Sample preparation including a concentration step

Transfer 600 ml of the well shaken sample to a 1-l glass bottle and follow the procedure given above using six times as much of the reagents specified. After cooling, add 30 ml of hydroxylammonium chloride solution (150 g l^{-1}) to reduce excess of oxidants and to redissolve any precipitated manganese dioxide. Transfer the sample to the 1-l bottle of the concentration apparatus when the sample is completely decolourized. Introduce 20 ml of the reducing solution, mix and aerate the solution for 10 min at 1 l min^{-1}, absorbing the mercury vapour in the 125-ml wash bottle containing 40 ml of water, 0.2 ml of potassium permanganate solution (50 g l^{-1}) and 10 ml of sulphuric acid (ca. 3.5 M) (see Notes 10 and 11). Measure the mercury content by the procedure given under *Determination of mercury content.*

Photometric measurement; calibration of photometer

For the method without concentration. Establish a calibration curve in the range 0—0.10 μg of mercury as follows. Use a series of six 250-ml glass bottles, each containing 100 ml of distilled water, 5 ml of preservation reagent, 10 ml of the mixed acids solution and 15 ml of potassium permanganate solution (50 g l^{-1}). Add (from a 1-ml microburette, for example) 0, 0.2, 0.4, 0.6, 0.8 and 1.0 ml of the standard mercury solution (0.10 mg Hg l^{-1}) to the glass bottles. Follow the procedure given under *Sample preparation without concen-*

tration step, starting with "Stopper the bottle ...". Convert the peak heights obtained to absorbance (if necessary), deduct the value obtained for no added mercury and construct a graph of absorbance against μg of mercury. Repeat the procedure using quantities of mercury in the range 0—1.0 μg.

For the method with concentration. Establish a calibration curve in the range 0—1.0 μg of mercury as follows. Use a series of six 1-l wash bottles, each containing 600 ml of water and 30 ml of preservative reagent. Add (from a 1-ml microburette, for example) 0, 0.2, 0.4, 0.6, 0.8 and 1.0 ml of the standard mercury solution (1 mg Hg l^{-1}) to the wash bottles.

Place each bottle in turn in the concentration apparatus, add 20 ml of reducing solution, mix and immediately aerate the solution for 10 min at 1 l min^{-1}, absorbing the mercury vapour in the 125-ml wash bottle containing 40 ml of water, 0.2 ml of potassium permanganate solution (50 g l^{-1}) and 10 ml of sulphuric acid (ca. 3.5 M) (see Note 10). Measure the mercury content by the procedure given under *Determination of mercury content* and convert the peak height obtained to absorbance (if necessary). Follow the same procedure for each solution, deduct the value obtained for no added mercury and construct a graph of absorbance against μg of mercury.

ULTRAVIOLET IRRADIATION IN THE PRESENCE OF POTASSIUM DICHROMATE AND SULPHURIC ACID OR NITRIC ACID (UV METHOD) [16]

Scope, field of application and principle

This u.v. method is suitable for the determination of total mercury in drinking and candidate drinking water at levels below 1 μg Hg l^{-1}. The lower limit of determination is ca. 0.2 μg Hg l^{-1} (see below).

The water sample is irradiated with u.v. radiation for 10 min, after addition of the preservative reagent (potassium dichromate and sulphuric or nitric acid). Organic mercury compounds are decomposed, liberating ionic mercury. The total mercury is either determined directly or concentrated into a smaller volume and then determined by cold-vapour atomic absorption spectrometry.

Apparatus and reagents

The apparatus is the same as for the chemical method with the following additions: an immersion-type u.v. lamp, e.g. a medium-pressure lamp such as Hanau TQ 150 or TQ 150/Z3 or Hanovia PCRIL; a low-pressure lamp such as Hanau TNN 15/32 (see Note 9); irradiation vessels with a sample capacity of at least 100 or at least 600 ml (see Note 9); magnetic stirrers.

The reagents are the same as for the chemical method, except for the mixed acids solution.

Procedure for u.v. irradiation. Measure 100 ml or 600 ml of the well shaken sample into the irradiation vessel, insert a magnetic follower, attach the vessel to the photochemical reactor and surround with an ice bath or turn on a chilled water supply. Irradiate the sample for 10 min, stirring continuously (see Note 12). Transfer the 100-ml sample, if necessary, to a 250-ml aeration flask

and determine the mercury content as given in *Determination of mercury content* (see Note 10).

For the 600-ml sample, concentrate the mercury as follows. Remove the irradiation vessel from the photochemical reactor assembly and transfer the contents to the 1-l wash bottle of the concentration apparatus. Introduce 20 ml of reducing solution and aerate the solution for 10 min at 1 l min^{-1}, absorbing the mercury vapour in the 125-ml wash bottle containing 40 ml of water, 0.20 ml of potassium permanganate solution (50 g l^{-1}) and 10 ml of sulphuric acid (ca. 3.5 M) (see Notes 10 and 11). Measure the mercury as described under *Determination of mercury content.*

Photometric measurement; calibration of photometer

For the method without concentration. Establish a calibration graph in the range 0—0.10 μg of mercury as follows. Use a series of six aeration/irradiation vessels, each containing 100 ml of distilled water and 5 ml of preservative reagent. Add (from a 1-ml microburette, for example), 0, 0.2, 0.4, 0.6, 0.8, and 1.0 ml of the standard mercury solution (0.10 mg Hg l^{-1}) to the aeration irradiation vessels (see Note 10). Measure the mercury content as given under *Determination of mercury content.* Convert the peak heights obtained to absorbance (if necessary), deduct the value obtained for no added mercury and construct a graph of absorbance against μg of mercury.

For the method with concentration. Follow the procedure given for the chemical method.

Determination of mercury content (applicable to both methods)

Adjust the solution to a temperature of 20 ± 0.5°C (unless the spectrophotometer is fitted with a drying tube), add 2 ml of reducing solution, and immediately attach the bottle to the aeration apparatus. Swirl to mix and aerate the sample 30 s after the addition of the reducing solution. Convert the peak height obtained to absorbance (if necessary) and read the result from the calibration graph.

Calculation. The mercury concentration in the sample is

$$\text{Hg } (\mu g\ l^{-1}) = [(C - C_0)/V] \times 1000 \times 1.05$$

where C = μg Hg in sample, C_0 = μg Hg in the blank and V = volume of sample in ml. The factor 1.05 is required to correct for dilution by the preservative reagent.

Blank measurement (applicable to both methods)

Transfer 100 ml or 600 ml of distilled water into the type of flask given in the appropriate procedure, add 0.2 ml or 1 ml of reducing solution and aerate in the normal manner to remove traces of mercury from the solution (see Note 5). Add the corresponding volume of preservative reagent and continue with the procedure to obtain the mercury content of all the reagents used.

Carry out a daily blank which should not significantly exceed the upper limit of the confidence interval determined as given below. If it is significantly higher, check the reagents used and replace any with high mercury levels. If

the blank still exceeds the upper limit or if it is significantly lower than the lower limit of the confidence interval, redetermine the confidence interval and recalculate the limit of detection.

Blank monitoring; determination of the limit of detection, limit of determination

For highly sensitive analyses at concentration levels close to the limit of detection, it is essential to monitor and control the blank values in order to ensure that the results obtained are meaningful and that a realistic value for the limit of detection is quoted, depending on the blank values which each individual laboratory can achieve.

For the method of analysis in use, run a series of ten blank determinations by the appropriate procedure. Calculate the standard deviation of a single blank and use it to calculate the confidence interval (*CI*) from the expression $CI = \bar{x} \pm s.t_{(P,f)}$, where $\bar{x}$ = mean of the blank values, s = standard deviation, t = Student's confidence coefficient (here 2.26), P = probability (here 95% two-sided), and f = degree of freedom (here, for 10 measurements, 9).

The limit of detection (*LD*) is given by the expression $LD = s.t_{(P,f)}$ where the symbols have the same meaning; in this case the Student's confidence coefficient is 3.25 and the probability is 99.5% (one-sided).

The limit of detection thus obtained will vary with the quality of the reagents available and also with the background contamination level of the relevant laboratory. In general, this result will be less than 0.2 μg Hg l^{-1}, but it is considered by members of the Working Group that this value is the lowest which can be reliably obtained. For this reason, a value (defined as the limit of determination) of 0.2 μg Hg l^{-1} has been given for all methods under Scope and field of application.

Notes

1. Deterioration of mercury solutions. Dilute solutions of mercury are not completely stable. Their mercury content tends to diminish with time. It is advisable to renew the standard 1 g Hg l^{-1} solution every two months and the diluted standard solutions daily. More recent knowledge about the preservation of mercury-containing solutions makes it advisable to stabilize the standard mercury solutions with acidic dichromate solution: 50 ml of the preservative reagent should be added before the standard mercury solution is diluted to 1 l.

2. Oxidation of the reducing solution. Tin(II) ions are oxidized by air to tin(IV) and so the reducing solution is useless if it becomes turbid.

3. Cleaning glassware. Before use, all glassware must be carefully cleaned with concentrated nitric acid and rinsed with an oxidizing solution such as acidic potassium dichromate (100 g l^{-1} in 10% nitric or sulphuric acid), also to destroy any residual tin(II). The glassware should be retained exclusively for this determination.

4. Preparation of reagents. Because of the low levels of mercury being dealt with, extreme care must be taken in the preparation of all the reagents,

especially the potassium permanganate, potassium dichromate (preservative reagent) and potassium persulphate solutions. These reagents must never be left unstoppered because they rapidly absorb mercury from the atmosphere. In order to minimize contamination still further, it is advisable to fit as many of the reagent bottles as possible with dispensers. This arrangement, if used permanently, also minimizes the need for pipettes and measuring cylinders.

5. *Distilled water.* It is assumed that only inorganic forms of mercury are present in supplies of laboratory distilled water.

6. *Gas velocity and glassware.* The height of the mercury peak obtained depends on the dimensions of the apparatus and the gas velocity. It must be confirmed that changes in the glassware, particularly the aeration flasks, do not alter the peak height. If difficulty is experienced in obtaining wash bottles which give a uniform response, all aerations should be done with one bottle reserved for this purpose. Reducing the gas velocity gives shorter, wider peaks. The optimal gas velocity must be determined experimentally and maintained at this value during measurement of sample and calibration.

7. *Samples with a high chloride content.* Waters with a high chloride content may require additional potassium permanganate. They also evolve chlorine during oxidation and it is advisable to purge the head-space over the solution in the aeration vessel with air after adding the hydroxylammonium chloride but before adding the reducing solution.

8. *Matrix effects.* The presence in the solution of ions which form complexes or compounds of low solubility with mercury(II) or (I) diminishes the absorbance of the mercury peaks, all other things being equal. The presence of chloride above a concentration of 2.5 g/60 ml in the aeration flask therefore causes low results. In the presence of bromide and iodide, this effect appears at even lower concentrations, particularly in the case of iodide, which forms very stable complexes with mercury. These ions also cause a significant decrease in the speed of reduction of mercury by tin(II) chloride. Accordingly, it is advisable when their presence in significant concentrations is suspected, to prolong the delay between the introduction of the tin(II) chloride and the aeration, in order to obtain reproducible signals. In such cases, the calibration curve is invalid and it is necessary to resort to the method of standard additions to avoid these interferences from matrix effects.

This is done by repeating the calibration procedure with aliquots of the sample solution instead of the distilled water as described under *Photometric measurement; calibration of photometer.* The sample solution aliquots should be of the same volume as that used in *Sample preparation* and depending on the importance of the sample the whole calibration graph or just one point may be measured. It is important to ensure that the mercury in the sample aliquot plus the addition does not exceed the amount for which the response of the instrument is linear, and that the same tin(II) chloride reaction time is used throughout. The presence of matrix interference is indicated by a lower slope for the standard addition graph than for the original calibration graph.

If this occurs the method of standard additions should be used for all samples of that type.

When volatile organic components that also absorb at 254 nm are present, a positive interference will occur, although the oxidation and concentration steps should largely eliminate them. This type of interference may be eliminated by using a deuterium background corrector or by using a bypass trap containing palladium chloride or silver foil in a difference procedure.

9. *U.v. lamps and irradiation vessels.* The instructions of the manufacturer of the u.v. lamp must be followed; the lamps should be operated only when the operator is protected by an amber glass screen. For medium-pressure lamps, sample cooling is essential, either by means of an ice bath or with a water jacket through which chilled water is circulated. In addition, some lamps need gas cooling. The lamps are best left on continuously while being used.

The irradiation vessels should be constructed to fit the u.v. lamp in use and should be designed so that the sample solution is exposed to the whole of the quartz window on the lamp. Effective mixing is essential to achieve complete destruction of organo-mercury compounds in a short time. The combination of the u.v. lamp and irradiation vessel must be checked before use to ensure that organo-mercury compounds are destroyed in an acceptably short time; as the lamp ages, repeat checks are necessary to confirm that this time remains correct.

These checks are carried out as follows. At the time of use, standard solutions (10 μg Hg l^{-1} and 100 μg Hg l^{-1}) of methylmercury chloride are prepared in water by appropriate dilution of an aqueous standard containing 0.1 g Hg l^{-1}. To check the 100-ml irradiation apparatus, a series of 8 solutions is prepared containing 5 ml of preservative reagent and 10.0 ml of 10 μg Hg l^{-1} standard diluted to 100 ml with water. (To check the 600-ml irradiation apparatus, a 600-ml portion of water containing 30 ml of preservative reagent and 10.0 ml of standard 100 μg Hg l^{-1} solution is used.) The whole procedure given is then applied with irradiation times of 2, 4, 6, 8, 10, 12, 14, and 16 min, respectively. The apparatus is satisfactory if 100% conversion of methylmercury chloride is achieved in less than 10 min.

10. Hydroxylammonium chloride is not added in this procedure because the amount of oxidant is small in comparison with the reducing power of the tin(II).

11. The acidity of the sample solution at the preconcentration aeration stage is not high enough to prevent completely the hydrolysis of tin salts and precipitation of tin hydroxide occurs after 20—30 min. It is recommended therefore that immediately after this stage, the solution should be discarded and the vessel rinsed out.

12. The preservative reagent added during sampling provides all reagents necessary for u.v. oxidation. If the dichromate has been reduced, a further 5 ml of preservative reagent should be added before irradiation.

TESTING THE METHODS

During the development of the methods a considerable amount of work was done by participating laboratories to evaluate certain sections such as the stability of solutions of low mercury levels on storage, the efficiency of the u.v. oxidation procedure on various organo-mercury compounds and the efficiency of the mercury concentration technique. Not all this work is reported here because the effectiveness of some of it is illustrated by the results of the interlaboratory trial. Some of the sections which are not substantiated in this way are given below.

Storage of dilute aqueous mercury solutions

Tests were carried out by two laboratories as shown in Table 1. It can be concluded that there are no losses of mercury under the conditions specified.

The efficiency of decomposition of organo-mercury compounds by u.v. irradiation

The results given in Table 2 were obtained by using 170 ml of mercury solutions containing the preservative reagent with irradiation times of 15 min and two different types of lamp. The low-pressure lamp emits considerably less heat than the high pressure lamp for which cooling by means of an ice bath or the circulation of cooling water is essential. Similar results were obtained by three other laboratories on most of the compounds listed. The only compound which failed to give a recovery of greater than 80% was mercury dicyanodiamide which gave about 60% recovery by both methods.

It was found that as long as the sample solution was efficiently stirred during u.v. irradiation, sample volumes of up to 2 l could be used without any reduction in the recoveries of mercury.

The interference of organic substances with the u.v. method

The discovery that isopropanol interfered in the irradiation process prompted an examination of the influence of some other organic compounds. This was done by irradiating and aerating 100-ml volumes of a solution containing 1 μg Hg/100 ml (as methylmercury chloride) and the appropriate volume of preservative reagent with the addition of varying concentrations of other organic compounds. To speed up the work and to accentuate the effect, the irradiation times were reduced to 1 min. The results, in percentage conversion of the methylmercury to ionic mercury, are given in Table 3.

Experiments were also done to identify the effect of ethanol on the standard procedure for irradiation times up to 10 min. The results, in percentage conversion, are given in Table 4.

From the results given in Tables 2—4, it can be concluded that while the concentration of ethanol necessary to cause interference for normal irradiation times is relatively large, the effect and the possibility that other organic compounds may interfere should not be ignored. Accordingly, it is recommended

TABLE 1

Storage of dilute aqueous mercury solutions after addition of preservative reagent (50 ml l^{-1}; 4 g of potassium dichromate per litre of 1 + 1 sulphuric acid).

Series 1
Mercury level, 0.30 μg Hg l^{-1} consisting of equal quantities of methylmercury chloride and mercury(II) chloride.
Method of analysis, u.v. procedure

Storage time (days)	Type of bottle	μg Hg l^{-1} found
0	Polyethylene	0.30, 0.32
	Glass	0.30, 0.26
7	Polyethylene	0.28, 0.32
	Glass	0.30, 0.25
66	Polyethylene	0.31, 0.28
	Glass	0.30, 0.31
130	Polyethylene	0.30, 0.36
	Glass	0.25, 0.25

Series 2
Mercury level, 0.70 μg Hg l^{-1} consisting of equal quantities of methylmercury chloride and phenylmercury acetate.
Method of analysis, chemical procedure.

Storage time (days)	Type of bottle	μg Hg l^{-1} found
0	—	0.68, 0.76
7	Polyethylene	0.70, 0.67
	Glass	0.69, 0.78
14	Polyethylene	0.73, 0.84
	Glass	0.59, 0.81
28	Polyethylene	0.62, 0.74
	Glass	0.67, 0.86

Series 3
Mercury level, 1.0 μg Hg l^{-1} consisting of equal quantities of methylmercury chloride and mercury(II) chloride.
Method of analysis, u.v. procedure.

Storage time (days)	Type of bottle	μg Hg l^{-1} found
0	Polyethylene	1.02, 1.06
	Glass	1.03, 1.07
7	Polyethylene	1.04, 1.06
	Glass	1.04, 1.05
66	Polyethylene	1.06, 1.10
	Glass	1.08, 1.12
130	Polyethylene	1.03, 1.04
	Glass	1.03, 1.05

that the use of the u.v. irradiation method should be confined to drinking water and candidate drinking water unless it has been established by another method of analysis that there is no interference.

TABLE 2

Efficiency of decomposition of organo-mercury compounds by u.v. irradiation

	Hanau TNN 15/32 (low-pressure)			Hanau TQ 150 (high-pressure)		
	Added ($\mu g\ Hg\ l^{-1}$)	Found ($\mu g\ Hg\ l^{-1}$)	Recovery (%)	Added ($\mu g\ Hg\ l^{-1}$)	Found ($\mu g\ Hg\ l^{-1}$)	Recovery (%)
Methylmercury chloride	0.61	0.63	103	0.61	0.57	94
	0.61	0.65	107	0.61	0.61	100
Phenylmercury acetate	0.54	0.55	102	0.54	0.55	102
	0.54	0.58	107	0.54	0.51	95
Phenylmercury borate	0.50	0.50	100	0.50	0.49	98
	0.50	0.46	92	0.50	0.45	90
Phenylmercury nitrate	0.50	0.45	90	0.50	0.59	118
	0.50	0.41	82	0.50	0.59	118
Phenylmercury chloride	0.47	0.43	92	0.47	0.56	119
	0.47	0.43	92	0.47	0.56	119

TABLE 3

Percentage recovery of organic mercury (1 μg as methylmercury chloride) with different amounts of organic substances in the u.v. irradiation process

Organic compound added (ppm)[a]	Isopropanol	Ethanol	Methanol	Urea	Citric acid	Tartaric acid	Acetic acid
10,000	25	45	—	—	—	—	95
5,000	30	—	—	—	—	—	—
2,000	—	40	—	—	—	—	—
1,000	25	—	—	—	—	—	100
100	30	30	50	90	90	90	100
10	65	75	75	100	100	100	—
1	>90	>90	>90	—	—	—	—

[a]ppm (v/v) for isopropanol, ethanol and methanol; ppm (w/v) for the other organics.

TABLE 4

Percentage recovery of organic mercury (1 μg as methylmercury chloride) with different amounts of ethanol and different irradiation times

Ethanol present (ppm v/v)	Irradiation time (min)			
	1	2	5	10
1,000	30	35	55	65
100	35	50	80	85
10	70	90	100	100

Concentration of mercury after oxidation or irradiation

Trials carried out by two laboratories indicated that quantities of ionic mercury in the range 0.1—1.0 μg Hg could be recovered to the extent of 85—95% by aeration under the following conditions:
aeration time and gas flow, 60 l h^{-1} for 10 min or 40 l h^{-1} for 20 min;
sample volume, 1000 ml;

acid concentration, 4 g l^{-1} hydrochloric acid or 9 g l^{-1} sulphuric acid; tin(II) chloride concentration, 2 g l^{-1}.

The acid concentrations quoted were sufficient to prevent precipitation of tin dioxide during aeration but if the sample solution was not discarded immediately after aeration precipitation occurred on standing. The quantity of tin(II) chloride used represents approximately a 10-fold excess. It was also found that the shape of the container was an important factor in the speed of mercury vapour release; the best results were obtained with a tall, narrow container such as a 1-litre graduated cylinder with a coarse glass frit reaching almost to the bottom.

Interlaboratory tests and results

Interlaboratory tests for the determination of very low mercury concentrations are difficult to organize, mainly because such solutions are not stable in time. Therefore the procedure followed was similar to an ASTM/EPA protocol [11], where the sample was distributed as a concentrated solution of mercury, that had to be diluted a thousand times before the analysis. Before the present interlaboratory test was carried out, it was experimentally proved that a solution of 1 mg of mercury as methylmercury chloride in 0.15% nitric acid is stable when stored in darkness. When stored in daylight, about a quarter of the methylmercury chloride is oxidized to inorganic mercury. When the preservative reagent is used, methylmercury chloride is completely oxidized to inorganic mercury in 21 days when stored in daylight, but only by about 10% when stored in the dark.

The interlaboratory test was organized at the end of 1976 as follows. About one month before the week in which the analysis had to be carried out, the concentrated samples were distributed to the different laboratories, situated throughout Western Europe. These samples had to be stored in the dark if unpacked. During the weeks before the time specified for the tests, all laboratories had to test the methods if they were not familiar with them. Every laboratory had to carry out the blank control procedures. On the first day of the week in which the analyses were to be done, the sample had to be diluted according to the following procedure.

Two 5-l stoppered glass bottles were cleaned by soaking with preservative reagent. The bottles were then washed with distilled water, 4750 ml of distilled water and 250 ml of preservative reagent were placed in each bottle and shaken vigorously to mix. Finally a dry pipette was used to pipette 5.0 ml of the sample solution provided for the interlaboratory trial into one of the bottles and the bottle was again shaken to mix. The other bottle was retained for use as a dilution water blank.

After this, the diluted sample was analyzed in triplicate by as many as possible of the procedures given. Also, three analyses of the dilution water blank solution were carried out and the mean of these results was deducted from each of the results obtained. The individual results obtained for the sample and the dilution water were then reported to one person for central data statistics. The results received are given in Table 5.

TABLE 5

Results of interlaboratory analysis for mercury in water (in μg Hg l^{-1})

Lab No.	Chemical method									U.v. method								
	Without concentration					With concentration				Without concentration					With concentration			
				Mean	s_r (%)				Mean	s_r (%)			Mean	s_r (%)				Mean	s_r (%)
1	0.69	0.74	0.72	0.717	3.5	0.70	0.78	0.69	0.723	6.8									
2	0.722	0.722	0.748	0.731	2.05	0.663	0.658	0.779*	0.700	9.8									
3	0.98	1.03	1.00	1.003	2.5	0.75	0.86	1.02	0.877	15.5									
4						0.743	0.743	0.760	0.749	1.3	0.778	0.740	0.757	0.758	2.5	0.710	0.667	0.739	0.705	5.1
5	1.3	1.3	1.3	1.300	0.0															
6	0.69	0.73	0.72	0.713	2.9															
7	0.77	0.78	0.72	0.757	4.2	0.53	0.56	0.58	0.557	4.5	0.65	0.65	0.80	0.700	12.4	0.49	0.39	0.48	0.453	12.1
9	0.69	0.65	0.66	0.667	3.1	0.58	0.59	0.58	0.583	1.0										
10	0.98	1.15	0.94	1.023	10.9	1.39	1.22	1.30	1.303	6.5	1.09	1.09	0.95	1.043	7.7	1.19	1.42	1.38	1.33	9.2
12	0.64	0.72	0.71	0.690	6.3	0.66	0.76	0.59	0.670	12.8	0.467	0.54	0.505	0.504	7.2	0.425	0.39	0.455	0.423	7.7
13	0.84	0.86	0.88	0.860	2.3	0.44	0.50	0.60	0.513	15.7	0.81	0.84	0.93	0.860	7.3					
14											0.683	0.699	0.699	0.694	1.3					
15	0.76	0.71	0.72	0.730	3.6	0.77	0.73	0.75	0.75	2.7	0.70	0.72	0.67	0.697	3.6	0.71	0.69	0.72	0.707	2.2
16	0.73	0.73	0.69	0.717	3.2						0.77	0.80	0.71	0.760	6.0					
18						0.663	0.630	0.608	0.634	4.4										
19	0.452	0.461	0.496	0.470	4.9	0.642	0.519	0.788	0.650	20.7										
20	0.65	0.65	0.85	0.717	16.1	0.55	0.36	0.50	0.470	20.9										
21	0.688	0.658	0.696	0.681	2.9	0.738	0.728	0.691	0.719	3.4	0.551	0.535	0.503	0.530	4.6	0.656	0.703	0.697	0.687	4.0
22	0.78	0.78	0.80	0.787	1.5															
23						0.83	0.65	0.85	0.777	14.2										
24	0.65	0.63	0.69	0.657	4.7						0.66	0.68	0.69	0.677	2.3					
25	0.69	0.67	0.77	0.710	7.5	0.63	0.79	0.77	0.730	11.9	0.65	0.72	0.72	0.697	5.8	0.60	0.67	0.67	0.647	6.3
26	1.09	0.97	0.97	1.010	6.9	1.10	1.17	1.11	1.127	3.4	0.83	0.86	0.77	0.820	5.6	0.69	0.65	0.86	0.733	15.2
29	0.73	0.70	0.69	0.707	2.9	1.00	0.97	0.75	0.907	15.1										
30	0.74	0.73	0.73	0.733	0.79	0.47	0.60	0.42	0.497	18.7										
31	0.71	0.70	0.70	0.703	0.82	0.64	0.63	0.63	0.633	0.91	0.68	0.69	0.69	0.687	0.84	0.66	0.65	0.66	0.657	0.88
35																0.71	0.67	0.69	0.690	2.9

At the end of 1977, the Working Party participated in an interlaboratory test with the International Organization for Standardization (ISO/TC 147/SC 2/WG 5 "Water—Mercury"). During this test, the chemical method and the u.v. method were also tested, but without the concentration step. The results obtained did not differ significantly from the results of the test that is presented here.

Statistical procedures

The procedures followed were the same as those used in Parts I and II [17, 2]. The means, repeatabilities and reproducibilities of the results are given in Table 6. The results were tested for significant differences from the true value by the Student *t*-test.

DISCUSSION AND CONCLUSIONS

In general, the results are good for all four methods. The results obtained for the methods including a concentration step are somewhat lower than for the methods without a concentration step. The difference between the value found and the true value is not significant when the Student *t*-test is applied, even for the u.v. method with concentration. It is possible that the lower results were due to some laboratories using a 1-l wash bottle with poor geometry for the concentration step and/or not aerating long enough during the concentration procedure. Therefore, the wording of the procedure was improved.

In comparison with the ASTM/EPA Interlaboratory Test [11], the bias of the mean found here was much lower at the 0.7 μg Hg l^{-1} level for the chemical method without concentration: ASTM/EPA + 20%; BITC + 2.2%.

TABLE 6

Results of statistical evaluation of interlaboratory analysis for mercury in water

Method	Chemical method		U.v. method	
	Without concn.	With concn.	Without concn.	With concn.
Number of participating laboratories	22	20	13	10
Sets of three results eliminated:				
Because of lack of repeatability	2	0	0	0
Because of lack of reproducibility	0	0	0	3
Results				
Arithmetic mean (μg l^{-1})[a]	0.767	0.728	0.725	0.689
Repeatability[b]				
Standard deviation (μg l^{-1})	0.029	0.079	0.046	0.049
Relative standard deviation (%)	3.8	10.9	6.3	7.1
Reproducibility[b]				
Standard deviation (μg l^{-1})	0.173	0.214	0.142	0.050
Relative standard deviation (%)	22.5	29.4	19.6	7.2

[a]The actual mercury content of the sample was 0.75 μg Hg l^{-1}.

[b]Repeatability means single-laboratory, single-operator and single-apparatus precision; reproducibility means multi-laboratory, multi-operator and multi-apparatus precision.

TABLE 7

Summary of data for blanks and calculated limit of detection[a]

Method		Mean of blanks (μg Hg)	s of blanks (μg Hg)	n	$t_{99.5}$	Limit of detection (μg Hg l^{-1})
Chemical method	Without concn.	0.020	0.0036	19	2.88	0.10
	With concn.	0.147	0.0345	20	2.86	0.16
U.v. method	Without concn.	0.0092	0.0022	10	3.25	0.07
	With concn.	0.0387	0.0141	10	3.25	0.08

[a] s = standard deviation; n = number of laboratories that reported blank values that were not eliminated; t = Student's confidence coefficient for 99.5% probability, one sided.

From the data for the blanks in Table 7 it is clear that the u.v. method gives a lower blank and a better repeatability than the chemical method. This is obviously due to the fact that the u.v. method needs fewer reagents than the chemical method. Therefore, the lower limit of detection of the u.v. method is about half that of the chemical method. The concentration procedures do not seem to give any advantage over the direct procedures in obtaining a lower limit of detection. This is probably due to the reagents used and the standard of working in many laboratories, because the value of the blank increases with the amount of reagents. As results of the preliminary tests showed, it is readily possible to obtain lower blanks with the concentration procedure.

REFERENCES

1 European Parliament Working Documents 1973-4. Document 350/73.
2 Mercury Analysis Working Party of BITC, Anal. Chim. Acta, 84 (1976) 231.
3 J. M. Lo and C. M. Wai, Anal. Chem., 47 (1975) 1869.
4 J. F. Kopp, M. C. Longbottom and L. B. Lobring, J. Am. Water Works Assoc., 64 (1972) 20.
5 U.S. Environmental Protection Agency, Methods for Chemical Analysis of Water and Wastes, 2nd edn., 1974, EPA publication 625-/6-74-003, STORET total 71900, pp. 118—126.
6 F. Frimmel and H. A. Winkler, Z. Wasser Abwasser Forsch., 8 (1975) 67.
7 G. Topping and J. M. Pirie, Anal. Chim. Acta, 62 (1972) 200.
8 E. Harsányi, L. Pólos and E. Pungor, Anal. Chim. Acta, 67 (1973) 229.
9 C. Feldman, Anal. Chem., 46 (1974) 99.
10 M. H. Bothner and D. E. Robertson, Anal. Chem., 47 (1975) 592.
11 J. A. Winter and H. A. Clements, Water Quality Parameters ASTM STP 573, American Society for Testing and Materials, 1975, pp. 566—580.
12 F. A. J. Armstrong, P. M. Williams and J. D. H. Strickland, Nature, 211 (1966) 481.
13 P. D. Goulden and B. K. Afghan, Technol. Bull., 27 (1970). Inland Waters Branch Dept. of Energy, Mines and Resources, Ottawa, Canada.
14 M. Dujmovic and H. A. Winkler, Chem. Ztg., 98 (1974) 233.
15 F. Frimmel and H. A. Winkler, Z. Wasser Abwasser Forsch., 9 (1976) 126.
16 A. M. Kiemeneij and J. G. Kloosterboer, Anal. Chem., 48 (1976) 575.
17 Mercury Analysis Working Party of BITC, Anal. Chim. Acta, 72 (1974) 37.

Analytica Chimica Acta, 109 (1979) 229—239
© Elsevier Scientific Publishing Company, Amsterdam — Printed in The Netherlands

ANALYTICAL AND SPECTRAL FEATURES OF GAS-PHASE CHEMILUMINESCENCE SPECTROMETRY OF ARSENIC AND ANTIMONY[‡]

K. FUJIWARA**, J. N. BOWER, J. D. BRADSHAW and J. D. WINEFORDNER*
Department of Chemistry, University of Florida, Gainesville, FL 32611 (U.S.A.)
(Received 5th January 1979)

SUMMARY

Intense emissions are produced in the u.v. and visible regions when arsine and stibine are introduced into a flow-type furnace—hydrogen diffusion flame system, when the flame is surrounded by oxygen. The emissions in the range 240—300 nm are attributed to AsO and SbO. The emission characteristics seem to be due to chemiluminescence based on the reaction between atomic analyte and oxygen. The detection limits are 0.05 μg As (10 ppb) at 429 nm and 0.1 μg Sb (20 ppb) at 369 nm.

Chemiluminescence spectroscopy (emission spectroscopy based on chemical excitation) is a sensitive and indispensable technique [1] for the determination of some organic or biological materials. Conversely, for inorganic species, although mechanisms of chemiluminescence have been well characterized in flames [2—5], furnaces [6—8], molecular beams [9—11] and gas flow systems [12—14] in terms of their potential for chemical lasers, applications to analytical chemistry have scarcely been taken into consideration.

The molecular emission bands of arsenic, antimony and selenium have been observed mainly in electrical discharges [15]. However, atomic absorption spectrometry (a.a.s.) [16—18] and atomic fluorescence spectrometry (a.f.s.) [19] have mainly been employed in quantitative analyses for these elements. Resonance atomic lines of these elements exist in the near vacuum u.v. region (180—200 nm) and their determination by a.a.s. is sometimes troublesome with regard to stability and noise of the light source and absorption interference by oxide gases, such as SO_2, H_2O, NO and O_2.

Recently, Belcher et al. [20—22] reported the molecular emission of arsenic, antimony and selenium in the region 350—500 nm by using molecular emission cavity analysis (m.e.c.a.). Also Kushawaha et al. [23, 24] investigated the chemiluminescence of arsenic monoxide based on the reaction between arsenic trichloride and oxygen in order to investigate the bands for the A″—X transition in the 580—655-nm region. Previously arsenic and antimony oxides were found to be present in flames by mass spectroscopy [25, 26].

**On leave from the University of Tokyo.
[‡]Research supported by AF-AFWR F44620-78C-0005.

In the present paper, the chemiluminescence of arsenic and antimony resulting from their oxidation reactions was investigated and applied to quantitative measurements of these species.

EXPERIMENTAL

Reagents

Standard solutions of arsenic, antimony and selenium were prepared by dissolving arsenic trioxide, antimony potassium tartrate and elemental selenium in dilute sodium hydroxide solution, distilled water and diluted nitric acid, respectively. For generating arsine, stibine and hydrogen selenide, 6 M hydrochloric acid, 2% sodium borohydride and a 1 M potassium iodide—5% ascorbic acid mixture were prepared (the last is not needed for hydride generation, but is used in sample preparation) [16—18].

Apparatus

The apparatus used and their manufacturers are listed in Table 1; some experimental conditions are also included.

For the spectral measurements, a silicon-intensified target (SIT) Vidicon sensor with an optical multichannel analyser (OMA) was used. The SIT was attached to a spectrometer. The 500 channels of the SIT covered a wave-

TABLE 1

Apparatus and manufacturers

Item	Model number	Manufacturer
OMA detection system		
SIT—Vidicon sensor	1205 D	Princeton Applied Research Co., San Carlos, CA 94070
OMA	1205 A	Princeton Applied Research Co., San Carlos, CA 94070
Monochromator	EU 700[a]	GCA McPherson, Acton, MA, 01720
X—Y recorder	690-2R-26	MFE Corporation, Salem, N.H. 03079
Single-channel detection system		
Photomultiplier	R-106 (1000 V)	Hamamatsu Co., Middlesex, N.J. 08846
High-voltage supply	412	John Fluke Manufacturing Co., Inc., Seattle, Washington
Monochromator	H-10V[b]	Jobin Yvon, Metuchen, N.J. 08840
Potentiometric recorder	SR	Sargent Welch, Birmingham, Ala., 60076

[a]With 0.2-nm spectral bandpass.
[b]With 4-nm spectral bandpass and 10-mm slit height.

length range of about 50 nm. About 200—300 accumulation times (32.8 ms for each accumulation period) were used for the spectral signal; background subtraction was performed. All spectra were displayed on an X—Y recorder.

For quantitative analyses, a conventional monochromator of 10-cm focal length was used. A laboratory-constructed nanoammeter was used for all d.c. measurements.

The hydride generator was constructed as described previously [18]. A laboratory-built ultrasonic nebulizer with an r.f. generator—piezoelectric crystal system was also used for the direct nebulization of sample solutions instead of hydride generation.

The decomposition of the hydrides or sample aerosol containing analyte and production of the oxide species was achieved by a continuous flow furnace [27] with a hydrogen diffusion flame (containing a trace of methane) in which the carbon tube (0.25-in. o.d., 0.185-in. i.d., 2.125-in. long) was electrically heated (generally 200 A, 8 V), giving a temperature of 2200°C (optical pyrometer). The furnace carbon was continuously coated by pyrolytic graphite owing to the methane flow as well as being precoated before use. The gas flows used are stated in the text. A block diagram of the instrumental set up is given in Fig. 1.

Procedures

Hydride generation. To 7 ml of hydrochloric acid and 1 ml of the potassium iodide—ascorbic acid solution was added the sample solution; 1 ml of sodium borohydride solution was then injected through the generator rubber cap. The hydride produced was expelled by a mixture of N_2 (or Ar), H_2 and CH_4, and, for quantitative analysis, was collected in a liquid nitrogen trap, and released later by insertion in hot water.

Ultrasonic nebulization. The mixed gases mentioned were used to transport the nebulized solution to the furnace via a desolvation system heated to about 200°C, for measurement of OMA spectra.

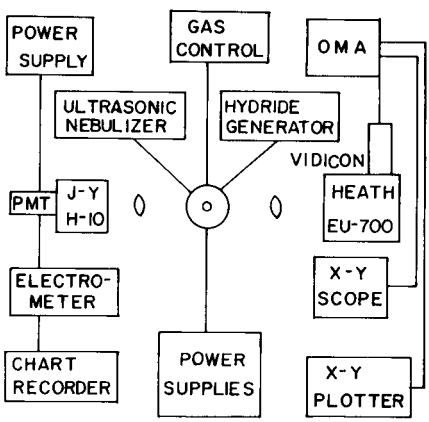

Fig. 1. Block diagram of instrumental system.

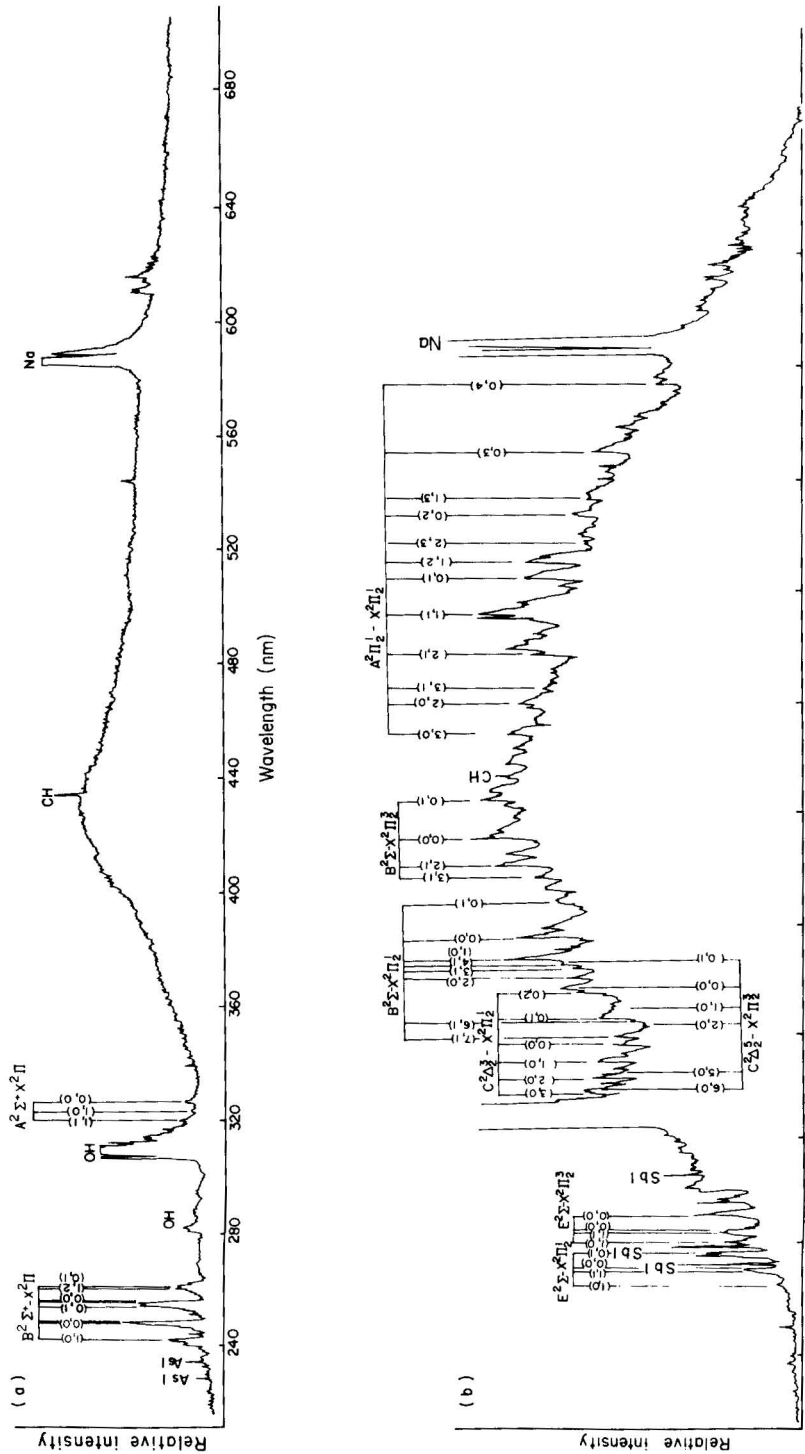

Fig. 2. Emission spectrum obtained for (a) 1.5 mg As and (b) 1.5 mg Sb. Conditions: hydride generation; H_2, 1.1 l min^{-1}; CH_4, 0.11 l min^{-1}; Ar, 0.8 l min^{-1}; furnace (internal) Ar, 1.2 l min^{-1}; sheath air, 2.0 l min^{-1}. Peaks assigned on basis of ref. 14.

Observation of chemiluminescence. The hydride or aerosol sample was passed through the continuous flow furnace and immediately into the hydrogen diffusion flame, which was sheathed with an oxidant gas (air, N_2O or O_2). The emission from the flame was monitored. The sheath gas outlet was composed of capillaries which were placed coaxially around the furnace outlet. The spectrometer was optically aligned with the flame at a height of 10—20 mm above the top of the furnace.

RESULTS

Spectroscopic observation

Figure 2(a) shows the emission spectrum obtained for arsenic. Several intense peaks ascribed to AsO were observed; the $B^2\Sigma^+—X^2\Pi$ transitions were observed at 240—260 nm. Because OH emission was strong, only three peaks of the AsO $A^2\Sigma^+—X^2\Pi$ transition near 300 nm were seen. Emissions corresponding to other AsO electronic transitions were not distinguishable. In the visible region, there was a broad molecular band (maximum 420—440 nm). After comparison of background flame emission without arsenic, the broad peak was also ascribed to one or more arsenic molecular species. Ultrasonic nebulization of arsenic trioxide solution did not result in an "emission" spectrum of AsO in the ultraviolet region, but did give the same broad peak in the visible region as with arsine.

Figure 2(b) gives the emission spectrum of antimony produced by stibine generation. Numerous peaks were ascribed to SbO. In the u.v. region, several intense peaks from SbO were evident as well as band emission and several atomic lines. In the visible region, several emission bands (B—X and A—X) of SbO were present in the region 350—650 nm. With ultrasonic nebulization of antimony potassium tartrate solution, only the broad peak (350—650 nm) appeared, and the emission peaks ascribed to SbO in the ultraviolet were not observed.

Neither hydride generation nor direct sample nebulization of selenium solutions by ultrasonic nebulizer gave any emission spectra, unlike m.e.c.a., in which Se_2 emission was reported [20]. However, in the present system, selenium hydride was decomposed to atoms in the furnace; apparently the association reaction of selenium atoms to form Se_2 does not occur very readily because of the low concentration of selenium.

Determination of arsenic and antimony

For analytical arsenic measurements, the AsO peaks at 250 nm ($B^2\Sigma^+—X^2\Pi$ transition) and at 429 nm (broad band) were chosen. For analytical antimony measurements, SbO peaks at 256.5 nm ($E^2\Sigma—X^2\Pi_{3/2}$) and at 369 nm ($B^3\Sigma—X^2\Pi_{1/2}$ and $C^2\Delta_{5/2}—\Pi_{3/2}$) were used.

Figure 3 shows the dependence of emission intensity on the current supplied to the carbon furnace (a current increase of 10 A corresponds to a 75°C increase of furnace temperature as measured by an optical pyrometer). Higher

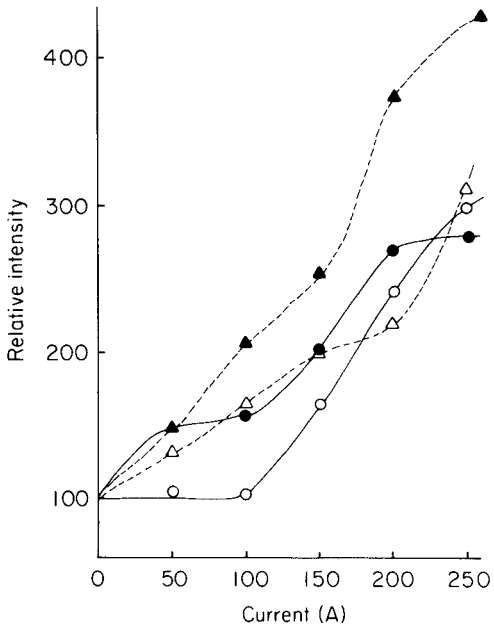

Fig. 3. Dependence of emission intensity on furnace current. Conditions: H_2, 0.94 l min^{-1}; CH_4, 0.11 l min^{-1}; Ar, 1.0 l min^{-1}; furnace Ar, 1.1 l min. (△) 60 μg As, 429 nm, air 2.1 l min^{-1}; (▲) 100 μg Sb, 369 nm, air 4.7 l min^{-1}; (○) 60 μg As, 245 nm, air 4.7 l min^{-1}; (●) 60 μg Sb, 256 nm, air 4.7 l min^{-1}.

furnace temperatures gave greater intensities for the u.v. and visible emission peaks. Therefore, the decomposition of arsine or stibine appears to be necessary for more intense emission.

Figure 4 shows the dependence of emission intensities on the flow rate of the sheath oxidant gas which surrounds the diffusion flame. Oxygen was the most effective sheath gas for enhancement of the emission signal regardless of the wavelength and the analyte. Conversely, nitrous oxide had only a small effect on the emission signal. Although nitrous oxide or active nitrogen has been found to be effective enhancers of chemiluminescence [29—31], the results obtained here indicate that only oxygen is suitable for the present emission processes.

From the above results, higher current to the furnace and higher flow rate of the oxygen sheath increased the sensitivity for measurement of arsenic and antimony. However, for the arsenic band at 245 nm, a higher flow rate of oxygen also increased the background noise, and the detection limit was the same as with the air sheath. The detection limit for arsenic at 245 nm was ca. 1 μg (signal-to-noise ratio of 3). For the 429-nm arsenic emission, the oxygen sheath improved the sensitivity and the detection limit, giving a detection limit of 50 ng (10 ppb) of arsenic. The responses obtained for calibration purposes at 429 nm are shown in Fig. 5.

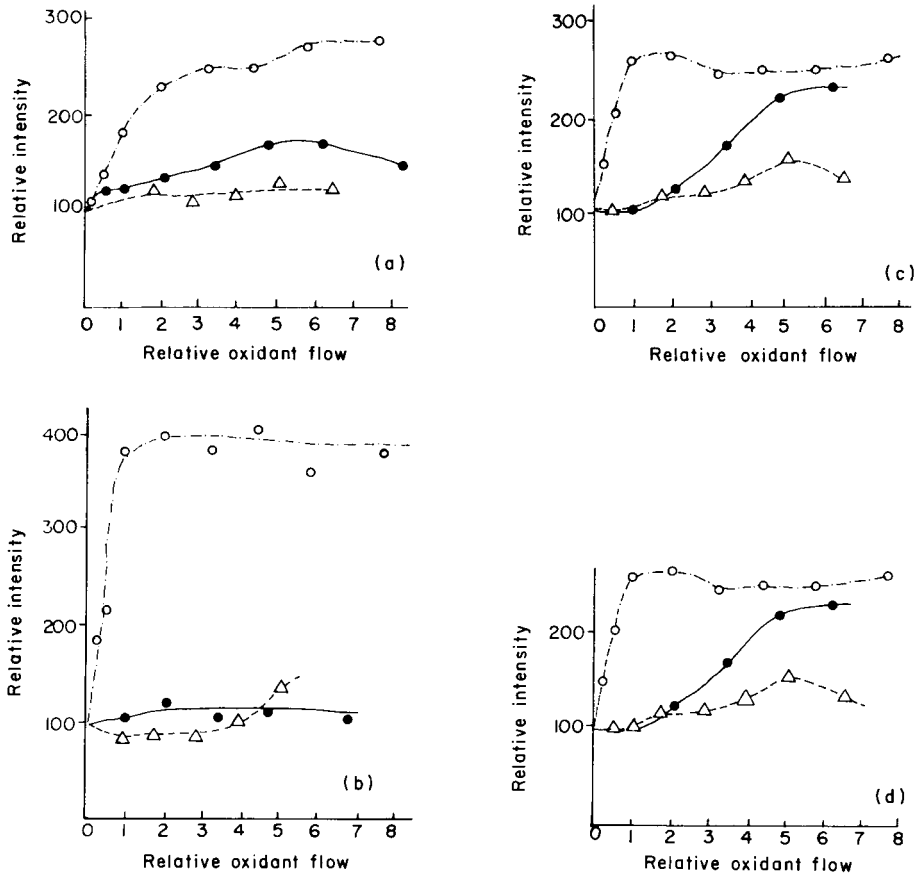

Fig. 4. Dependence of emission intensity on flow rate of sheath oxidant gases. Conditions: H_2, 0.58 l min^{-1}; CH_4, 0.11 l min^{-1}; Ar, 1.1 l min^{-1}, furnace Ar, 0.95 l min^{-1}. (a) 40 μg As, 245 nm; (b) 40 μg Sb, 429 nm; (c) 100 μg Sb, 256 nm; (d) 100 μg Sb, 369 nm. Sheath gas: (○) oxygen; (●) air; (△) nitrous oxide.

The antimony emission at 369 nm was much more intense than that at 256 nm. The detection limit at 369 nm was 0.1 μg (20 ppb); the signals obtained for 0.5—3.0 μg of antimony were similar to those shown in Fig. 5.

In all the cases, decrease in the spectral band width to less than 4 nm decreased the signal-to-noise ratio. Because the determination of arsenic or antimony based on the visible broad peak was not specific, it was difficult to correct for background by use of a different wavelength. Therefore, interference by concomitants in the sample must be minimized by the hydride generation method.

DISCUSSION

The emission intensities of arsenic and antimony are directly related to the oxidant concentration and to the concentration of atomic species. These

results indicate that the emission observed is most likely due to a chemical reaction between these species. This conclusion is especially viable for the emission around 250 nm (ca. 5 eV) where thermal excitation cannot account for the intense emissions observed. The u.v. bands were not reported in the m.e.c.a. studies [21]. Furthermore, the flame used (in the furnace) was extremely lean (the hydrogen was used primarily to provide a reducing atmosphere). Also, an increase in hydrogen flow rate over 1 l min^{-1} did not increase the emission signal. These results are contrary to those expected for a thermal excitation mechanism but are understandable for a chemical excitation mechanism (chemiluminescence).

Broad band in visible region

One possible origin of the broad band in the visible region could be the recombination of arsenic and oxygen atoms. When this process occurs (transition from antibonding to bonding orbital) such as $As + O \rightarrow AsO + h\nu$, the resulting emission might be a quasi-continuum. This type of emission is well known in flames, particularly for H + OH and CO + O [32]. However, the respective energy differences between ground and lowest antibonding states must be more than 4.1 and 4.0 eV for AsO and SbO, respectively; therefore maxima at 430 nm for arsenic and 450 nm for antimony, which correspond to 2.88 eV and 2.76 eV, are at longer wavelengths than expected. Therefore, this mechanism seems to be unlikely if the transition occurs from an antibonding orbital to the ground state.

From mass spectral observations of oxyhydrogen flames [25, 26] (average temperature 2300 K), H_3AsO_4, $HAsO_3$ and AsO formed from $AsCl_3$, and H_3SbO_4, $HSbO_3$ and SbO formed from $SbCl_5$, are the major flame gas molecules when arsenic and antimony are present. Because the flame temperature in the present system is also close to 2300 K (as determined by line reversal

TABLE 2

Enthalpies of arsenic and antimony reactions of interest to the present study [21, 29]

Reaction	ΔH (eV)	Reaction	ΔH (eV)
$AsO + 3H_2O(g) \rightarrow H_3AsO_4(g) + \frac{3}{2}H_2(g)$	−4.46	$SbO(g) + 3H_2O \rightarrow H_3SbO_4(g) + \frac{3}{2}H_2$	−4.68
$AsO + 2H_2O(g) \rightarrow HAsO_3 + \frac{3}{2}H_2(g)$	−2.06	$SbO(g) + 2H_2O \rightarrow HSbO_3(g) + \frac{3}{2}H_2$	−1.77
$HAsO_3(g) + H_2O \rightarrow H_3AsO_4(g)$	−2.43	$HSbO_3(g) + H_2O \rightarrow H_3SbO_4(g)$	−2.94
$As + O \rightarrow AsO$	−4.47	$Sb + O \rightarrow SbO$	−4.69
$As + OH \rightarrow AsO + H$	0.11	$Sb + OH \rightarrow SbO + H$	0.32
$As_2 + O_2 \rightarrow 2AsO$	0.16	$Sb_2 + O_2 \rightarrow 2SBO$	−1.10
$As_2 + O \rightarrow As + AsO$	0.49	$Sb_2 + O \rightarrow Sb + SbO$	−120
$As + O_2 \rightarrow AsO + O$	0.66	$Sb + O_2 \rightarrow SbO + O$	0.14
$AsH_3 + 2O_2 \rightarrow AsO + 3OH$	0.26	$SbH_3 + 2O_2 \rightarrow SbO + 3OH$	[a]
$AsH_3 + \frac{5}{4}O_2 \rightarrow AsO + \frac{3}{2}H_2O$	−1.26	$SbH_3 + \frac{5}{4}O_2 \rightarrow SbO + 3H_2$	[a]
$As + 2OH \rightarrow AsO + H_2O$	−5.28	$Sb + 2OH \rightarrow SbO + H_2O$	−5.55
$As_2 + 2O \rightarrow 2AsO$	−4.97	$Sb_2 + 2O \rightarrow 2SbO$	−5.58

[a]Not available.

measurement [28]), H_3AsO_4, $HAsO_3$, H_3SbO_4, and $HSbO_3$ seem to be possible as major analyte species. The reactions involved in formation of these species are listed in Table 2. These formation reactions are sufficiently exothermic for $HAsO_3$ ($HSbO_3$ or H_3SbO_4) to emit in the visible spectral region. In this case, these polyatomic molecules would give rather broad bands as can be seen in the case of HPO in other flame studies [15].

Emission of AsO and SbO

For AsO, the main emission transition is $B^2\Sigma^+ - X^2\Pi$. Because As + O → AsO is the only greatly exothermic reaction in the two-body interactions of AsO formation (Table 2), this reaction seems to be the main one responsible for the production of the $B^2\Sigma^+$ state of AsO. From the data calculated by Callomon et al. [35, 36], it can be assumed that $B^2\Sigma^+$ is produced from $As(^4S^0) + O(^1D)$ (Fig. 6). Because the $As(^4S^0)$ state is the ground state (lowest energy level), most arsenic atoms produced in the flame belong to this state. However, $O(^1D)$ can be produced via the following processes [34] in an air–hydrogen flame:

$$O_2(^3\Sigma_g^-) + H(^2S) \rightarrow HO_2(^2A'') \xrightarrow[\text{transition}]{\text{radiationless}} HO_2(^2A'')$$

$$HO_2(^2A'') \rightarrow OH(^2\Sigma^+) + O(^3P)$$

$$OH(^2\Sigma^+) + H_2(^1\Sigma_g^+) \rightarrow O(^1D) + H(^2S) + H_2(\Sigma_g^+)$$

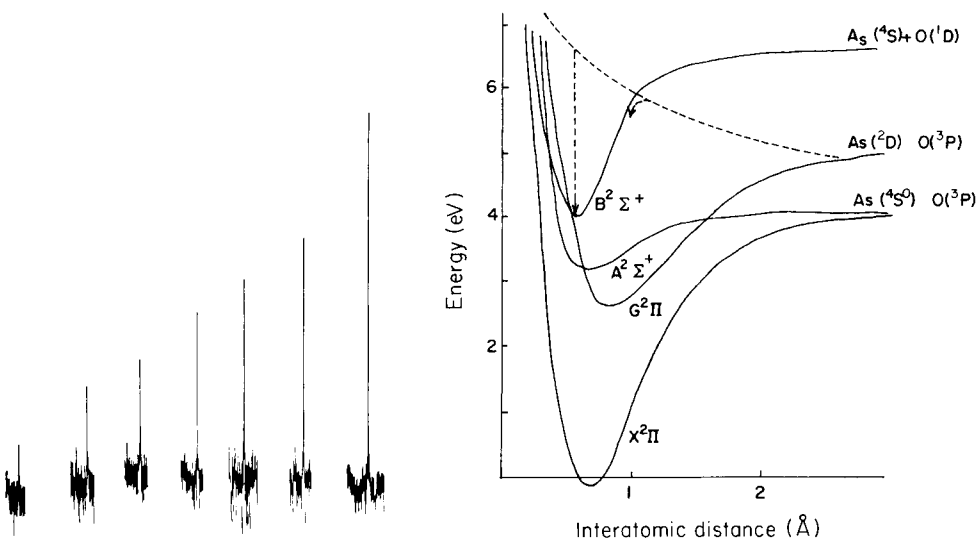

Fig. 5. Calibration responses for (left to right) blank, 0.1, 0.2, 0.5, 0.7, 1.0 and 2.0 μg of arsenic at 429 nm. Conditions: H_2, 1.9 l min^{-1}; N_2, 1.84 l min^{-1}; furnace N_2, 0.36 l min^{-1}; O_2, 5.80 l min^{-1}.

Fig. 6. Schematic potential curve of AsO. Dotted line is the assumed curve of the lowest antibonding level of which spin multiplicity is a doublet [35, 36].

Therefore, the reaction between As($^4S^0$) and O(^1D) is assumed to be the major mechanism for producing the $B^2\Sigma^+$ state. Another possibility is the radiative or non-radiative transition from the antibonding orbital of As($^2D^0$) + O(^3P) (for which an assumed potential curve is shown in Fig. 6 as a dotted line). As ($^2D^0$) accounts for 0.2% of the total number of arsenic atoms according to the Boltzmann distribution (at 2300 K). Both processes could result in the selective formation of the $B^2\Sigma^+$ state in the present studies. Transitions from antibonding orbitals of As($^4S^0$) plus O(^3P) to $B^2\Sigma^+$ are spin-forbidden.

For SbO, many transitions from various excited levels to the ground level are observable. The reaction of Sb + O → SbO is sufficiently exothermic that non-radiative transition via crossing of energy levels might also occur.

The detection limits of arsenic and antimony are 50 ng (10 ppb) and 100 ng (20 ppb), respectively. These values are ~ 20 × more sensitive than by m.e.c.a. [22] but are not as impressive as those obtained by a.a.s. or a.f.s. However, there are several merits to the present method. The measurement system is simple and its cost is low. The emission signal is free from the noise commonly present in arsenic a.a.s. light sources, and practical analytical difficulties are minimized compared to a.a.s. and a.f.s. where absorption or fluorescence of atomic lines in the 180—220-nm region is affected by absorption by atmospheric gases.

K. Fujiwara thanks Yoshida Scientific Foundation, Japan, for a travel grant.

REFERENCES

1 J. Isacsson and G. Wettermark, Anal. Chim. Acta, 68 (1974) 339.
2 C. Lintox and H. P. Broida, J. Mol. Spectrosc., 64 (1977) 382.
3 S. E. Johson, P. B. Scott and G. Watson, J. Chem. Phys., 61 (1974) 2384.
4 K. J. Kaufmann, J. L. Kinsey, H. B. Palmer and A. Tewarson, J. Chem. Phys., 60 (1974) 4023.
5 M. Luria, D. J. Eckstrom and S. W. Benson, J. Chem. Phys., 65 (1976) 158.
6 S. Rosenwaks, J. Chem. Phys., 65 (1976) 3668.
7 H. Luria, D. M. Eckstrom and S. W. Benson, J. Chem. Phys., 64 (1976) 3103.
8 M. M. Hessel, R. E. Drullinger and H. P. Broida, J. Appl. Phys., 46 (1975) 2317.
9 F. Engelke, R. K. Sander and R. N. Zare, J. Chem. Phys., 65 (1975) 1146.
10 C. D. Jonah, R. N. Zare and Ch. Ottinger, J. Chem. Phys., 56 (1972) 263.
11 T. P. Parr, A. Freedman, R. Behrens, Jr. and R. R. Herm, J. Chem. Phys., 67 (1977) 2181.
12 R. Shanker, C. Linton and R. D. Verma, J. Mol. Spectrosc., 60 (1976) 197.
13 C. L. Chalek and J. L. Goel, J. Chem. Phys., 65 (1976) 2845.
14 G. Harger, R. Harris and S. G. Hadley, J. Chem. Phys., 63 (1975) 2810.
15 R. W. B. Pearse and A. G. Gaydon, (Eds.), The Identification of Molecular Spectra, Chapman and Hall, London, 1976.
16 F. J. Schmidt and J. L. Royer, Anal. Lett., 6 (1973) 17.
17 D. D. Siemer and L. Hagemann, Anal. Lett., 8 (1975) 323.
18 D. D. Siemer, P. Koteel and V. Jarwale, Anal. Chem., 48 (1976) 836.
19 E. M. Heithmar and F. W. Plankey, Appl. Spectrosc., 32 (1978) 208.
20 R. Belcher, T. Kouimtzis and A. Townshend, Anal. Chim. Acta, 68 (1974) 297.

21 R. Belcher, S. L. Bogdanski, S. A. Ghonaim and A. Townshend, Anal. Chim. Acta, 72 (1974) 183.
22 R. Belcher, S. L. Bogdanski, E. Henden and A. Townshend, Anal. Chim. Acta, 92 (1977) 33.
23 V. S. Kushawaha, B. P. Asthana and C. M. Pathak, J. Mol. Spectrosc., 41 (1972) 577.
24 V. S. Kushawaha, Chem. Phys. Lett., 30 (1975) 130.
25 M. Farber and R. D. Srivastava, Combust. Flame, 25 (1975) 101.
26 J. W. Hastie, Combust, Flame, 21 (1973) 49.
27 C. J. Molnar and J. D. Winefordner, Anal. Chem., 46 (1974) 1419.
28 J. N. Bower, K. Fujiwara, J. D. Bradshaw and J. D. Winefordner, FACSS 5th Annual Meeting, Nov. 2, 1978, Boston.
29 R. G. Gann, F. Kaufmann and M. A. Biondi, Chem. Phys. Lett., 16 (1972) 380.
30 D. J. Benard, W. D. Slafer and J. Hecht, J. Chem. Phys., 66 (1977) 1012; D. J. Benard and W. D. Slafer, J. Chem. Phys., 66 (1977) 1017.
31 C. J. Hsu, W. D. Krugh and H. B. Palmer, J. Chem. Phys., 60 (1974) 5118.
32 J. D. Winefordner, Spectrochemical Methods of Analysis, Wiley, New York, 1971, p. 79.
33 F. D. Rossini, D. D. Wagman, W. H. Evans, S. Levine and I. Jaffe, (Eds.), Selected Values of Chemical Thermodynamic Properties, NBS publication, 1952.
34 K. J. Laidler, The Chemical Kinetics of Excited States, Oxford University Press, London, 1955, pp. 113 and 116.
35 J. H. Callomon and J. E. Morgan, Proc. Phys. Soc., 86 (1965) 1091.
36 V. M. Anderson and J. H. Callomon, J. Phys. B, 6 (1973) 1664.

Analytica Chimica Acta, 109 (1979) 241—249
© Elsevier Scientific Publishing Company, Amsterdam — Printed in The Netherlands

FOUR-LINE METHOD FOR CORRECTION OF INTER-ELEMENT EFFECTS ON EXCITATION AND IONIZATION PROCESSES IN ATOMIC EMISSION SPECTROMETRY IN PLASMAS

KUNIYUKI KITAGAWA* and TOSHIYUKI KOYAMA

Department of Synthetic Chemistry, Faculty of Engineering, Nagoya University, Furo-cho, Chikusa-ku, Nagoya (Japan)

TSUGIO TAKEUCHI

School of Materials Science, Toyohashi University of Technology, 1-1 Hibarigaoka, Tenpaku-cho, Toyohashi, Aichi (Japan)

(Received 9th April 1979)

SUMMARY

A four-line method is described for correction of inter-element effects caused by variations of excitation temperatures and the degree of ionization in a plasma. Four lines with different upper-level energies in the atomic-ionic system are compared. The total number of atoms and ions is used as the response instead of the spectral intensity. Plasma torch symmetry is one of the most important factors for successful corrections. The correction method is demonstrated for the determination of manganese in a capacitively coupled plasma torch, where strontium interferes strongly.

In previous papers [1, 2], a method was described for determining the degree of ionization in a plasma emission source. It was shown that the method gave useful information about excitation sources used in atomic emission spectrometry. In several types of emission source, there are inter-element effects in the excitation and ionization processes; practical applications have therefore been restricted to special cases. Recently, it has been proved that the inductively coupled plasma (ICP) has the advantage that such interference effects are much smaller than those given by other kinds of plasma source [3, 4].

In this paper, a novel method is proposed for correction of interferences from variations in the excitation temperature and the degree of ionization in a capacitively coupled plasma. This is also expected to be useful for the ICP when small inter-element effects change with the fluctuation in r.f. power or flow rate of carrier gas [5, 6]. However, it should not be applied to interferences arising from variations in nebulization [7] or atomization efficiency.

THEORY

For interference correction, it is necessary to estimate a quantity indepen-

dent of the variation in the excitation temperature and the degree of ionization. This quantity, which is used here for calibration instead of the emission intensity, is the total number of atoms and ions.

The spontaneous emission intensity can be expressed for a transition (upper level 1 to lower level 1') by

$$I_{a1} = h\nu_{a1} A_{a1} N_{a1} \tag{1}$$

where h is Planck's constant, ν the frequency, A the Einstein transition probability for spontaneous emission, N_{a1} the number of atoms with an electron in the upper level 1, and the subscripts a and 1 indicate the atom and level number, respectively. Unless selective excitation occurs, the Boltzmann distribution can be applied to the energy system:

$$N_{a1} = N_a \frac{g_{a1}}{Q_a(T_a)} \exp(-E_{a1}/kT_a) \tag{2}$$

where N_a is the number of atoms, g_{a1} the statistical weight, E_{a1} the energy of the upper level, k the Boltzmann constant, T_a the excitation temperature and $Q_a(T_a)$ the partition function equal to $\Sigma_j g_{aj} \exp(-E_{aj}/kT_a)$.

The number of atoms N_a can be replaced by $N_t(1 - \chi)$, where N_t is the total number of atoms and ions and χ the degree of ionization. If the degree of atomization or the nebulization efficiency varies, N_t must be replaced by $N_s\eta\beta$, where η is the nebulization efficiency and β is the degree of atomization. However, this case is not dealt with here. Combining the above relationships gives

$$I_{a1} = h\nu_{a1} N_t(1 - \chi) \frac{g_{a1}A_{a1}}{Q_a(T_a)} \exp(-E_{a1}/kT_a) \tag{3}$$

To determine the excitation temperature T_a, this equation is written for transitions with different upper energies, and the intensity ratio I_{a1}/I_{a2} is obtained. Rearrangement of this expression gives

$$T_a = (E_{a2} - E_{a1})/k \ln\left(\frac{\nu_{a2}g_{a2}A_{a2}I_{a1}}{\nu_{a1}g_{a1}A_{a1}I_{a2}}\right) \tag{4}$$

This is the well-known two-line method.

For the ionic system, the following equations can be introduced in the same fashion as for the atomic system. As the number of ions $N_i = N_t\chi$:

$$I_{i3} = h\nu_{i3}N_t\chi \frac{g_{i3}A_{i3}}{Q_i(T_i)} \exp(-E_{i3}/kT_i) \tag{5}$$

where the subscript i stands for ion. Thus

$$T_i = (E_{i4} - E_{i3})/k \ln\left(\frac{\nu_{i4}g_{i4}A_{i4}I_{i3}}{\nu_{i3}g_{i3}A_{i3}I_{i4}}\right). \tag{6}$$

These two equations are valid independently of the values of η, β and χ.

The degree of ionization χ can be determined by taking a ratio I_a/I_i or I_i/I_a:

$$\frac{I_a}{I_i} = \frac{\nu_a g_a A_a Q_i(T_i)\,(1-\chi)}{\nu_i g_i A_i Q_a(T_a)\chi} \exp\left(\frac{E_i}{kT_i} - \frac{E_a}{kT_a}\right) \tag{7}$$

Any combination between the atomic and ionic lines is allowed, e.g., I_{a1}/I_{i3}, I_{a2}/I_{i3}, I_{a1}/I_{i4} or I_{a2}/I_{i4}. Consequently,

$$\chi = \left[1 + \frac{I_a \nu_i A_i g_i Q_a(T_a)}{I_i \nu_a A_a g_a Q_i(T_i)} \exp\left(\frac{E_a}{kT_a} - \frac{E_i}{kT_i}\right)\right]^{-1} \tag{8}$$

From eqns. (3) and (5), N_t is given by:

$$N_t = I_i \frac{Q_i(T_i)}{h\nu_c \chi g_i A_i} \exp\,(E_i/kT_i) \tag{9}$$

and

$$N_t = I_a \frac{Q_a(T_a)}{h\nu_a(1-\chi) g_a A_a} \exp\,(E_a/kT_a) \tag{10}$$

Equation (9) is suitable for small values of χ, and eqn. (10) for large values.

The partition functions for the atomic and ionic systems have been obtained for various elements, developed in the form of a series [8]. Thus, if the intensities of four lines I_{a1}, I_{a2}, I_{i3} and I_{i4} are measured experimentally, the total number of atoms and ions N_t can be determined.

Manganese was chosen as the element to be measured because intense radiation was observed for the four lines required. The lines selected and their physical properties are listed in Table 1 [9]. The atomic and ionic partition functions for manganese are:

$$Q_a(T_a) = 5.7492 + 0.36614\,(T_a/10^3) - 0.17998\,(T_a/10^3)^2 + 0.031845\,(T_a/10^3)^3 + 0.000991\,(T_a/10^3)^4$$

$$Q_i(T_i) = 6.9764 + 0.09951\,(T_i/10^3) - 0.09092\,(T_i/10^3)^2 + 0.027782\,(T_i/10^3)^3 - 0.001495\,(T_i/10^3)^4$$

Lithium, strontium and barium were selected as interferents because of their strong interference effects on the intensity of the manganese lines.

TABLE 1

The four lines selected and their properties

Wavelength (nm)	Upper energy (cm^{-1})	gA value ($10^8\ s^{-1}$)	Response factor
Mn(I) 403.08	24,802	1.4	5.9
Mn(I) 279.48	35,770	8.3	8.4
Mn(II) 294.92	43,370	66	9.0
Mn(II) 260.57	38,366	33	8.0

EXPERIMENTAL

Apparatus

A Hitachi UHF plasma torch spectrometer Model 300 [10] was used for the excitation source. It forms a capacitively coupled plasma supplied by microwave power of 300—400 W at 2450 MHz. In order to avoid interferences from variations in efficiency, a desolvation system was not incorporated in the sample-introducing system and the nebulizer was fitted directly to the plasma cavity. A brass cone for mounting the aluminum discharging electrode was replaced by an aluminium cone to avoid contamination when acidified sample solutions were used. Spectral measurements were made through a small rectangular aperture constructed by an additional slit of 2.0-mm width located in front of the entrance slit of the monochromator. The profile of the plasma torch was imaged onto the slits with a magnification ratio of unity.

The working conditions for the plasma torch are listed in Table 2. To stabilize the plasma discharge, small amounts of nitrogen were mixed with the argon. However, too much nitrogen rapidly damaged the aluminum electrode.

Reagents

A stock standard solution of manganese (100 μmol ml^{-1}) was prepared by dissolving manganese metal in distilled hydrochloric acid. The solution was diluted with distilled deionized water to 10 μmol ml^{-1} just before use. The acidity of the solution was adjusted to 0.1 M.

Stock standard solutions of the interfering elements were prepared by dissolving their reagent-grade carbonates in distilled hydrochloric acid. They were added to the manganese solution before dilution.

RESULTS AND DISCUSSION

To estimate the net intensity, the instrumental response was divided by a response factor. The factor is a product of the efficiency of the grating and the quantum yield of the photocathode in the photomultiplier tube. These depend on the wavelength. Figure 1 shows the response factor for the combination of a grating of blaze wavelength 250 nm (Hitachi) and photomultiplier

TABLE 2

Working conditions for plasma and spectrometer

Flow rate of nebulizing gas	1.5 l min^{-1}
Flow rate of plasma sheath gas	3.5 l min^{-1}
Field current for magnetron	400 mA
Anode current for magnetron	300 mA
Entrance slit width	50 μm
Exit slit width	50 μm
Measurement position	16 mm above electrode

tube R106 (HTV). The response factors for each of the four lines are listed in Table 1.

For practical purposes, the radiation was observed at a defined sectional point and the Abel transformation [11] was not applied in the calculation.

Figure 2 shows the dependence of the excitation temperatures of manganese atoms and ions (T_a and T_i) on the concentration of strontium. There is no local thermal equilibrium between the atomic and ionic systems, and the excitation temperatures change significantly with the concentration of strontium. The change suggests that energy is transferred to the manganese ionic system and removed from the manganese atomic system.

Figure 3 demonstrates the dependence of the degree of ionization, χ, on the concentration of strontium. Ionization is suppressed by the presence of strontium. This phenomenon is similar to those encountered for a nitrous oxide—acetylene flame in atomic absorption spectrometry [12], which are attributed to changes in equilibrium between the ionization processes of the two elements. Although this could be the case in the present system, this interpretation cannot generally be applied to plasma torch spectroscopy. As suggested previously, the degree of ionization could increase as a function of the total concentration of the two elements. This also applies to the variations in the excitation temperatures.

However, regardless of the physical mechanisms, it is possible to correct the interference if the excitation temperatures and the degree of ionization are determined. Figure 4 shows the dependence of the uncorrected intensity of the atomic radiation and the corrected value, i.e. the total number of atoms and ions N_t, on the concentration of the interfering element. The former is strongly affected by strontium as a result of the variation in the ex-

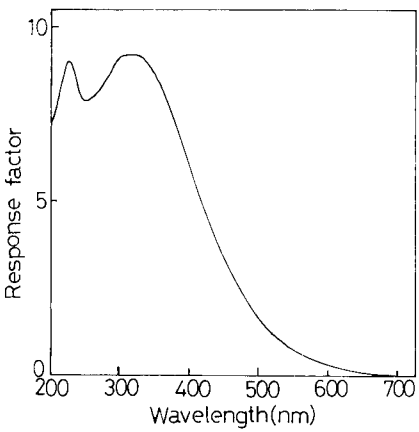

Fig. 1. Variation of instrumental response factor with wavelength.

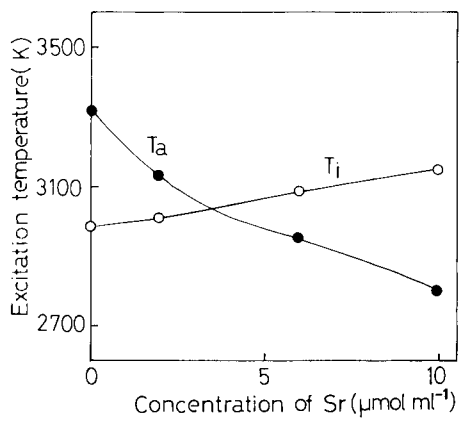

Fig. 2. Dependence of the manganese excitation temperatures on strontium concentration: T_a atomic, T_i ionic excitation temperature.

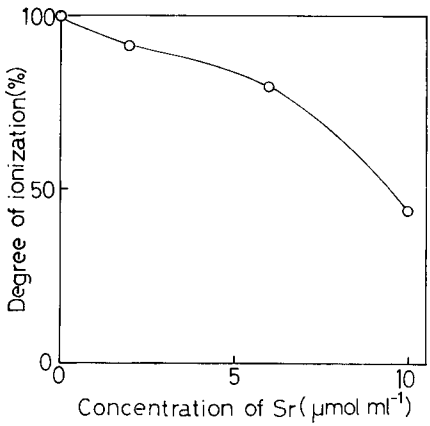

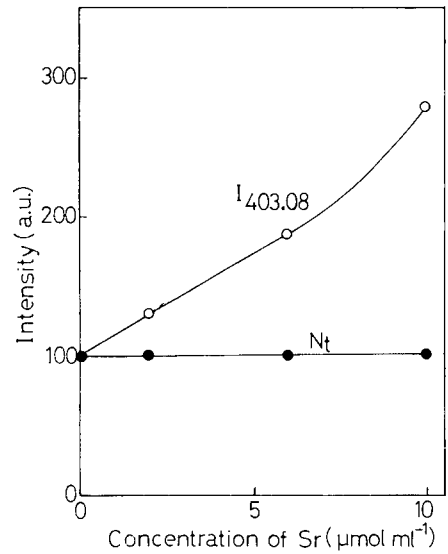

Fig. 3. Dependence of the degree of manganese ionization on strontium concentration.

Fig. 4. Corrected and uncorrected responses for manganese in the presence of strontium.

citation temperature and the degree of ionization. In spite of such a strong interference effect, the corrected value remains essentially unaffected by the strontium concentration.

Symmetry in the plasma torch

There is a problem concerned with the symmetry of spatial distribution of spectral line intensity in the plasma torch. Figure 5 depicts the projected profile of the intensity distribution for the atomic line Mn(I) 403.08 nm after successful correction. The distribution is reasonably symmetrical. Figure 6, however, demonstrates that when lithium or barium is the interfering element, the corrected distributions are asymmetrical. The corresponding dependences of the excitation temperature and the degree of ionization are illustrated in Figs. 7 and 8, and the corrected results in Fig. 9. The correction fails in both cases. It should be pointed out that there are inflection points on the excitation temperature curves for atoms or ions in the presence of these elements.

Apparently, the plasma torch was supported asymmetrically about the coaxis of the discharging and cylinder electrodes, and an anomalous discharge to the cylinder electrode partly occurred. This lack of symmetry in the plasma torch causes the asymmetrical profile of the spectral intensity and the anomalous inflection on the excitation temperature curves. An error in the calculated temperature leads to a significant error in the total number of atoms and ions on calculating the exponential terms involved, which would be increased by the effect of lack of symmetry increasing an error from the

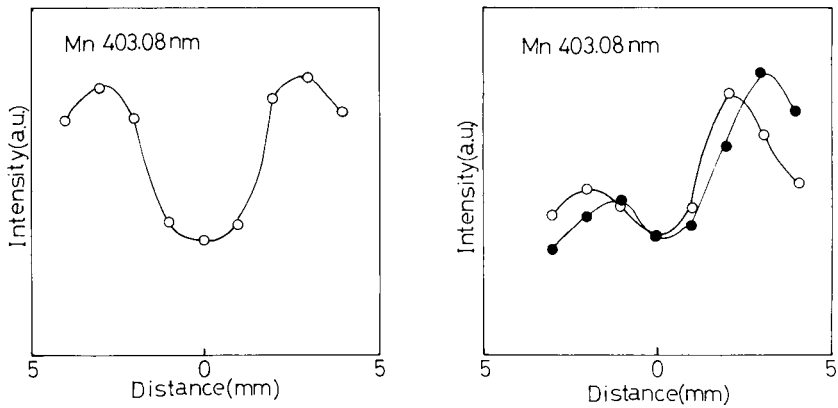

Fig. 5. Profile of the intensity distribution for 10 μmol Mn ml^{-1} + 5 μmol Sr ml^{-1}.

Fig. 6. Profile of the intensity distribution for 10 μmol Mn ml^{-1} + 5 μmol Li ml^{-1} (•) or 5 μmol Ba ml^{-1} (○).

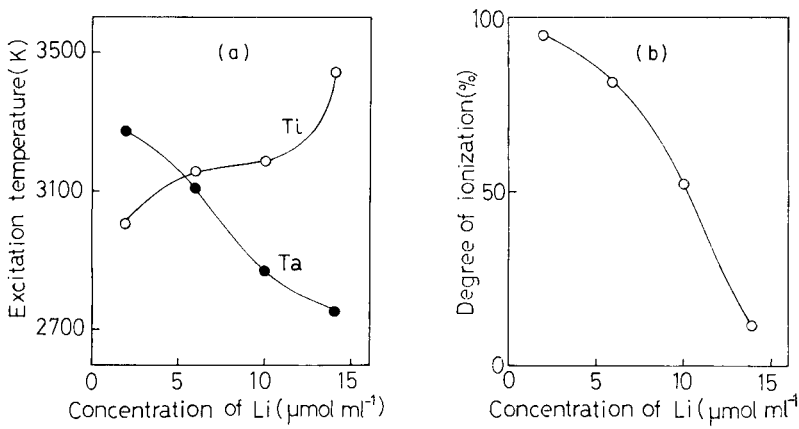

Fig. 7. Dependence of (a) the manganese excitation temperatures and (b) the degree of manganese ionization on lithium concentration.

net value determined by the Abel transformation. It was reported earlier that for a plasma such as an ICP in which the sample is introduced into a narrow region near the central axis of discharge, the Abel transformation is not necessarily required for measurement of the excitation temperature in the central region [13]. From this point of view, therefore, the present correction method is expected to be most promising if used with the ICP source.

However, the type of plasma supplied with low-power microwaves [14] and fitted with an electrothermal atomizer, seems to be a useful technique, for example, for microbiological samples, because its sample requirement is very small. This type of plasma also suffers from interferences connected with

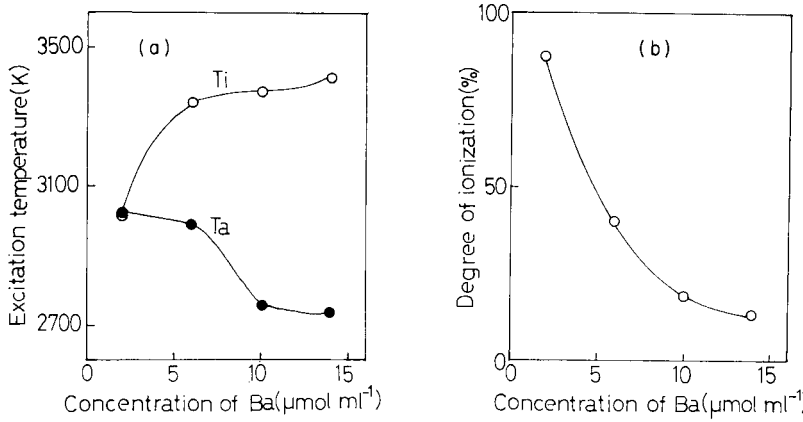

Fig. 8. Dependence of (a) the manganese excitation temperatures and (b) the degree of manganese ionization on barium concentration.

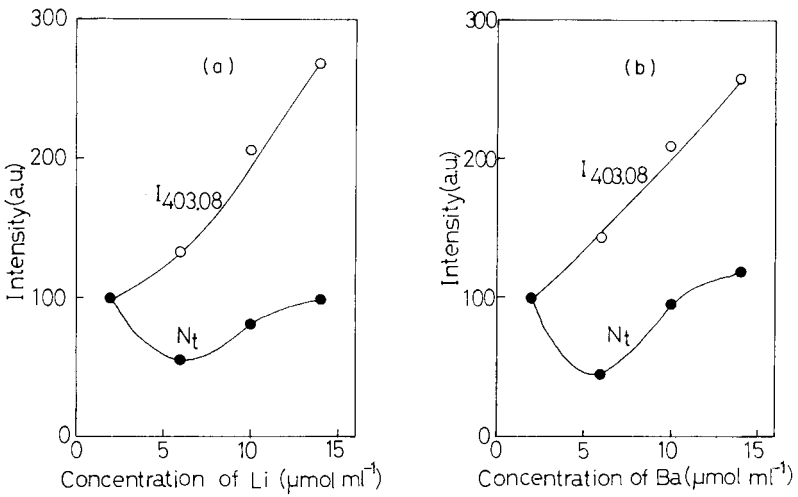

Fig. 9. Corrected and uncorrected responses for manganese in the presence of (a) lithium and (b) barium.

excitation and ionization processes [14]. This type of plasma is supported within the quartz capillary, so that it forms a relatively symmetrical intensity profile. If the system is evacuated, high temperatures for the atomic and ionic systems are established. Therefore, the lines utilized for correction are increased in intensity. This feature is expected to make the correction method versatile enough for the determination of other elements.

For on-line measurement of the intensity of the four lines, a rapid scanning monochromator coupled to a microcomputer is under development. This will be described at a later date.

REFERENCES

1 K. Kitagawa and T. Takeuchi, Anal. Chim. Acta, 60 (1972) 309.
2 K. Kitagawa and T. Takeuchi, Anal. Chim. Acta, 67 (1973) 453.
3 D. J. Kalnicky, R. N. Kniseley and V. A. Fassel, Spectrochim. Acta, Part B, 30 (1975) 511.
4 D. J. Kalnicky, R. N. Kniseley and V. A. Fassel, Appl. Spectrosc., 31 (1977) 137.
5 G. F. Larson, V. A. Fassel, R. H. Scott and R. N. Kniseley, Anal. Chem., 47 (1975) 238.
6 P. W. J. M. Boumans and F. J. de Boer, Spectrochim. Acta, Part B, 32 (1977) 356.
7 S. Greenfield, H. McD. McGeachin and P. B. Smith, Anal. Chim. Acta, 84 (1976) 67.
8 L. de Galan, R. Smith and J. D. Winefordner, Spectrochim. Acta, Part B, 23 (1968) 521.
9 C. H. Corliss and W. R. Bozman, NBS Monograph, 53 (1962).
10 S. Murayama, H. Matsumoto and M. Yamamoto, Spectrochim. Acta, Part B, 23 (1968) 513.
11 C. J. Cremers and R. C. Birkebak, Appl. Opt., 5 (1966) 1057.
12 T. Maruta, T. Takeuchi and M. Suzuki, Anal. Chim. Acta, 58 (1972) 452.
13 J. Jarosz, J. M. Mermet and J. P. Robin, Spectrochim. Acta, Part B, 31 (1976) 459.
14 H. Kawaguchi, I. Atsuya and B. L. Vallee, Anal. Chem., 49 (1977) 266.

Analytica Chimica Acta, 109 (1979) 251—258
© Elsevier Scientific Publishing Company, Amsterdam — Printed in The Netherlands

REDUCTION OF TIN AND GERMANIUM TO HYDRIDES FOR DETERMINATION BY INDUCTIVELY-COUPLED PLASMA ATOMIC EMISSION SPECTROMETRY

M. THOMPSON* and B. PAHLAVANPOUR

Applied Geochemistry Research Group, Department of Geology, Imperial College, London SW7 2BP (Gt. Britain)

(Received 10th January 1979)

SUMMARY

The effect of a range of acids on the reduction of tin and germanium to their hydrides in aqueous solutions by means of sodium tetrahydroborate(III) solution in a continuous flow system is investigated. Interference effects in hydrochloric acid and tartaric acid reaction media are tabulated. Tartaric acid decreases many interference effects. Detection limits for both elements are low (ca. 0.2 $\mu g\ l^{-1}$) and the linear calibration ranges span nearly four orders of magnitude.

Thompson et al. [1, 2] have described a method for the continuous reduction of arsenic, antimony, bismuth, selenium and tellurium in aqueous solutions to their hydrides by means of sodium tetrahydroborate(III). The volatile hydrides were carried into an argon-supported inductively-coupled plasma (ICP) for excitation of the elements, which were simultaneously determined by atomic emission spectrometry. Detection limits of about 1 $\mu g\ l^{-1}$ and good working ranges were obtained for each of the five elements. However, under the compromise conditions required for reduction of the five elements, tin and germanium could not be satisfactorily reduced, and so were investigated separately.

In this paper, conditions are reported under which tin and germanium can be reduced and determined simultaneously with good sensitivity in a number of aqueous reaction media; the interference effects found in two of them are also described. The ICP and a polychromator were used to determine the elements simultaneously, but the study of the reduction conditions and interference effects in solution are independent of the determination and can reasonably be compared to atomic absorption studies which have been carried out by other workers using sodium tetrahydroborate(III). However, the comparisons are not exact because of the widely differing experimental conditions employed in those studies.

Fernandez [3] reported the determination of As, Sb, Bi, Se, Te, Ge, and Sn after reduction with sodium tetrahydroborate(III). The hydrides were collected in a balloon reservoir and subsequently determined in an argon—

hydrogen—entrained air flame. Thompson and Thomerson [4] reduced the same elements plus lead and carried the hydrides into a heated silica tube for atomization. Smith [5] studied the interferences of a wide variety of elements, but did not report results for tin. Bedard and Kerbyson [6] reported the determination of these elements (except Pb and Ge) in pure copper after a separation procedure, and Fleming and Ide [7] studied the determination of all the elements (except germanium) in steel. Vijan and Chan [8] have used the method for the determination of tin in air particulate matter, with a continuous flow method for mixing the reagent and sample and a heated silica tube for atomization.

EXPERIMENTAL

Equipment

The equipment used was as previously reported [1]. A Radyne R50 cavity controlled oscillator with a maximum forward power of 8 kW was fitted with a plasma torch as described by Wendt and Fassel [9]. The Applied Research Laboratories 29000B quantometer used has lines for about 40 elements including tin and germanium at 284.0 and 303.9 nm, respectively. Light from the tail flame of the plasma was focused onto the slit of the spectrometer in such a way that the effective viewing height of the plasma could be varied.

The hydride generator consisted of a glass separation cell and a peristaltic pump [1]. The glass cell provided mixing of the sample solution and reducing agent, separation of the hydrides and hydrogen from the spent liquids, and mixing of the gaseous products with the argon carrier gas for transmission to the injector of the plasma torch. The Watson—Marlow Pump (type MRHE 200) used was fitted with tubing of narrow diameter (0.5 and 0.8 mm) to provide fast linear flow rates and hence fast sample uptake and low dead space.

Reagents

The germanium solution was prepared from GeO_2 by dissolution in a minimum amount of sodium hydroxide and dilution with 5 M hydrochloric acid. The tin solution was made by dissolving high-purity tin metal in 5 M hydrochloric acid. The acid concentration was maintained at 5 M in these solutions until the final dilution, as dilute acid solutions of these elements deteriorate rapidly. However, even very dilute solutions of tin in tartaric acid are stable for at least a week.

Sodium tetrahydroborate(III) solution was prepared from the powder (Aldrich Chemical Co.) by dissolution in 0.1 M sodium hydroxide. All other solutions were prepared from analytical-grade reagents and demineralized water. Laboratory-grade tartaric acid contains tin impurity, as do some batches of analytical-grade reagent. Most batches of analytical grade are free from troublesome levels of tin, but if necessary can be readily purified

by extraction with a solution of diethylammonium diethyldithiocarbamate in chloroform.

Operating parameters

The magnitude and stability of an analytical signal from an ICP depends on a number of factors: three argon flow rates (for the coolant, plasma support gas and injector flows), the power coupled to the plasma and the viewing height in the tail flame. When the hydride generator is used, the flow rates and compositions of the sample solution and the reducing solution also affect the analytical signal. The problem of adjusting the system to provide the required analytical characteristics has been discussed [1]. Briefly, the procedure followed consisted of fixing the carrier gas flow rate at an arbitrary maximum to give a ceiling to operating costs, and then finding an optimum by trial and error. The conditions found were similar to those previously described and are as follows: coolant flow rate, 15 l Ar min^{-1}; carrier gas flow rate, 0.8 l Ar min^{-1}; viewing height above load coil, 11 mm; forward power in plasma, 2.7 kW; concentration of reducing agent, 10.0 g l^{-1}; reducing agent flow rate, 4.5 ml min^{-1}; sample flow rate, 9.2 ml min^{-1}. The analytical characteristics were then studied as a function of the composition, especially the acid concentration, of the aqueous solution.

RESULTS AND DISCUSSION

Hydrochloric acid reaction medium

The relative intensities of the analytical signals for the two elements were studied in a reaction medium of hydrochloric acid with concentrations varying between 0.05 M and 5 M. The concentrations of tin and germanium were 0.1 mg l^{-1}. Both tin and germanium show a sharp maximum at about 0.1 M (Fig. 1), at which concentration the acid is neutralized by the reducing solution. The response for germanium increases slightly at higher concentrations of acid, but that of tin remains low. The behaviour of tin is similar to that reported by Fernandez [3] and other workers, but the germanium results differ, probably because of the continuous reduction system used here. Subsequent studies were carried out with 0.1 M hydrochloric acid. The

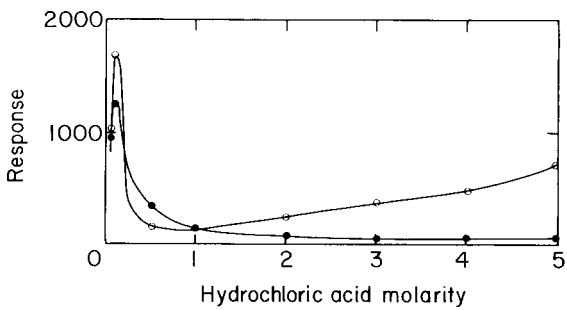

Fig. 1. The effect of hydrochloric acid concentration on the sensitivity of the reduction. (○) Germanium; (●) tin. Response in arbitrary units.

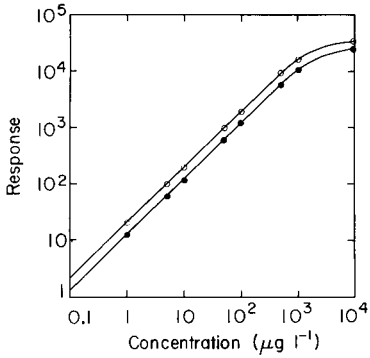

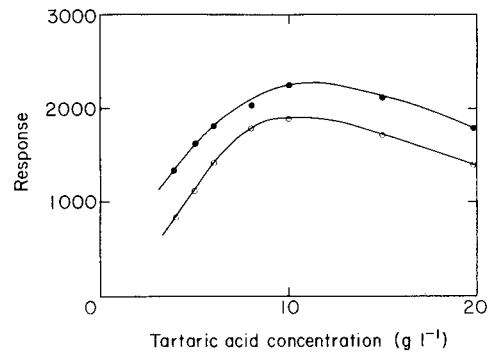

Fig. 2. Calibration curves for tin (•) and germanium (○) in 0.1 M hydrochloric acid. Response in arbitrary units.

Fig. 3. The effect of tartaric acid concentration on the sensitivity of the reduction for tin (•) and germanium (○). Response in arbitrary units.

TABLE 1

Performance characteristics of a.a.s. methods and the proposed method for determination of tin and germanium after reduction to hydrides by sodium tetrahydroborate(III) (Values in parentheses were obtained from calibration curves, not the texts.)

Method	Germanium		Tin	
	Detection limit ($\mu g\ l^{-1}$)	Upper limit of linearity ($\mu g\ l^{-1}$)	Detection limit ($\mu g\ l^{-1}$)	Upper limit of linearity ($\mu g\ l^{-1}$)
Fernandez [3]	10	(750)	0.2	(25)
Thompson and Thomerson [4]	500	—	0.5	(40)
Smith [5]	4.1	—	8.2	—
Bedard and Kerbyson [6]	—	—	10	(75)
Fleming and Ide [7]	—	—	40	(200)
Vijan and Chan [8]	—	—	0.1	40
This work (ICP)	0.3	500	0.2	500

calibration curves obtained are shown in Fig. 2. The graphs for both elements are linear up to 0.5 mg l^{-1}. The detection limits and linear ranges compare favourably with those reported by other workers using atomic absorption systems (Table 1).

Possible interference effects fall into two classes, those caused by mutual compound formation by the reduced elements in the atomization stage, and those caused by changes in the efficiency of hydride formation at the reduction stage. In atomic absorption work the former are significant, but could not be detected with the much hotter plasma excitation source. Other workers, using atomic absorption detection, have shown that considerable interference of the latter type could also be expected, especially from tran-

sition metal ions [5, 7]. This source of interference was investigated by the following method, which used four solutions for each concentration of each ion studied. The four solutions were: (i) 0.1 M hydrochloric acid; (ii) as (i) plus the analytes at 100 $\mu g\ l^{-1}$; (iii) as (i) plus the potential interferent at a suitable level; (iv) as (ii) plus the interferent at a suitable level. If there is no interference, the differences between the signals produced by (i) and (ii) and between (iii) and (iv) should be identical. A positive difference between (i) and (iii) would probably indicate analyte impurity in the interferent, but this was not detected here. Where severe interference was found, the experiment was repeated with a lower concentration of interferent. The metal solutions were prepared from reagent-grade chemicals, usually the metal chloride. Solutions of silver and lead contained an equivalent amount of nitrate ion, which caused no interference at the concentrations used. The results obtained for tin and germanium (Table 2) are very similar, except when zinc or cadmium is present. Sodium, potassium, calcium and magnesium have no effect at high concentration, nor has manganese(II), chromium(III), titanium(IV), bromide or iodide. Most transition metals produce depressive effects, those of copper, cobalt and nickel (and probably iron) being especially severe at concentrations as low as 1 mg l^{-1}. These results are consistent with the findings of Smith [5] and Fleming and Ide [7] (for tin only), but are at variance with those of Vijan and Chan [8] (for tin only). The interfering effect of aluminium is surprising and may be due to occlusion of the analytes in the hydrous oxide which forms. The interferences are considerable; clearly this system could not be used for the determination of tin and germanium unless the analytes could be freed from the effects of most of the transition metals and aluminium before the reduction stage. In view of the difficulties encountered with the hydrochloric acid reaction medium, viz., the very narrow acidity range for peak sensitivity and the serious interferences, other media were studied.

Other acids

The experiment to determine the reduction efficiency was repeated with a number of other acids. The results for oxalic acid, hydrobromic acid, perchloric acid and sulphuric acid were very similar to those found for hydrochloric acid. In phosphoric acid, the germanium signal was enhanced somewhat, although the tin signal remained low throughout. In nitric acid no consistent reduction of the elements could be achieved. In chloracetic acid the acidity—response curve was reasonably flat over the range 1—4 M but the response was low compared with the best obtained with hydrochloric acid. With tartaric acid, the response for tin was slightly enhanced and had a broad maximum at a concentration of about 1% acid (Fig. 3). Germanium also gave a broad maximum over this range, and the signal was only slightly diminished (Fig. 3) compared to that in hydrochloric acid. As tartaric acid proved to be suitable in this respect as a reaction medium, further studies were made with this acid (10 $g\ l^{-1}$).

TABLE 2

Effect of diverse ions on recovery of tin and germanium (0.1 mg l^{-1}) in 0.1 M HCl and tartaric acid (10 g l^{-1}) solutions

Other ion	Concn. (mg l^{-1})	Recovery (% change in response)			
		Ge		Sn	
		HCl	Tartaric acid	HCl	Tartaric acid
Na(I)	10,000	0	0	0	0
K(I)	10,000	0	0	0	0
Mg(II)	10,000	0	0	0	0
Ca(II)	10,000	0	0	0	0
Al(III)	10,000	−77	−3	−18	−1
	1,000	−39	—	−2	—
	100	−3	—	0	—
Fe(II)	10,000	−99	—	−91	—
	1,000	−99	—	−90	—
	100	−93	—	−79	—
	10	−76	—	−63	—
Fe(III)	10,000	−96	−12	−93	−10
	1,000	−92	—	−90	—
	100	−88	—	−84	—
	10	−64	—	−63	—
Mn(II)	10,000	0	0	0	0
V(V)	1,000	−10	0	−44	−10
	100	−6	—	−10	—
Ni(II)	1,000	−99	−82	−98	−80
	100	−99	—	−84	—
	10	−90	—	−70	—
	1	−80	—	−65	—
Co(II)	1,000	−99	−80	−99	−80
	100	−98	—	−94	—
	10	−82	—	−87	—
	1	−55	—	−55	—
Zn (II)	1,000	−99	−60	0	0
	100	−70	—	0	—
	10	−35	—	0	—
Cu(II)	1,000	−99	−75	−97	−72
	100	−97	—	−95	—
	10	−76	—	−83	—
	1	−34	—	−40	—
Cr(III)	1,000	0	− 1	0	0
Cr(VI)	1,000	−50	—	−40	—
	100	0	—	0	—
Ti(IV)	1,000	0	0	0	0
Cd(II)	1,000	−60	−12	−40	−10
	100	−40	—	−21	—
	10	−25	—	−5	—
Ag(I)	1,000	−26	− 6	−19	−2
	100	− 7	—	−3	—

TABLE 2 (cont.)

Other ion	Concn. (mg l^{-1})	Recovery (%)			
		Ge		Sn	
		HCl	Tartaric acid	HCl	Tartaric acid
Mo(VI)	1,000	−80	−12	−60	−8
	100	−26	—	−30	—
	10	0	—	−6	—
Pb(II)	1,000	−26	−5	−24	0
	100	−1	—	0	—
Hg(II)	1,000	+7	0	0	0
F^-	10,000	−82	−80	−68	−50
Br^-	10,000	0	0	0	0
I^-	10,000	0	0	0	0

The detection limits and the upper limits of linearity were the same as found for the hydrochloric acid medium. Interference effects were studied as described above, and the results are shown for comparison in Table 2. It can be seen that the interference effects of most transition metal ions and of aluminium are significantly decreased when compared with the hydrochloric acid medium. Consequently, the tartaric acid medium offers more analytical scope. This is consistent with the work of Fleming and Ide [7], who used a tartaric acid medium when determining tin in steel by reduction to the hydride, to prevent interference from iron. Interference from the other volatile hydride-forming elements was found to be insignificant in the tartaric acid medium, as was mutual interference between germanium and tin. For example, the responses from 0.1 mg l^{-1} each of germanium and tin were unaffected by 100-fold amounts of the other element. The effects of very large amounts of the volatile hydride-forming elements were not studied, because of problems of contaminating the equipment.

Conclusion

It has been confirmed that tin and germanium can be reduced to the hydrides in hydrochloric acid and tartaric acid media by means of sodium tetrahydroborate(III), and, in combination with the inductively-coupled plasma, determined with high sensitivity. There is a wide range of interferences but their effects are considerably decreased by addition of tartaric acid. The elements are best reduced when the final solution produced by mixing the analyte solution with the reducing solution is almost neutral. Higher concentrations of either hydrochloric acid or tartaric acid in the sample solution could thus be accommodated by appropriately increasing the alkali content of the tetrahydroborate(III) solution. In such a case, the increased tartrate content would undoubtedly further improve the masking effect observed at 10 g l^{-1}.

There is a substantial improvement in detection limits or linear calibration ranges compared with atomic absorption spectrometry. Successful application of this work to trace analysis awaits the investigation of methods for attacking samples to obtain tin and germanium simultaneously in solution with the bulk of transition metals either removed or eliminated by masking.

REFERENCES

1 M. Thompson, B. Pahlavanpour, S. J. Walton and G. F. Kirkbright, Analyst, 103 (1978) 568.
2 M. Thompson, B. Pahlavanpour, S. J. Walton and G. F. Kirkbright, Analyst, 103 (1978) 705.
3 F. J. Fernandez, At. Absorpt. Newsl., 12 (1973) 93.
4 K. C. Thompson and D. R. Thomerson, Analyst, 99 (1974) 595.
5 A. E. Smith, Analyst, 100 (1975) 300.
6 M. Bedard and J. D. Kerbyson, Can. J. Spectrosc., 21 (1976) 64.
7 H. D. Fleming and R. G. Ide, Anal. Chim. Acta, 83 (1976) 67.
8 P. N. Vijan and C. Y. Chan, Anal. Chem., 48 (1976) 1788.
9 R. H. Wendt and V. A. Fassel, Anal. Chem., 37 (1965) 920.

Analytica Chimica Acta, 109 (1979) 259—278
© Elsevier Scientific Publishing Company, Amsterdam — Printed in The Netherlands

COMPARISON OF TIME CONSTANTS FOR LIQUID ION-EXCHANGE MEMBRANE ELECTRODE RESPONSES DETERMINED BY AN IMPEDANCE METHOD AND AN ACTIVITY STEP METHOD

F. S. STOVER, T. R. BRUMLEVE** and R. P. BUCK*

William R. Kenan Laboratories of Chemistry, University of North Carolina, Chapel Hill, NC 27514 (U.S.A.)

(Received 12th February 1979)

SUMMARY

Linear current-step perturbations and resulting membrane potential responses of liquid ion-exchange membranes have been analyzed and the numerous possible time constants examined and catalogued. Ideal activity steps at a single membrane interface produce potential—time responses similar to those resulting from current steps. The common time constants have nearly identical values. However, fewer time constants are observed for activity steps than for current steps. Slow processes at the active interface dominate and obscure short time processes. For liquid ion-exchange membranes it is concluded that an activity step on one side is not identical to a current step because processes involving bulk membrane transport and the far side of the membrane are not involved to the same extent for the two excitation modes. Two analog circuit models (one active, one passive) are proposed for the potential—time response to an activity step. Systems containing neutral carriers are not considered.

Reports of ion-selective electrode responses frequently include time dependences (measured cell or membrane potentials vs. time) after "step" activity changes are made on one side [1—9]. If an activity step were, indeed, one with hypothetical infinite slope at the leading edge, then the resulting $\Delta\phi$ vs. t response would be a measure only of electrode properties. However, the "step" is never an ideal, abrupt activity change on the outer test-solution side of a membrane-type electrode. Except for a few studies based on stopped flow and related techniques [10—13], a dip method is used; the measurement is complicated by convolution of a further time constant into the response. This additional time constant reflects establishment of the new bulk concentration at an electrode surface by diffusion within the external static Nernst layer of bathing electrolyte or dissolving membrane species. In our experience, this latter time constant is often longer than the electrical relaxation time or the kinetic relaxation time for slow ion transfers at an electrode. This activity-step time constant can be confused with properties of the electrode itself. In

**Present address: Department of Chemistry, Colorado State University, Fort Collins, CO 80523, U.S.A.

this paper, pure response to ideal, rapid activity steps at one interface are compared with responses for current steps. Slow attainment of external stepped activity by diffusion relaxation of concentration polarization is not included in the simulation.

It is common experience that an ion-selective electrode exposed suddenly to a fresh solution will change its initial measured potential to a new one through a series of stages [5, 7, 9]. These stages are not necessarily obvious or resolved steps in time. The transient is often a featureless monotonic with a decreasing slope. However, analysis of the $\Delta\phi$ vs. t transient shows that there are generally several time constants, even though there are no arrests between the segments. The processes and their associated time constants can, for ideal systems, be identified, itemized and ranked from impedance theory [14—16]. Yet, the complete detailed analysis and derivation of exact equations for some of the time constants are not available. The reason is that the theory of mass transport, concentration, field and potential profiles for single activity steps on one side of a membrane is not completely developed. The non-linear Nernst—Planck—Poisson system has been partially [17, 18] but not generally solved, even for parallel-faced, homogeneous, conducting phases with charge carriers of constant mobilities. In addition, real systems are not ideal, and many factors such as heterogeneities [19], microcracks [20, 21], high-resistance surface layers (in or on supports) [22—25], time-dependent resistances of supports (e.g., because of hydration) [26, 27], slow extraction or dissolving of membranes and crystals into test solution [28, 29], and other unrecognized processes, conspire to complicate analysis further.

Our opinions concerning time constants and their origins are colored by the presumed corresponding time constants for the same systems when perturbed by a.c. voltages, i.e. by time constants deduced from impedance measurements. Identification of processes and analysis of time constants and their ranking for activity steps follow from the equivalent impedance analysis of electrochemical cells. The latter is the more completely developed field, and many results are now available for liquid membranes [17, 18, 26—29], solid membranes [30, 31], single crystals [32—34] and electrolyte/metal interface systems [35], based on both theoretical and experimental impedance results. Electrochemical cells can be represented as passive networks when the intrinsic e.m.f. is biased out so that the current—voltage curve of the system passes through zero at zero applied voltage [35]. Current—voltage—time responses of most electrochemical cells can be derived from linear partial differential equations, subject to boundary conditions, and probable system functions (or impedance—frequency spectrum functions) may be derived. These functions often show complicated, irrational dependences on frequency, but in most cases, electrochemical cells can be represented as passive networks involving combinations of resistance and capacitance components including transmission lines among the circuit elements [36, 37].

Testing of theory and establishment of numerical values of an equivalent, analog, passive network and its components follow from experimental im-

pedance measurements and determination of the impedance—frequency spectrum. The quantities are determined by analysis of transient responses of electrochemical cells. The process can be conveniently accomplished for linear perturbations by use of a.c. impedance, pulsed and stepped current or voltage methods. The choice of experiments is determined by experimental preference because $\Delta\phi$ vs. t at constant I, or I vs. t at constant $\Delta\phi$ are simply related to each other and to the a.c. impedance function through the relationship

$$\bar{Z}(j\omega) = \bar{\Delta}\phi(j\omega)/\bar{I}(j\omega) \tag{1}$$

(For definition of symbols, see Table 1.)

The construction of passive network equivalent (analog) circuits can be achieved by any of the methods. In electrical engineering the construction is not unique, but preferred circuits often occur in electrochemistry because chemical sources and locations of resistances and capacitances are recognized from properties of homogeneous bulk electrolytes and interfaces, respectively.

Resulting characteristic system functions, the impedance functions $Z(j\omega)$, contain time constants which appear experimentally in $\Delta\phi$ vs. t plots at constant I or, in a more readily apparent way, in impedance plane plots. Time constants, when widely spaced, give rise to responses to constant I in the form [7, 38]:

$$\Delta\phi = \sum_i k_i[1 - \exp(-t/\tau_i)] + \Delta\phi^0 \tag{2}$$

When a finite transmission line is involved, as in finite diffusion processes of potential-determining ions within liquid membrane electrodes and within external Nernst layers, a series of closely-spaced time constants leads to an apparent $t^{-1/2}$ dependence of $\Delta\phi$ on t over a range of short times, but these appear as a single time constant

$$\tau_w = M^2\tau_\infty/2.53 \simeq d^2/2D_{salt} \quad \text{for } z_+ = z_- \,,\ u_+ = u_- \tag{3}$$

at longer times approaching d.c. For idealized, homogeneous, ion-transporting systems and many electronic-conducting systems, these time constants can be computed from first principles, in terms of system parameters: conductivities, space charge distributions and concentrations of charge carriers [32].

Equation (2) is a monotonic function which can show arrests or general featureless behavior similar to experimental results for activity steps on one side of a membrane in an electrochemical cell. The identifiable time constants are sufficiently similar to the time constants expected for equivalent current or voltage perturbations that it seems important to make theoretical comparisons between the origins and magnitudes of the time constants found by the two different experimental methods. This paper addresses the following questions. Which processes are common to the two excitation methods? And in which membrane electrodes would the experimental response time constants from activity step experiments agree with time constants determined from current steps or other related a.c. perturbation methods?

TABLE 1

Symbols and their definitions

a_+, a_-	Ionic activities in bathing solutions
A	Geometric area
$c_i, \bar{c}_i$	Concentration inside and outside membrane
$c_{oi}, \bar{c}_{oi}$	Concentration inside and outside membrane at "o" side
$c_o(t)$	Concentration inside membrane surface
$\bar{c}_o$	Step concentration outside membrane at the surface
c_b	Interior or bulk membrane species concentration
c_+, c_-	Ionic concentrations
C	Capacitance
C_g	Geometric capacitance
$C_{o,b}$	Series combination of Gouy—Chapman capacitances inside membrane
$C_{o,r}$	Diffusional "pseudo" capacitance at low frequencies
d	Membrane thickness
D, D_i, D_{salt}	Diffusion coefficients of species and salt
$E(x,t)$	Local electrical field varying in time
$f_i, f_i', f_i(x,t)$	Ionic fluxes
F	Faraday
i^0	Ionic exchange current density
I	Current density
$\bar{I}(j\omega)$	Fourier transform of current density
k_0^+, k_0^-	Rate constants for ion transfer at a surface (cm s^{-1}) at the standard potential
k_i	Coefficients in the empirical step-activity response equation
k_{fi}, k_{bi}	Rate constants for forward and backward transfer of ions at a surface in the space charge region
K_{eq}	Single ion partition coefficient at the surface in the space charge region
k_b	Rate constant for slow ion transfer in the model eqn. (20), related to k_{fi}
L_D	Debye thickness
M	Number of Debye thicknesses in one half of a membrane
p	Laplace transform parameter equal to $j\omega$
R	Resistance
R	Gas constant
R_∞	High-frequency resistance
R_θ	Slow ion transfer, or "activation" resistance
R_0	D.c. resistance of a membrane
t	Time
T	Absolute temperature
u_+, u_-	Ionic mobilities in a membrane (mol cm^2 V^{-1} A^{-1} s^{-2} = D/RT)
z, z_+, z_-	Ionic charges with sign
$\bar{Z}(j\omega)$	Impedance function
ϵ	Dielectric constant, conventional unrationalized
$\Delta\phi^0$	Standard or reference membrane potential
$\Delta\phi$	Membrane potential taken as right minus left
$\Delta\bar{\phi}(j\omega)$	Fourier transform of a membrane potential
τ_∞	High-frequency time constant
τ_W	Equivalent low-frequency "Warburg" time constant
τ_k	Kinetic time constant for interfacial transfers
$\tau_1, \tau_2 \ldots \tau_i$	Model time constants
ω	$2\pi \times$ frequency (in Hz)

The results reported here make use of digital simulation of the Nernst—Planck—Poisson system of equations that describe both faradaic and non-faradaic current flow within the membrane and in the external double layer. The method does not compute external bathing electrolyte concentration polarization and consequently does not compute long-time diffusion time constants in the external Nernst layer. The same set of equations is used regardless of the system perturbation but ideal activity steps and current steps are emphasized. Numerical magnitudes of the perturbations can be adjusted to give equivalent results. For example, if the activity step of a typical uni-univalent salt is two-fold, the final steady state or equilibrium membrane potential will change by 17.7 mV. Similarly, currents can be determined and used in the simulation which will also lead to a 17.7-mV change in membrane potential. One can tailor activity steps (on one or both sides of a membrane) and currents so that the resulting potential differences are identical and much less than 25.6 mV, or more generally $25.6/z$ mV for permeable ions of absolute charge z. Because the factor $\Delta\phi F/\mathbf{R}T$ occurs in the exponential functions in the time-dependent solutions of voltage-step problems, this factor must be less than unity for linearization of any exponentials in the solution of voltage-step, current-step and a.c.-perturbation problems. Consequently, there is a widely-held belief, supported by reduction of transport equations to dimensionless form, that perturbations of voltage (and therefore the magnitude of activity steps) should be small and such that $zF\Delta\phi/\mathbf{R}T \ll 1$ or $\Delta\phi \ll \mathbf{R}T/zF = 25.6/z$ mV at 25°C.

TIME CONSTANTS FROM IMPEDANCE THEORIES

Theories and experiments on homogeneous membrane electrode systems suggest that at least four widely disparate time constants may be observed; however, this statement does not imply that voltage-time responses after a bathing solution activity step or impulse can be resolved into four exponentials [32]. Not all processes necessarily occur, and there may be an overlapping of processes with similar or identical time constants. The following results of theory were derived for perturbations of equilibrium, zero-current membrane conditions. It is probable that steady-state, zero-current conditions (e.g. permselective membranes bathed with non-identical salt electrolytes with equal and opposite permeable ion fluxes) will obey similar laws when linear perturbations are used. However, in the latter bi-ionic cases, especially for liquid membranes, overshoots of potential and inductive behavior are possible. These effects have not been included here.

by dielectric relaxation only. It is traceable to solvent dipoles and reorganization of dissolved species in liquids, and to ionic inertia in solids. It is not expected to be important for ion-selective electrodes. However, the next longer time constant is caused by charging of the external space—charge surface regions (for electrolyte-bathed membranes) coupled to the high-frequency or a.c. bulk-electrode resistance. More generally, it is charging of the dielectric

material, coupled to a.c. resistance. The capacitance per unit area is geometric and is given by $C_g = \epsilon/4\pi d$. The high-frequency resistance multiplied by area for an electroneutral, two-ion system of arbitrary charges and mobilities is

$$R_\infty = d/F^2(z_+^2 u_+ C_+ + z_-^2 u_- C_-) \tag{4}$$

For solid membranes, typically involving only one charge carrier, there is only one term in the denominator. The time constant τ_∞ corresponds to the highest-frequency processes determined by transport of charged species in a medium of constant dielectric and constant resistivity. It is the product $R_\infty C_g$ and corresponds to no change in the internal ionic-concentration profiles. It is the usual high-frequency space-charge relaxation time found in conducting systems and it is independent of membrane thickness. For silver bromide [33] and chloride [34], it is about 50 μs and 0.3 ms, respectively, at 25°C, while for glass pH electrode membranes, studied by Buck and Sandifer [22] 100—200 ms is typical for tight, low-error pH glasses.

The third time constant that may be observed is an intermediate value which arises from coupling of slow surface rates and the relaxed, doubly diffuse (or compact) capacitance of each interface. When surface rate processes are rapid and reversible, this time constant does not appear. The effective resistivity at the equilibrium or steady-state potential corresponding to activities $\bar{a}_+$, a_+, for slow surface rate control is

$$R_\theta = 2RT/zFi^0 = 2RT/z^2F^2k_0^+(\bar{a}_+a_+)^{1/2} \tag{5}$$

for single cation transport, and

$$R_\theta = 2RT/F^2[z_+^2 k_0^+(\bar{a}_+a_+)^{1/2} + z_-^2 k_0^-(\bar{a}_-a_-)^{1/2}] \tag{6a}$$

when ions of both signs transfer slowly with rate constants k_0^+ and k_0^- at unit activities in symmetric bathing solutions. The factor two occurs because two interfaces are passing current. For asymmetric bathing electrolytes, individual surface rate processes may predominate. Far from equilibrium, a single resistance is defined by

$$R_\theta = RT/z^2F^2k_{fi}\bar{C}_o \tag{6b}$$

For symmetric bathing electrolytes, the appropriate relaxed capacitance $C_{o,b}$ (ignoring the compact value) is the series combination of the Gouy—Chapman capacitances ($C'_{o,b}$), and is related to the geometric capacitance C_g by $C_{o,b} = MC_g$, where $M = d/2L_D$ is the number of Debye lengths (L_D) in half of the membrane. Of course, the single interfacial capacitance $C'_{o,b} = 2MC_g$. The theory for blocked electrodes contains the capacitance $C_{o,b} - C_g$ in series with the membrane resistance. For slow surface rates and thick membranes such that $C_{o,b} \gg C_g$, the time constant is $R_\theta C_{o,b}$. However, it should be noted that in the linearized theory, $C_{o,b}$ is independent of interfacial potential. Actually, this cannot be true over a wide range of bathing solution concentrations and so $C_{o,b}$ is expected to increase at all potentials away from the potential of zero charge (p.z.c.) and to reach limiting values given by the capacitance of the compact layers.

Slow surface rates behave as apparent resistances and can have a significant effect only if the value exceeds the bulk resistance. However, surface resistances can be identified as long as they are a measurable fraction, say 10% or more, of the bulk resistance. The slow time response of glass electrodes has been attributed to this source because the time constant can be shortened by surface etching [22]. However, it is possible and even likely that the apparent surface resistance in this instance (and possibly in OH^- interference at LaF_3 electrodes) is associated with mass transport through the surface film of protonated and hydrolyzed glass. At 25°C, time constants as great as 30 s for E-2 glass and 7 s for GP glass were observed [22]. While these measurements were obtained by voltage perturbations across electrodes in homogeneous solutions, values of the same order of magnitude were obtained by activity pulses [5]. Markovic and Osburn [5] also cite many other references to long time-constant values in the 1—10-s range for glass electrodes. These time constants for electrodes with glass surface films are longer than expected for relaxation of concentration polarization in the electrolyte at electrode surfaces without surface films.

An apparent surface rate semicircle and time constant can also be generated in liquid ion-exchange membrane systems. A recent study [26, 27] makes use of an Aliquat nitrate—nitrobenzene, free-standing liquid between platinum electrodes, and between thin films of various stable, wettable support materials, bathed in aqueous potassium nitrate electrolytes. Depending on the thickness of the support and its wettability by water or by nitrobenzene, one or two geometric semicircles occur in the impedance plane, corresponding to transport through bulk liquid phase and through liquid phase contained in support voids. Some membrane supports are inert structures as demonstrated by identical transport enthalpies in bulk and in supports. Other membranes such as cellulose acetate tend to partially dissolve, and impede ion transport.

As the free standing volume is diminished, so that all of the liquid is truly supported in the voids of the polymer, the two semicircles in the impedance plane collapse into a single semicircle. Surprisingly, PVC—acrylonitrile copolymer, 0.1 mm thick containing Aliquat nitrate in nitrobenzene, still shows two semicircles. The low-frequency semicircle is independent of membrane thickness and must, therefore, be a true surface kinetic semicircle. In this case, the analysis gives a heterogeneous rate constant for nitrate of 2.5×10^{-5} cm s^{-1}. A further unusual feature of this system is an increase in the apparent rate constant as water permeates the support. One interpretation is that water penetration gives a "rougher" surface so that the actual exchange area between water and nitrobenzene is larger.

The longest membrane-controlled time constant arises from concentration polarization of charge carriers within a membrane electrode and is observed when a current passes the membrane, and when a change occurs in compensating fluxes of different ions. The latter situation corresponds to bi-ionic cases of two or more permeable ions at different concentrations on the two sides. This is the Warburg finite-diffusion process, and the appropriate resis-

tance is the d.c. value, which is significantly greater than the a.c. value because only permeable ions carry current under d.c. conditions. The d.c. capacitances are large and arise from charge separations caused by transport. The Warburg behavior requires at least two charge carriers, both of which contribute to high-frequency current, but one ion is partially or completely blocked under d.c. conditions. Thus, Warburg behavior is not expected for fixed-site membranes through which ions of only one sign are permeable and transported by a single mechanism. It is possible that long membrane-controlled time constants for single ion conductors may appear when the generation rate of charge carriers (from lattice ions) is slow, or when adsorption/reaction is slow [39].

In the low-frequency or finite Warburg region, the membrane-controlled time constant is that required to adjust concentration profiles throughout the membrane. If only cations are permeable, the d.c. resistivity R_0 is

$$R_0 = d/F^2\, z_+^2\, u_+\, C_+ = [1 + (u_- |z_-|/u_+ z_+)]\, R_\infty \tag{7}$$

for ions of charge z_+ and z_-. The d.c. capacitance is approximately

$$C_{o,r} = \frac{dF^2}{2RT}\,\frac{[z_+^2\, C_+ + z_-^2\, C_-]}{[1 + u_- |z_-|/u_+ z_+]} \approx M^2 C_g\, [1/(1 + u_- |z_-|/u_+ z_+)] \tag{8}$$

and the time constant (defined as the reciprocal frequency at maximum imaginary impedance) is given by:

$$\tau_W = [1/2.53]\, [z_+ z_-/(z_+ + |z_-|)^2]\, [(u_+ + u_-)^2/u_+ u_-]\, C_{o,r} R_o \tag{9}$$

Diffusion and migration through a whole ideal liquid ion exchanger to reach a steady-state concentration and potential profiles have been discussed before [15, 40]. The interior diffusion potential is not an exact derivative. The total membrane potential cannot reach a steady-state value until both the interfacial potential difference, determined by the ion-exchange rate of charging as discussed above, and the diffusion component reach steady values. There are several corollaries of this theory. (1) Ideal, rapid ion-exchange, homogeneous, fixed-site membranes permeable to, and bathed in ions of a single charge show no long-time, interior diffusion—migration time constant; (2) ideal, rapid ion-exchange, homogeneous, fixed-site membranes bathed in permeable ions of different charge (i.e. Ca^{2+} and Na^+) show a long-time diffusion component and time constant, while complex formation has no further complicating effect; (3) liquid (mobile site), rapid ion exchangers and related neutral-carrier membranes show long time constants from interior diffusion and migration, the time constant depending on ion charge and on complex formation.

A further application of this theory for long, membrane-controlled diffusion-migration time constants is to inhomogeneous membranes. Particularly, liquid and solid membranes covered with site-free or nearly site-free films of adsorbed layers of foreign material (or decomposition products) are worth considering. At the limit of site-free, pure diffusion barriers, on the outside of ion-exchange

membranes, the $t^{-1/2}$ Warburg transport time constant can appear. The reason is well known in the context of external bathing electrolyte transport, viz., the need to bring bathing electrolyte to uniform activity at an electrode surface so that the surface ion-exchange process becomes equilibrated with bulk activities. Because interfacial potentials depend on establishment of ion-exchange equilibrium, they reflect only the activities of electrolytes immediately adjacent to both sides of an interface. Thus, if an ion exchanger is covered with a site-free film, a long time may be required for a bulk bathing activity step or current step to be reflected in a corresponding activity change at the film—ion-exchanger interface [23, 41, 42].

However, an ion-exchange membrane may be covered with a film which has high resistance and high site density and may behave as if it had a single RC time constant. The difference between a surface film causing an apparent surface resistance, (RC time constant) and one which is diffusive ($t^{-1/2}$, transmission line) is a matter of the size of the time constant $d^2/2D$. If the film is resistive, D is virtually zero because co-ions are excluded. A diffusional time constant would not be expected. Furthermore, both kinds of films may be present. For example, glasses with hydrolyzed films (low site-content) can be in series with a high resistance layer at the intact glass surface. These systems show mainly the surface-resistance time constant. In contrast, liquid membranes with site-free surface layers are likely to be more nearly diffusional because ions of both signs may penetrate.

Presumably, many situations can arise when several layers or regions are present. Of course, for film time-constants to appear in impedance studies, the films must be sufficiently resistive that the time constants are greater than, or at least comparable to, the bulk membrane transport time constants.

SIMULATION COMPARISON OF TIME CONSTANTS FROM ACTIVITY STEPS AND FROM CURRENT STEPS (IMPEDANCES)

The recent development of a numerical method by Brumleve and Buck [17] has significantly expanded the possibilities of treating problems involving both space charge and transport in electroneutral regions of membranes. This method is an implicit finite-difference simulation for the solution of the Nernst—Planck—Poisson equation system. This extremely efficient and general procedure was applied to such cases as charge steps at a blocked interface, and impedance—frequency responses of membranes under concentration polarization, with surface rates, in systems containing up to three ions.

The availability of this new powerful technique for studying various membrane processes has led to its use in investigating total potential—time responses of mobile-site ion-exchange membranes to bathing solution activity variations of a single salt. In this simulation section, three problems are discussed: (1) the differences between time responses to activity perturbations and time reponses to current (or potential) perturbations; (2) the effect of surface kinetics on these responses; and (3) the changes in time responses induced by using

non-linear activity perturbations, such as those commonly encountered in ion-selective electrode dip experiments.

Simulation model

Details of the simulation algorithm have been given [17]. The three basic equations solved are the dilute solution form of the Nernst—Planck equation,

$$f_i(x,t) = -D_i[\partial c_i(x,t)/\partial x - z_i c_i(x,t)(F/RT)\, E(x,t)] \tag{10}$$

the continuity equation,

$$\partial c_i(x,t)/\partial t = -\partial f_i(x,t)/\partial x \tag{11}$$

and the displacement current equation (equivalent to Poisson's equation),

$$I = F\sum z_i f_i(x,t) + (\epsilon/4\pi)(\partial E(x,t)/\partial t) \tag{12}$$

where, for the ith species, f_i is the flux, c_i is the concentration, D_i is the diffusion coefficient, and z_i is the valence; E is the electric field and ϵ is the unrationalized dielectric permittivity.

The total membrane potential, $\Delta\phi(t)$, is computed by integrating the electric field across the membrane thickness, d.

$$\Delta\phi(t) = -\int_0^d E(x,t)\, dx \tag{13}$$

The kinetic boundary conditions related the interfacial fluxes to heterogeneous rate constants and interfacial concentrations. For permeable ions

$$f_i'(t) = \pm k_{fi}\, \bar{c}_{oi}(t) \mp k_{bi}\, c_{oi}(t) \tag{14}$$

where f_i' is the flux through the interface, $\bar{c}_{oi}$ is the bathing solution surface concentration, c_{oi} is the membrane surface concentration, and k_{fi} and k_{bi} are the forward and backward heterogeneous rate constants. The sign of the terms on the right of eqn. (14) is determined by whether the flux is at the left or right interface. Single ion extraction coefficients at equilibrium are defined by $K_{eq} = k_{fi}/k_{bi} = c_{oi}/\bar{c}_{oi}$.

Equations (10)—(14) are converted to a set of dimensionless equations through the appropriate variable transformations (see the Appendix and reference [17]) and written in finite difference form. The Newton—Raphson method is then employed to solve this system for concentrations and fields as functions of distance and time. Scaling of both the space and time discretization grids is used to achieve accurate and efficient characterization of the concentration, field profiles and time constants. In this method, diffusion of ions in the external bathing solution is not considered. Activity steps at a membrane surface are taken to have occurred at $t = 0$.

RESULTS

The system under study is a permselective membrane containing totally

blocked, mobile, negative sites. Positive counter-ions are permeable and may be rate-limited at the interfaces. The dimensionalizing formulae are given in the Appendix. Numerical values of reduced constants are given to achieve the following ends: the membrane parameters are given values such that M, the number of Debye lengths in half the membrane, is 10^5; this results in well-separated time constants for the geometrical and diffusional processes; the reduced geometric capacitance has the value 5×10^{-6}, and the reduced high-frequency resistance R_∞ has the value 10^{-6}, while R_0 (d.c.) is 2×10^{-6} (for reversible counter-ions). The reduced charging time constant ($\tau_\infty = R_\infty C_g$) is 5×10^{-12}, and the reduced diffusional time constant ($\tau_W = (M^2/2.53)\tau_\infty$) is 2×10^{-2}. The initial state is the flat band condition: $I = 0$, $\Delta\phi = 0$ with symmetrical bathing solutions.

Case I

The first case to be considered is the membrane bathed in a single salt whose counter-ions are completely reversible at the interfaces. The salt activity in the left bathing solution is raised by 1% corresponding to a linear activity step. The final reduced membrane potential $\Delta\phi_\infty$ is ln (1.01) = 0.01. For analysis of the time response of the system, a quantity ln $(\Delta\phi_\infty - \Delta\phi(t))$ is calculated; this is plotted in Fig. 1, curve (a). It should be noted that the zero time intercept is ln $(\Delta\phi_\infty) = -2 \times 2.303$ or -4.606 reduced units.

For the activity step, the counter-ion concentration at the membrane surface establishes its equilibrium value instantaneously, and a diffuse space charge region begins to develop just inside the membrane. At longer times, the electric fields near the interface grow; the sites become depleted and a diffuse double-layer resembling an equilibrium Gouy—Chapman distribution forms. Eventually, the salt concentration in the bulk of the membrane is raised very slightly (in the absence of electric fields), and a small equilibrium diffuse double-layer forms at the right interface. The first time constant (when $\Delta\phi(t)$ has approached within $1/e$ of the net change) proves to be 5×10^{-12} reduced time units. This result is expected and demonstrates that the electric space-charge relaxation time has the same value for space charge that occurs across a membrane as for diffuse regions external to the two interfaces, or as for two diffuse regions across a single interface. There is no longer time constant in this case, and the membrane potential continues to approach the steady-state value with a $t^{-1/2}$ dependence.

Case II

The membrane is the same as in Case I, but a current step is made, which results in the same steady-state potential change as in Case I. For this perturbation, the expected $\tau_\infty = 5 \times 10^{-12}$ is seen. In contrast to the single-salt activity step result, a second time constant also appears in the potential response, as shown in Fig. 1, curve (b). Polarization of the bulk concentration gives rise to the long-time diffusional time constant. The current step produces rearrangement in the bulk concentration profiles that the previous activity

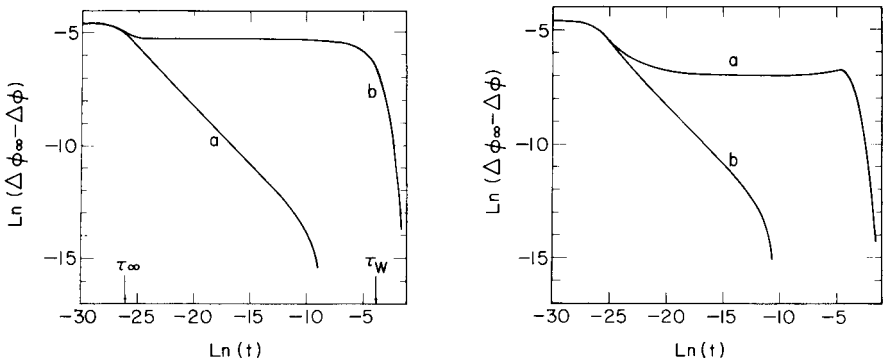

Fig. 1. Curve (a): logarithmic potential—time plot for a linear single-salt activity-step at a thick permselective liquid ion-exchange membrane with equilibrium surface extraction rates; membrane parameters (see text and Appendix) are $D_+ = D_- = 5.0 \times 10^{12}$, $d = 10^6$, $K = 5.0$, $K_{eq} = 1.0$, $k_b = 10^{15}$, and $I = 0$; membrane salt concentration is 0.1; initial salt activity in the bathing solutions is 0.1; left bathing solution salt activity is stepped to 0.101; final reduced potential is 0.01. Curve (b): logarithmic potential—time plot for linear current step; membrane parameters are the same, except that the left bathing solution salt activity is held at 0.1, and current density is stepped from 0 to 5000, resulting in a final reduced potential of 0.01; low-frequency time constant, $\tau_W = 2.0 \times 10^{-2}$; geometric time constant, $\tau_\infty = 5.0 \times 10^{-12}$.

Fig. 2. Curve (a): logarithmic potential—time plot for a multi-ion activity step at a thick permselective liquid ion-exchange membrane with equilibrium surface extraction rates; membrane parameters are the same as for Fig. 1(a) except for external activities; original permeable ion is at an activity of 0.1 in both bathing solutions; step in left bathing solution is to a pure solution of a second permeable ion at an activity of 0.1005; membrane diffusion coefficient for the second ion is 5.025×10^{12}; final reduced potential is 0.01. Curve (b): logarithmic potential—time plot for a multi-ion activity step displaying no low-frequency time constant; original bathing solutions contain two ions with diffusion coefficients of 5.1×10^{12} and 5.0×10^{12} at equal activities of 0.05; step raises the left bathing solution activity of the first ion to 0.051; final reduced potential is 0.01.

step cannot produce. The salt concentration profile remains flat at short times, and the electric fields grow uniformly throughout the membrane. After this charging process has been completed and the time scale reaches the diffusion time, the salt concentration profile tips, and equilibrium diffuse double-layers containing equal and opposite charge form at the interfaces.

Case III

Although thick membranes exposed to a single-salt linear activity step (as in Case I) do not show a second, diffusional time constant, certain activity steps may produce internal bulk concentration changes and long time-constant responses in two different ways.

First, a membrane exposed to two or more permeable ions will display potential transients with long time constants when a significant change in the ratio of the external activities of permeable ions occurs, and the mobilities

of the permeable ions are different. For membranes exposed to a single permeable ion, variations in external activity result in potential changes through the adjacent space-charge region only. When more than one permeable ion is present, activity variations can lead to substantial changes in the value of the internal electric fields (diffusion potential changes) as well as potential changes through the opposite space-charge region. These latter two processes will occur with a diffusional time constant, τ_W.

An example of the potential—time response is shown in Fig. 2, curve (a). The membrane is exposed to a single salt solution of a second permeable ion. This activity change to a bi-ionic system displays an identical geometric time constant to that seen in Case I, because the mobility of the second species is nearly the same as the first. The magnitude of the geometrical time response accounts for approximately 90% of the total potential change. As can be seen from Fig. 2, the final 10% of the potential transient is due to the potential drop through the membrane bulk and the right space-charge region, and is delayed with a time constant τ_W, which agrees with that calculated from eqn. (3).

Membranes exposed to more than one permeable counter-ion will not always display the long time-constant potential response. The potential—time response to a 1% change in the ratio of permeable counter-ion activities is shown in Fig. 2, curve (b). The geometrical potential transient accounts for the total potential change, and no long time response is seen. In this case, bulk rearrangement of the internal concentration profiles produces insignificant changes in the diffusion potential.

With regard to the second possibility, thin membranes are also capable of displaying diffusional time constants with a single-salt bathing solution. In thick membranes, formation of the diffuse space-charge region at the interface where the activity step occurs causes little change in the bulk ionic concentration profiles. However, formation of diffuse space-charge regions in thin membranes can substantially affect bulk concentrations. Activity steps may be large enough to displace significant fractions of the total sites from the interface into the bulk of the membrane. Bulk concentration changes result in variations in the diffuse space-charge region at the opposite interface. The potential drop through the second space-charge region will then account for a substantial portion of the total potential transient, and will change on a time scale equivalent to the membrane diffusion time.

Case IV. Membranes with slow interfacial transfer rates

Single-salt activity steps at permselective membranes result in potential—time responses governed by geometrical and, in some cases, diffusional time constants. These membranes have surface rate processes which are rapid and reversible. A different time response is expected when permeable-ion transport across the interface is limited by slow surface rates, and the resulting apparent interfacial resistance is larger than the bulk resistance.

An approximate expression for a slow interfacial time response to an activity step may be derived by assuming that the charging process establishes

an equilibrium diffuse double-layer at each instant of time. Consideration of the linearized Gouy—Chapman concentration distribution and eqn. (14) yields

$$c_o(t) = \bar{c}_o K_{eq} - [\bar{c}_o K_{eq} - c_b] \exp [-(k_b/2L_D)t] \quad (15)$$

where c_b is the concentration of the ion in the bulk membrane. Since the time-dependent membrane potential is simply $(RT/F) \ln (c_o(t)/c_b)$, and the steady-state potential is $(RT/F) \ln (\bar{c}_o K_{eq}/c_b)$, the potential—time response should be of the form

$$\Delta\phi(t) = (RT/F) \ln \{\exp (F\Delta\phi_\infty/RT) - [\exp (F\Delta\phi_\infty/RT) - 1] \exp (-t/\tau_k)\} \quad (16)$$

This expression is formally equivalent to that given by Morf et al. [41] for boundary-layer diffusion-controlled potential transients. In practice, surface film and interfacial rate control are distinguishable. The time constant for surface film control is approximately $\delta^2/2D$ (where δ is the Nernst thickness and D is the diffusion coefficient of the bathing solution salt) and should depend on the stirring rate.

The time constant used in eqn. (16), $\tau_k = 2L_D/k_b$, is exactly the value obtained from impedance measurements, $R_\theta \cdot C_{o,b}$. As a check on eqn. (16), Fig. 3 plots $\ln (\Delta\phi_\infty - \Delta\phi(t))$ vs. t for two time constants, along with digitally-simulated data from an activity step. Rate constants ($k_b = 10^6$) are given such that $R_\theta = 2 \times 10^{-5}$, $C_{o,b} = 0.5$, and $\tau_k = 1 \times 10^{-5}$. The simulated activity step

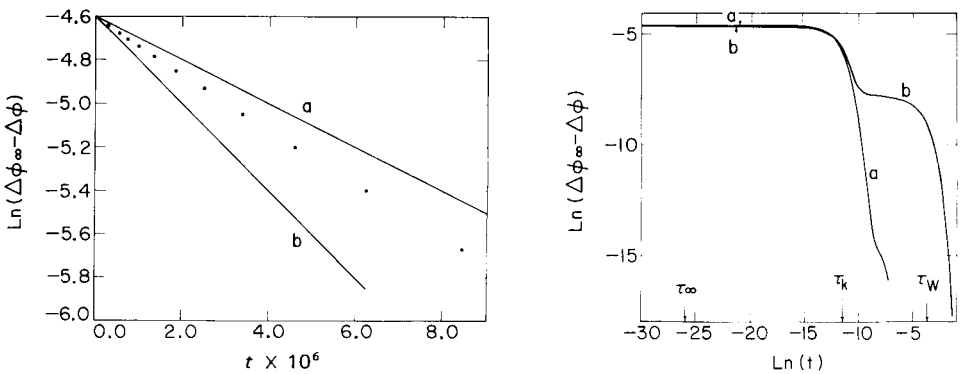

Fig. 3. Logarithmic potential—time plot for linear single-salt activity step at a thick permselective ion-exchange membrane with slow surface extraction rates. Curve (a) plots eqn. (16) with a time constant $\tau_k = 1.0 \times 10^{-5}$, as calculated for impedances ($R_\theta C_{o,b}$) and the expected time constant $2L_D/k_b$. Curve (b) plots eqn. (16) with a time constant $\tau_k' = 5.0 \times 10^{-6}$. Plotted points are simulated data for a membrane with parameters the same as for Fig. 1, curve (a), except $k_b = 1.0 \times 10^6$. Simulated points lie between these two calculated curves.

Fig. 4. Logarithmic potential—time plots for linear activity and current steps at a membrane with slow surface extraction rates. Curve (a) plots activity step; membrane parameters are the same as for Fig. 3. Curve (b) plots current step; membrane parameters are the same as for Fig. 1 (curve b), except that $k_b = 1.0 \times 10^6$ and current density is stepped to 833. Final reduced potential is 0.01. $\tau_\infty = 5.0 \times 10^{-12}$, $\tau_k = 1.0 \times 10^{-5}$, $\tau_W = 2.0 \times 10^{-2}$.

response displays a smaller time constant than predicted from eqn. (16). This discrepancy may be caused by the coupling of the interfacial charging with diffusional processes which were ignored in the derivation of eqn. (16).

Rate-limited membrane potential responses from activity-step perturbations are compared with current step responses in Fig. 4. The striking feature of the activity step response is that no geometrical charging response is seen. A single surface-rate time constant is displayed, which accounts for the entire potential transient. As in the earlier cases, long-time diffusional response is not observed. The current-step time-response displays potential changes which are due to all three membrane processes: geometrical, interfacial, and diffusional. The values of the time constants for the current-step responses are in excellent agreement with the theoretical expressions given earlier.

Case V. Time responses to non-linear activity steps

Figure 5 plots the potential—time response to a ten-fold increase in bathing salt activity along with the linear step data. The membrane interfacial transfer rates are rapid and reversible. The two curves shown in Fig. 5 are congruent, indicating that non-linear activity changes give rise to equivalent potential-determining processes within the membrane. The non-linear step response does yield a smaller geometrical time constant, however. This is probably due to reduction of the bulk resistance of the membrane by extraction of permeable ions from the external solution.

Similar effects are shown in Fig. 6 for non-linear activity steps at membranes

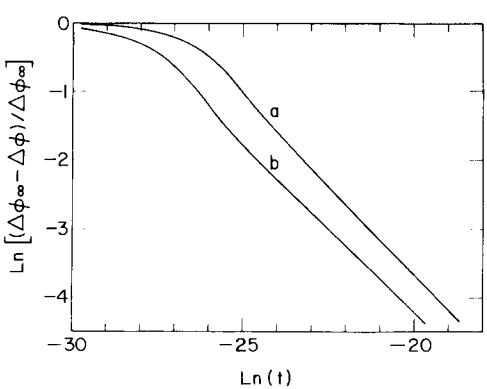

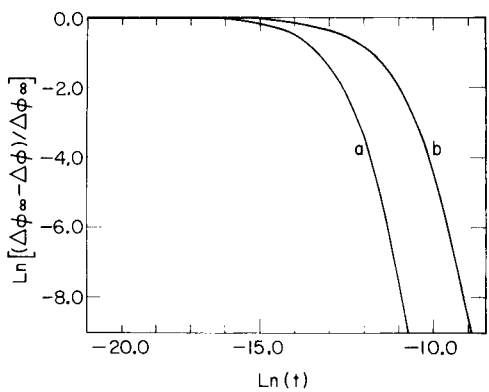

Fig. 5. Normalized logarithmic potential—time plot for linear and non-linear single-salt activity steps at a membrane with equilibrium surface extraction rates. Membrane parameters are: (a) the same as for Fig. 1, curve a, and (b) the same as for Fig. 1, curve a, except that the left bathing solution salt activity is stepped to 1.0.

Fig. 6. Normalized logarithmic potential—time plot for linear and non-linear single-salt activity steps at a membrane with slow extraction rates. Membrane parameters are: (a) the same as for Fig. 4, curve a, and (b) the same as for Fig. 4, curve a, except that the left bathing solution salt activity is stepped to 1.0.

with slow interfacial rates. Again, the non-linear response is similar to the linear response, but is displaced to shorter times. In this case, larger membrane surface concentrations give smaller Debye lengths, which may be responsible for the smaller observed interfacial time constant. Neither Fig. 5 nor Fig. 6 exhibits diffusional time responses. This will be true as long as the activity steps, while non-linear, are still small enough not to perturb the bulk membrane salt concentration, as discussed for the second possibility under Case III.

Analog circuit of equation (2) and its significance

Equation (2) for the response of a membrane to an ideal or non-ideal activity step gives $\Delta\phi\ (t = 0) = \Delta\phi^0$, and $\Delta\phi\ (t = \infty) = \Delta\phi^0 + \Sigma_i\, k_i = \Delta\phi_\infty$. The k_i values can be identified as fractions of the final less initial voltage, i.e. fractions of the voltage step size: $k_i = f_i(\Delta\phi_\infty - \Delta\phi^0) = f_i\Delta\phi_{\text{step}}$, with $\Sigma_i\, f_i = 1$. These fractions can be computed from the time constants τ_i by using an electrical analog model.

Whenever a two-port network shows a time response E_{out} vs. E_{in} (in this case, $\Delta\phi_{\text{memb.}}$ vs. $\Delta\phi_{\text{step}}$) which is the sum of exponentials, it is likely that the transfer function is given by:

$$L\Delta\phi(t)/L\Delta\phi_{\text{step}} = \{L\Delta\phi(t)\}/\{L(\mathbf{R}T/F)\ \ln\ [\Delta a_{\text{step}}(t) + a(t = 0)/a(t = 0)]\}$$
$$= [(p\tau_1 + 1)(p\tau_2 + 1) \ldots (p\tau_i + 1)]^{-1} \qquad (17)$$

Here L indicates Laplace transforms and $\Delta\phi_{\text{step}}$ is expressed in terms of the activity step. The circuit which gives this transform is active, and is illustrated in Fig. 7(a). The time constants $\tau_1, \tau_2 \ldots \tau_i$ are $R_1C_1, R_2C_2 \ldots R_iC_i$. These are ranked $\tau_1 \ll \tau_2 \ll \tau_3 \ldots \ll \tau_i$. From the well-known inversion method for functions of this type [43], the expected measured $\Delta\phi(t)$ can be expressed in terms of $\Delta\phi_{\text{step}}$ and τ values. Four cases are considered below, including the effect of imperfect activity steps.

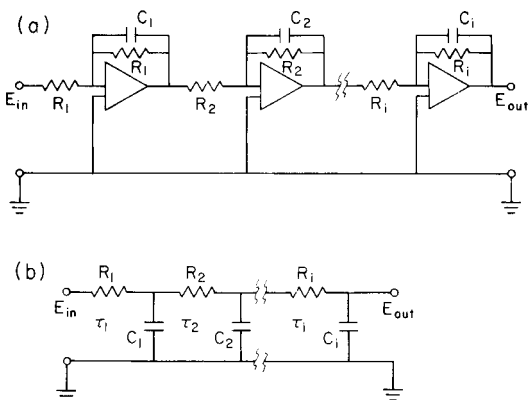

Fig. 7. Analog equivalent circuit models for activity-step time responses. (a) Active circuit with transfer function given by eqn. (17). (b) Passive circuit for membrane time responses.

(a) The membrane is a single RC *combination* τ_1 *with an ideal activity step.* In this case,

$$L\Delta\phi_{step} = \Delta\phi_{step}/p \tag{18}$$

Then, $\Delta\phi(t) = \Delta\phi_{step}\,[1 - \exp(-t\tau_1^{-1})] + \Delta\phi^0$, with $k_i = k_1 = f_i = f_1 = 1$.

(a') The membrane is a single RC *combination* τ_1, *but the activity step is not ideal, showing a time constant* τ. In this case,

$$L\Delta\phi_{step} = \Delta\phi_{step}/[\tau p(p + \tau^{-1})] \tag{19}$$

Then,

$$\Delta\phi(t) = \Delta\phi_{step} f_1\,[1 - \exp(-t\tau_1^{-1})] + \Delta\phi_{step} f_2\,[1 - \exp(-t\tau^{-1})] + \Delta\phi^0 \tag{20}$$

where $f_1 = 1/(1 - \tau/\tau_1)$ and $f_2 = -(\tau/\tau_1)/(1 - \tau/\tau_1)$. It should be noted that the second time constant dominates the response because $f_2 \approx 1$.

(b) The membrane has two time constants τ_1 *and* τ_2 *as in Fig. 7(a), and the step is ideal.* In this case,

$$\Delta\phi(t) = \Delta\phi_{step} f_1\,[1 - \exp(-t\tau_1^{-1})] + \Delta\phi_{step} f_2\,[1 - \exp(-t\tau_2^{-1})] \tag{21}$$

where $f_1 = -\tau_1/(\tau_2 - \tau_1)$ and $f_2 = \tau_2/(\tau_2 - \tau_1)$.

(b') The membrane has two time constants τ_1 *and* τ_2 *and the step is imperfect.* In this case,

$$\Delta\phi(t) = \Delta\phi_{step} f_1\,[1 - \exp(-t\tau_1^{-1})] + \Delta\phi_{step} f_2\,[1 - \exp(-t\tau_2^{-1})] + \Delta\phi_{step} f_3\,[1 - \exp(-t\tau^{-1})] \tag{22}$$

where $f_1 = \tau_1^2/(\tau_1 - \tau)(\tau_1 - \tau_2)$, $f_2 = \tau_2^2/(\tau_2 - \tau)(\tau_2 - \tau_1)$, and $f_3 = \tau^2/(\tau - \tau_1)(\tau - \tau_2)$. There are cyclic rules for generating the coefficients [43].

The important point to note is that all time constants occur, and are weighted according to their increasing size. The error, however, in this simple description of the system is that membranes are assumed to be passive. Circuit 7(a) must be replaced by circuit 7(b). It is well known that such passive integrators do not respond ideally at high frequencies (short times). Long time constants "mix" into the exponentials containing the expected shorter time constants. The exponentials which again occur, as in eqn. (2) are not pure τ_1, τ_2, etc., but contain effects of all longer τ values. For the two-time constant case with an ideal step (b above), the observed first time constant $\tau_1 \neq R_1C_1$, but is given by $(R_1 + R_2)C_1$, while τ_2 remains R_2C_2, with first-order approximation accuracy.

CONCLUSIONS

Back-to-back computer experiments can be used to generate membrane potential vs. time response data for a small activity step on one side of a membrane, and for a current step. The results show both similarities and differences for ideal, permselective membrane with reversible and rate-limited

surface ion exchange. Values of the observed time constants for both perturbations (excitations) are identical or within error of approximations, and they agree well with the values calculated for the isolated, identified processes. However, activity-step perturbations are not identical with applied cell voltage-step perturbation, and are obviously not identical with applied current steps. The result is that processes involving the far (unperturbed) side during an activity step, do not give isolated time constants. Furthermore, the slowest steps at the perturbed interface dominate the overall response. This result was unexpected and demonstrates an essential loss of information from activity-step experiments that can be recovered by using current-step experiments. The latter "excite" all membrane processes (both interfaces and interior) while the activity step "excites" interfacial processes at one side and to a much lesser extent, interior and far-side processes.

A model is offered for the equivalent R and C values which correspond to the time constants of the potential-generating sources. This active network analog has a necessary transfer function which reproduces the form of the empirical $\Delta\phi$ vs. t behavior of many ion-selective electrodes. A passive version is also suggested, but this network does not give exact correspondence between activity-step and current-step time constants. A major uncertainty in modelling comes from the assumption that an ideal abrupt activity step at one interface corresponds to a voltage step at one interface. This postulate must serve in the absence of any other model.

Appendix I. Transformation of membrane parameters to dimensionless simulation parameters

Table 1-A lists the appropriate transformations from dimensioned (starred) quantities to the dimensionless quantities used in the simulation.

TABLE 1-A

Simulation parameter	Transformation of dimensioned parameter
Thickness, d	$= d^*/l_o$
Diffusion coefficient, D	$= D^*/D_o$
Concentration, c	$= c^*/c_o$
Time, t	$= t^* D_o/l_o^2$
Potential, $\Delta\phi$	$= \Delta\phi^* F/RT$
Current density, I	$= I^* l_o/FD_o c_o$
Unrationalized dielectric permittivity, K	$= \epsilon^* RT/4\pi c_o l_o^2 F^2$
Heterogeneous rate constant, k	$= k^* l_o/D_o$
Capacitance, C	$= C^* l_o K\, 4\pi/\epsilon^* = C^* RT/c_o l_o F^2$
Resistivity, R	$= R^* D_o c_o F^2/l_o RT$
Time constant, τ	$= \tau^* D_o/l_o^2$

Choice of the scaling factors, c_o, D_o, and l_o, is determined by consideration of the values of the dimensioned parameters for the membrane system of interest. Employment of the scaling factors used earlier [17] gives $c_o = 1.0 \times 10^{-5}$ mol cm^{-3}, $D_o = 1.0 \times 10^{-16}$ cm^2 s^{-1} and $l_o = 2.0 \times 10^{-8}$ cm. The values of the dimensioned quantities given in Table 2-A result in the parameter values used in the simulations.

TABLE 2-A[a]

Parameter	Dimensioned quantity	Simulation value
c	1.0×10^{-6} mol cm^{-3}	0.1
D	5.0×10^{-4} cm^2 s^{-1}	5.0×10^{12}
d	2.0×10^{-2} cm	1.0×10^{6}
K	$\epsilon^* = 9.4 \times 10^{-13}$ A s V^{-1} cm^{-1}	5.0
k	5.0×10^{-3} cm s^{-1}	1.0×10^{6}
ΔI	2.41×10^{-5} A cm^{-2}	5.0×10^{3}
$\Delta\phi$	2.56×10^{-4} V	0.01
R_∞	5.32 ohm cm^2	1.0×10^{-6}
R_θ	106.4 ohm cm^2	2.0×10^{-5}
R_0	10.64 ohm cm^2	2.0×10^{-6}
C_g	3.77 pF cm^{-2}	5.0×10^{-6}
$C_{o,b}$	0.377 μF cm^{-2}	.5
$C_{o,r}$	18.9 mF cm^{-2}	2.5×10^{4}
τ_∞	2.0×10^{-11} s	5.0×10^{-12}
τ_k	4.0×10^{-5} s	1.0×10^{-5}
τ_W	8.0×10^{-2} s	2.0×10^{-2}

[a]The values for k, R_θ, and τ_k apply to the membrane with intermediate rates at the interfaces. The value of R_0 applies to the membrane with rapid, reversible interfacial transfer.

Appendix *II. Derivation of equation (15): inner surface concentration* c_{oi} *determined by slow surface kinetics after an external activity step.*

The parameter c_{oi} is written in terms of the corresponding charge q: $c_{oi}(q) = c_b/((1 + 1/A^2)^{\frac{1}{2}} + z_i/A)^2$, where

$A = -2(2c_bK)^{\frac{1}{2}}q = -4c_bL_D/q$.

Linearizing for small q gives $c_{oi}(q) \approx c_b[1 + q/2c_bL_D]$. Because the flux of positive ions is the sole contributor to double-layer charge, eqn. (14) gives

$dq/dt = k_b[K_{eq}\bar{c}_o - c_o(t)] = k_b[K_{eq}\bar{c}_o - c_b - q/2L_D]$

For $z_i = 1$, integrating from $q = 0$ at $t = 0$ gives

$q/2L_D = [K_{eq}\bar{c}_o - c_b]\,(1 - e^{-tk_b/2L_D})$

Substituting into the approximation for $c_{oi}(q)$ just above gives

$c_o(t) = c_b + [K_{eq}\bar{c}_o - c_b]\,(1 - e^{-tk_b/2L_D})$

and eqn. (15) is a simple rearrangement.

Support of this work by the National Science Foundation under grants CHE-7500970-A01 and CHE-77-20491 is gratefully acknowledged.

REFERENCES

1 K. Tóth, L. Gavaller and E. Pungor, Anal. Chim. Acta, 57 (1971) 131.
2 J. Bagg and R. Vinen, Anal. Chem., 44 (1972) 1773.
3 B. Karlberg, J. Electroanal. Chem., 42 (1973) 115.
4 R. E. Reinsfelder and F. A. Schultz, Anal. Chim. Acta, 65 (1973) 425.
5 P. L. Markovic and J. O. Osburn, A.I. Ch.E.J., 19 (1973) 503.

6 B. Karlberg, J. Electroanal. Chem., 49 (1974) 1.
7 B. Fleet, T. H. Ryan and M. Brand, Anal. Chem., 46 (1974) 12.
8 G. J. Moody and J. D. R. Thomas, Lab. Pract., 23 (1974) 475.
9 A. Shatkay, Anal. Chem., 48 (1976) 1039.
10 G. A. Rechnitz, Acc. Chem. Res., 3 (1970) 69.
11 K. Tóth and E. Pungor, Anal. Chim. Acta, 64 (1973) 417.
12 E. Lindner, K. Tóth and E. Pungor, Anal. Chem., 48 (1976) 1071.
13 A. Denks and R. Neeb, Fresenius Z. Anal. Chem., 285 (1977) 233.
14 R. P. Buck, Anal. Chem., 48 (1976) 23R.
15 R. P. Buck, Crit. Rev. Anal. Chem., 5 (1975) 323.
16 R. P. Buck, Anal. Chem., 50 (1978) 17R.
17 T. R. Brumleve and R. P. Buck, J. Electroanal. Chem., 90 (1978) 1.
18 T. R. Brumleve and R. P. Buck, unpublished results.
19 R. D. Armstrong, T. Dickinson and P. M. Willis, J. Electroanal. Chem., 53 (1974) 389.
20 R. deLevie, Adv. Electrochem. Electrochem. Eng., 6 (1976) 329.
21 R. D. Armstrong and R. A. Burnham, J. Electroanal. Chem., 72 (1976) 257.
22 R. P. Buck and J. R. Sandifer, J. Electroanal. Chem., 56 (1974) 385.
23 W. E. Morf, Anal. Lett., 10 (1977) 87.
24 F. G. A. Baucke, in E. Pungor (Ed.), Ion Selective Electrodes, Akademiai Kiado, Budapest, 1978, p. 215.
25 Z. Boksay, in E. Pungor (Ed.), Ion Selective Electrodes, Akademiai Kiado, Budapest, 1978, p. 245.
26 D. E. Mathis and R. P. Buck, J. Membr. Sci., 4 (1979) 379.
27 D. E. Mathis, F. S. Stover and R. P. Buck, J. Membr. Sci., 4 (1979) 395.
28 J. P. Sandblom, Biophys. J., 12 (1972) 1118.
29 J. P. Sandblom, J. L. Walker, Jr. and G. Eisenman, Biophys. J., 12 (1972) 587.
30 R. D. Armstrong, T. Dickinson and P. M. Willis, J. Electroanal. Chem., 48 (1973) 47.
31 R. D. Armstrong and K. Taylor, J. Electroanal. Chem., 63 (1975) 9.
32 J. R. Macdonald, Trans. Faraday Soc., 66 (1970) 953; J. Electroanal. Chem., 32 (1971) 317; 53 (1974) 1; J. Chem. Phys., 54 (1971) 2026; 58 (1973) 4982; 60 (1974) 343; 61 (1974) 3977; J. Appl. Phys., 45 (1974) 73.
33 R. P. Buck, D. E. Mathis and R. K. Rhodes, J. Electroanal. Chem., 80 (1977) 245.
34 R. K. Rhodes and R. P. Buck, J. Electroanal. Chem., 86 (1978) 349.
35 M. Sluyters-Rehbach and J. H. Sluyters, in A. J. Bard (Ed.), Electroanalytical Chemistry, 4 (1970) 1.
36 G. C. Barker, Pure Appl. Chem., 15 (1967) 239; J. Electroanal. Chem., 41 (1973) 201.
37 T. R. Brumleve, Ph.D. Thesis, University of North Carolina, October 1978.
38 R. P. Buck, in H. Freiser (Ed.), Ion-Selective Electrodes in Analytical Chemistry, Plenum Press, N.Y., 1978, p. 1.
39 J. R. Macdonald, in G. D. Mahan and W. L. Roth (Eds.), Superionic Conductors, Plenum Press, N.Y., 1976, p. 81.
40 F. Conti and G. Eisenman, Biophys. J., 6 (1966) 227.
41 W. E. Morf, E. Lindner and W. Simon, Anal. Chem., 47 (1975) 1596.
42 W. E. Morf and W. Simon, in H. Freiser, (Ed.), Ion-selective Electrodes in Analytical Chemistry, Plenum Press, N.Y., 1978, p. 233.
43 A. Erdelyi, W. Magnus, F. Oberhettinger and F. G. Tricomi, Tables of Integral Transforms, McGraw-Hill, N.Y., 1950, Vol. 1.

Analytica Chimica Acta, 109 (1979) 279—290
© Elsevier Scientific Publishing Company, Amsterdam — Printed in The Netherlands

THE SURFACE MORPHOLOGY OF ION-SELECTIVE MEMBRANE ELECTRODES
Part 2. Studies on the Copper(II)-selective Electrode

E. PUNGOR*, K. TÓTH, M. K. PÁPAY and L. PÓLOS

Institute for General and Analytical Chemistry, Technical University, Budapest (Hungary)

H. MALISSA, M. GRASSERBAUER and E. HOKE

Institut für Analytische Chemie und Mikrochemie der Technischen Universität Wien (Austria)

M. F. EBEL and K. PERSY

Institut für Technische Physik der Technischen Universität Wien (Austria)

(Received 5th March 1979)

SUMMARY

The response of copper(II)-selective electrodes based on copper(II) sulphide incorporated in silicone rubber or compressed to pellets is described, with particular reference to electrode behaviour after treatment with various oxidizing agents and regeneration by chemical procedures. Changes in the surface state of the membranes were examined by electron microprobe analysis and photoelectron spectroscopy. The electrochemical behaviour of the membranes can be correlated with surface morphology changes, primarily connected with formation of sulphate monolayers.

The preparation and fundamental electrochemical properties of the silicone rubber-based copper(II)-selective electrode and its behaviour in the presence of complexing agents have been described in earlier papers [1—3]. In later studies, it was found that these electrodes lose their sensitivity towards copper(II) ions in highly oxidizing systems; the electrode potential increases gradually during treatment in such redox systems and finally reaches a constant value. This effect of redox systems was found to be reversible, as the electrode function could be restored by suitable chemical treatment [4].

Johansson and Edström [5] were the first to draw attention to the redox sensitivity and regeneration of the Orion copper(II)-selective electrode which consists of a pressed mixture of copper(II) sulphide and silver(I) sulphide. These workers attributed the redox sensitivity to corrosion of the electrode and preferred a mechanical method of regeneration (diamond polishing) to chemical treatment. They stated that the deterioration of the surface takes place mainly at the crystal interstices.

Hansen et al. [6] pointed out that treatment with EDTA solution improves the characteristics of electrodes activated with a metal sulphide, but they also

stated that treatment with EDTA solution is not effective in the case of commercial electrodes, including those produced by Orion. This difference in behaviour is probably due to the differences in the surface characteristics of the types of electrode studied.

The redox sensitivity of electrodes containing mixed sulphides, e.g. copper(II) sulphide and silver(I) sulphide, was also observed by Koebel [7], who attributed the effect to the dissolution or precipitation of the metal at the electrode surface.

The behaviour of an iodide-selective electrode consisting of silver iodide and silver sulphide was investigated by Baucke [8]. The electrode did not respond in dilute hydriodic acid solution, possibly because of the oxidizing effect of the iodine present in small amounts in hydriodic acid. During oxidation of sulphide, amorphous sulphur was formed which produced an inactive blocking layer at the electrode surface.

More recently, Gulens and Ikeda [9] drew attention to the effect of surface heterogeneity on the electrochemical behaviour of silver sulphide-based sulphide-selective electrodes. It was shown that the presence of silver metal films or deposits on the electrode surface result in the formation of mixed potentials indicated by slow and non-Nernstian electrode responses at low sulphide concentrations.

From the above, as well as from the studies of Sorrentino and Rechnitz [10] and earlier work [11] on the surface morphology of iodide-selective electrodes based on silver iodide, it is clear that quite a number of phenomena observed with precipitate-based ion-selective electrodes can be correlated with the surface morphology and heterogeneity of the ion-selective membranes, i.e. with the formation of deposits or recrystallization of the electrode surface or leaching of the electrode membrane.

EXPERIMENTAL

Preparation of the electroactive copper sulphide precipitate

An aliquot (25 ml) of a stock solution of copper(II) sulphate pentahydrate (200 g l^{-1}) was transferred to a 750-ml Erlenmeyer flask, and 7 ml of concentrated sulphuric acid, 200 ml of distilled water and 27 ml of sodium thiosulphate pentahydrate solution (316 g l^{-1}) were added. After a funnel had been placed into the neck of the flask, the solution was heated to boiling. The initial yellow precipitate soon became brown and then black. To promote the agglomeration of the precipitate, the solution was boiled gently for 15 min. The pH of about 100 ml of the decanted mother liquor was adjusted to about 9 with concentrated ammonia solution. The precipitate was then filtered on a G4 sintered glass crucible, washed with the pH 9 mother liquor, and then with eight 50-ml portions of distilled water, until the pH of the filtrate was 7. The precipitate was dried at 100°C for 4 h in a hydrogen sulphide or nitrogen atmosphere. The average composition of the precipitate was then determined, by using relative conductometry to measure sulphur and atomic absorption spectrometry to measure copper.

Preparation of the copper sulphide electrodes

The electrodes were made from the above copper sulphide precipitate in two ways.

(1) The copper sulphide (0.5 g) was pressed to a pellet (1-cm diameter) under a pressure of about 15 tons/cm^2, and the pellet was sealed to the end of a glass tube.

(2) The copper sulphide precipitate (70 parts by weight) was mixed with 30 parts (wt.) of dimethylpolysiloxane (Silopren K 1000, Farbenfabrik Bayer) to form a homogeneous dispersion. A mixture of a cross-linking agent and a catalyst (1 part of dibutyl tin dilaurate and 2 parts of hexaethoxysiloxane) was then added to the dispersion in a proportion of 1% by weight and mixed thoroughly. The material thus obtained was spread on a plastic sheet, covered with another plastic sheet and pressed gently to obtain the necessary layer thickness (0.01—1 mm). About an hour was needed for polymerization. After removal of the plastic sheets, discs were cut out and stuck to the end of glass tubes with silicone adhesive.

The internal electrolyte was 10^{-4} M $CuSO_4$—10^{-2} M KCl, and the internal reference electrode was a silver—silver chloride electrode.

Checking of the electrode response. The electrodes were calibrated in 10^{-1} M, 10^{-2} M, 10^{-3} M and 10^{-4} M copper sulphate solutions, the latter three solutions being 0.1 M in potassium nitrate. A saturated calomel electrode (Radelkis, Type 830) was used as reference electrode.

Investigation of the effect of redox systems and the regeneration process of the electrodes

The effects of various oxidizing agents such as cerium(IV), potassium permanganate and chlorine water on the electrochemical behaviour of these copper sulphide electrodes were studied in stationary solutions, in a batch-wise manner, as a function of time. The solutions used were a 0.02 M cerium(IV) solution in 0.5 M sulphuric acid, a saturated aqueous chlorine solution, and a 0.1 N potassium permanganate solution in 0.5 M sulphuric acid. The same volume of fresh oxidizing solution was used in each experiment. In the regeneration tests, the electrodes were treated with 10^{-2} M ascorbic acid, 10^{-2} M perchloric acid or 10^{-1} M EDTA solutions for various periods of time.

In some cases, the concentration of the cerium(IV) solution was determined by potentiometric titration during the pretreatment, by using a platinum—calomel electrode couple (Radelkis Type OP-612 and Radelkis OP-830) with 0.01 M sodium oxalate solution as titrant. The amount of copper dissolved from the membrane during pretreatment was measured by atomic absorption spectrometry. From the results the amount of cerium(IV) consumed by oxidation was calculated.

Apparatus and reagents

Potentials were measured with a precision pH meter (Type OP-205, Radelkis, Budapest).

Morphological studies were done with an electron microscope (International Scientific Instruments Type MSM-2) and an electron microprobe analyser (Applied Research Laboratories Type EMX-SM).

A Varian-Techtron AA6 atomic absorption spectrometer was used to determine metal ions in solutions.

A photoelectron spectrometer (McPherson GCA Corporation, ESCA-36) and a MOM derivatograph were also used.

All chemicals were of analytical grade.

RESULTS AND DISCUSSION

The composition of the copper sulphide precipitate

Earlier studies [12] indicated that copper(II)-selective electrodes show satisfactory electrochemical behaviour only if the electroactive component, i.e. the copper sulphide precipitate, has been prepared under oxygen-free, or reducing conditions. Accordingly, the composition of the precipitates prepared under different conditions was determined in order to establish if there is a correlation between composition and electrochemical properties. The results (Table 1) show that the precipitate prepared with sodium thiosulphate and then heated in a hydrogen sulphide atmosphere consists mainly of copper(II) sulphide, whereas the composition of the precipitate prepared with hydrogen sulphide in the presence of air is quite different. The composition of the former precipitate was studied in oxygen-free nitrogen by thermal methods (Derivatograph). The results are shown in Fig. 1; the weight change and the derivative of the weight change with respect to temperature are plotted as functions of the temperature. The first change (between 200 and 400°C) indicates the reaction between copper sulphide and the sulphur formed in small amounts during the precipitation. In the second stage (between 400 and 650°C), the copper(II) sulphide is completely converted to Cu_2S, releasing sulphur: $2\ CuS = Cu_2S + S$. These results indicate that the precipitate is mainly copper(II) sulphide (cf. Table 1).

Electrochemical studies

The copper(II) responses of homogeneous pellet and heterogeneous silicone-rubber copper sulphide electrodes made with the precipitate prepared in a reducing atmosphere are shown in Fig. 2. These results, in accordance with many other experimental findings, show that the copper(II) ion sensitivity of the silicone rubber electrode is better than that of pressed pellet electrodes. However, electrodes prepared with precipitates dried in air (see Table 1) do not respond to copper, which suggests that oxidation of the copper sulphide precipitate is not beneficial to the electrochemical behaviour.

The effects of cerium(IV) on the copper-ion responses of the two types of electrode are shown in Fig. 3 as a function of treatment time. The experiment was done as follows: an electrochemically correct copper-selective electrode was placed in 10 ml of 0.02 M cerium(IV) solution in 0.5 M sulphuric acid

TABLE 1

Compositions of copper sulphide precipitates prepared in different ways

Sample	Cu (%)	S (%)	Total Cu + S (%)
Theoretical composition of CuS	66.46	33.54	100.00
Theoretical composition of Cu_2S	79.85	20.15	100.00
CuS precipitated with $Na_2S_2O_3$ and dried under H_2S	62.53	35.05	97.58
CuS precipitated with H_2S in presence of air	55.60	29.01	84.61

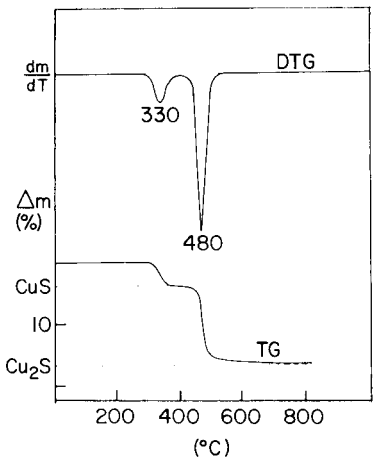

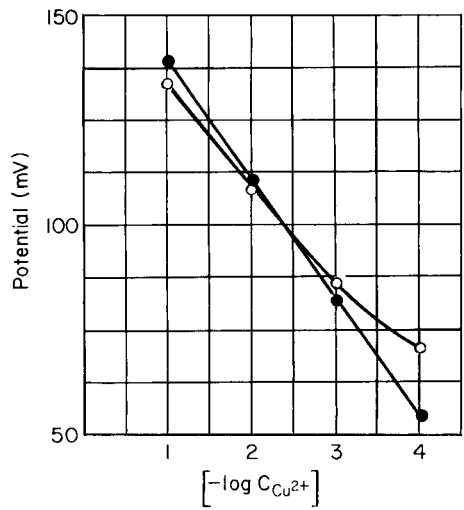

Fig. 1. Thermal properties of the copper sulphide precipitate used for electrode preparation.

Fig. 2. Copper(II)-ion response of a pressed pellet and a silicone-rubber copper(II) sulphide electrode. (•) Silicone rubber membrane; (○) pressed pellet.

(for 10 or 30 min) and then the oxidizing solution was renewed; before the solution was changed, the copper(II) function of the electrode was checked (Fig. 3) and the copper dissolved by the soaking solution was determined (Fig. 4). The results show clearly that the amount of dissolved copper(II) is much smaller for the silicone rubber electrodes than for the pressed pellet electrodes. Moreover, the electrode function ceases later in the case of the silicone rubber electrodes, owing to the protecting effect of the rubber. These findings indicate that the electrode function ceases as a result of surface corrosion; it is supposed that corrosion is slower at the rubber-covered surface than at the pellet surface.

In further experiments, a pressed pellet electrode was treated with cerium(IV) solutions for periods of 1, 3, 6 h, etc.; after the specified time, the

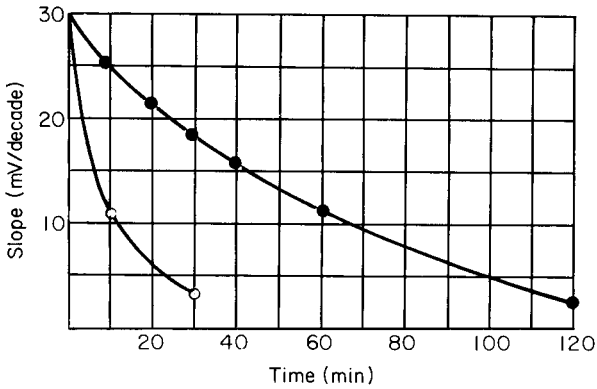

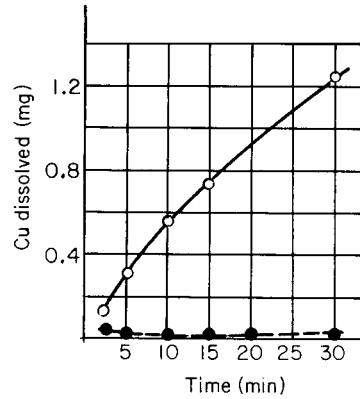

Fig. 3. The effect of the time of treatment in 2×10^{-2} M Ce^{4+} solution on the slope of the copper(II)-selective electrode response, determined in the range 10^{-2}—10^{-3} M Cu^{2+}. (•) Silicone rubber membrane; (○) pressed pellet electrode.

Fig. 4. Copper dissolved from pressed pellet and silicone rubber electrodes with membranes of the same geometric surface area. (•) Silicone rubber membrane; (○) pressed pellet electrode.

soaking solution was renewed, and the copper content and the amount of the cerium(IV) consumed were determined. The procedure was repeated three times with the same electrode. The following results were obtained. The amount of copper dissolved increased with increasing time of treatment, but the greatest amount of copper was dissolved in the first portion of the oxidizing solution. The amount of cerium(IV) consumed in oxidation also increased with the time of soaking but the trend did not correlate well with that found for dissolved copper. This apparent phenomenon may be due to the fact that the reaction path of the oxidation process is not known; it seems likely that not only sulphide but also copper(I) at the membrane surface may be oxidized.

The copper(II) responses of pressed pellet electrodes treated for different time intervals with different oxidizing agents — cerium(IV), potassium permanganate, chlorine—as well as with ascorbic acid are shown in Figs. 5—7. The amounts of copper in the oxidizing solutions and in the regenerating ascorbic acid solutions were determined in each case, as described above for the tests with cerium(IV) solutions, i.e. the soaking solution was renewed at the intervals given. These results, summarized in Table 2, show that copper is mainly dissolved by the oxidizing agents.

The results in Figs. 5—7 show that, in accordance with earlier results, the normal potential of copper sulphide electrodes is shifted to more positive values in the presence of oxidizing agents. After treatment with a reducing agent, i.e. ascorbic acid, the calibration curves shift towards more negative potentials. In a separate experiment, the copper(II) responses were deter-

TABLE 2

Studies of the copper dissolution rate with pressed pellet membranes

Time	Amount of copper dissolved (mg)						
	Ce^{4+}	Ascorbic acid	Cl_2	Ascorbic acid	$KMnO_4$	Ascorbic acid	
						Cu	Mn
2.5 min	0.15		1.05		1.00		
5 min	0.31		1.60		0.37		
10 min	0.56	0.003	2.00	0.08			
15 min	0.73		3.30	0.02	0.36		
30 min	1.25	0.006	2.75	0.08		0.023	1.05
						0.002	0.14
60 min		0.002	3.30		1.73	0	0
4 × 6 h	10.5						
4 × 24 h	24.3						

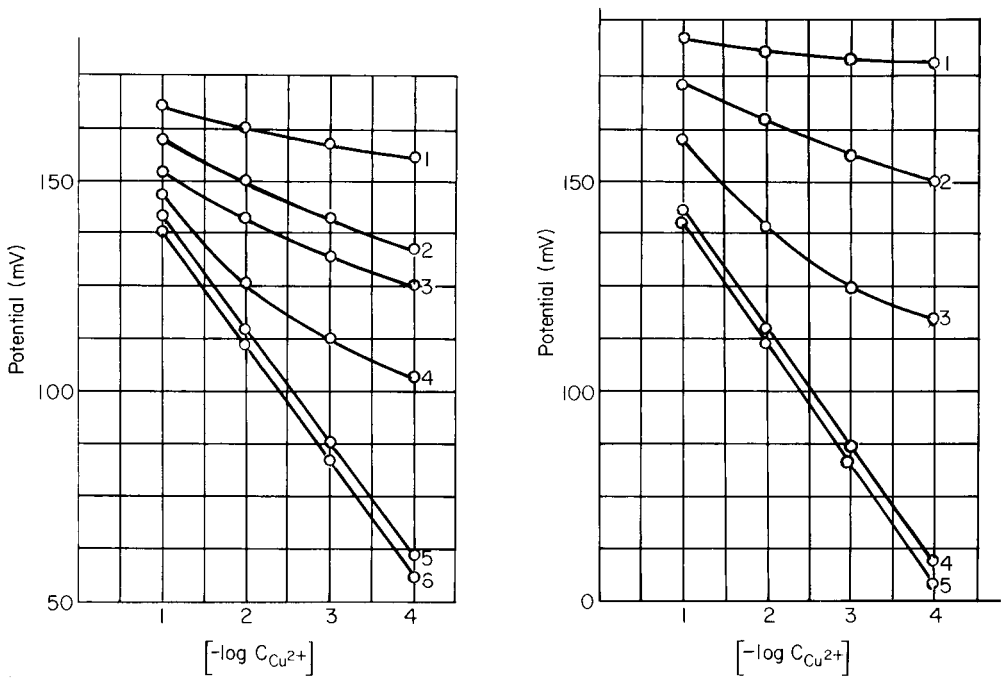

Fig. 5. Copper(II) response of a pressed pellet electrode after soaking in cerium(IV) solutions and regenerating in ascorbic acid solutions for different times. (1) Soaking for 30 min in Ce(IV); (2) soaking for 10 min in Ce(IV); (3) regenerating in ascorbic acid for 10 min; (4) for 30 min; (5) for 80 min; (6) untreated electrode.

Fig. 6. Copper(II) response of a pressed pellet electrode after soaking in potassium permanganate and regenerating in ascorbic acid solutions. (1) Soaking for 30 min in $KMnO_4$; (2) soaking for 10 min in $KMnO_4$; (3) regenerating in ascorbic acid for 30 min; (4) for 60 min; (5) untreated electrode.

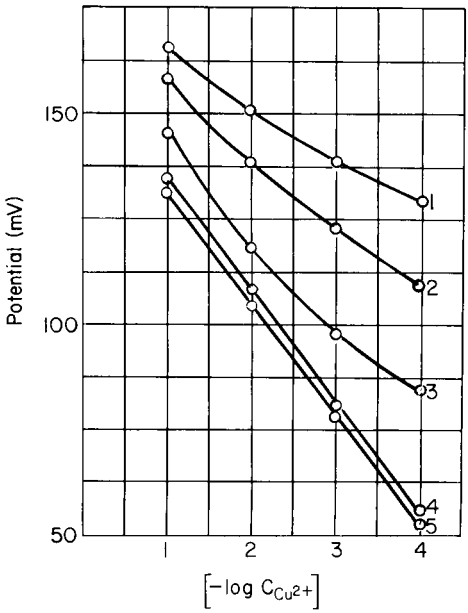

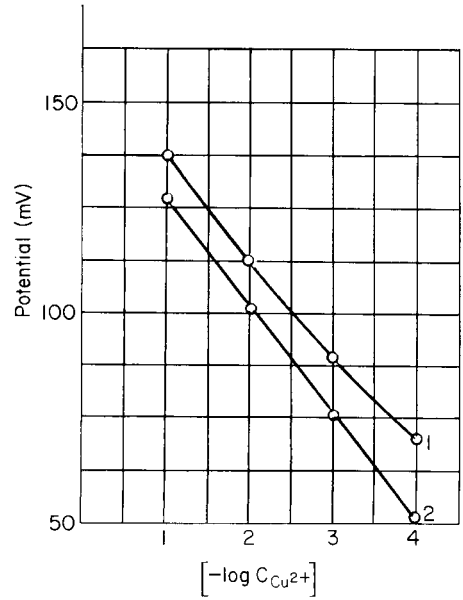

Fig. 7. Copper(II) response of a pressed pellet electrode after soaking in saturated chlorine water and regenerating in ascorbic acid solutions. (1) Soaking in Cl_2 water for 5 min; (2) soaking in Cl_2 water for 2.5 min; (3) soaking in Cl_2 water for 1 min; (4) untreated electrode; (5) after regenerating in ascorbic acid for 30 min.

Fig. 8. Copper(II) responses of an untreated and a pretreated pressed pellet electrode. (1) Untreated electrode; (2) after soaking in 10^{-2} M ascorbic acid solution for 5 h.

mined for a pressed pellet electrode first untreated and then treated in 10^{-1} M ascorbic acid. The absolute potentials were found to shift to more negative values (Fig. 8) as a result of the ascorbic acid treatment, which tends to indicate that slight oxidation had taken place during the preparation of the precipitate itself.

The effects of various regenerating agents (ascorbic acid, EDTA, perchloric acid) on the behaviour of electrodes which had completely lost their electrode function are illustrated in Fig. 9. Ascorbic acid is clearly the best regenerating agent. This fact and the data in Table 2 indicate that oxidizing agents cause changes in the surface stoichiometry of the electrode material which may block the electrode surface. The failure of the electrode response cannot be ascribed solely to simple surface dissolution.

Investigation of the morphology and surface composition of electrode membranes

Electron micrographs of the surfaces of an electrode membrane pressed from copper sulphide treated in a hydrogen sulphide atmosphere and of a heterogeneous silicone rubber membrane are shown in Fig. 10. In the pressed pellets

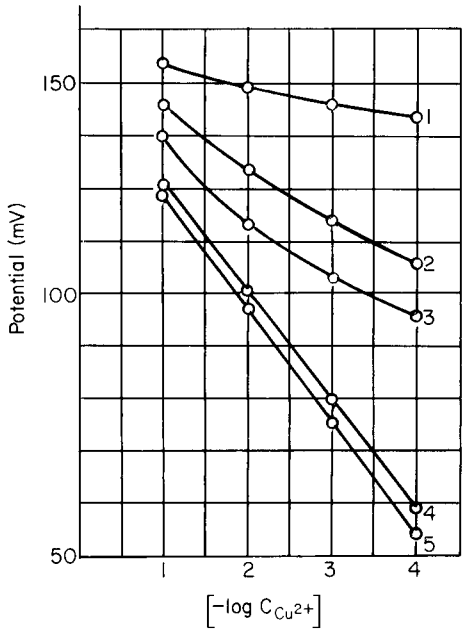

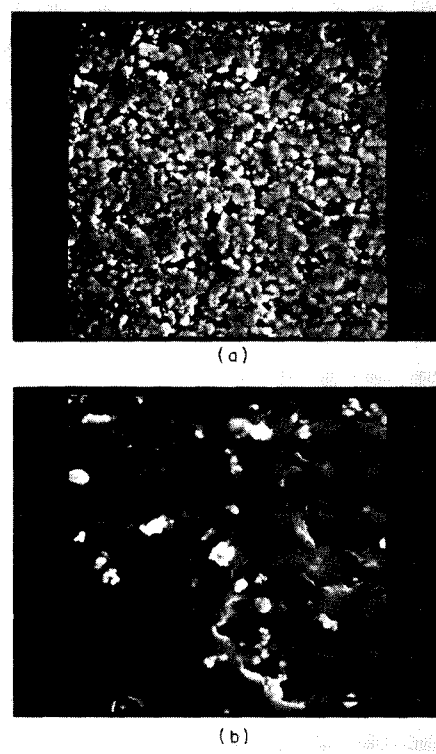

Fig. 9. Copper(II) responses of pressed pellet electrodes treated in different ways. (1) Soaked in Ce(IV) solution for 30 min; (2) soaked in EDTA solution for 120 min; (3) soaked in $HClO_4$ solution for 120 min; (4) soaked in ascorbic acid solution for 80 min; (5) untreated electrode.

Fig. 10. Scanning electron micrographs of CuS pressed pellet electrode membranes at 4000 × magnification. (a) Pressed pellet; (b) silicone rubber.

the precipitate particles are clearly dispersed homogeneously. Similar homogeneous distribution was apparent from the "element-specific" pictures of copper and sulphur obtained with an electron microprobe analyzer.

The distribution of oxygen on the surface of an electrode membrane pressed from a copper sulphide precipitate treated in air was established by scanning the surface with an electron microprobe. The scans illustrated in Fig. 11 show that the oxygen is present on the surface in islets. In Fig. 11(a) the dark spots indicate the presence of light elements. In the oxygen-specific scan (Fig. 11b), the light spots indicate the presence of oxygen. In the copper-specific scan (Fig. 11c), the dark spots correspond to the light spots on the oxygen-specific micrograph. The precipitate treated in air obviously contains a considerable amount of sulphate, as was confirmed by the x-ray valence band spectrum (Fig. 12) and by the results of the thermo-analytical investigations.

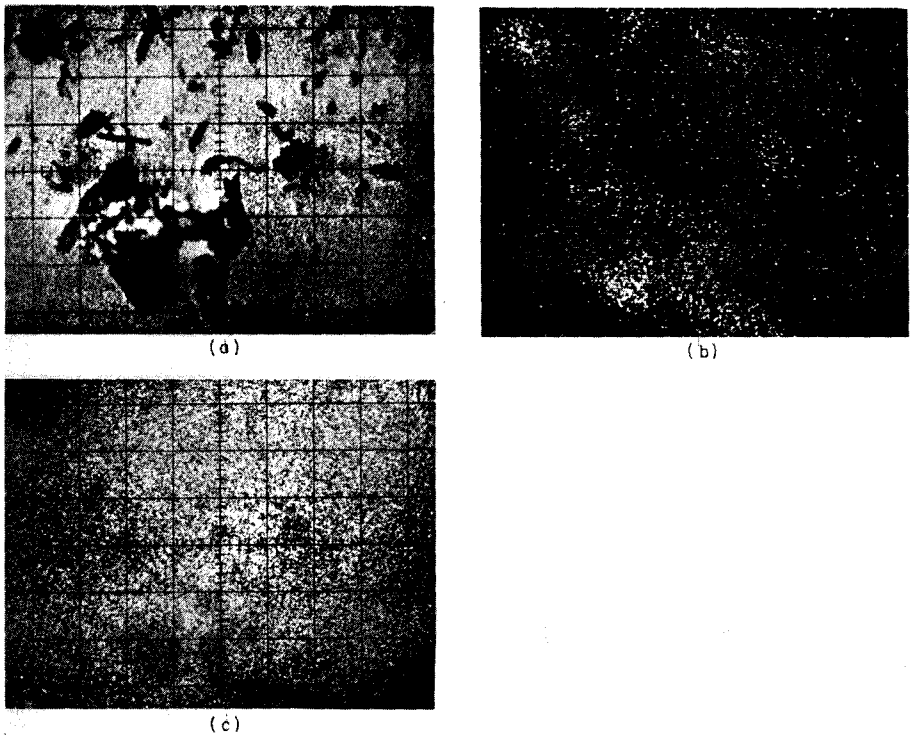

Fig. 11. Micrographs of CuS pressed pellet electrode membranes with an electron probe analyzer at 500 × magnification. (a) Back-scattered electron image of CuS membrane; (b) oxygen distribution image; (c) copper distribution image.

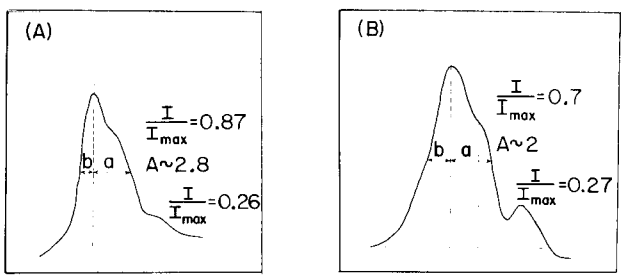

Fig. 12. X-ray valence band spectra (O $K\alpha$) of copper compounds. (A) oxygen compound on CuS pellet; 20 keV, 1.0 μA, RAP crystal; asymmetry number = a/b = 2.8. (B) $CuSO_4$ standard; 10 keV, 1.0 μA, RAP crystal; a/b = 2.

The composition of the surface layer of the pressed pellets of copper sulphide was also studied by x-ray photoelectron spectroscopy. Pellets were examined in the original state, after oxidation with potassium permanganate and after reduction with ascorbic acid following oxidation. As photoelectrons can escape only from very short distances (ca. 30 Å) beneath the surface, the technique is valuable for surface studies.

Typical spectra of S 2*p* photoelectrons are shown in Fig. 13. In all cases, copper sulphate and copper(II) sulphide were present, but they occurred in different amounts. In order to determine the thickness and the kind of the sulphate surface layer for electrodes treated with permanganate, experiments were done with argon-ion etching, and by the variable take-off angle technique [13, 14]. Figure 14 gives an impression of the reduction of the sulphate signal after argon-ion treatment of the sample surface for 5 min and 10 min. This experiment provides evidence for a thin continuous superficial layer of sulphate. A model based on thick separate particles of sulphate on the sulphide does not hold. The thickness of the sulphate layer can be estimated from Fig. 15; the sulphide signal was measured at 20 different take-off angles. A least-squares fit leads to the reduced thickness D/L value of 0.26 (where D is the thickness of sulphate plus the contamination layer, and L is the mean free path of the photoelectrons). If L is assumed to be 30 Å, the total thickness is about 8 Å, which means that the sulphide is coated with a monolayer of

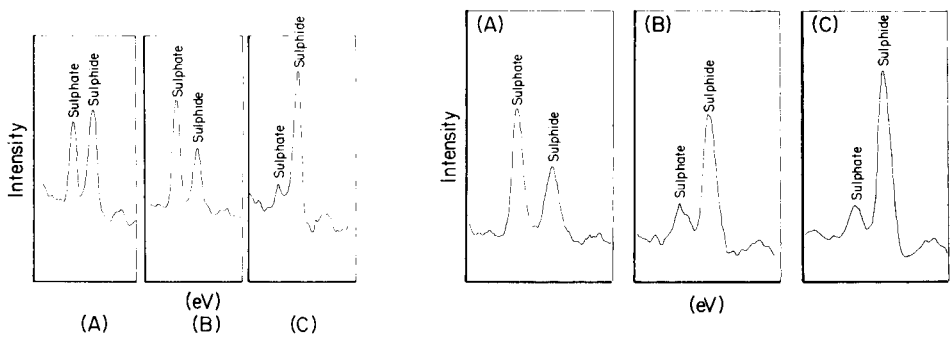

Fig. 13. Photoelectron spectra. Mg $K\alpha$ x-ray, 6 keV, 40 mA, 240 W, 1.3×10^{-4} Pa. (A) Untreated CuS electrode; (B) electrodes treated in $KMnO_4$; (C) after treatment with $KMnO_4$ and then ascorbic acid.

Fig. 14. Photoelectron spectra of CuS electrode surfaces, without argon-ion etching (A) and with etching for 5 min (B) and 10 min (C).

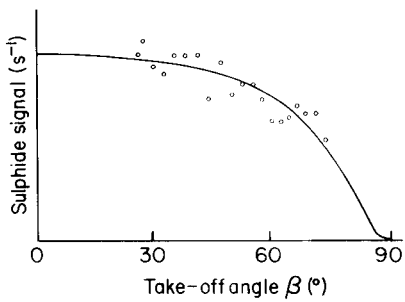

Fig. 15. Determination of the thickness of the sulphate layer by application of the variable take-off angle technique.

sulphate. Whereas even untreated electrodes contain some sulphate, after regeneration with ascorbic acid only a weak sulphate signal can be observed (see Fig. 13).

Conclusion

The chemical composition studies show that the electro-active material of the copper(II)-selective electrodes developed earlier is copper(II) sulphide precipitate. The thermoanalytical investigations of the precipitate and the surface morphology studies of pressed pellet copper(II) sulphide electrodes show that copper sulphate may also be present in small amounts.

Strong oxidants destroy the copper(II)-sensitivity of the electrode and simultaneously the surface morphology of the membrane changes; copper sulphate is formed on the surface in a thickness of one monolayer. Regeneration in ascorbic acid solution restores the copper(II) response of the electrode, the copper sulphate on the surface being eliminated. These results draw attention to the fundamental importance of the surface state — morphology — of electrode membranes in studies of the electrochemical behaviour of precipitate-based ion-selective electrodes.

The authors are indebted to Drs. F. Paulik and J. Paulik for providing the thermoanalytical results.

REFERENCES

1 J. Pick, K. Tóth and E. Pungor, Anal. Chim. Acta, 61 (1972) 169.
2 J. Pick, K. Tóth and E. Pungor, Anal. Chim. Acta, 65 (1973) 240.
3 M. Fayez El-Taras, E. Pungor and G. Nagy, Anal. Chim. Acta, 82 (1976) 285.
4 J. Pick, K. Tóth and E. Pungor, paper presented at IUPAC International Symposium on Selective Ion-Sensitive Electrodes, UWIST, Cardiff, April 1973.
5 G. Johansson and K. Edström, Talanta, 19 (1972) 1623.
6 E. H. Hansen, C. G. Lamm and J. Růžička, Anal. Chim. Acta, 59 (1972) 403.
7 M. Koebel, Anal. Chem., 46 (1974) 1559.
8 F. G. K. Baucke, Fresenius Z. Anal. Chem., 282 (1976) 105.
9 J. Gulens and B. Ikeda, Anal. Chem., 50 (1978) 782.
10 M. H. Sorrentino and G. A. Rechnitz, Anal. Chem., 46 (1974) 943.
11 H. Malissa, M. Grasserbauer, E. Pungor, K. Tóth, M. K. Pápay and L. Pólos, Anal. Chim. Acta, 80 (1975) 223. (Part 1).
12 J. Pick, Ph.D. Thesis, Technical University, Budapest, 1972.
13 M. F. Ebel, Habilitationsschrift, Technische Hochschule Wien, 1977; J. Electron. Spectrosc. Relat. Phenom., 14 (1978) 287.
14 R. J. Baird and C. S. Fadley, J. Electron Spectrosc. Relat. Phenom., 11 (1977) 39.

Analytica Chimica Acta, 109 (1979) 291—305
© Elsevier Scientific Publishing Company, Amsterdam — Printed in The Netherlands

COMPARISON BETWEEN MEASURED AND CALCULATED CONCENTRATIONS OF CALCIUM IONS IN BUFFERS

OLE SCHARFF

Department of Clinical Physiology, The Finsen Institute, DK-2100 Copenhagen (Denmark)

(Received 15th December 1978)

SUMMARY

Concentrations of ionic calcium found by careful calculation from stability constants (corrected for temperature and ionic strength) and by direct measurement with a calcium-selective electrode are compared. The two methods give almost identical results in several calcium buffers in the range pCa 3.5—7.2. In series of calcium buffers at given pH values, two calcium-chelating ligands (EGTA and NTA) were used. In these calcium buffers, which were adapted for use in biological experiments, the two methods led to almost identical pCa values, even in the presence of magnesium and adenosine triphosphate. The greatest discrepancies between results from the two methods were observed at calcium/ligand concentration ratios of 0.9—1.0. Under these conditions calculations, in contrast to electrode measurements, led to calcium ion concentrations which were up to 7 times too low, judging from measurements of the enzyme activities of a calcium-sensitive ATPase. The results demonstrate that the calcium electrode is essential for reliable determination of the actual calcium ion concentration in complex calcium buffers.

The increasing evidence of low physiological calcium ion concentrations in the cytoplasm of various biological tissues makes experiments at the pCa level of 4—8 important and necessitates the availability of solutions with well-defined calcium concentrations in this range. Such calcium buffer solutions consist of a calcium salt, a calcium-chelating ligand in excess, and a pH buffer. The calcium ion concentration of the buffer may be calculated by use of stability constants taken from the literature.

In the following sections, the calculations of calcium ion concentrations are compared with the results of direct measurements by a calcium-selective electrode which permits determination of concentrations down to about 10^{-7} M [1]. Further, the electrode measurements in different calcium buffers are compared with the responses of a calcium-sensitive enzyme to the same calcium buffers.

THEORY

Conditional stability constants

The main reaction involving the calcium ion and the calcium-chelating ligand L is defined as shown in Table 1. Under physiological conditions, the

TABLE 1

Logarithmic stability constants for complexes of reactants involved in main reaction and side reactions
(The constants (M^{-1}) are valid at 25°C and ionic strength of 0.1 M. NTA and EGTA refer to nitrilotriacetic acid and ethyleneglycol bis(β-aminoethylether)-*N*,*N*′-tetraacetic acid, respectively, and ATP refers to adenosine 5′-triphosphate. Numbers in square brackets are references.)

Equilibrium reaction	Stability constant	Logarithmic stability constants	
		L = NTA^{3-}	L = $EGTA^{4-}$
Main reaction			
Ca + L ⇌ CaL	K_{CaL}	6.40 [5]	10.90 [7]
Side reactions related to the chelating ligand L			
H + L ⇌ HL	K_{HL}	9.75 [6]	9.54 [7]
H + HL ⇌ H_2L	K_{H_2L}	2.63 [6]	8.87 [7]
H + H_2L ⇌ H_3L	K_{H_3L}	1.66 [6]	2.65 [8]
H + H_3L ⇌ H_4L	K_{H_4L}	—	2.0 [8]
Mg + L ⇌ MgL	K_{MgL}	5.36 [6]	5.2 [2—4]
H + MgL ⇌ MgHL	K^{H}_{MgHL}	—	7.7 [2—4]
		Z = ATP^{4-} [9]	Z = PO_4^{3-} [2]
Side reactions related to calcium			
Ca + Z ⇌ CaZ	K_{CaZ}	3.97	—
Ca + HZ ⇌ CaHZ	K^{Ca}_{CaHZ}	2.13	1.7
H + Z ⇌ HZ	K_{HZ}	6.53	11.7
H + HZ ⇌ H_2Z	K_{H_2Z}	4.06	6.9
H + H_2Z ⇌ H_3Z	K_{H_3Z}	—	2.0
Mg + Z ⇌ MgZ	K_{MgZ}	4.22	—
Mg + HZ ⇌ MgHZ	K^{Mg}_{MgHZ}	2.24	1.9

reactants participate in side reactions as shown in Table 1. The logarithmic stability constants [2—9] for all the complexes considered are also given in Table 1. The impact of the side reactions can be described by α-coefficients (cf. [2, 10, 11]) which are defined as

$$\alpha_{Ca} = [Ca']/[Ca] = ([Ca] + [CaZ] + [CaHZ])/[Ca] \quad (1)$$

$$\alpha_{L} = [L']/[L] = ([L] + \sum_{n} [H_nL] + [MgL] + [MgHL])/[L] \quad (2)$$

Here, [Ca] and [L] are the concentrations of free calcium ions and free ligand L, and [Ca′] and [L′] are the concentrations of all calcium and L not bound to L and calcium, respectively. H_nL refers to the proton-ligand complexes (cf. Table 1). The α-coefficients can be calculated from the stability constants:

$$\alpha_{Ca(Z)} = 1 + [Z]\,K_{CaZ} + a_H\,[Z]\,K_{CaZ}\,K^{H}_{CaHZ} \quad (3)$$

$$\alpha_{L(H)} = 1 + a_H\,K_{HL} + a_H^2\,K_{HL}\,K_{H_2L} + \cdots + a_H^n\,K_{HL} \cdots K_{H_nL} \quad (4)$$

$$\alpha_{L(Mg)} = 1 + [Mg]\,K_{MgL} + a_H\,[Mg]\,K_{MgL}\,K^{H}_{MgHL} \quad (5)$$

where a_H refers to the hydrogen ion activity. The stability constants K^H_{MHZ} (M refers to Ca or Mg) are derived from $K_{HZ}\, K^M_{MHZ}/K_{MZ}$. The total α-coefficient of L is $\alpha_L = \alpha_{L(H)} + \alpha_{L(Mg)} - 1$, and correspondingly is $\alpha_{Ca} = \alpha_{Ca(Z)}$ if Z is the only ligand, other than L, which binds a significant part of the total calcium. In all the present calculations, $\alpha_{CaL} = 1$, as neither the NTA nor the EGTA complex of calcium binds hydrogen or other reactants to a measurable extent.

The equilibrium between calcium ions and the calcium-chelating ligand L in the presence of interfering reactants may now be expressed by the conditional stability constant, K'_{CaL}, as defined [2, 11] by

$$K'_{CaL} = [CaL']/[Ca'][L'] = K_{CaL}\, \alpha_{CaL}/\alpha_{Ca}\, \alpha_L = K_{CaL}/\alpha_{Ca}\, \alpha_L \qquad (6)$$

which can be calculated for any given pH and concentrations of magnesium and ligand Z.

Calculation of pCa

From the definitions in eqns. (1), (2) and (6) it follows that

$$[CaL'] = [CaL] = Ca_t - [Ca'] \qquad (7)$$

$$[L'] = \alpha_L\, [L] = L_t - [CaL] = L_t - Ca_t + [Ca'] \qquad (8)$$

where Ca_t and L_t are the total concentrations of calcium and ligand L. By inserting eqns. (7) and (8) into eqn. (6), [Ca'] may be calculated from the quadratic equation

$$[Ca']^2 + (L_t - Ca_t + 1/K'_{CaL})\, [Ca'] - Ca_t/K'_{CaL} = 0 \qquad (9)$$

From eqn. (1) it follows that $[Ca] = [Ca']/\alpha_{Ca}$. Therefore pCa (= $-\log [Ca]$) can be calculated from eqn. (9) and is referred to as pCa_{calc}. Furthermore, it follows from eqn. (6) that

$$pCa = \log (K_{CaL}/\alpha_L) + \log ([L']/[CaL']) \qquad (10)$$

which corresponds to the equation for a pH buffer. Equation (10) shows that small changes in $\log \alpha_L$ change pCa by the same amount.

pCa in the calibrating calcium buffers. In the buffers used (cf. Experimental section) magnesium ions and competing calcium-chelating ligands are absent. Consequently, the calculation of pCa can be made from eqn. (9) combined with the calculation of $\alpha_{L(H)}$ from the stability constants and the measured values of a_H (= 10^{-pH}), cf. eqn. (4), since $\alpha_{L(Mg)} = \alpha_{Ca} = 1$. In the presence of interfering reactants other than hydrogen ions, the calculation of pCa is more complex.

Effect of interfering reactants on calculation of pCa. In the presence of magnesium ions or a competing calcium-chelating ligand Z, the calculations of α_L and α_{Ca} include the concentrations of uncomplexed magnesium ions and Z, cf. eqns. (3) and (5). Setting the total concentrations of added magnesium and Z-ligand to $Mg_t = [Mg] + [MgL] + [MgHL] + [MgZ]$ and $Z_t = [Z] + \Sigma_n\, [H_nZ] + [CaZ] + [MgZ]$, respectively, eqns. (11) and (12) may be derived for $Z = ATP^{4-}$ (cf. Table 1). The complexes MgHZ and CaHZ occur in

small amounts compared to MgZ and CaZ and can be neglected in the calculations, as the pH exceeds the log K^{H}_{MHZ} values by more than 2.

$$[Mg] = Mg_t/(1 + [L]\,K_{MgL} + a_H\,[L]\,K_{MgL}\,K^{H}_{MgHL} + [Z]\,K_{MgZ}) \quad (11)$$

$$[Z] = Z_t/(\alpha_{Z(H)} + [Ca]\,K_{CaZ} + [Mg]\,K_{MgZ}) \quad (12)$$

$\alpha_{Z(H)}$ is calculated analogously to $\alpha_{L(H)}$, cf. eqn. (4); α_L, α_{Ca}, and [Ca] may now be calculated by iterations, combining eqns. (3)—(5), (8), (9), (11), and (12), leading to pCa_{calc}. Expressions like eqns. (11) and (12) may also be derived for $Z = PO_4^{3-}$.

Correction of stability constants

The stability constants necessary for calculation of pCa in the investigated calcium buffers are given in Table 1. The constants are mixed constants, i.e., the activity term of hydrogen ions is used together with the concentration term for the other ions [2]. Most of the constants were selected from Sillén and Martell's compilations [3, 4]. However, all these constants have to be corrected in order to allow calculations at different temperatures and ionic strengths.

Temperature correction. Correction for the temperature T (in Kelvin) may be done by the equation, $\ln K = (T\Delta S^0 - \Delta H^0)/RT$ (derived from $\Delta G^0 = \Delta H^0 - T\Delta S^0 = -RT \ln K$), provided that the values of both enthalpy (ΔH^0) and entropy (ΔS^0) are available for the equilibrium in question; K is the stability constant and R the gas constant.

In Table 2, log K_{CaL} (cf. Table 1) has been calculated for both NTA and EGTA, by using the values for ΔH^0 and ΔS^0 given by Hull et al. [5] and Boyd et al. [7]. The values of log K_{CaL} for NTA [5] differed by less than 0.05 from those determined by Hughes and Martell [6] at the temperatures concerned. Similar corrections were made for K_{HL} and K_{H_2L} (see Table 2).

TABLE 2

Logarithmic stability constants at various temperatures and ionic strengths
(The correction of log K for ionic strength is valid at 20°C but may be used at the other temperatures without significant error.)

Ligand	Stability constant	Log K at I = 0.1 M at temperature (°C)					Correction of log K for transition from I = 0.1 M to I = 0.03 M
		0	10	20	30	40	
NTA	K_{CaL}	6.49	6.45	6.42	6.38	6.35	+0.43
	K_{HL}	10.06	9.92	9.80	9.70	9.60	+0.19
	K_{H_2L}	2.63	2.63	2.62	2.64	2.66	+0.11
EGTA	K_{CaL}	11.43	11.21	11.00	10.80	10.62	+0.43
	K_{HL}	9.97	9.79	9.62	9.46	9.32	+0.18
	K_{H_2L}	9.20	9.06	8.93	8.81	8.70	+0.12

Ionic strength correction. The stability constants may be corrected for ionic strength in a way similar to that shown in eqn. (13)

$$K_{CaL(o)} = K_{CaL(p)} \, (\gamma_{Ca(o)} \, \gamma_{L(o)} \, \gamma_{CaL(p)})/(\gamma_{Ca(p)} \, \gamma_{L(p)} \, \gamma_{CaL(o)}) \qquad (13)$$

where o and p designate two different ionic strengths, and γ_{Ca}, γ_{L} and γ_{CaL} are the activity coefficients of the reactants participating in the main reaction, Ca + L $\rightleftharpoons$ CaL (cf. Table 1).

The activity coefficients may be calculated from the Debye—Hückel formula, $-\log \gamma_i = Az_i^2 \, I^{\frac{1}{2}}/(1 + Ba_i I^{\frac{1}{2}})$, where z_i is the valency of the ion in question, I is the ionic strength, A and B are constants at a fixed temperature [12], and a_i is the effective diameter of the hydrated ion in Ångstrom (0.1 nm) i.e., 0.6 nm for the calcium ion and 0.8 nm for the magnesium ion [13]. The values of a_i were estimated as 0.9 and 0.5 nm for the various molecular species of EGTA and NTA, respectively, based on a_i values of similar molecules, i.e., EDTA [14] and citric acid [13], respectively. The value of a_i was estimated as 1.1 nm for the molecular species of adenosine 5'-triphosphate (ATP), (cf. [13, 15]).

Calculation of activity coefficients from the Debye—Hückel formula is, of course, an approximation. However, the following example indicates that the use of eqn. (13) combined with the calculated activity coefficients may well lead to a satisfactory correction of stability constants. Hughes and Martell [6] determined the value of log K_{CaL} for NTA at $I \rightarrow 0$ and 20°C as 7.61 which may be corrected by eqn. (13) to 6.37 at I = 0.1 M. This corrected value is in good accordance with the value of 6.42 (cf. Table 2) determined at I = 0.1 M by Hull et al. [5].

In Table 2 some corrections for ionic strength of various stability constants are given. Similar corrections were made for other stability constants from Table 1.

EXPERIMENTAL

Calibrating calcium buffers

All chemicals were of analytical-reagent grade, and water redistilled immediately before use was employed throughout.

pCa values of all the investigated calcium buffers were measured by a calibrated calcium-selective electrode. The electrode was calibrated with different solutions having well-defined pCa values. Three types (A—C) of solutions were prepared [1]. (A) Solutions with pCa values in the range 7.3—4.8 were obtained with 47 mM sodium tetraborate decahydrate solutions containing 1—4 mM nitrilotriacetic acid (NTA) and 0.1—1.0 mM calcium nitrate, providing Ca_t/L_t ratios from 0.02 to 0.9, with pH in the range 9.0—9.2. (B) Solutions with pCa values in the range 4.6—3.6 were obtained with solutions of 40 mM maleic acid and 99 mM sodium hydroxide containing 11—14 mM NTA and 1—4 mM calcium nitrate, providing Ca_t/L_t ratios from 0.1 to 0.3, with pH in the range 6.4—6.8. (C) Solutions with pCa 3.0—2.0 were obtained with

100 mM sodium nitrate solutions containing 1—10 mM calcium nitrate. The ionic strength was about 0.1 M.

To permit measurement of pCa at lower ionic strengths, an analogous set of calibrating buffers with ionic strength about 0.03 M was prepared by reducing the concentration of the pH-buffering substance or sodium nitrate.

The pH (= pa_H) was measured with a precision of 0.01 in order to ensure reliable conditional stability constants and pCa_{calc} values. The pH values of the pCa buffers of types (A) and (B) remained nearly constant for several months; the pH could be reproduced with a standard deviation of 0.02 pH units without readjustment. There was no indication of precipitation of calcium carbonate in the calcium buffers, not even at pH 9.

The pCa value of each calibrating buffer was calculated from eqn. (9). The low calcium-binding effect of maleic acid [3] is of minor importance and can be neglected in the calculations. The mV readings obtained by the electrode measurements of the calibrating buffers were plotted vs. the corresponding pCa_{calc} values (see Fig. 1). The points (mV vs. pCa) could be fitted by a straight regression line in the pCa range 7.3—2.0, in agreement with the equation (derived from the Nernst equation):

$$E = E_0 + \frac{2.303RT}{2F} \log a_{Ca} = E_0 + \beta \log \gamma_{Ca} + \beta \log [Ca] \qquad (14)$$

where a_{Ca} refers to calcium ion activity. The slope β of the straight line depicting the electrode potential E (mV) vs. log [Ca] is determined by the temperature T (K), the gas constant R, and the Faraday constant F; E_0 is a temperature-dependent constant. From these calibration curves pCa values corresponding to measured mV values could be read with a standard deviation of 0.08 pCa units (based on the variation of the pCa_{calc} values around the regression line in 8 calibration curves).

Changes in pH, temperature, and ionic strength (I) caused changes of pCa_{calc} which were, respectively, 0.01—0.02 pCa units per 0.01 pH units, maximally 0.01 pCa units per degree, and 0.02—0.03 pCa units per 0.01 M change in I at the 0.1 M level (at the 0.03 M level the corresponding change was 0.04—0.06 pCa units).

In the following sections, the term pCa_{obs} refers to pCa values determined from mV measurements in buffers and a calibration curve. In a series of 27 calcium buffers in the pCa range 6.6—4.5, repeated measurements provided a standard deviation of pCa_{obs} of 0.07 pCa units (a total of 97 measurements).

A linear regression analysis of several calibration curves, determined during several months, showed that the different curves were parallel ($P > 0.5$) but not identical ($P < 0.001$). The levels of the calibration curves shifted by up to 20 mV. For that reason the calcium electrode had to be calibrated every day. The mean slopes of several calibration curves, corresponding to different sets of conditions, are shown in Table 3. The deviations of the observed slopes from the theoretical values are negligible for the present purpose. In general, it can be concluded that the buffers are very suitable for calibration of the calcium electrode, as suggested previously by Růžička et al. [1].

TABLE 3

Slopes of calibration curves depending on temperature
(The observed slopes are calculated from regression lines and given as mean ± standard error of the mean (n experiments); deviations from the theoretical slopes which are calculated from eqn. (14) are tested by Student's t test.)

Temperature (°C)	Ionic strength (M)	Slope (mV/pCa)		Significance
		Observed	Theoretical	
8	0.03	28.4 ± 0.2 (8)	27.9	$P < 0.05$
22	0.1	29.2 ± 0.2 (6)	29.3	$P > 0.5$
35	0.1	30.6 ± 0.1 (14)	30.6	$P > 0.5$

Calcium buffers for physiological experiments

For physiological experiments it is necessary to prepare calcium buffers with a given pH, as biochemical reactions depend on catalytic proteins which show optimum activity over rather narrow pH ranges. In order to prepare calcium buffers with pCa values covering the range 4—8 it is necessary to change both the Ca_t/L_t ratio and K_{CaL}/α_L (cf. eqn. (10)). K_{CaL}/α_L can be changed easily by altering pH. However, when it comes to calcium buffers for a given pH value, K_{CaL}/α_L can be changed only by shifting from one chelating ligand L to another, e.g., from NTA to EGTA.

In order to investigate the properties of calcium buffers suitable for physiological experiments, different calcium buffers containing NTA or EGTA were prepared in various combinations with pH-buffering substances.

Sodium maleate buffers. Solutions with pCa 3.7—7.2 were obtained by using 40 mM maleic acid and 95—100 mM NaOH containing 10 mM EGTA and 0.5—8.0 mM $Ca(NO_3)_2$ with pH in the range 5.9—6.7.

Tris buffer. Solutions of pCa 3.5—7.2 were obtained by using 70 mM tris-(hydroxymethyl)aminomethane (Tris · HCl, Sigma) and 20 mM NaOH containing 10 mM of either NTA or EGTA and 0.5—8.0 mM $Ca(NO_3)_2$ with pH in the ranges 7.2—9.3 (NTA) or 5.7—7.2 (EGTA).

Sodium phosphate buffer. Solutions of pCa 4.0—7.2 were obtained by using 6.7 mM sodium phosphate containing 1 mM of either NTA or EGTA and 0.02—0.9 mM $CaCl_2$ with a pH of 7.43 ± 0.07 (s.d., n = 22). The phosphate ions compete with NTA or EGTA for calcium, which leads to log α_{Ca} = 0.1. The ionic strengths of these solutions were about 0.03 M. In some experiments, 9 volumes of the solutions were mixed with 1 volume of human red blood cells which hemolyzed because of the low ionic strength [16, 17]. After mixing, the pH was 7.79 ± 0.10 (s.d., n = 32). The mixed solutions contained about 0.2 mM Mg^{2+} which originated from the cells, leading to a log $\alpha_{L(Mg)}$ value of about 1.5 (NTA) or 1.8 (EGTA) and an unchanged α_{Ca}. The occurrence of an intracellular calcium-binding buffer in human erythrocytes, which has been described quantitatively [18], caused a pCa change of 0.01 (maximum) in the mixed solutions, judging from calculations.

Tris, HEPES, and histidine—imidazole buffers with given pH. Solutions with pCa 4.5—6.6 were obtained by using 65 mM solutions of pH-buffering substance and 25 mM NaOH or NaCl containing 1 mM NTA or EGTA and 0.02—0.9 mM $Ca(NO_3)_2$ with a pH of 7.10. The pH buffer used was Tris or *N*-2-hydroxyethylpiperazine-*N'*-2-ethanesulfonic acid (HEPES), or histidine and imidazole in equimolar amounts (histidine—imidazole). In some experiments, the solutions also contained various concentrations of $MgCl_2$ and adenosine 5'-triphosphate ($Na_2 \cdot$ ATP, Sigma): 0.2 mM ATP or 1 mM $MgCl_2$ or 3 mM ATP and 4 mM $MgCl_2$ (for α_L and α_{Ca}, see Tables 5 and 6).

When magnesium was present in these buffers the concentration of free magnesium ions was about 1 mM. The magnesium sensitivity of the calcium electrode (see below) implies that pCa_{obs} values above 5.3 could not be determined at 1 mM Mg^{2+}. For that reason, pCa_{obs} was determined in the absence of Mg^{2+} and ATP in the EGTA-containing buffers, and pCa_{obs} was then corrected for the presence of Mg^{2+} and ATP by calculation. The correction was only about —0.04 pCa units because of the relatively low magnesium binding of EGTA (cf. Table 1). In addition, one of the NTA-containing buffers (Ca_t/L_t = 0.02) had to be measured without Mg^{2+} and ATP and corrected afterwards, the correction of pCa_{obs} being about —0.20 pCa units.

The pH value of 7.10 in these buffers was selected on account of the pH optimum of the calcium-sensitive enzyme used for checking the calcium ion concentrations found potentiometrically (see below). At this and higher pH values, which are commonly used in physiological experiments, the EGTA-containing calcium buffers provide only pCa values about or higher than 6. For instance, a Ca_t/L_t ratio of 0.9 provides a pCa_{calc} of 5.8 at pH 7.1 (37°C, I = 0.1 M, no Mg^{2+}). Lower pCa values can be provided by NTA-containing calcium buffers; for instance, at a Ca_t/L_t ratio of 0.1, a NTA buffer provides a pCa_{calc} value of 4.9 at pH 7.1

The examples demonstrate a discontinuity between the pCa ranges covered by the EGTA-containing and NTA-containing calcium buffers prepared at a given pH value.

In some of the prepared EGTA-containing solutions the concentration of $Ca(NO_3)_2$ was increased, leading to Ca_t/L_t ratios from 0.95 to 1.20. In this range of Ca_t/L_t, the calcium-buffering effect of EGTA is poor or even absent (cf. eqn. 10).

Calcium-sensitive enzyme

In some calcium buffers the calcium ion concentrations found potentiometrically were checked by measurement of the enzyme activity of a calcium-sensitive ATPase (ATP phosphohydrolase, E.C. 3.6.1.3). The enzyme was prepared from human erythrocytes in the native membrane-bound state in two different ways (A-membranes and B-membranes), as described previously [16, 17]. The enzyme in the A-membranes is most sensitive to calcium ions in the pCa range 4.0—5.5, and in the B-membranes to the pCa range

5.0—6.5. The enzyme activity was assayed by measuring the production of inorganic phosphate arising from the catalyzed hydrolysis of ATP, as described previously [16]. The activity was expressed as μmol min^{-1} g^{-1} or in relative units; here, the mass refers to the dry cell membrane, corrected for contaminating hemoglobin.

Instruments

The potentiometric calcium measurements were done with a F2112 calcium Selectrode and other equipment from Radiometer, Copenhagen. The reference was a calomel electrode (K401). Both electrodes were connected to a titrator (TTT 1c) supplied with scale expansion, allowing accurate mV readings (±0.1 mV). The calomel electrode was connected to a pH meter (PHM 26) together with a glass electrode (G222C), so that pH (±0.01) could be determined simultaneously with the mV readings for pCa.

The calcium Selectrode is sensitive to magnesium ions. A magnesium/calcium concentration ratio of 80 corresponds to a maximum interference of 1 mV on the Selectrode response (according to Radiometer); 1 mV corresponds to about 0.03 pCa units.

RESULTS AND DISCUSSION

Comparison of NTA and EGTA as calcium-chelating ligand

In calcium buffers containing sodium maleate and EGTA, the values of pCa_{obs} and pCa_{calc} were equal in the range pCa 3.7—7.2. Since the pCa_{obs} values are based on the pCa values of the calibrating calcium buffers which contain NTA (cf. Experimental section), the results of Fig. 2 indicate that EGTA can be used instead of NTA.

Results similar to those obtained with EGTA and maleate were obtained with calcium buffers containing EDTA and maleate (not shown), the pCa_{calc} values being calculated from the stability constants given by Bohigian and Martell [3].

Comparison of different pH buffering substances

Table 4 shows a comparison between pCa_{obs} and pCa_{calc} in calcium buffers containing EGTA and sodium phosphate. Except for one buffer, the differences between observed and calculated values are not significant. The relatively high standard deviations are mainly due to the variation of the pH values. Similar results were obtained with calcium buffers containing NTA and sodium phosphate (not shown). In these buffers, which provide a pCa range of 4.0—6.2, the average difference between pCa_{obs} and pCa_{calc} varied only from 0.04 to 0.07. The presence of 10% organic material (hemolyzed erythrocytes) did not affect the determination of ionic calcium by the calcium electrode (Table 4).

In calcium buffers containing NTA and HEPES, Tris, or histidine—imidazole, the pCa_{obs} and pCa_{calc} values were in fairly good agreement, even in the

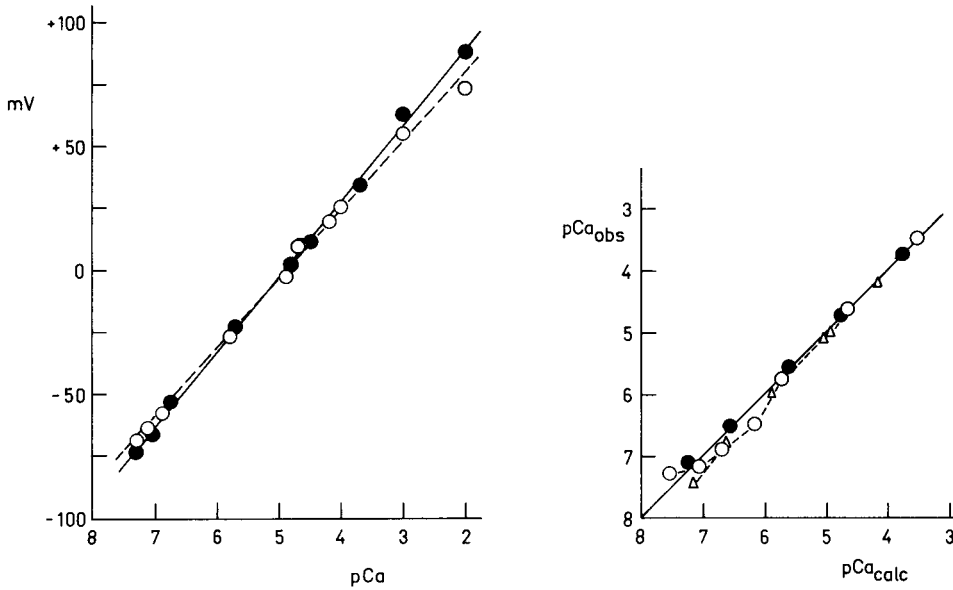

Fig. 1. Calibration curves showing mV vs. pCa_{calc} at two different ionic strengths(I). For composition of buffers, see Experimental. (•) I = 0.1 M, 35°C (the solid line was calculated by linear regression analysis, $y = -30.5x + 150.1$); (○) I = 0.03 M, 8°C (the dashed line was calculated as before, $y = -27.9x + 136.3$).

Fig. 2. pCa_{obs} vs. pCa_{calc} at 35°C in calcium buffers containing different calcium-chelating ligands and buffer substances. The buffers contained 0.5—8.0 mM $Ca(NO_3)_2$ and 10 mM EGTA or NTA in addition to either 40 mM maleic acid and 95—100 mM NaOH or 70 mM Tris and 20 mM NaOH. (•) EGTA + maleate (pH 5.9—6.7); (○) EGTA + Tris (pH 5.7—7.2); (△) NTA + Tris (pH 7.2—9.3). The points represent the means of 4—6 experiments (± s.e.m. less than point diameter). The solid line is $y = x$ (or $pCa_{obs} = pCa_{calc}$).

presence of magnesium and ATP (Table 5). The greatest discrepancy was found in histidine—imidazole in the absence of magnesium and ATP. The effect of magnesium ions was to reduce pCa, whereas ATP had the opposite effect (Table 6).

At pCa values above 6, greater deviations between pCa_{obs} and pCa_{calc} were found in calcium buffers containing HEPES, Tris, or histidine—imidazole. This is shown for Tris in Fig. 2 with both EGTA and NTA as calcium-chelating ligand.

The results suggest a difference between calcium buffers containing phosphate or maleate and those containing HEPES, Tris, or histidine—imidazole at pCa values above 6. This agrees with the findings of Ogawa [19] who found discrepancies between calculated and observed conditional stability constants for the calcium—EGTA complex using Tris, histidine, or imidazole buffer but not with phosphate or maleate buffer, when ionic calcium concentrations were measured by the murexide method. The explanation of these

TABLE 4

Observed and calculated pCa in buffers containing sodium phosphate with organic material absent or present
(In addition to $CaCl_2$, the buffers contained 1 mM EGTA and 6.7 mM sodium phosphate; pH was 7.4 in absence and 7.8 in presence of organic material (hemolyzed erythrocytes). Temperature was 8°C. The difference between the mean values of pCa_{obs} and pCa_{calc} was tested by Student's *t* test; standard deviations (s.d.) were calculated by Bartlett's test).

$CaCl_2$ in buffer (mM)	Organic material (%, v/v)	pCa_{obs}	pCa_{calc}	Significance
0.80 (n=4)	0	6.57	6.61	$P > 0.2$
0.85 (n=3)	0	6.36	6.40	$P > 0.4$
0.90 (n=6)	0	6.14	6.29	$P < 0.02$
0.80 (n=2)	10	7.25	7.18	$P > 0.5$
0.90 (n=7)	10	6.98	7.01	$P > 0.4$
	S.d.	0.20	0.15	

TABLE 5

Effect of simultaneous addition of Mg^{2+} and ATP to calcium buffers
(Buffer composition as in Fig. 3, except for the buffer substances shown, with 0.2 mM $Ca(NO_3)_2$ and 1 mM NTA. With 4 mM $MgCl_2$ + 3 mM ATP added, log α_L was 2.87 and log α_{Ca} was 0.36. Mean values of five experiments are given; differences between observed and calculated values were tested by Student's *t* test.)

Buffer substance	No addition			Mg^{2+} + ATP added		
	pCa_{obs}	pCa_{calc}	Significance	pCa_{obs}	pCa_{calc}	Significance
HEPES	4.67	4.61	$P < 0.05$	4.45	4.47	$P > 0.4$
Tris	4.59	4.59	$P > 0.5$	4.45	4.46	$P > 0.5$
Histidine—imidazole	4.72	4.59	$P < 0.01$	4.50	4.46	$P > 0.2$
S.d.	0.056			0.059		

TABLE 6

Effect of single addition of Mg^{2+} or ATP to calcium buffers
(Buffer composition as in Fig. 3, except for Mg^{2+} and ATP, with 0.2—0.5 mM $CaCl_2$ and 1 mM NTA. With 1 mM $MgCl_2$ added, log α_L was 2.71. With 0.2 mM ATP added, log α_{Ca} was 0.39. Difference between observed and calculated mean values (± s.e.m.) was tested by Student's *t* test.)

Addition	Effect of addition on pCa		Significance
	Observed	Calculated	
Mg^{2+} (n=8)	−0.37 ± 0.03	−0.24 ± 0.01	$P < 0.05$
ATP (n=3)	+0.07 ± 0.01	+0.10 ± 0.01	$P > 0.05$

discrepancies is not known. The observed discrepancy between pCa_{obs} and pCa_{calc} in calcium buffers containing Tris (Fig. 2) was found to depend on pCa and not on pH, since the pH of the buffers containing EGTA and NTA at high pCa values were about 7 and 9, respectively. The discrepancies are probably due to interference between the buffer substance and the calcium—ligand complex and not to simple binding phenomena between calcium and the buffer substance.

Calcium buffers with a given pH; checking of pCa by enzyme measurements

pCa_{obs} and pCa_{calc} were determined in three different sets of calcium buffers containing Tris, HEPES, and histidine—imidazole, respectively. The buffers covered the pCa range 4.5—6.6.

pCa_{obs} vs. pCa_{calc}. Figure 3 shows pCa_{obs} in dependence on pCa_{calc} in Tris-containing buffers. The lower curve shows that the pCa_{obs} value of the calcium buffers, of which some contained EGTA (high pCa) and others NTA (low pCa), deviate from pCa_{calc} in some regions. Consequently, the curve is not a straight line, but exhibits a characteristic break near the transition from EGTA to NTA (marked by arrows).

To check whether the discrepancies between pCa_{obs} and pCa_{calc} were due to the electrode measurements or to the calculations, the two sets of pCa values were compared with the activity of the calcium-sensitive enzyme.

Enzyme activity vs. pCa_{calc} and vs. pCa_{obs}. In Fig. 3, the middle curve shows the relative ATPase activities (B-membranes) obtained by assay in the same calcium buffers which were used to obtain the lower curve. Apart from the deflection caused by the saturating effect of ionic calcium on the enzyme, the shapes of the middle and lower curves are similar.

The plot of the enzyme activity vs. pCa_{obs} (Fig. 3, upper curve) does not show any break. Results quite similar to those obtained with Tris were found with buffers containing HEPES or histidine—imidazole (not shown). All these results suggest that the enzyme activity reflects the same variations in the calcium ion concentrations as were detected with the electrode.

The breaks in the lower and middle curves in Fig. 3 occur in the interval between the pCa ranges covered by the EGTA-containing and the NTA-containing calcium buffers. In this interval, the calcium-buffering effect of both EGTA and NTA is expected to be poor because of the high and the low Ca_t/L_t ratios, respectively (cf. eqn. 10). Nevertheless, the results indicate a good agreement between pCa_{obs} and pCa_{calc} in the NTA-containing buffers, despite Ca_t/L_t ratios as low as 0.02 and 0.05. In contrast, pCa_{obs} was lower than pCa_{calc} in the EGTA-containing calcium buffers with a Ca_t/L_t ratio of 0.9. At Ca_t/L_t ratios below 0.9, the pCa_{obs} values were in better accordance with the pCa_{calc} values (see also Table 4). Further increase in the Ca_t/L_t ratio in the EGTA-containing calcium buffers led to observed ionic calcium concentrations which were 4—7 times higher than the calculated concentrations (Table 7). In the buffers containing NTA with Ca_t/L_t ratios of 0.1 and 0.2, the observed and calculated ionic concentrations are almost equal and corre-

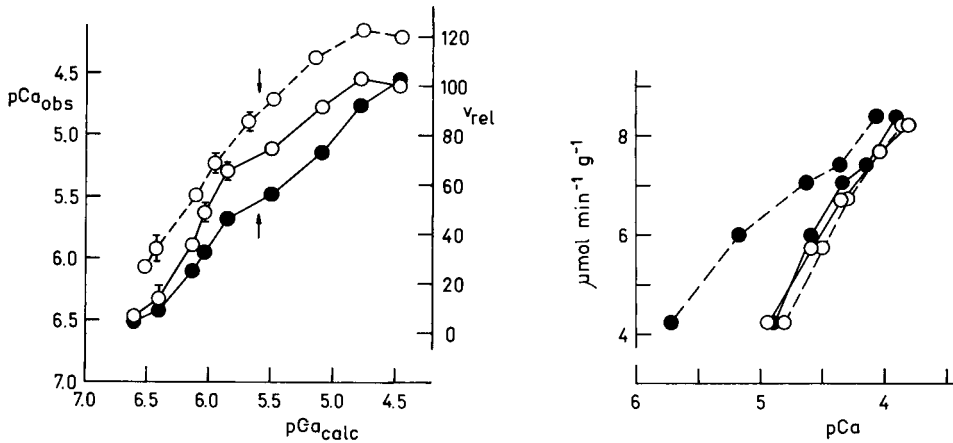

Fig. 3. Responses of calcium-selective electrode and calcium-sensitive enzyme to calcium buffers. Buffers contained either 0.6—0.9 mM $Ca(NO_3)_2$ and 1.0 mM EGTA (to the left of arrows) or 0.02—0.20 mM $Ca(NO_3)_2$ and 1.0 mM NTA (to the right of arrows) in addition to 25 mM NaCl, 4 mM $MgCl_2$, 3 mM Na_2-ATP (Sigma), and 65 mM Tris. pH was 7.1 and temperature 37°C. ATPase activity (B-membranes) was measured as production of inorganic phosphate (see Experimental). Lower curve, pCa_{obs} vs. pCa_{calc}. Middle curve, relative enzyme activity (v_{rel}) vs. pCa_{calc}. Upper curve, v_{rel} + 20 (in order to displace the curve from the former one) vs. pCa_{obs}. The points represent means of five experiments (with vertical bars referring to the standard error of the mean).

Fig. 4. Enzyme activity of calcium-sensitive ATPase (A-membranes) vs. calculated and observed pCa values in calcium buffers with different calcium/ligand concentration ratios. Buffer composition as in Fig. 3. (•) Calcium/EGTA ratio 0.95—1.20; (○) calcium/NTA ratio 0.1—0.7. Dashed lines, pCa_{calc}. Solid lines, pCa_{obs}. Single experiments.

spond to the observed ionic concentrations in the EGTA-containing buffers (Table 7).

Figure 4 demonstrates the responses of the calcium-sensitive enzyme (ATPase, A-membranes) to buffers with calcium/EGTA ratios of 0.95—1.20 and calcium/NTA ratios of 0.1—0.7. The curve depicting enzyme activity vs. pCa_{calc} in the buffers containing EGTA deviates significantly from the three other curves, indicating that the calculation of the ionic calcium concentration at the high calcium/EGTA ratios has led to erroneous results (cf. Table 7). Similar effects of high Ca_t/L_t ratios were obtained with NTA and EDTA and, in addition, at pH values lower than 7.2 (not shown).

These results show that use of calculations alone may lead to an underestimate of the ionic concentration in calcium buffers at high Ca_t/L_t ratios. This may be one of the reasons why varying values of calcium concentrations have been reported to affect single physiological responses, e.g., muscle contraction [20].

It has to be emphasized that the erroneous results of the calculations (Table 7 and Fig. 4) cannot be ascribed to wrong methods of calculation. At pH 7.0 and a calcium/EGTA ratio of 0.5, the method of calculation used

TABLE 7

Observed and calculated concentrations of ionic calcium depending on total calcium concentration in buffers
(Buffer composition as in Fig. 3 with 1 mM of EGTA (pH 7.20) or NTA (pH 7.25). Mean values ± s.e.m. of four experiments are given.)

Parameter	Calcium concentration			
	EGTA		NTA	
Total calcium (mM)	0.95	1.00	0.10	0.20
Ionic calcium (μM)				
observed	14.5 ± 1.6	27.8 ± 1.9	13.0 ± 0.6	28.2 ± 1.3
calculated	1.9 ± 0.1	6.9 ± 0.2	15.3 ± 0.1	32.0 ± 1.3

gives a pCa of about 6.7, in accordance with the calculations reviewed recently by Weber and Murray [20].

Conclusions

The results show that the electrode measurements provide values for the ionic concentrations of calcium which are in good agreement with careful calculations from stability constants. In some calcium buffers, however, the calculations lead to calcium ion concentrations which are erroneous, judging from measurements of calcium-sensitive enzyme activities. In contrast to the calculations, the results of electrode measurements in these buffers are in excellent agreement with the results of enzyme measurements. The results demonstrate that the calcium electrode is essential for reliable determinations of the actual calcium ion concentrations in calcium buffers. The electrode measurements provide security against errors arising from the calculations, provided, of course, that suitable precautions are taken against possible interferences in the electrode measurements [21].

The use of the calcium-selective electrode has the advantage of confining the necessary calculations of pCa to the calibrating buffers. The composition of the calibrating buffers can be quite simple, which facilitates calculations and reduces the possibility of errors, compared to the more complex calcium buffers used in biological experiments. The determination of pCa in complex buffers by a calibrated calcium-selective electrode is in principle analogous to the conventional pH electrode measurement.

The results of the present investigation differ in many respects from those reported recently, with the same calcium-selective electrode [22]. In contrast to the present results, Kim and Padilla [22] found an extremely low calcium-binding effect of NTA and great deviations between observed and calculated pCa in the presence of ATP, apparently because of differences in both calculations and experimental techniques.

The author thanks Dr. Elo H. Hansen, Technical University of Denmark,

for stimulating discussions and reading of the manuscript, and Dr. Bent Vestergaard-Bogind, Professor Ulrik V. Lassen and Dr. Leon Pape, University of Copenhagen, for valuable criticisms.

REFERENCES

1 J. Růžička, E. H. Hansen and J. C. Tjell, Anal. Chim. Acta, 67 (1973) 155.
2 A. Ringbom, Complexation in Analytical Chemistry, Interscience, New York, 1963.
3 L. G. Sillén and A. E. Martell, Stability Constants of Metal-Ion Complexes, The Chemical Society, Spec. Publ. No. 17, London, 1964.
4 L. G. Sillén and A. E. Martell, Stability Constants of Metal-Ion Complexes Suppl. No. 1, The Chemical Society, Spec. Publ. No. 25, London, 1971.
5 J. A. Hull, R. H. Davies and L. A. K. Staveley, J. Chem. Soc., (1964) 5422.
6 V. L. Hughes and A. E. Martell, J. Am. Chem. Soc., 78 (1956) 1319.
7 S. Boyd, A. Bryson, G. H. Nancollas and K. Torrance, J. Chem. Soc., (1965) 7353.
8 G. Anderegg, Helv. Chim. Acta, 47 (1964) 1801.
9 M. M. Taqui Kahn and A. E. Martell, J. Am. Chem. Soc., 88 (1966) 668.
10 G. Schwarzenbach, Complexometric Titrations, Interscience, New York, 1957.
11 E. H. Hansen, C. G. Lamm and J. Růžička, Anal. Chim. Acta, 59 (1972) 403.
12 R. G. Bates, Determination of pH, J. Wiley, New York, 1964.
13 J. Kjelland, J. Am. Chem. Soc., 59 (1937) 1675.
14 J. L. Hall, P. R. Wilkinson and J. A. Gibson, Proc. West. Va. Acad. Sci., 36 (1964) 87.
15 D. B. Boyd and W. N. Lipscomb, J. Theor. Biol., 25 (1969) 403.
16 O. Scharff, Biochim. Biophys. Acta, 443 (1976) 206.
17 O. Scharff and B. Foder, Biochim. Biophys. Acta, 509 (1978) 67.
18 H. G. Ferreira and V. L. Lew, Nature, 259 (1976) 47.
19 Y. Ogawa, J. Biochem. (Tokyo), 64 (1968) 255.
20 A. Weber and J. M. Murray, Physiol. Rev., 53 (1973) 612.
21 J. M. Grima and M. J. D. Brand, Clin. Chem., 23 (1977) 2048.
22 Y. S. Kim and G. M. Padilla, Anal. Biochem., 89 (1978) 521.

Analytica Chimica Acta, 109 (1979) 307—317
© Elsevier Scientific Publishing Company, Amsterdam — Printed in The Netherlands

POTENTIOMETRIC DETERMINATION OF SULFUR IN WATERS, CHEMICALS, IRON, STEEL AND FLY ASH WITH A CADMIUM SULFIDE MEMBRANE ELECTRODE

D. CHAKRABORTI* and F. ADAMS

Department of Chemistry, University of Antwerp (U.I.A.), 2610 Wilrijk (Belgium)

(Received 12th March 1979)

SUMMARY

Hydrogen sulfide is generated from sulfur compounds in the samples by reduction with hydrogen iodide—sodium hypophosphite—acetic acid mixture. After absorption in sodium hydroxide, sulfide is titrated with lead nitrate solution, the equivalence point being detected potentiometrically with a cadmium sulfide membrane electrode. The method is applied to the determination of sulfur in sea water, river water, tap water, deionized water, distilled—deionized water, iron, steel and analytical-grade chemicals. Several methods (Schöniger combustion, acid digestion and fusion) are compared for the determination of total sulfur in fly ash; acid digestion prior to reduction is most satisfactory. The amounts of water-soluble sulfur compounds in fly ashes are reported.

The use of a silver sulfide membrane electrode has already been reported for selective determination of different sulfur compounds [1]. The principle followed was to generate hydrogen sulfide from sulfur compounds by treatment with a reducing mixture consisting of hydrogen iodide—sodium hypophosphite—acetic acid, absorb hydrogen sulfide in sodium hydroxide and titrate with lead nitrate to a potentiometric end-point. This method was rapid and free of interferences from most common anions and cations. However, it appeared during its exploitation that only ca. 96% of the sulfur was recovered from many samples. The incomplete recovery was thought to be due to the formation and subsequent loss of small amounts of sulfur dioxide during the reaction of the reducing mixture with sulfur compounds. The conditions which were maintained for the reduction [1], i.e. rapid removal of hydrogen sulfide by nitrogen gas, highly acidic conditions, a high ratio of iodide to iodine, a low water activity and high temperature, favour the reduction of the sulfur compounds to hydrogen sulfide, but even in these conditions the possibility of loss of partially reduced sulfate as sulfur dioxide cannot be ignored [2] in a single reducing flask apparatus.

The method described here is based on the same principles as the earlier method [1] with the following changes to insure complete recovery. A second vessel with reducing reagent is added so that the small amount of sulfur dioxide coming over with hydrogen sulfide from the first stage is completely reduced to hydrogen sulfide in the second vessel. A cadmium sulfide

membrane electrode is used instead of the silver sulfide electrode because the sensitivity of the latter electrode deteriorates in sodium hydroxide solution after long periods of use.

The modified apparatus and procedure are applied to the determination of sulfur in sea water, river water, tap water, deionized water, distilled—deionized water, sulfate impurities in pure laboratory chemicals, iron, steel and fly ash.

Detailed studies of sulfur compounds and total sulfur in aerosols have been described [3—11]; results for fly ash samples are not generally available. Moreover, it has been reported [12] that there are no significant differences between total and water-soluble sulfur in ambient aerosols. In the case of fly ash, although most of the sulfur compounds are water-soluble, about 30% is water-insoluble. This paper also deals with the determination of total sulfur in fly ash after destruction by various methods and the degree of solubility of the sulfur compounds present in fly ash, in water, alkali, acid, acid mixture and in the final residue.

EXPERIMENTAL

Apparatus

A Radiometer PHM 64 millivoltmeter was used with an Orion model 94-48A cadmium electrode and a Tacussel double-junction $Hg/HgO/OH^-$ reference electrode with 1 M sodium hydroxide in the outer compartment. For titration, a Radiometer ABU-II automatic burette was used with a potentiometric recorder. Oxygen flask combustions were done with a Heraeus Mikro K Schöniger apparatus [13]; For x-ray fluorescence measurements, an energy-dispersive instrument with secondary target set-up was used, consisting of a Kevex 0810 system, a Siemens Kristalloflex 2 generator and Northern NS 720 multichannel analyzer. A filtering unit (Gelman Instruments No. 4700) was employed with Nuclepore filters (47-mm diameter, 0.4-μm pore size). Figure 1 shows the apparatus used for the hydrogen sulfide generation and evolution.

Reagents

All chemicals were of analytical-reagent grade. The reducing mixture of hydrogen iodide (57%, d = 1.7), acetic acid (98%) and sodium hypophosphite was prepared as described earlier [1]. The lead nitrate was standardized by the EDTA method with xylenol orange indicator and normally used after dilution at a concentration of 0.327 g Pb l^{-1}. The standard sulfate solution (1 g l^{-1}) was prepared from potassium sulfate previously dried at 125°C. More dilute solutions were prepared by suitable dilution. Distilled—deionized water was used for all experiments.

General procedure

Solid samples are placed directly in the 25-ml distillation flask (A). Liquid samples are first evaporated to dryness ina distillation flask at about 100°C,

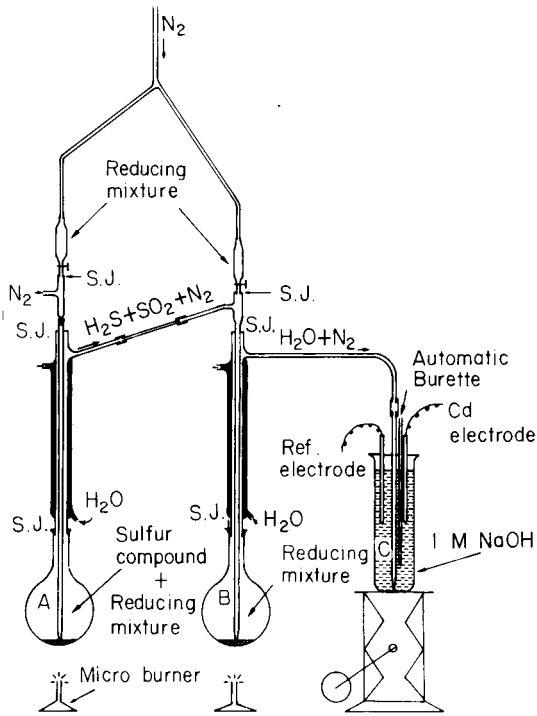

Fig. 1. Apparatus for hydrogen sulfide evolution.

before the evolution apparatus is assembled. The reducing mixture (3—4 ml) is added to each of flasks A and B. Flask B is heated first and after 2—3 min flask A is also heated. Nitrogen is passed at 2—3 bubbles per second through the absorption vessel (C) which contains about 50 ml of 1 M sodium hydroxide. The potential increases rapidly when flask A is heated and after some time becomes stable. The stabilization time depends on the form in which sulfur is initially present. For slightly soluble sulfates, the hydrogen sulfide evolution and potential stabilization takes up to a maximum of 30 min.

The tip of the autoburette remains well immersed in the sodium hydroxide solution. When the potential has stabilized, lead nitrate titrant is added in the usual way, and the titration curve is recorded. The equivalence point is evaluated graphically from a second derivative curve or by a linearization procedure [14]. These methods give similar results, but the former was preferred.

Determination of sulfur in waters

Sea or river water contains variable amounts of suspended particles. Samples are filtered and 1 ml of concentrated hydrochloric acid is added per litre of water. As natural waters usually contain significant concentrations of sulfate, dilution may be required depending on the titrant strength.

An aliquot of the water is evaporated in the generating flask below 100°C in an oven, and the sulfur content is measured by the general procedure.

As the sulfur or sulfate concentrations of deionized and distilled—deionized water is very low, preconcentration is needed. This is done by evaporating 1 l of water to 100 ml on a hot plate at about 100°C in a covered beaker. An aliquot of the sample is then analyzed by the standard addition method described below for iron and steel.

Determination of sulfate impurities in analytical-grade chemicals

Samples of 0.1—1 g, according to sulfate content, are weighed into the generating flask, and the general procedure is applied. If the titration value is too low for direct evaluation even on 1-g samples, a standard addition method is preferable to diluting the titrant.

Determination of sulfur in iron and steel

The sulfur content of powdered iron and steel samples can sometimes be determined directly without prior dissolution in acids, but this is not satisfactory for all standard steels. Pretreatment can be done by two procedures.

Method A. About 1.0 g of sample is digested with 15—20 ml of concentrated nitric acid in a 200-ml beaker on a hot plate. If dissolution is incomplete after some time, concentrated hydrochloric acid is added as required. After complete dissolution, 100—150 mg of sodium chloride is added and the solution is evaporated almost to dryness. Then 10 ml of concentrated hydrochloric acid is added and evaporated nearly to dryness; this operation is repeated. Finally the residue is treated with dilute 0.1 M hydrochloric acid and quantitatively transferred to a volumetric flask. A known aliquot is placed in the hydrogen sulfide generating flask and evaporated, and the sulfur is determined as described above.

Method B. About 100 mg of sample is weighed into the generating flask and heated with about 2 ml of concentrated nitric acid on a low flame. If the sample does not dissolve within a few minutes, a few drops of concentrated hydrochloric acid are added to obtain dissolution. After addition of 10—15 mg of sodium chloride, the solution is evaporated almost to dryness, then about 2 ml of concentrated hydrochloric acid is added and evaporated, and addition of hydrochloric acid and evaporation are repeated. The generating apparatus is then assembled and the sulfur content is determined as described above. This method is quicker than method A and gives lower blanks.

The reagents used contain small impurities of sulfur, so that blanks are not negligible, especially when small samples of iron and steel are used or when the sulfur contents are low. To avoid this error a blank is determined under the same conditions and with the same amounts of reagents as are used for the iron and steel samples. The amount of sulfur from the reagents is low; for accurate determinations, the titrant strength should be the same as for analysis of samples and a standard addition method should be used. For

this purpose a known amount of standard sulfate solution is added to the reagent blank, the mixture is evaporated to dryness, and the sulfur content is determined by the usual procedure. Hydrogen sulfide is also evolved from the standard sulfate solution and titrated. The blank is obtained from difference of these measurements. The reagents are responsible for a blank of 0.00098% of sulfur for method A and 0.00015% for method B.

Determination of total sulfur in fly ash

Two fly ash samples were used. The first was an aliquot of a thoroughly homogenized material intended by the Community Bureau of Reference (BCR, Brussels) as a reference material. The second was taken as a typical material from a conventional coal and oil burning electricity plant.

Method C. Direct decomposition in the generating flask. Fly ash samples (5—10 mg) are weighed into the hydrogen sulfide flasks, the actual weight depending on the strength of the titrant and the percentage of sulfur expected. After addition of reducing mixture, both flasks are heated. At first, the potential changes quickly but final stabilization of the potential may take 25—30 min, probably because of the presence of slightly soluble sulfur compounds. When the potential reaches a stable value, determinations are completed in the usual way.

Method D. Decomposition of samples with oxygen flask combustion. The fly ash (20—25 mg) is weighed on a suitable filter paper, which is then folded and mounted in the platinum gauze. The flask is charged with 25 ml of 1% hydrogen peroxide solution and filled with oxygen. The combustion and absorption are completed in the conventional manner, and the solution is transferred quantitatively to a volumetric flask and diluted to the mark with water. An aliquot is placed in the generating flask and 10—15 mg of sodium chloride is added. The solution is evaporated to dryness at about 100°C and the sulfur is determined by the usual procedure.

A blank for the reagents and filter paper is prepared in the same way and measured by the standard addition method. The reagents and filter paper are responsible for a blank of 12 μg of sulfur.

Method E. Wet oxidation with acid. The fly ash sample (0.2—0.3 g) is weighed into a 50-ml Kjeldah flask, 20 ml of concentrated nitric acid is added and heated very slowly under reflux until almost evaporated. The residue is then heated to dryness with 10 ml of concentrated nitric acid and 2 ml of concentrated hydrochloric acid. The residue is evaporated almost to dryness with two further 20-ml portions of concentrated hydrochloric acid. After addition of 2 ml of concentrated hydrochloric acid, heating, and addition of 25 ml of water, the mixture is filtered on a Nuclepore filter and the filtrate is diluted to 100 or 250 ml according to the weight of material taken. Suitable aliquots are analyzed as in the general procedure.

A blank is prepared under the identical conditions and measured by standard addition method. The blank value for reagents is 6 μg of sulfur.

Method F. Fusion. Direct weighing of fly ashes in a platinum or zircon-

ium crucible and fusion with sodium carbonate—sodium peroxide or sodium hydroxide—sodium peroxide, followed by potentiometric titration invariably provided results which were low by 15—20%, although the second fusion mixtures has been recommended for the determination of sulfur in fly ash [15]. Accurate results were obtained when the fusion was applied to the residue obtained by removing the water-soluble sulfur compounds from the sample by refluxing for about 10 h. The following procedure was therefore adopted.

About 500 mg of fly ash is refluxed with water in a 250-ml flask with water for about 10 h. After filtration on a Nuclepore filter, the residue is washed several times with water, the filtrate is quantitatively transferred to a volumetric flask, and aliquots are measured for water-soluble sulfur compounds. After drying in an oven at about 80°C, the residue is quantitatively transferred to a zirconium crucible, mixed thoroughly with 1 g of anhydrous sodium carbonate and 2—3 g of sodium peroxide, and heated slowly in a furnace to 550°C; after 5 min at 550°C, the crucible is allowed to cool and the contents are dissolved in water. Finally hydrochloric acid is added until the solution is faintly yellow.

The solution is transferred to a volumetric flask and aliquots are analyzed. Total sulfur is obtained by combining the two results. Blanks for the fusion procedure amount to about 0.001% of sulfur in the fly ash.

RESULTS AND DISCUSSION

Table 1 shows that with the modified apparatus almost 100% of the sulfur was recovered. Lead nitrate was used as titrant as it gave the most precise results [16]. For accurate results, the following conditions are essential. Before a series of measurements, the cadmium electrode is calibrated 3 or 4 times against known amounts of sulfate. Once the electrode has been cali-

TABLE 1

Accuracy and relative standard deviation (s_r) for the determination of sulfate after reduction

Sulfate (μg S)		Recovery (%)	s_r (%)	No. of detns.
Present	Found			
160	160.5	100.2	2.1	5
100	99.4	99.4	0.9	5
80	80.2	100.2	1.5	5
30	30.3	100.1	0.7	7
16	15.9	99.4	1.2	7
10	10.1	100.1	0.5	7
5	5	100	1.9	8
3	3.01	100.3	2.3	7
1	1.01	101	6.9	8

TABLE 2

Determination of sulfur in waters

Sample	Sulfur Found (mg l^{-1})	s_r (%)	No. of detns.
North Sea	794.6	1.4	15
Schelde river, (1) Antwerp region[a]	441	1.1	10
(2)	127.8	0.9	10
(3)	114.3	0.7	10
Tap water (Wilrijk, Belgium)	29.1	0.6	10
Deionized water	0.109	4.9	15
Distilled—deionized water	0.056	5.4	16

[a](1) At the confluence of river and sea; (2) 1 km away from a metallurgical factory; (3) near the factory.

brated, it behaves reproducibly for several hours, but its performance should be checked after each set of measurements. After use, the electrode must be washed with water, dried with soft tissues and stored dry. Storage in 1 M sodium hydroxide causes a slow decrease in sensitivity.

Table 2 shows the results obtained for water samples. Sea water contains more sulfur, probably as sulfate, than river water. The sulfur content of river water is even lower near a factory which emits metallic wastes in the river, probably because of precipitation of heavy metal sulfates.

For the determination of sulfur in deionized water and distilled water, pre-concentration was necessary. For these determinations, standard addition proved more satisfactory than direct determinations.

Table 3 shows the results for sulfur impurities in various analytical-grade laboratory chemicals. The method fails when some volatile compounds are formed which deposit on the cooler part of the condenser, e.g. K_2CrO_4 or $K_2Cr_2O_7$. In some cases there is no apparent change of potential, e.g., for $(NH_4)_3PO_4$ or $SnCl_2$. It has been reported [12] that the sulfur content of lead sulfate, barium sulfate and strontium sulfate can be determined by evolving hydrogen sulfide from this reducing mixture. However, consistently low results were found when these sulfates were present, which shows that complete reduction of these sulfates is not possible.

The results obtained for iron and steel samples by method B are reported in Table 4. This method is accurate for determination of amounts of sulfur down to 0.009%. Some powdered steel samples can be analyzed by direct treatment with the reducing mixture, but the procedure is not universally applicable so that acid pre-treatment is mandatory. The entire procedure takes about one hour.

Table 5 shows the results of at least three determinations in fly ash samples by each of methods C—F (see Experimental). Each individual measurement is the result of five determinations on aliquots of the solution after the decomposition method. The results obtained by direct treatment of the fly ash with the reducing solution (method A) are too low, apparently because not all sulfur compounds in fly ash are completely reduced by the reducing mixture. The results of wet oxidation (method E) are higher, probably because possible losses are minimized in this case.

TABLE 3

Determination of sulfate as impurity in analytical-grade reagents

Compound	Sulfate (%)		s_r (%)	No. of detns.
	Certified	Found		
Potassium dihydrogenphosphate[a]	<0.003	0.0029	2.5	5
Calcium hydroxide[a]	≤0.15	0.068	3.9	5
Sodium chloride[b]	<0.001	0.0012	5.1	6
Disodium hydrogenphosphate[a]	<0.005	0.0084	0.9	4
Sodium pyrophosphate[a]	≤0.005	0.0205	3.1	6
Calcium carbonate[bc]	<0.005	0.0055	2.2	5
Magnesium oxide[ac]	<0.005	0.0039	1.1	5

[a]Pro analysi; U.C.B. Belgium. [b]Pro analysi, Merck. [c]This compound was moistened with 11 M HCl and dried before analysis.

TABLE 4

Determination of sulfur in iron and steel samples

Sample	Sulfur (%)		s_r (%)	No. of detns.
	Present	Found		
Mild steel BAS-I(e)	0.052	0.0515	0.6	5
Alloy steel BAS-60(b)	0.036	0.0362	0.4	5
Cast iron BAS-4(a)	0.051	0.0521	0.7	6
Cast iron BAS-35(b)	0.036	0.0367	0.9	6
Stahl 25/126[a]	0.0095	0.00913	1.7	7

[a]Analysen-kontrollprobe, Max-Planck Institut fur Eisenforschung, Düsseldorf.

TABLE 5

Determination of sulfur in fly ashes by methods C—F (see Experimental)

Sample	Method C		Method D		Method E		Method F			
	Found (%)	s_r (%)	Found (%)	s_r (%)	Found (%)	s_r (%)	S Found in H_2O (%)	S in residue (%)	Total (%)	s_r (%)
BCR-38										
No. 1202	0.3429	3.4	0.3795	5.4	0.3949	0.4	0.2694	0.1189	0.3883	1.1
No. 11	0.2856	2.8	0.3481	4.8	0.3502	0.2	0.2552	0.0893	0.3445	1.8

Moreover, any organic sulfur compounds present are also oxidized to sulfate by the wet oxidation procedure.

The mean result from the oxygen flask combustion (method D) is similar to that from wet oxidation but the reproducibility is poorer.

When the fusion method was applied to the fly ash without prior removal of water-soluble compounds by refluxing with water, the results were invariably low. However, when the fusion method was used after removal of the water-soluble sulfur compounds, the combined results were in good agreement with those obtained by other methods.

Discrimination between sulfur species in fly ash

As a practical application of the method, the stepwise solubility of sulfur compounds in the fly-ash samples was studied. The sample (0.1—0.3 g) was mixed with 75 ml of water in a 250-ml standard flask, which was placed in an ultrasonic vibrator for 24 h. The residue was removed on a Whatman 42 filter and washed with water. The filtrate was evaporated to about 75 ml on a hot plate and diluted to exactly 100 ml; 5-ml aliquots were taken for potentiometric titration. This titration corresponds to the sulfur compounds in fly ash which are soluble in water at room temperature. The residue along with the filter paper was refluxed with 75 ml of water for about 10 h, filtered and washed with hot water. The filtrate was evaporated to about 75 ml and then diluted to exactly 100 ml with water. Aliquots (15 ml) were analyzed to obtain values for the sulfur compounds soluble in hot water.

This residue along with the filter paper was then refluxed with 1 g of anhydrous sodium carbonate and 75 ml of water for 10 h, filtered and washed with water. The filtrate was evaporated to 75 ml and diluted to exactly 100 ml; 20-ml portions were taken for determination of the sulfur compounds soluble in sodium carbonate.

The residue again with filter paper, was refluxed with 75 ml of 8 M hydrochloric acid for about 10 h and given the same treatment. Aliquots (20 ml) were analyzed to obtain values for the hydrochloric acid-soluble sulfur compounds. This residue and filter paper were refluxed with 75 ml of hydrochloric acid—nitric acid (3 + 1) mixture for 10 h, evaporated to dryness, and then evaporated to dryness with 10 ml of concentrated hydrochloric acid. The residue was finally heated with 2 ml of concentrated hydrochloric acid and 25 ml of water, and the solution was cooled and diluted to exactly 100 ml; 10-ml aliquots were analyzed.

Energy-dispersive x-ray fluorescence analysis was applied to determine the sulfur in the residue after the aqua regia treatment, following transference to a mylar foil. The sulfur K x-rays were measured under titanium excitation. Data reduction and quantification of the sulfur peaks were done as described previously [17, 18]. The accuracy of the determinations can be estimated as 10—20%.

Blanks were taken throughout the entire procedure and measured by the standard addition method.

TABLE 6

A stepwise study of solubility and total sulfur in fly ashes

Sample	Sulfur (%) after treatment with						Total S (%)
	H_2O, 22°C (ultrasonic)	H_2O, 100°C (reflux)	0.15 M Na_2CO_3	8 M HCl	$HCl-HNO_3$ (3 + 1)	X.r.f.	
BCR-38 no. 1202	0.2321 ±0.0026	0.0334 ±0.0013	0.0072 ±0.0009	0.01 ±0.0004	0.0954 ±0.0067	0.001 ±0.0001	0.3791 ±0.0087
No. 11	0.2373 ±0.0033	0.0148 ±0.0016	0.0075 ±0.0014	0.0045 ±0.0002	0.0756 ±0.0001	0.0007 ±0.0001	0.3404 ±0.0017

The sum of the sulfur content in each of these extracts and the x-ray fluorescence value for the final residue give the total sulfur in fly ash (Table 6). It can be seen from Table 6 that most of the sulfur compounds in fly ash are soluble in water at room temperature under ultrasonic vibration. Very similar results were obtained when a mechanical shaker was used. A small additional amount of sulfur is soluble in hot water. Very small amounts are soluble in sodium carbonate and hydrochloric acid solutions but appreciable amounts are again soluble in aqua regia. The residue from the aqua regia treatment contains a neglible quantity of sulfur compound, as indicated by x.r.f.

These results for water-soluble sulfur compounds in BCR-38 are in good agreement with the result 0.233 ± 0.006% S obtained elsewhere [19] by a standard barium sulfate turbidimetric method [20].

The blank values for sulfur from filter paper and reagents in refluxing with water, sodium carbonate, hydrochloric acid and aqua regia were, respectively, 0.0007%, 0.004%, 0.0036%, 0.0046% of apparent sulfur in fly ash.

When fly ash samples (0.1—0.3 g) were refluxed for various times (4, 10, 16, 48 h) in water and the water extracts were analyzed for sulfur, by the general procedure, the results were almost identical (Table 7). Thus the refluxing time has no effect on the solubility of sulfur compounds in water. The sum of the results shown in columns 2 and 3 of Table 6 is consistent with the results of Table 7.

TABLE 7

Amounts of sulfur compounds in fly ashes extracted with water after different times

Sample	Sulfur (%) found after refluxing for			
	4 h	10 h	16 h	24 h
BCR-38 no. 1202	0.2668 ± 0.003	0.2688 ± 0.005	0.2679 ± 0.005	0.2703 ± 0.004
No. 11	0.2521 ± 0.004	0.2495 ± 0.006	0.2511 ± 0.008	0.2571 ± 0.004

REFERENCES

1 H. Clysters and F. Adams, Anal. Chim. Acta, 92 (1977) 251.
2 J. B. Davis and F. Lindstrom, Anal. Chem., 44 (1977) 524.
3 P. T. Roberts and S. L. Friedlander, Atmos. Environ., 10 (1976) 403.
4 J. D. Husar, R. Husar and P. Stubits, Anal. Chem., 47 (1975) 2062.
5 K. Pötzl, Staub Reinhalt. Luft, 34 (1974) 55.
6 J. L. Johnson, Mikrochim. Acta, (1974) 145.
7 D. Leahy, R. Siegel, P. Koltz and L. Newman, Atmos. Environ., 9 (1975) 219.
8 Sulfur in the atmosphere, Proc. Int. Symp., Dubrovnik, Yugoslavia, 1977, Atmos. Environ., 12 (1978).
9 R. J. Charlson, A. H. Vanderpol, D. S. Covert, A. P. Waggoner and C. Ahlquist, Sulfur in the atmosphere, Proc. Int. Symp., Dubrovnik, Yugoslavia, Atmos. Environ., 8 (1974) 1257.
10 P. T. Roberts and S. K. Friedlander, Sulfur in the atmosphere, Proc. Int. Symp., Dubrovnik, Yugoslavia, Atmos. Environ., 10 (1976) 403.
11 R. L. Tanner, R. Cederwall, R. Garber, D. Leahy, W. Marlow, R. Meyers, M. Phillips and L. Newman, Atmos. Environ., 11 (1977) 1978.
12 L. Newman, Atmos. Environ., 12 (1978) 113.
13 W. Schöniger, Mikrochim. Acta, (1955) 123.
14 G. Gran, Analyst, 77 (1962) 662.
15 M. C. Van Grondelle, F. Van de Graats and J. D. Vander Laarse, Anal. Chim. Acta, 97 (1977) 267.
16 H. Clysters, Doctoral thesis, University of Antwerp, Belgium, 1976.
17 R. Dewolfs, R. De Neve and F. Adams, Anal. Chim. Acta, 75 (1974) 47.
18 P. Van Espen and F. Adams, Anal. Chim. Acta, 75 (1974) 61.
19 R. Dams, private communication
20 Air Pollution Measurements of the National Air Sampling Network, Analysis of Suspended Particulates 1957—1961, and Supplement 1962—1963, Public Health Service Publication No. 978, U.S. Department of Health, Education and Welfare, Washington, 1962 and 1964.

Analytica Chimica Acta, 109 (1979) 319—326
© Elsevier Scientific Publishing Company, Amsterdam — Printed in The Netherlands

POTENTIOMETRIC TITRATION OF FLUORIDE, SULFATE, CHROMATE, MOLYBDATE, TUNGSTATE, OXALATE, PHOSPHATE, PYROPHOSPHATE AND HEXACYANOFERRATE(II) IONS WITH LEAD(II) SOLUTIONS AND A FLUORIDE-SELECTIVE ELECTRODE

C. E. EFSTATHIOU and T. P. HADJIIOANNOU*

Laboratory of Analytical Chemistry, University of Athens, Athens (Greece)

(Received 2nd February 1979)

SUMMARY

A semi-automatic potentiometric method is described for the direct titration of fluoride with lead(II) solutions in the presence of added chloride. Sulfate, chromate, molybdate, tungstate, oxalate, phosphate, pyrophosphate, and hexacyanoferrate(II) are titrated similarly in the presence of added chloride and fluoride. A fluoride-selective electrode is used to detect the end-points. Fluoride in the range 0.57—5.7 mg can be determined with a precision of about 0.3%. The other ions can be determined in the range 0.025— 0.30 mmol with a precision of 0.5—1%.

The lanthanum fluoride membrane electrode [1] is undoubtedly the most widely used ion-selective electrode, second only to pH-measuring glass electrodes. At present, the fluoride-selective electrode is the only selective electrode officially recommended for the analysis of water and wastes [2]. Direct potentiometry is the standard technique for the determination of micro-quantities of fluoride, but titration with lanthanum nitrate offers greater accuracy for moderately large quantities of fluoride [3]. The fluoride-selective electrode has also been used for the indirect titration of phosphate [4] and arsenate [5], by adding a known excess of lanthanum nitrate and back-titrating the unreacted lanthanum with standard fluoride solution.

In this paper, methods are described that greatly extend the possibilities of the fluoride-selective electrode in titrimetry. Several ions (X^{n-} = sulfate, chromate, molybdate, tungstate, oxalate, phosphate, pyrophosphate, and hexacyanoferrate(II)) are titrated semi-automatically by continuous addition of lead nitrate solution in the presence of fixed amounts of fluoride and chloride. The precipitation reaction is monitored with a fluoride-selective electrode and the end-point is detected by the large potential change near the equivalence point, which is due to the formation of the insoluble mixed halide PbClF [6]. The formation of this mixed halide marks also the end-point in the titration of fluoride with lead solution in the presence of added chloride. In all cases, the titrated solution contains appropriate amounts of propan-2-ol to ensure a relatively rapid precipitation reaction. Fluoride in the

range 0.57—5.7 mg in a 5.00-ml sample and a total volume of 25 ml can be determined with good precision. Sulfate, chromate, molybdate, tungstate, oxalate and phosphate in the range 0.05—0.3 mmol, and pyrophosphate and hexacyanoferrate(II) in the range 0.025—0.15 mmol, can also be determined rapidly.

EXPERIMENTAL

Apparatus

A block diagram of the semi-automatic titration system is shown in Fig. 1. A pH/pIon electrometer (Heath—Schlumberger Model EU-200-30) was used as a follower—amplifier for impedance matching. A potentiometric recorder (Heath—Schlumberger Model EU-205B) monitored the output from the electrometer and recorded the titration curve. A stepper motor-driven multi-speed burette (Model S-11120-12, E.H. Sargent Co.) was used to deliver the titrant. The internal square-wave clock was disconnected and the square-wave output of a sine-square wave audio generator (Heath Model SG-5218) was connected directly to the input of the driving circuit of the stepper motor. Parallel connection of the generator output to the recorder chart external drive allowed complete synchronization of the burette with the recorder at any titrant delivery rate. Any frequency in the 5—100-Hz range could be selected, resulting in a titrant delivery rate of 0.0667—1.333 ml min^{-1}. The same frequency range resulted in a chart speed of 0.40—8.00 cm min^{-1} when the nominal chart speed of 4.00 cm min^{-1} (50 Hz internal clock) was selected.

During titration, the driving pulses from the audio generator were counted with a programmable timer (Heath—Schlumberger Model SM-102A). The gating circuits of the timer were bypassed and the pulses were fed directly to the five-decade counter circuit through the external clock input of the timer. This arrangement resulted in a 9-fold improvement in the resolution of the readings. Thus a delivery of 1.000 ml was displayed as 4500 counts on the timer panel instead of 500 on the electromechanical counter of the burette.

A frequency of 50 Hz on the sine-square wave audio generator was used for all titrations, giving a titrant delivery rate of 0.667 ml min^{-1}. This was the normal delivery rate of the unmodified burette. Frequencies in the range 7—100 Hz were used in studies of the effect of delivery rate on the blank. Titrant delivery, chart moving and pulse counting were initiated simultaneously on turning the amplifier switch from position ×1 (insufficient pulse amplitude) to position ×10 (sufficient pulse amplitude to drive burette, recorder and counter). The concentric amplifier—variable potentiometer should always be in the fully clockwise position.

An Orion combination fluoride-selective electrode (Model 96—09) was used as the indicator electrode; its outer chamber was filled twice a week with the recommended electrolyte solution (Orion 90-00-01).

All titrations were done at room temperature in 50-ml polypropylene beakers with constant magnetic stirring.

Reagents

All solutions were prepared from reagent-grade materials with deionized, distilled water.

Sodium fluoride, 0.1000 M. Dissolve 4.199 g of sodium fluoride, purified as described by Lingane [3], in water, dilute to 1 l and store in a polyethylene bottle. Prepare working solutions (0.00600, 0.02000, 0.0400 and 0.0600 M) by dilution.

Lead nitrate, 0.1000 M. Dissolve 33.12 g of $Pb(NO_3)_2$ in water and dilute to 1 l. Standardize against standard EDTA solution with xylenol orange indicator at pH 6. Each count on the timer corresponded to $(2.223 \pm 0.004) \times 10^{-5}$ mmol Pb ($n = 5$).

Lanthanum nitrate, 0.03333 M. Dissolve 5.431 g of pre-ignited (1000°C) La_2O_3 (99.99%, G. F. Smith Co., Columbus, Ohio) in excess of (1 + 1) nitric acid, continue as described by Lingane [3] and dilute to 1 l.

Sulfate, chromate, molybdate, tungstate, oxalate, phosphate, pyrophosphate, and hexacyanoferrate(II) solutions. Prepare 0.1000 M solutions from Na_2SO_4, K_2CrO_4, $Na_2MoO_4 \cdot 2H_2O$, $Na_2WO_4 \cdot 2H_2O$, $Na_2C_2O_4$, $Na_3PO_4 \cdot 12H_2O$, $Na_4P_2O_7 \cdot 10H_2O$, and $K_4Fe(CN)_6 \cdot 3H_2O$. Prepare working solutions (0.00500, 0.01000, 0.0200 and 0.0300 M for pyrophosphate and hexacyanoferrate(II); 0.01000, 0.0200, 0.0400 and 0.0600 M for the other anions) by dilution. Molybdate, tungstate, oxalate, pyrophosphate, and hexacyanoferrate(II) solutions should be prepared fresh when needed, to eliminate problems arising from hydrolysis, bacterial attack or oxidation. Titers are based on the purity indicated by the manufacturer and are accurate to ± 0.5%. Further standardization was deemed unnecessary for this study, because standards and unknowns were prepared from the same stock solutions.

Solid lead chlorofluoride. Mixing equal volumes of 0.100 M $Pb(NO_3)_2$ and a composite 0.100 M NaF—0.100 M NaCl solution. Collect the precipitate on a sintered glass funnel, wash with water, dry with suction and heat at 140°C to constant weight.

Total ionic strength adjustment buffer (TISAB). Prepare in the usual way with *trans*-1,2-diaminocyclohexane-*N*,*N*,*N*',*N*'-tetraacetic acid [7] but use 117 g of NaCl (final molarity 2.0 M NaCl).

Procedures

Semi-automatic titration of fluoride. Select on the recorder a span of 200 mV, a chart speed of 4.00 cm min^{-1} and a frequency of 50 Hz on the audio generator. Pipet into the titration cell a 5.00-ml aliquot of the standard or unknown fluoride solution, 5.00 ml of 0.50 M NaCl solution and 15.0 ml of propan-2-ol. Start the stirrer, press the servo button on the recorder and adjust the recorder pen to one side (lower potential) of the chart. Turn the amplifier switch of the audio generator to position ×10, terminate the titra-

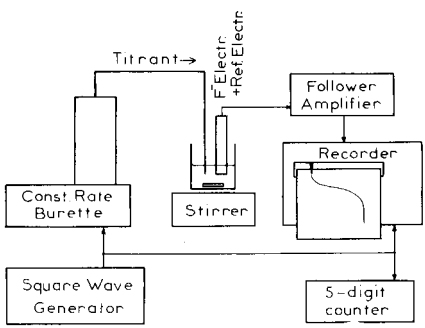

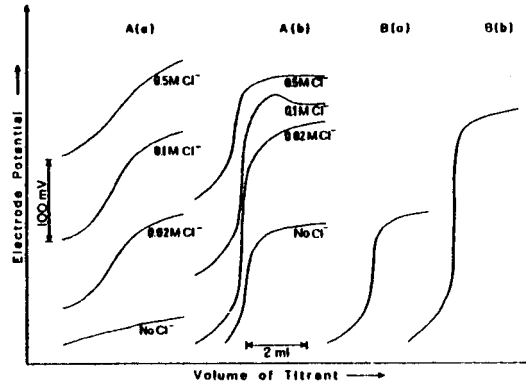

Fig. 1. Block diagram of the semi-automatic titration system.

Fig. 2. Recorded curves for the semi-automatic titration of 25.0 ml of 6.00×10^{-3} M NaF with (A) 0.1000 M $Pb(NO_3)_2$ or (B) 0.03333 M $La(NO_3)_3$ in water (a) or 60% (v/v) propan-2-ol (b) in the presence of various chloride concentrations.

tion after obtaining the titration curve by turning the switch to position X1, and record the counter reading y. Press the reset button of the timer to clear the reading. Locate the end-point (point of maximum slope of the titration curve) and calculate from y the number of counts z corresponding to the end-point. Calculate the fluoride content of the unknown from a working curve obtained with standard fluoride solutions (number of counts vs. molarity of fluoride in the titrated 5.00-ml sample). The number z is also used to calculate the blank.

Semi-automatic titration of other anions. Proceed as for the titration of fluoride, but use 5.00 ml of composite 0.50 M NaCl—0.0100 M NaF solution instead of the 0.5 M NaCl solution. For the titration of hexacyanoferrate-(II), use a 60% (v/v) propan-2-ol solution, and for the titration of oxalate, phosphate, and pyrophosphate a 50% (v/v) propan-2-ol solution.

Determination of the solubility of PbClF. Transfer to 50-ml polyethylene vials 0.50-g amounts of finely pulverized PbClF and 30 ml of sodium chloride solutions of various concentrations. Shake the vials mechanically for 4 h at room temperature (22 ± 1°C) and filter through a Whatman No. 42 filter paper. Mix 1.00-ml aliquots of each filtrate with 15.00 ml of TISAB solution and determine the fluoride concentration of the mixtures with the fluoride-selective electrode, by comparing it with standard fluoride—TISAB mixtures (1+15). The solubility of the mixed lead halide is taken as equal to the fluoride concentration.

RESULTS AND DISCUSSION

Titration of fluoride

Typical recorded curves for the semi-automatic potentiometric titration of fluoride with lead and lanthanum ions at various initial chloride concentra-

tions in aqueous or propan-2-ol media are shown in Fig. 2. Although sharper end-points were obtained with lanthanum, lead was chosen as titrant because it is not only much cheaper than lanthanum but forms insoluble salts with all nine of the anions of interest and gives satisfactory end-points in propanolic media.

The titration of fluoride with lead(II) in aqueous solutions was possible only in the presence of chloride (Fig. 2). The sharpest potential inflection was obtained with an initial chloride concentration of 0.1 M. Similar results but with slightly less sharp potential inflections were obtained when bromide was substituted for chloride, whereas trials with iodide failed because of the formation of the highly insoluble lead iodide. The large potential change near the equivalence point is due to the formation of lead chlorofluoride. The optimal chloride concentration was close to the chloride concentration which results in the largest value for the mole fraction Φ_{PbCl^+}. Thus from the overall stability constants β_{PbCl^+}, β_{PbCl_2}, $\beta_{PbCl_3^-}$ and $\beta_{PbCl_4^{2-}}$ [8], it was calculated that the maximum value 0.71 for Φ_{PbCl^+}, occurs at a chloride ion concentration of 0.12 M.

The addition of a water-miscible organic solvent in precipitation titrations is generally known to improve the end-point sharpness. Titrations of fluoride with lanthanum(III) solutions in the presence of various organic solvents have been reported [9]. In the present study, the effectiveness of the organic solvents tested decreased in the order acetone > ethanol ≃ propan-2-ol > dioxane. However, acetone slowly attacked the plastic body of the electrode and therefore was not used. Propan-2-ol was chosen because it offered better precision and lower cost. The 60% (v/v) propan-2-ol medium selected was a compromise between ensuring sufficiently sharp end-points and avoiding problems from the insolubility of many metal salts in solutions containing large amounts of propan-2-ol. For certain anions, smaller amounts of propan-2-ol had to be used, because of solubility problems.

In contrast to aqueous solutions, the sharpness of the potential inflection in propanolic solutions increased with decreasing chloride concentration (Fig. 2). Therefore, the background chloride concentration should be made equal to the largest fluoride concentration to be titrated. However, there is always a blank which depends on the chloride concentration. An initial concentration of about 0.1 M chloride was chosen to eliminate problems arising from small variations in chloride concentration. At this concentration, the end-point could still be located easily and reproducibly, according to conventional techniques [10].

In propan-2-ol solutions and in organic media generally, the potential inflection occurred a few tenths per cent after the equivalence point, because of partial precipitation of lead as lead chloride in such solutions. The blank depended on the titrant (it was smaller with lanthanum than with lead), the chloride concentration and experimental conditions such as stirring, electrode geometry, titrant delivery rate (Fig. 3), etc. However, all these factors could be kept constant and the blank was very reproducible under a particular set of experimental conditions, so that working curves were also reproducible.

Titrations of other anions

For the titration of any of the other eight anions examined (sulfate, chromate, etc.), a fixed amount of fluoride (0.05 mmol) was added as indicator. The amount was relatively large in order to obtain well-defined end-points. A working curve obtained with standard solutions of the titrated ion under the selected experimental conditions is always essential. The back-titration technique with standard fluoride solution was not considered as an alternative, to avoid any possible problems arising from prolonged contact of fluoride solutions with the glass parts of the burette.

Titration curves obtained for these eight ions are shown in Fig. 4. Interesting phenomena of fluoride adsorption and desorption on the precipitates formed during the titration can be observed as shoulders on the titration curves, before the end-point in the titrations of sulfate, chromate and phosphate, or after it in the titration of oxalate.

In all these titrations, the solutions were unbuffered; no problems were found even with phosphate and pyrophosphate solutions. However, acidic solutions should be neutralized before the titration to ensure quantitative precipitation.

Results for the solubility of lead chlorofluoride are given in Table 1. Because of the low stability of the PbF^+ ion in comparison with the $PbCl^+$ ion ($\beta_{PbF^+} < 2; \beta_{PbCl^+} = 39.8$ [8]), lead should be considered bound covalently

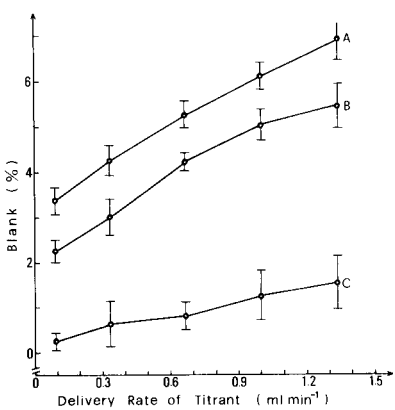

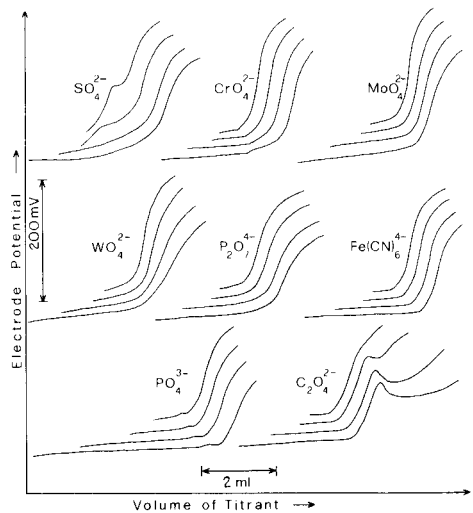

Fig. 3. Effect of titrant delivery rate on the blank in the titration of fluoride. Titrations with (A and B) 0.1000 M $Pb(NO_3)_2$ in the presence of 0.10 M and 0.02 M initial chloride concentration, respectively, in 60% (v/v) propan-2-ol; (c) 0.03333 M $La(NO_3)_3$ in water. Initial fluoride concentration, 6.00×10^{-3} M; initial volume, 25.0 ml.

Fig. 4. Recorded curves for the titration of 25 ml of the specified anion solution with 0.100 M $Pb(NO_3)_2$, in the presence of 0.1 M chloride and 0.05 mmol of fluoride in propan-2-ol (30—60% v/v). Amounts titrated: 50, 100, 200, and 300 μmol of sulphate, chromate, molybdate, tungstate, phosphate, and oxalate; 25, 50, 100, and 150 μmol of pyrophosphate and hexacyanoferrate(II).

TABLE 1

Solubility of [PbCl]F in various concentrations of chloride at 22 ± 1°C

[NaCl] (M)	0.000	0.010	0.030	0.080	0.150	0.300	1.00
Soly. ($\times 10^{-4}$ M)	12.9[a]	5.13	3.89	3.80	3.61	5.37	20.4

[a]This corresponds to a solubility of 0.338 g PbClF l^{-1}. Reported values (in the same units, but at 25°C): 0.35 [6], 0.370 [11], 0.357 [12].

to chlorine and ionically to fluorine. From the data in Table 1 ($\mu < 0.1$) and the overall stability constants of the chloro complexes of lead, the thermodynamic solubility product of [PbCl]F was calculated to be (5.5 ± 0.2) × 10^{-8} M^2.

General precision and blanks

Results for aqueous solutions of nine anions of known concentrations are summarized in Table 2. There is always a blank, which is larger for low fluoride concentrations and in titrations of tungstate and phosphate. The positive blank is probably due to coprecipitation of basic lead salts. Under the experimental conditions, the blank is determined mainly by the nature and solubility of PbX, and the speed with which Cl^- or OH^- is displaced by X^{n-} in the coprecipitated salts. The blanks necessitate the use of calibration graphs. The precision of the method for these dilute solutions is in the range 0.3—1.0%. Correlation coefficients are given (Table 2) to indicate the scatter of the experimental points on each graph; the linearity is clearly excellent.

Although the applications reported here deal with the determination of

TABLE 2

Summary of results for aqueous solutions of F^-, SO_4^{2-}, CrO_4^{2-}, MoO_4^{2-}, WO_4^{2-}, $C_2O_4^{2-}$, PO_4^{3-}, $P_2O_7^{4-}$ and $Fe(CN)_6^{4-}$

Anion	Concentration range in 5-ml sample (M)	Range of blank (%)	Correlation coefficient[a]	Average error (%)[b]
F^-	0.006—0.060	(+15.0)—(+3.7)	0.99996	0.32
SO_4^{2-}	0.010—0.060	(+0.3)—(−1.2)	0.99990	0.54
CrO_4^{2-}	0.010—0.060	(+2.7)—(+2.5)	0.999990	1.00
MoO_4^{2-}	0.010—0.060	(+4.0)—(+3.4)	0.99990	0.79
WO_4^{2-}	0.010—0.060	(+13.5)—(+15.0)	0.9997	0.86
$C_2O_4^{2-}$	0.010—0.060	(+2.5)—(+0.7)	0.99993	1.01
PO_4^{3-}	0.010—0.060	(+9.3)—(+8.1)	0.99995	0.94
$P_2O_7^{4-}$	0.005—0.030	(+1.1)—(−0.8)	0.9998	0.96
$Fe(CN)_6^{4-}$	0.005—0.030	(+4.5)—(+3.9)	0.999998	0.77

[a] From least-squares fit on data obtained from four different standard solutions; average of 2 measurements.

[b]The average error for six samples covering the analyte range; single measurements.

nine anions, the scope of the method should be more general. It should be possible to determine other anions or molecules forming insoluble lead salts or stable lead complexes with lead(II) solutions in the presence of fluoride ion as indicator with the fluoride selective electrode as end-point detector. The applications of this widely-available electrode are thus greatly extended.

REFERENCES

1 M. S. Frant and J. W. Ross, Jr., Science, 154 (1966) 1553.
2 Methods for Chemical Analysis of Water and Wastes, U.S. Environmental Protection Agency, Washington, D.C., 1974, p. 65.
3 J. J. Lingane, Anal. Chem., 39 (1967) 881.
4 Orion Newsletter, III, 1—2 (1971) 6.
5 W. Selig, Mikrochim. Acta, (1973) 349.
6 I. M. Kolthoff and P. J. Elving, Treatise on Analytical Chemistry, Part II, Vol. 7, Wiley-Interscience, New York, 1961, p. 257.
7 Analytical Methods Guide, 8th edn., Orion Research, Cambridge, Massachusetts, May 1977, p. 29.
8 J. Inczédy, Analytical Applications of Complex Equilibria, Ellis Horwood, Chichester, 1976, p. 319.
9 See, e.g., W. E. Bazzelle, Anal. Chim. Acta, 54 (1971) 29.
10 W. J. Blaedel and V. W. Meloche, Elementary Quantitative Analysis, Harper and Row, New York, 1963, p. 350.
11 W. F. Linke and A. Seidell, Solubilities of Inorganic and Metal Organic Compounds, Vol. II, 4th edn., Am. Chem. Soc., Washington, D.C., 1965, p. 1293.
12 CRC Handbook of Chemistry and Physics, 55th edn., CRC Press, Cleveland, 1974, p. B-101.

Analytica Chimica Acta, 109 (1979) 327—339
© Elsevier Scientific Publishing Company, Amsterdam — Printed in The Netherlands

STUDIES OF CADMIUM—ETHYLENEDIAMINE COMPLEX FORMATION IN SEAWATER BY COMPUTER-ASSISTED STRIPPING POLAROGRAPHY

SAMUEL P. KOUNAVES* and ALBERTO ZIRINO

Chemistry and Environmental Sciences, Code 5132, Naval Ocean Systems Center, San Diego, California 92152 (U.S.A.)

(Received 15th May 1978)

SUMMARY

An equation for stripping polarography is derived, relating the half-wave potential ($E^*_{1/2}$), ligand concentration, and dissociation constant of a complexed metal ion. This equation is similar to that for classical polarography, but contains an additional term which makes $E^*_{1/2}$ a linear function of the logarithm of the time. A computer-assisted system for generating stripping polarographic curves is also described. This system is used to characterize 10^{-8} M cadmium in a potassium nitrate solution and in sea water.

Current awareness of the importance of trace metals in natural waters has stimulated interest in the development of analytical techniques capable of determining the chemical speciation of these metals at levels of less than 10^{-8} M.

It has been shown experimentally [1] and theoretically [2—4] that trace metals in sea water exist in different forms. They may be complexed with simple inorganic ligands such as water, halides, carbonates, and sulfate, or by organic ligands such as amino acids, humic acids, sugars, carbohydrates and polymers. Their availability for biological and geochemical processes is largely determined by such species characteristics as oxidation state, degree of hydration, and complexation [5]. Because of the low levels at which these metals normally occur in the environment, direct determinations by classical methods cannot be made without prior concentration which usually modifies the species under investigation.

Classical d.c. polarography was one of the first analytical techniques capable of determining metal ion concentrations and speciation in aqueous solutions for levels of 10^{-5} to 10^{-7} M [6—8]. Numerous modifications of the classical method have been developed to increase sensitivity and also provide signals that are easier to measure. At present, one of the best methods for trace metal characterization is anodic stripping voltammetry (a.s.v.) [9, 10].

Stripping polarography is a variation on the normal a.s.v. technique. In stripping polarography, the peak stripping currents observed during the normal a.s.v. trace are plotted as a function of the deposition potential, so that a curve analogous to the classical d.c. polarogram is obtained (Fig. 1, a, b). The value at which the peak currents level off after the sharp rise and become

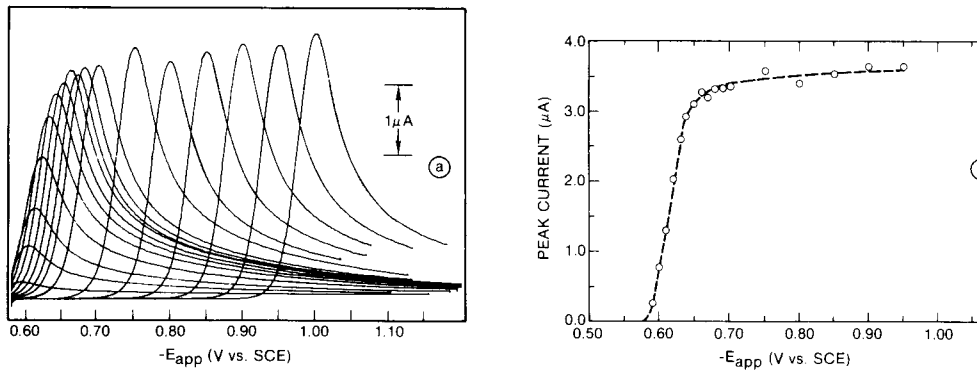

Fig. 1. (a) A.s.v. peaks obtained at each indicated applied potential; (b) stripping polarographic curve constructed from a.s.v. peaks (10^{-8} M cadmium(II) in sea water).

independent of the applied potential is known as the limiting current (i_{pl}). The potential at which the current is half the limiting current is the half-wave potential ($E^*_{1/2}$).

The method has been used for qualitative analysis of metals in natural waters at concentrations too low for direct polarographic analysis. Matson [11] and Fitzgerald [12], using the mercury composite graphite electrode (MCGE), suggested that the speciation of trace metals in sea water could be studied from peak current—electrolysis potential plots. However, Seitz et al. [13] demonstrated that deteriorating electrodes could alter the shape of these plots. Bubic and Branica [14] used stripping polarography with the hanging mercury drop electrode (HMDE) to establish that $Cd(H_2O)_6^{2+}$, $CdCl^+$ and $CdCl_2$ were the predominant species of cadmium in sea water. They did this by comparing values of the potential at the foot of the sigmoidal curve (E^*_p) obtained from natural sea water, with E^*_p observed for a model system.

Recently, Zirino and Kounaves [15] showed that for electrochemically reversible, simple-ion systems, the peak current—electrolysis potential relationships obtained by stripping polarography can be described by:

$$E = E^0 + \beta \ln [(i_{pl} - i_p)/i_p] + \beta \ln [2\delta_s r f_s / 3 D_s f_a] - \beta \ln(t) \quad (1)$$

where E is the applied potential; E^0 the standard potential for the amalgam electrode; f_a and f_s are the activity coefficients for amalgam and simple ion; δ_s is the thickness of the diffusion layer; D_s the diffusion coefficient; r the radius of the mercury drop; t the electrolysis time; i_p the peak current; i_{pl} the peak current obtained under limiting conditons, and $\beta = RT/nF$, where R, T, n and F have their usual meanings.

This paper will show the derivation of the stripping polarographic relationship for an electrochemically reversible system containing a reagent which forms a complex with the depolarizer. The method is applied to studies of cadmium—ethylenediamine complexation in sea water by means of a computer-assisted system for generation of the curves.

THEORY

In the manner of the simple-ion relationship given earlier (15), the current is linearized over the electrolysis interval t, and it is assumed that $q = \bar{i}t$, where q is the charge accumulated over time t and $\bar{i}$ is the average current which flows over this period. However, for the complexed metal, $\bar{i}$ is controlled by the flux of complexed metal to the electrode and, from the mean value theorem [16],

$$\bar{i} = nFA\bar{F}_c \tag{2}$$

where $\bar{F}_c$ is the average flux of the complexed ion, A the area of the electrode and n and F have their usual meanings.

Similarly, when the bulk concentration of the complexed metal C_c is not significantly altered during electrolysis, the quantity $\bar{F}_c$ is proportional to $C_c - \bar{C}_c^0$ as given by the Nernst diffusion layer approximation

$$\bar{F}_c = (D_c/\delta_c)(C_c - \bar{C}_c^0) \tag{3}$$

where D_c is the diffusion coefficient of the complex, δ_c is the thickness of the diffusion layer, and $\bar{C}_c^0$ is the average concentration of the complex at the drop surface.

Combining these last three equations gives

$$q = nFA(D_c/\delta_c)(C_c - \bar{C}_c^0)t \tag{4}$$

At the limiting conditions, $\bar{C}_c^0 \to 0$, $q_l = nFA(D_c/\delta_c)C_c t$. Combining this with eqn. (4) gives

$$\bar{C}_c^0 = (q_l - q)/nFA(D_c/\delta_c)t \tag{5}$$

It is now assumed that the system is in equilibrium over the entire interval and that

$$K_c = (f_s C_s^0)(f_x C_x)^P / f_c C_c^0 \tag{6}$$

where K_c is the dissociation constant of the complex, f_c, f_x and f_s are activity coefficients of the complex, ligand and simple ion, respectively, P is the stoichiometric coefficient of the ligand with the metal ion, and C_x^0 is the concentration of ligand at the electrode surface. The following conditions are also assumed: (a) the solution contains a large excess of the complexing ligand compared to the complex, thus making the liberation of free ligand at the electrode surface, as the complex is reduced, insignificant, i.e. $C_x^0 = C_x$; (b) K_c is so small that the contribution of the simple ion to the overall current is negligible, i.e., $C_c \gg C_s$; (c) all activity coefficients remain constant over the interval.

Under these circumstances, use of the mean value theorem gives

$$\bar{C}_c^0 = (f_x C_x)^P f_s \bar{C}_s^0 / f_c K_c \tag{7}$$

Since the system is at equilibrium, the Nernst equation is obeyed at all times and at any instant of time

$$\theta = C_s^0 f_s / C_a^0 f_a = \exp\left[\beta^{-1}\,(E - E^0)\right] \tag{8}$$

where C_a^0 is the concentration of the reduced metal at the surface of the drop and f_a is its activity coefficient. C_a^0 remains at present an unspecified function of t, thus $C_a^0 = f(t)$. Simplification of eqn. (8) gives $C_s^0 = \theta' f(t)$, and further application of the mean value theorem gives the average value of C_s^0

$$\bar{C}_s^0 = (\theta'/t) \int_0^t f(t)\,\mathrm{d}t \tag{9}$$

But by definition, $\int_0^t f(t)\,\mathrm{d}t/t = \bar{C}_a$, and thus $\bar{C}_s^0/\bar{C}_a^0 = \theta'$, which means that the ratio of the average values is identical to the ratio of the instantaneous values.

The actual value of $\bar{C}_a^0$ is then obtained from the equation proposed for C_a^0 [17] under conditions of constant flux. Integrating again, and neglecting those terms not experimentally significant, gives

$$\bar{C}_a^0 = 3\bar{i}t/2nFAr = 3q/2nFAr \tag{10}$$

Algebraically, use of the constant flux equation is justified because, by definition, $\bar{i}$ is constant over the entire interval. In actuality, this approximation introduces a small error at very low overvoltages and large values of t which is not experimentally resolvable under the usual a.s.v. conditions [15].

Substitution of the equivalent values for $\bar{C}_s^0$ and $\bar{C}_a^0$ in the Nernst expression gives

$$\bar{C}_s^0 = K_c(q_l - q)fc/(C_x f_x)^P nFA(D_c/\delta_c)t \tag{11}$$

As shown above

$$\bar{C}_s^0 f_s / \bar{C}_a^0 f_a = C_s^0 f_s / C_a^0 f_a = \exp\left[\beta^{-1}\,(E - E^0)\right] \tag{12}$$

Substituting eqns. (10) and (11) into this equation gives

$$\exp\left[\beta^{-1}\,(E - E^0)\right] = \left[(q_l - q)/q\right]\, 2\delta_c K_c f_c r/3(C_x f_x)^P f_a D_c t \tag{13}$$

When $q = q_l/2$, the half-wave potential $E_{1/2}^*$ is obtained from

$$E_{1/2}^* = E^0 + \beta \ln\left[2\delta_c f_c r/3D_c f_a\right] + \beta \ln(K_c) - \beta P \ln(C_x f_x) - \beta \ln(t) \tag{14}$$

Ordinarily, the ratio $\delta_c f_c/D_c$ for the complex is approximately equal to the ratio $\delta_s f_s/D_s$ for the simple ion. Thus the collection of terms $E^0 + \beta \ln\left[2\delta_s f_s r/3D_s f_a\right] - \beta \ln(t)$ is the half-wave potential for the simple ion ($E_{1/2s}^*$), and

$$E_{1/2c}^* = E_{1/2s}^* + \beta \ln(K_c) - \beta P \ln(C_x f_x) \tag{15}$$

This result is similar to that for the classic polarographic wave of a complexed ion [18] but in addition, there is the linear dependency of $E_{1/2c}^*$ with $\ln(t)$.

Development of automated instrumentation for stripping polarography

It became apparent from preliminary efforts to confirm the theoretical relationships that obtaining the data points for the stripping polarographic curves required an excessive amount of time and effort. Each curve is composed from a minimum of 10—15 points, each point being at least one nor-

mal a.s.v. experiment. Under the best conditions, with deposition times of 10—30 min, the stripping polarographic curve would take at least 2 days, during which the operator has to monitor the instrument constantly, changing mercury drops and deposition potentials, and collecting output data.

Several workers [19—22] have demonstrated the utility of on-line computer systems for controlling electrochemical analysis. Since a large amount of data is produced by stripping polarography, interfacing with a computer also becomes extremely advantageous for the storage and evaluation of data. With the on-line computer, processing of data such as peak heights or integration of peak areas, can be done rapidly.

Interfacing of a computer with a commercial polarograph is relatively straightforward, and this technique was adopted to save time in the development of the necessary hardware and software. Within these constraints, a general, completely automated system for stripping polarography was developed. The system is extremely flexible and can be programmed to carry out any conceivable experiment of this type, with the experimental parameters selected by the user. The system can also accommodate other inputs such as pH and temperature sensors with only minor changes in hardware and software.

EXPERIMENTAL

Instrumentation

The computer used was a Hewlett-Packard 21MX (HP21MX) with 32K of RAM working memory and an HP disc drive for mass storage. In addition, the system contained 16 general-purpose I/O registers, a 91000A analog-to-digital 8-channel interface (A/D), and the ISA-FORTRAN extension software package for the above.

A Princeton Applied Research Polarographic Analyzer model 174A was used as the potentiostat. The electrolysis cell consisted of a PAR model 9323 HMDE fitted into a PAR model 9300 polarographic cell top, and a model 3343 cell bottom. The cell was not thermostated, but room temperature was maintained at 25 ± 1°C, and the cell temperature was continuously monitored. The solution was stirred with a 1.1-cm Teflon-covered stirring bar coupled to a Sargent-Welch 600-rpm synchronous-speed magnetic stirrer (model 576492). The reference electrode was a Markson model 1202 Ag/AgCl with a platinum-banded tip, which also served as the counter electrode. The PAR 174A was modified as described below.

Scan Control. The potential scan on the 174A is normally initiated by pressing the scan button, which disconnects the −15 V d.c. power to the ramp control circuit and allows the potential to start changing according to a preselected rate and direction. Modification for computer control consisted of providing the −15 V d.c. power through contacts on a relay, which in turn was controlled by bit 0 from the computer.

Cell control. Normally, the applied potential is controlled by a selector switch on the front panel. Even though this switch has only three positions

(dummy cell on—off—cell on), it also simultaneously controls circuits for the summing amplifer, ramp generator, and potential feedback. Because of its many functions, this switch was replaced by a 10-contact relay connected in series with the selector switch. With the switch set to EXT (cell on), the cell can be turned on/off by the computer.

Initial potential selection. The initial deposition potential is normally selected by setting the initial potential control on the front panel of the 174A to the desired potential. For computer control, a digital-to-analog converter (D/A) was used to provide a controlled current to the 174A summing amplifier.

X-axis output voltage. A modification was required to the x-axis output circuit to provide the 0—10 V d.c. range necessary for operation of the HP21 A/D converter. The x-axis output, normally 0—1 V d.c., was increased by replacing resistor R118 on the programmer—potentiostat board by a 10 kohm variable resistor. It was then adjusted so that the x-axis output was 0—10 V d.c.

Stirrer control. The 174A does not provide any control for a stirrer. To provide for computer control, a solid-state relay was used. The state of bit 1 from the computer controls the 115-V a.c. power to the stirrer motor.

Gas control. The 174A does not provide any gas control. Nitrogen is normally used to purge the sample before an a.s.v. cycle and to maintain a gas blanket during the deposition and stripping steps. Gas control was achieved by addition of a solenoid-controlled three-way valve. The valve under computer control selects the purge or blanket outlet.

Drop dislodger and dispenser. To provide for the dislodging and dispensing of the mercury drop, a modified version of the PAR model 314 automated hanging mercury drop electrode (HMDE) was incorporated into the system (see Fig. 2). The Model 314 consists of a small metal enclosure that is mounted on the same stand as the cell and contains the stepper motor drive circuits and dislodge solenoid. The motor is a four-phase stepper type that rotates a precise number of degrees each time it is pulsed by its drive circuit. Reduction gears between the motor and the drive shaft set the drive shaft rotation at 0.25 degree per step. The drive circuits are controlled by 10-ms pulses provided by the computer. The duration and number of pulses can be specified in the control program.

Systems interconnections and operation

The system can basically be separated into three subsystems: (1) the HP21MX minicomputer; (2) the interfaces (IF1, IF2); and (3) the polarographic analyzer (PAR-174A). A block diagram of the system interconnections is shown in Fig. 3.

The HP21MX, apart from the CPU, includes a 16-bit I/O register and an A/D converter. The 16-bit output register provides a pathway for transferring data from the CPU to a peripheral device. Each of the 16 output lines can be set high (1) or low (0) by software control. The A/D converter (20-kHz A/D interface—HP91000A) is used for converting the x-axis (potential) and y-axis (current) outputs to digital form for manipulation and storage by the CPU.

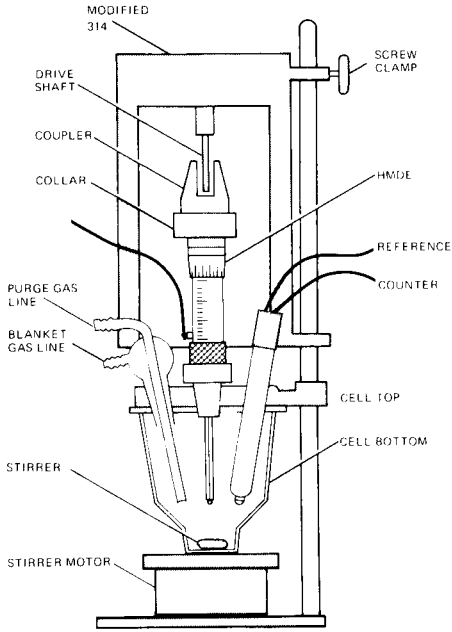

Fig. 2. Diagram of automated HMDE and cell.

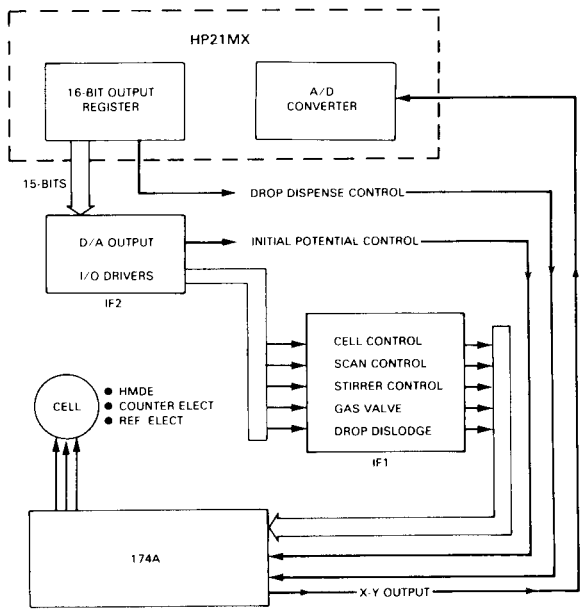

Fig. 3. Block diagram of automated system.

The A/D is directly connected to the x—y output posts on the rear panel of the 174A.

Two interface cards, IF1 and IF2, are located within the 174A. IF1 contains the cell control relay, stirrer control relay, scan control relay, voltage regulator, and gas control circuit. IF2 contains the D/A converter and the I/O drivers. The outputs from the 16-bit register, except bit 12, go to IF2. Depending on the state of bits 14 and 15, both the D/A and I/O drivers can be controlled by the same 16 bits.

For dislodging the drop, a pulse from the computer is applied to the drop-dislodge solenoid, which then hits the clamp that holds the HMDE.

With bit 14 high, and bit 15 low, bits 0—10 control the output current of the D/A. This output is connected to the input of the 174A summing amplifier which controls the initial potential applied to the cell. The D/A provides 1 μA/bit. Adding 1 bit decreases the current by 1 μA. When bits 0—10 are all set to 1, the output current to the summing amplifier will be 0 μA, and the potential applied to the cell will be 0 V. Each bit added will increase the potential 10 mV until at 100 μA the applied potential is —1.0 V. When bit 15 is high (1) and bit 14 is low (0), bits 0—4 and bit 12 set the I/O drivers high or low; these, in turn, control the various relays.

Software. All software was written in FORTRAN V. The programs allow the user to select purge time, initial potential, final potential, current range, deposition time, and equilibration time. The values for the applied deposition potential $E_{(app)}$ are selected from E(initial) to E(initial) + (0.3 V) from a set of originally randomized potentials. A normal a.s.v. experiment is run at a selected potential and the data are then stored in the first file. Each subsequent set of data is stored in a new file. The program selects 30 potentials, 0.01 V apart, in covering the 0.3-V range chosen. While the program is running, the status of the 174A is displayed by the "S" register on the HP21MX front panel.

Reagents

All solutions were prepared with deionized water. Standard stock solutions of cadmium(II) were prepared from cadmium nitrate. Unless otherwise indicated, all chemicals used were analytical-reagent grade. All sea water used was collected from Scripps Pier, San Diego, California, and filtered through a 0.22-μm Millipore system.

The mercury used for filling the capillary was reagent-grade and was triple distilled; it was further cleaned by washing with nitric acid and then passing through a pinhole made in a filter paper.

The nitrogen gas used was ultra-pure (99.95%) (Airco Co.) passed once through a Messer Griesheim Oxisorb filter (Parco).

Procedures

For each experiment the cell was washed with 8 M nitric acid and then rinsed several times with quartz-distilled water. The cell was filled with 25 ml of quartz-distilled water and the appropriate reagents added. The experiment was then placed under computer control after the operator had entered the

necessary experimental and instrument parameters. The following steps were carried out under the program control: (1) the solution was purged with nitrogen gas for 30 s (15 min for the first run); (2) the old drop was dislodged and a new drop formed; (3) the specified deposition potential was applied for the specified time; (4) the stirrer was turned off, and the solution allowed to equilibrate for 15—30 s; (5) the applied potential was decreased by 5 $mV s^{-1}$, starting at the deposition potential; (6) while the potential was decreasing, the A/D converter sampled the x-axis (E_{app}) and y-axis (I) outputs at 500-ms intervals. These (E_{app}, I) data points were stored in a data file.

After the scan, the experiment was either terminated or a new deposition potential was selected by the program and the procedure repeated. A typical computer plot for stripping polarography is shown in Fig. 4.

To verify the relationship indicated by eqn. (15), solutions of 10^{-5}—10^{-8} M cadmium(II) which contained 10^{-1}—10^{-4} M ethylenediamine in 0.1 M KNO_3 were studied.

RESULTS AND DISCUSSION

Addition of 10^{-2} M ethylenediamine (en) to a solution containing 10^{-8} M cadmium(II) in 0.1 M KNO_3 caused a shift of the half-wave potential of —168 mV ± 2 mV (Fig. 5). The value for $\Delta E^*_{1/2}$, calculated from eqn. (15) is —166 mV. The slope of the reduction wave was 27 mV ± 1 mV, indicating the reversibility of this system and thus allowing application of eqn. (15). This same equation can also be used to determine the formula of the complex by solving for P, which may be determined from the variation of $E^*_{1/2c}$ with C_x. A simple analytical expression is obtained by differentiation of eqn. (15) to give:

$$d(E^*_{1/2c})/d(\log C_x) = -0.0592\, P/n \qquad (16)$$

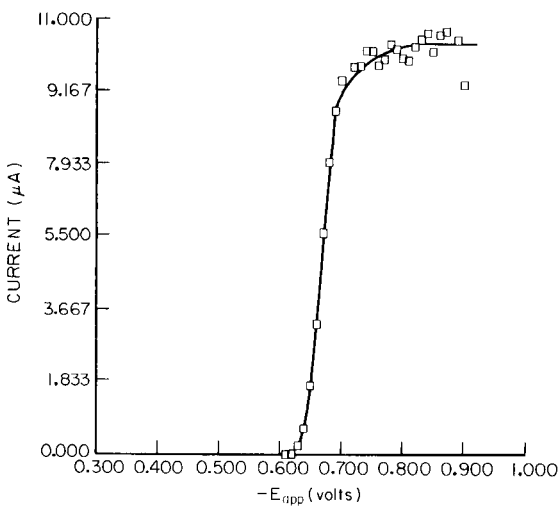

Fig. 4. Computer-generated plot of 10^{-5} M cadmium(II) in 0.1 M KNO_3.

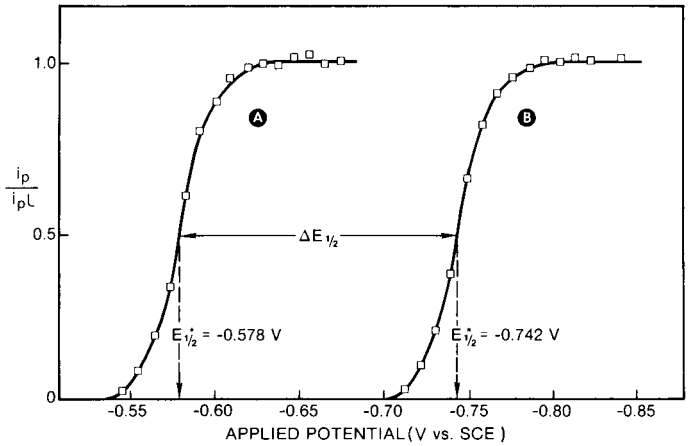

Fig. 5. Shift of the half-wave potential on addition of 10^{-2} M ethylenediamine to 10^{-8} M cadmium(II) in 0.1 M KNO_3. (A) 10^{-8} M cadmium(II); (B) 10^{-8} M cadmium(II) + 10^{-2} M ethylenediamine.

where $E^*_{1/2s}$ and f_x in eqn. (15) are assumed to be constants as C_x is varied; x is also assumed to be non-ionic in this case. Subject to these assumptions, the value of P can be obtained directly from the slope of the plot (solid line) shown in Fig. 7. With ethylenediamine concentrations of 10^{-1}—10^{-4} M, the experimental value of the slope $d(E^*_{1/2c})/d(\log [en])$ is —0.087 V ± 0.001 V. Since n = 2 for the reduction of the cadmium(II) complex, P = 2.89. This indicates that under the given conditions, the predominating complex is $Cd(en)_3^{2+}$.

To find the dissociation constant of the $Cd(en)_3^{2+}$ complex, eqn. (15) was used. Substituting —0.578 V for $E^*_{1/2s}$, —0.742 for $E^*_{1/2c}$, 1×10^{-2} M for C_x, and P = 3, the value obtained was $K_c = 2.48 \times 10^{-12}$, which within experimental error, is in good agreement with a literature value of $K_c = 2.32 \times 10^{-12}$ [23].

Application to sea water

Addition of 10^{-1}—10^{-3} M ethylenediamine to sea water containing 10^{-8} M Cd(II) caused a shift of the half-wave potential of —126 mV ± 2 mV (see Fig. 6). This shift is less than that observed for $Cd(en)_3^{2+}$ in 0.1 M KNO_3 and reflects the competitive complexation of cadmium by chloride ions. The slope of the stripping polarographic reduction wave for Cd(II) in sea water was found to be 29 mV ± 1 mV for all concentrations of ethylenediamine and cadmium used. This indicates that the reduction/oxidation reaction $Cd^{2+} \rightleftharpoons Cd(Hg)$ in sea water is reversible and allows the application of eqns. (1) and (15) for investigative purposes.

The complexation of cadmium(II) in sea water was further studied by observing the effect of successive additions of ethylenediamine on $E^*_{1/2}$ values (Fig. 7). It can be predicted from eqn. (15) that no change in $E^*_{1/2}$ will be ob-

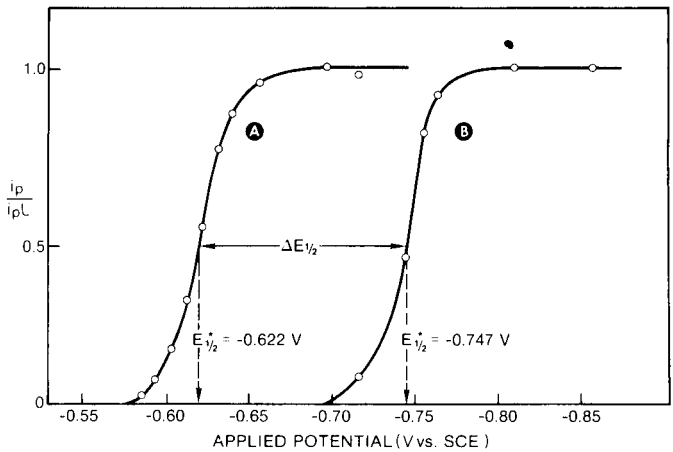

Fig. 6. Shift of the half-wave potential on addition of 10^{-2} M ethylenediamine to 1×10^{-8} M cadmium(II) in sea water. (A) and (B) as in Fig. 5.

served until $(C_x f_x)^P \leqslant K_c$. For $Cd(en)_3^{2+}$ ($K_c = 2.3 \times 10^{-12}$), the slope $d(E^*_{1/2})/d(\log [en])$ would be expected to be 0 mV up to a concentration of ca. 10^{-4} M ethylenediamine; at values above 10^{-4} M, the slope should be equal to 87 mV. As can be seen in Fig. 7, the theoretical and experimental points are practically identical for the KNO_3 solution. The second curve in Fig. 7 describes the behavior of $E^*_{1/2}$ for Cd(II) in sea water. In contrast to the KNO_3 system, the curve for sea water shows a gradual change of $E^*_{1/2}$ between 10^{-5} and 10^{-3} M ethylenediamine. This change can be explained by the competitive complexation of Cd(II) by chloride and ethylenediamine.

Figure 8 shows the calculated distribution of Cd(II) in 0.1 M KNO_3 and in sea water at various concentrations of ethylenediamine. The data were obtained by use of a modified version of a computer program which calculates the equilibrium concentration distribution of chemical species in aqueous systems [24]. In a 0.1 M KNO_3 solution, cadmium(II) is approximately 98% complexed with 10^{-4} M ethylenediamine. In model sea water (0.55 M Cl^-, 0.45 M Na^+; 0.052 M Mg(II); 0.01 M Ca(II); 0.0097 M K^+; 0.0012 M CO_3^{2-}; 0.028 M SO_4^{2-}; pH 8.0) the cadmium(II) is initially 95% complexed as $CdCl_2$. As ethylenediamine is added, the chloride is slowly replaced. However, the Cd(II) is not significantly (ca. 98%) complexed by ethylenediamine until ca. 10^{-3} M has been added.

The agreement between the calculated and experimental results indicates the usefulness of stripping polarography for studying and verifying at realistic concentrations, model systems of trace metals in natural media.

In conclusion, computer-assisted stripping polarography offers a means of applying classical polarographic methods to the study of ligand complexation of trace metals at sub-10^{-8} M levels. These initial investigations of cadmium—ethylenediamine complexes in sea water indicate the feasibility of using this

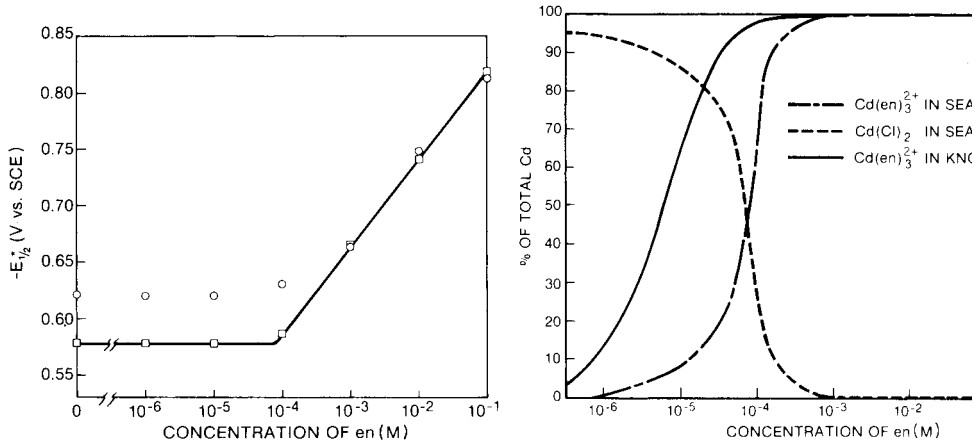

Fig. 7. Effect of ethylenediamine concentration on the half-wave potential for 10^{-8} M cadmium(II) in sea water (○) and 0.1 M KNO_3 (□). The line represents the theoretical plot for 0.1 M KNO_3.

Fig. 8. The calculated distribution of cadmium(II) in 0.1 M KNO, and in sea water at various concentrations of ethylenediamine.

method for further characterization studies of other trace metals, such as lead, zinc, and copper, at sub-10^{-8} M levels.

The use of the mini-computer was found to be essential because of the amount of data and time required for stripping polarographic curve generation.

We thank S. Yamamoto and E. P. Cooper for their continuing support of this effort, and J. J. Morgan, J. Westall and F. M. M. Morel for making the computer programs REDEQL and MINEQL available. We are also indebted to Jacques Buffle for many constructive suggestions. This work was funded by the Naval Ocean Systems Center IR/IED program and by the Office of Naval Research under contract NR083-301.

REFERENCES

1 R. Fukai, L. Huynh-Ngoc and C. N. Murray, J. Oceanogr. Soc. Jpn., 29 (1973) 44
2 A. Zirino and S. Yamamoto, Limnol. and Oceanogr., 17 (1972) 661.
3 D. Dyrssen and M. Wedborg, in E. D. Goldberg (Ed.), The Sea, Vol. 5, Wiley-Interscience New York, 1974.
4 W. Stumm and P. A. Brauner, in J. P. Riley and R. Skirrow (Eds.), Chemical Ocean ography, Academic Press, New York, Vol. 1, 1975, Ch. 3.
5 J. Shapiro, Chemical Environment in the Aquatic Habitat, North-Holland, Amsterdam 1967.
6 H. A. Laitinen and I. M. Kolthoff, J. Phys. Chem., 45 (1941) 1079.
7 J. J. Lingane, Ind. Eng. Chem., Anal. Ed., 15 (1943) 583.
8 N. H. Furman, Anal. Chem., 22 (1950) 33.
9 E. Barendrecht, Electroanalytical Chemistry, Vol. 2, M. Dekker, New York, 1967, pp 53—109.

10 M. Whitfield in J. P. Riley and R. Skirrow (Eds.), Chemical Oceanography, Academic Press, New York, 1975, Vol. 4, Ch. 20.
11 W. R. Matson, Ph.D. Thesis, Massachusetts Institute of Technology, Cambridge, Mass., 1968.
12 W. F. Fitzgerald, Ph.D. Thesis, Massachusetts Institute of Technology and Woods Hole Oceanographic Institution, Cambridge, Mass., 1969.
13 W. R. Seitz, R. Jones, L. Klatt and W. D. Mason, Anal. Chem., 45 (1973) 840.
14 S. Bubic and M. Branica, Thalassia Jugosl., 9 (1973) 47.
15 A. Zirino and S. Kounaves, Anal. Chem., 49 (1977) 56 (correction, 51 (1979) 592).
16 T. A. Bak and J. Lichtenberg, Mathematics for Scientists, W. A. Benjamin, New York, 1966, p. 143.
17 I. Shain and J. Lewinson, Anal. Chem., 33 (1961) 187.
18 L. Meites, Polarographic Techniques, Interscience, New York, 1955, p. 97.
19 H. E. Keller and R. A. Osteryoung, Anal. Chem., 43 (1971) 342.
20 Q. V. Thomas, L. Kryger and S. P. Perone, Anal. Chem., 48 (1976) 761.
21 L. Kryger, D. Jagner and H. J. Skov, Anal. Chim. Acta, 78 (1975) 241.
22 A. M. Bond and B. S. Grabaric, Anal. Chim. Acta., 88 (1977) 227.
23 B. E. Douglas, H. A. Laitinen and J. C. Bailar, J. Am. Chem. Soc., 72 (1950) 2484.
24 J. C. Westall, J. J. Zachary and F. M. M. Morel, MINEQL — A Computer Program for the Calculation of Chemical Equilibrium Composition of Aqueous Systems, Massachusetts Institute of Technology, Cambridge, Mass. (1976).

Analytica Chimica Acta, 109 (1979) 341—349
© Elsevier Scientific Publishing Company, Amsterdam — Printed in The Netherlands

VOLTAMMETRIC DETERMINATION OF PHENYLBUTAZONE AND OXYPHENBUTAZONE AT A GLASSY CARBON ELECTRODE

H. K. CHAN

Wyeth Laboratories, Huntercombe Lane South, Maidenhead, Berkshire SL6 0PH (Gt. Britain)

A. G. FOGG*

Department of Chemistry, Loughborough University of Technology, Loughborough, Leicestershire LE11 3TU (Gt. Britain)

(Received 22nd February 1979)

SUMMARY

Linear-sweep and differential-pulse voltammetric methods are reported for the determination of phenylbutazone and oxyphenbutazone and of their pharmaceutical dosage forms. The methods are based on the electrochemical oxidation of phenylbutazone and oxyphenbutazone at a glassy carbon electrode in 0.1 M sodium acetate—0.1 M acetic acid in 98% ethanol. The mechanisms are discussed. The proposed methods show good reproducibility and are not subject to interference from common tablet excipients and from possible therapeutically active drug substances used in combination with phenylbutazone and oxyphenbutazone. A simple interrupted-sweep procedure can be used to determine phenylbutazone in the presence of oxyphenbutazone.

Phenylbutazone (4-butyl-1,2-diphenylpyrazolidine-3,5-dione) and oxyphenbutazone (4-butyl-2-(4-hydroxyphenyl)-1-phenylpyrazolidine-3,5-dione monohydrate) are widely prescribed anti-inflammatory drugs and have the following structures:

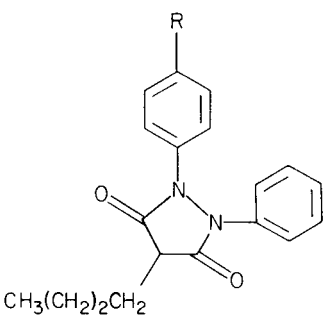

R=H, phenylbutazone
R=OH, oxyphenbutazone

The analytical chemistry of phenylbutazone and oxyphenbutazone has received considerable attention. Many analytical techniques such as spectrophotometry [1, 2], gas—liquid chromatography [3—5] and high-performance liquid chromatography [6], have already been applied in analyses for the drugs and their metabolites in biological fluids. The official BP method involves a non-aqueous titration with acetone as the solvent [7]. The same method has been used for the determination of the drugs in tablets. Recently, a non-aqueous titration in tetramethylurea as solvent has been reported [8] for determinations in pharmaceutical preparations.

The polarographic inactivity of phenylbutazone and oxyphenbutazone at the dropping mercury electrode led to the introduction of a derivatization procedure [9], which involves hydrolysis of the drugs in a mixture of acetic and hydrochloric acids, diazotization, coupling with 1-naphthol, and differential-pulse polarography of the resulting azo dyes. Although voltammetry is becoming popular for the analysis of pharmaceutical compounds [10, 11], no attempt seems to have been made previously to apply voltammetry to phenylbutazone and oxyphenbutazone.

This paper describes the development of procedures for the voltammetric determination of phenylbutazone and oxyphenbutazone at a glassy carbon electrode by both linear-sweep voltammetry (l.s.v.) and differential-pulse voltammetry (d.p.v.), and in particular the evaluation of the techniques as alternative, convenient methods for the determination of these drugs and their dosage forms. A simple precise interrupted-sweep voltammetric procedure based on the method of Perone et al. [12] proved successful for the determination of phenylbutazone in the presence of its metabolite, oxyphenbutazone.

EXPERIMENTAL

Instrumentation

A PAR 174A polarographic analyzer (Princeton Applied Research Corp.) was used with an Advance X-Y recorder (Model LR 100). The electrode system consisted of a glassy carbon electrode (PAR 9333; nominal surface area 0.28 cm^2), a platinum wire counter electrode and a saturated calomel reference electrode held by means of a rubber O-ring in a salt bridge (PAR 9332) containing a saturated aqueous solution of potassium nitrate. The close-fitting O-ring ensured the minimum flow of aqueous electrolyte into the voltammetric cell; this was important in ensuring good results. The voltammetric cell (PAR 9301) had a working volume of 5—50 ml. All potentials are quoted versus the SCE.

In order to obtain reproducible results, a standard pretreatment procedure was applied to the glassy carbon electrode before each recording. The electrode was first washed with 95% ethanol and with chloroform, then cleaned carefully with a non-abrasive paper tissue soaked in chloroform, and finally dried with a dry tissue. When not in use, the clean electrode was stored in

a boiling tube fitted with a ground-glass joint. Test solutions were not deaerated. No difference between the voltammograms with normal and deaerated solutions was observed.

Reagents

The purity of samples of phenylbutazone and oxyphenbutazone (R. W. Unwin & Co. Ltd.) was checked by the BP procedure [7] and confirmed by thin-layer chromatography. Other reagents were of analytical-reagent grade.

Supporting electrolyte. Dissolve 8.2 g of anhydrous sodium acetate in 20 ml of water. Add 5.8 ml of glacial acetic acid and dilute to 1 l with absolute ethanol.

Standard solutions (1 mg ml^{-1}). Dissolve 100 mg of the drug to be determined in 100 ml of 95% ethanol. Prepare working solutions by suitable dilution.

Preparation of calibration graphs

Solutions of phenylbutazone and oxyphenbutazone (0.5—70 μg ml^{-1}) in the supporting electrolyte were used. D.c. voltammograms were obtained from 0 to +0.8 V with the low pass filter at 0.3. The scan rate and the current sensitivity were in the range 5—20 mV s^{-1} and 1—5 μA full scale deflection, respectively. Differential-pulse voltammograms were obtained from 0 to +0.8 V at a scan rate of 5 mV s^{-1}; a 50-mV pulse and a 1-s pulse cycle were used. The current sensitivity ranged from 0.02 to 0.05 mA full scale deflection. Peak heights were measured in the usual way.

Recommended procedure for the analysis of tablets

Accurately weigh into a 50-ml stoppered centrifuge tube an amount of well-ground tablet — generally reserved from the average weight determination — containing about 25 mg of the drug. Add by pipette 25 ml of 95% ethanol, stopper the tube and shake it vigorously for 30 min to extract the drug. Centrifuge and pipette 5 ml of the supernatant layer into a dry 100-ml volumetric flask. Dilute to 100 ml with the supporting electrolyte and mix well. Transfer a portion of the solution to the voltammetric cell and obtain both d.c. and differential-pulse voltammograms as before. Compare the peak heights with those obtained with standards prepared in the same batch of supporting electrolyte.

RESULTS AND DISCUSSION

Oxidation process

Linear-sweep and differential-pulse voltammetry for phenylbutazone and oxyphenbutazone is based on oxidation at the glassy carbon electrode in a supporting electrolyte consisting of 0.1 M sodium acetate—0.1 M acetic acid in 98% ethanol. The use of organic solvents not only enhances the solubilities

of the drugs but also reduces the possibility of strong adsorption at the electrode surface; this is in marked contrast to aqueous media where adsorption is common [13]. The linearity of response over a wider concentration range in predominantly aprotic organic solvents is also an obvious advantage in rapid and direct formulation assays. The voltammetric behaviour of phenylbutazone and oxyphenbutazone under the above conditions depends on oxidation probably associated with a carbonyl group in the pyrazolone ring. The phenolic group also facilitates the electrochemical oxidation of oxyphenbutazone. Chan and Fogg [14] have shown that the same supporting electrolyte is suitable for the voltammetric determination of several phenolic analgesics in pharmaceutical dosage forms by linear-sweep voltammetry at a glassy carbon electrode. This electrolyte gives a sufficiently positive potential range to allow the anodic waves of the drugs to be observed clearly. The residual currents were negligible for both d.c. and d.p. scans at normal current sensitivities of 5 μA and 0.05 mA, respectively. Typical linear-sweep and differential-pulse voltammograms for the two compounds at the 50 μg ml^{-1} level are shown in Fig. 1.

Calculations based on the sensitivity setting of the instrument indicate that d.p.v. is approximately 10 times more sensitive than l.s.v.; because of the high residual current at low concentration, however, the sensitivity of d.p.v. is only slightly better than that of l.s.v. Although d.p.v. is generally much slower than l.s.v., the d.p.v. current—potential curve is more convenient because the peaks are symmetrical and the current drops almost to zero after the peak.

The peak potentials (E_p) obtained for phenylbutazone and oxyphenbutazone are 0.62 and 0.42 V, respectively, in l.s.v. and 0.56 and 0.37 V,

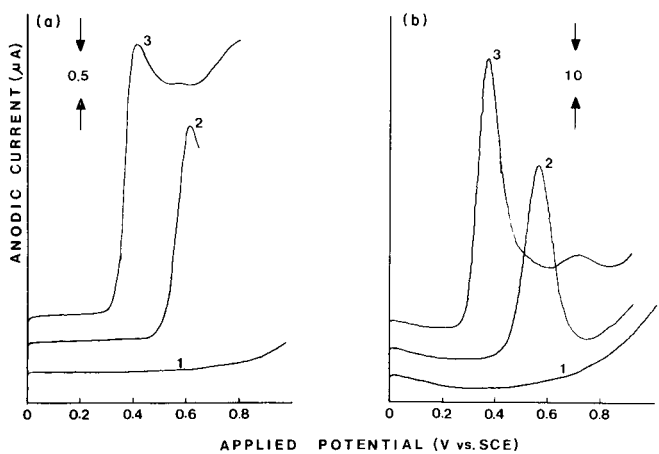

Fig. 1. Typical voltammograms obtained with standards. (a) Linear sweep; (b) differential pulse. (1) blank; (2) phenylbutazone; (3) oxyphenbutazone.

respectively, in d.p.v. These d.p.v. peak potentials are identical to the $E_{p/2}$ values obtained in l.s.v.

Calibration graphs of peak height against concentration for phenylbutazone and oxyphenbutazone by both techniques were plotted over the range 0—70 μg ml^{-1} in the recommended supporting electrolyte. Rectilinear plots were obtained down to the limit of detection of 0.5 μg ml^{-1}. The precision of both voltammetric methods was ascertained by carrying out 10 replicate analyses on freshly prepared 50 μg ml^{-1} solutions. The coefficients of variation for phenylbutazone and oxyphenbutazone were 1.4% and 1.8%, respectively, for l.s.v. and 0.7% and 2.7%, respectively, for d.p.v.

The effect of the water content of the supporting electrolyte on the l.s.v. peak currents and peak potentials was investigated (see Table 1). The peak current of both drug compounds decreases with increasing water content, and it is clearly important that the same batch of supporting electrolyte be used for both samples and standards.

The effect of the voltage scan rate (v) on the i_p, E_p and $i_p v^{-1/2}$ values was examined. Figure 2 shows the values $i_p v^{-1/2}$ and E_p as functions of the logarithmic scan rate for oxyphenbutazone. The plot of E_p vs. logarithmic scan rate shows the typical exponential increase, whereas the plot of peak current function $i_p v^{-1/2}$ vs. logarithmic scan rate shows a linear relationship which means that the voltammetric oxidation process is essentially diffusion-controlled [15] and is a first-order reaction.

The electrochemical oxidation of phenylbutazone and oxyphenbutazone is irreversible, as was shown by cyclic voltammetric measurements (Fig. 3) in which no cathodic peak corresponding to the reduction of the oxidation product was observed at any scan rate (10—100 mV s^{-1}).

In d.p.v., the peak current was proportional to the pulse amplitude between 5 and 100 mV. There is a rectilinear relationship between the pulse amplitude and the peak current for oxyphenbutazone but not for phenylbutazone. The peak current for a constant pulse amplitude of 50 mV is independent of the length of pulse cycles between 0.5 and 2 s, and independent of the sweep rate between 2 and 10 mV s^{-1}.

Determination of phenylbutazone in the presence of oxyphenbutazone

The determination of an electroactive compound by l.s.v. in the presence of a more readily oxidizable compound is difficult, owing to the characteristic shape of the voltammograms. Perone et al. [12] described a method which alleviates this situation to some extent: the linear sweep is interrupted at a potential at which only the first compound is oxidized, so that the concentration of this compound is depleted in the diffusion layer; when the scan is continued the second peak is more clearly defined. This procedure was examined for phenylbutazone in the presence of oxyphenbutazone.

The selectivity of the method was tested by adding various amounts of oxyphenbutazone to a 50 μg ml^{-1} solution of phenylbutazone. Figure 4 shows the effect of successive additions of oxyphenbutazone with an interrupt delay time of 1 min at +0.46 V. The peak current of phenylbutazone at

TABLE 1

Effect of water content on i_p and E_p (l.s.v.) for phenylbutazone and oxyphenbutazone (50 μg ml^{-1}) at the glassy carbon electrode

Water content (%)		2	3	5	7	12
Phenylbutazone	i_p (μA)	2.23	2.18	2.16	2.03	1.88
	E_p (V)	0.62	0.62	0.62	0.62	0.62
Oxyphenbutazone	i_p (μA)	2.65	2.60	2.59	2.53	2.48
	E_p (V)	0.42	0.42	0.42	0.44	0.45

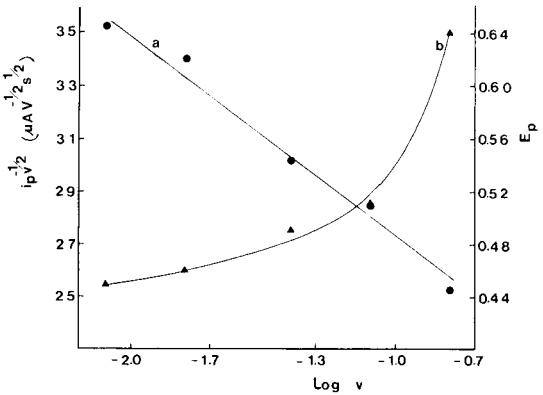

Fig. 2. Curve (a) Relationship of the logarithmic scan rate and the oxidation diffusion current function of oxyphenbutazone ($i_p v^{-1/2}$). Curve (b) Effect of the logarithmic scan rate on the peak potential (E_p) of oxyphenbutazone (50 μg ml^{-1}).

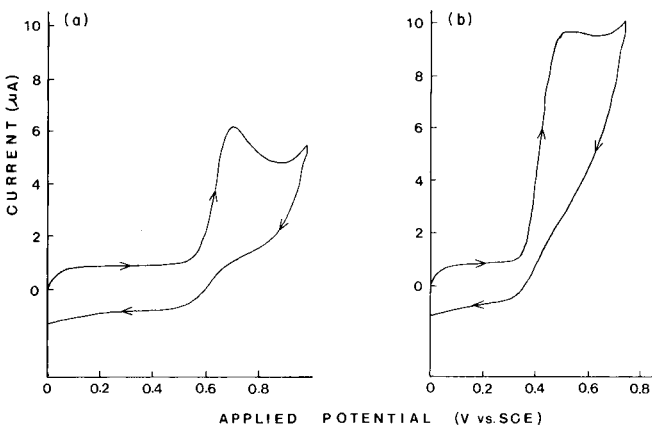

Fig. 3. Cyclic voltammograms of (a) phenylbutazone (50 μg ml^{-1}) and (b) oxyphenbutazone (50 μg ml^{-1}) at the glassy carbon electrode. Voltage scan rate, 100 mV s^{-1}.

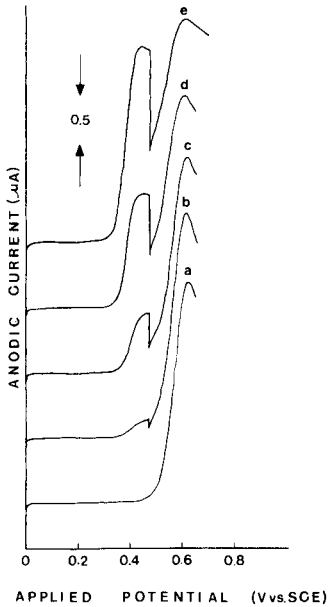

Fig. 4. Interference by oxyphenbutazone on interrupted-sweep voltammograms for 50 μg ml^{-1} solutions of phenylbutazone. Oxyphenbutazone additions of (a) 0.0, (b) 2.0, (c) 5.0, (d) 10.0, and (e) 20.0 μg ml^{-1}. Scans (b)—(e) are interrupted for 1 min at +0.46 V vs. SCE after oxidation of oxyphenbutazone.

+0.62 V is seen to be unaffected by its metabolite, oxyphenbutazone, up to a concentration level of 20 μg ml^{-1}. Above this concentration, longer interrupt delay times would be required which would cause serious convection problems and allow significant electrolysis of the second electroactive species (phenylbutazone). It is therefore impossible to determine small amounts of phenylbutazone in the presence of a much larger amount of oxyphenbutazone as both reactions occur to a significant extent at the peak potential of the latter molecule. However, this metabolite is only present normally at less than 10% of the original phenylbutazone.

Analytical applications

The data given above prove that l.s.v. and d.p.v. are simple and precise methods for the determination of phenylbutazone and oxyphenbutazone. The results obtained for the analysis of six commercially available pharmaceutical solid dosage forms of phenylbutazone and oxyphenbutazone by the recommended procedures are given in Table 2. These are in good agreement with results obtained by u.v. spectrophotometry.

The following excipients which are commonly found in tablets were checked for possible interference with the method: lactose, microcrystalline cellulose, Amberlite IRP88, magnesium stearate and starch. For each, an

TABLE 2

Comparison of recoveries (%) of phenylbutazone and oxyphenbutazone from commercial tablet forms

Sample	Compound	Labelled amount (mg)	L.s.v. method[a]	D.p.v. method[b]	U.v. method
A	Phenylbutazone	200	97.5 ± 0.1	97.5 ± 0.1	97.0[c]
B	Phenylbutazone	100	99.0 ± 0.6	99.7 ± 0.1	99.2[c]
C	Phenylbutazone	100	100.0 ± 0.3	99.7 ± 0.1	99.6[c]
D	Phenylbutazone	100	94.2 ± 0.6	94.5 ± 0.5	94.5[c]
E	Oxyphenbutazone	100	99.2 ± 1.8	99.4 ± 0.6	100.0[d]
F	Oxyphenbutazone	100	103.0 ± 1.5	102.0 ± 1.0	101.0[d]

[a]Each value is the average of three determinations. [b]Each value is the average of three determinations. [c]Assay from USP monograph for phenylbutazone content. [d]Assay from NF monograph for oxyphenbutazone content.

TABLE 3

Effect of other drugs (50 mg) on the recoveries of 50 μg each of phenylbutazone and oxyphenbutazone and voltammetric data for 50 μg ml^{-1} solutions in the recommended supporting electrolyte

Drug	Phenylbutazone recovered (%)	Oxyphenbutazone recovered (%)	E_p (V vs. SCE)	i_p (μA)
Codeine phosphate	100	100	Inactive	
Meprobamate	100	102	Inactive	
Caffeine	98	102	Inactive	
Aspirin	100	100	+ 0.95	0.60
Pentazocine	119	100	+ 0.78	3.43

ethanolic 1 mg ml^{-1} solution was prepared, 1 ml of the supernatant solution was pipetted into the voltammetric cell and 19 ml of the supporting electrolyte were added. No oxidation waves were observed.

The effects of possible combinations with other drugs on the voltammograms were also studied. The l.s.v. behaviour of 50 μg ml^{-1} solutions of five drugs in the recommended supporting electrolyte and the effects of these drugs on phenylbutazone and oxyphenbutazone recoveries are shown in Table 3. Of these drugs, only pentazocine interferes with the determination of phenylbutazone, as it produces an anodic wave at +0.78 V [14], close to the oxidation peak potential for phenylbutazone.

Direct determination of phenylbutazone and oxyphenbutazone in biological fluids was impossible owing to serious interferences from a large number of compounds of both endogenous and exogenous origin. Prior separation is therefore essential, and an h.p.l.c. method with electrochemical detection is currently being studied.

REFERENCES

1 J. J. Burns, R. K. Rose, T. Chenkin, A. Goldman, A. Schulert and B. B. Brodie, J. Pharmacol. Exp. Ther., 109 (1953) 346.
2 E. Jänchen and G. Levy, Clin. Chem., 18 (1972) 984.
3 K. K. Midha, I. J. McGilveray and C. Charette, J. Pharm. Sci., 63 (1974) 1234.
4 I. J. McGilveray, K. K. Midha, R. Brien and L. Wilson, J. Chromatogr., 89 (1974) 17.
5 K. K. Midha, I. J. McGilveray and C. Charette, J. Pharm. Sci., 63 (1974) 1751.
6 N. J. Pound, I. J. McGilveray and R. W. Sears, J. Chromatogr., 89 (1974) 23.
7 British Pharmacopoeia 1973, H.M. Stationery Office, London, 1973, pp. 336, 364—5.
8 M. I. Walash and M. Rizk, Indian J. Pharm., 39 (1977) 82.
9 A. G. Fogg and Y. Z. Ahmed, Anal. Chim. Acta, 94 (1977) 453.
10 R. N. Adams, J. Pharm. Sci., 58 (1968) 1171.
11 H. Hoffmann and J. Volke, in H. W. Nürnberg (Ed.), Electroanalytical Chemistry, J. Wiley, London, 1974.
12 S. P. Perone, D. O. Jones and W. F. Gutknecht, Anal. Chem., 41 (1969) 1154.
13 D. H. Evans, Acc. Chem. Res., 10 (1977) 313.
14 H. K. Chan and A. G. Fogg, Anal. Chim. Acta, 105 (1979) 423.
15 R. N. Adams, Electrochemistry at Solid Electrodes, M. Dekker, New York, 1969.

Analytica Chimica Acta, 109 (1979) 351—359
© Elsevier Scientific Publishing Company, Amsterdam — Printed in The Netherlands

A U.V.-ABSORPTIOSTAT AND ITS APPLICATIONS
Determination of Catalase, Ascorbate Oxidase, Peroxidase, Sorbitol Dehydrogenase and Lactate Dehydrogenase

SIEGBERT PANTEL and HERBERT WEISZ*

Lehrstuhl für Analytische Chemie, Chemisches Laboratorium der Universität, Freiburg i. Br. (Federal Republic of Germany)
(Received 19th February 1979)

SUMMARY

The instrumental set-up and applications of a u.v.-absorptiostat are described. It is used to determine enzymes such as catalase (1.5—15 U), ascorbate oxidase (3—30 mU), peroxidase (10—100 mU), sorbitol dehydrogenase (15—150 mU) and lactate dehydrogenase (15—150 mU). It is also shown that this method is of special interest for the determination of enzymes with low substrate concentrations.

"Stat" methods are an important tool in analytical chemistry [1], primarily because in these methods it is possible to maintain well-defined mild reaction conditions in the reaction mixture by keeping constant the concentration of a reactant. This is done by controlled addition of the essential substance as it is consumed. Therefore it is not necessary — in contrast to closed systems — to use a large excess of this substance for maintaining the conditions of the "initial state". This is of importance for the determination of rather unstable catalysts, e.g. enzymes, as the substance to be added is in many cases a strongly oxidizing agent. Furthermore, "stat" methods often produce linear addition curves, which are easily evaluated by using the tangent method.

Another advantage of the "stat" methods is their flexibility. For almost all physicochemical indication methods, the instrumental set-up needs only some simple equipment in addition to the basic unit. The basic unit may be a commercial or a home-made instrument [2—4] and consists of a comparator, a burette and a millivoltmeter. Around this it is possible to build pH-stats [1, 5, 6] and potentiostats [7—9] as well as absorptiostat [10], biamperostat [11, 12] and luminostat [13] instruments. The "thermostat" should be mentioned in this context; although it uses the "stat" principle, however, no solution is added from a burette [14].

From the absorptiostat methods already described [10] it seemed obvious to extend the use of this apparatus to the u.v. region. This would be especially favourable to biochemistry, as many substrates for enzyme-catalyzed reactions absorb in this region.

In this paper it will be shown that the u.v.-absorptiostat can be successfully applied for the determination of catalysts. A number of enzymes are determined in the U to mU range.

EXPERIMENTAL

Apparatus

The apparatus used consists of a u.v. spectrophotometer and a "stat" unit. The PMQ II spectrophotometer (Carl Zeiss, Oberkochen-BRD) is fitted with a temperature-controlled (rotary thermostat) cuvette holder with magnetic stirrer in the cell compartment, an important requirement for kinetic measurements. The quartz cuvette has a path length of 20 mm (10-ml total volume). For the "stat" unit, the home-made apparatus shown in Fig. 1 is coupled with a motor-driven 1-ml burette, mechanically coupled to a recorder (Microdosigraph; Metrohm, Herisau-Switzerland). In this case, it was not possible to use the Combi-Titrator 3D employed in earlier "stat" methods, because in general the electronic output of the photometer could not be adapted to the input of the Impulsomat.

The reaction termperature was 25 ± 0.1°C and the recorder speed 10 mm min^{-1} in all cases.

Mode of operation

In the regulating device of the "stat" apparatus (Fig. 1) the measured potential is compared electronically with a preset "working potential" (e.g. a current-analog voltage, equivalent to the u.v. transmittance of the substance to be kept constant in the solution); any difference between the

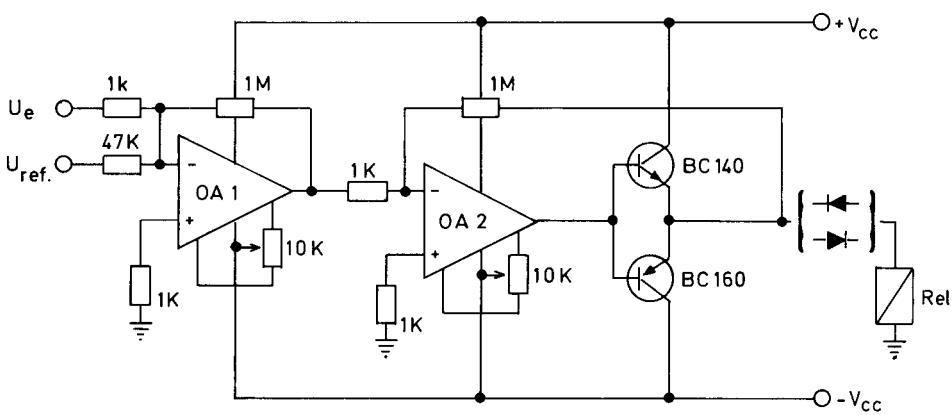

Fig. 1. Circuit for the comparator used. OA 1, operational amplifier Teledyne type 2740; OA 2 operational amplifier Teledyne type 741; Rel., Reed relay Elfein type 804-1R29 (12 V); V_{cc} = ±15 V; stabilized voltage source.

two opens the burette so that the substance to be kept constant is added to the system until the two potentials are identical again. The stepwise additions are plotted vs. time as shown in Fig. 2.

The range for determination of the catalyst depends essentially on the absorptivity of the substrate measured. From the instrumental point of view, the concentration of the reactant to be kept constant should be such that it causes an approximately 10% decrease in the transmittance and should be reached by the addition of 50—500 μl. This obviously defines the range of concentration of the solution to be added from the burette and so the range of the determination. If the stationary concentration of the reactant corresponded to less than 50 μl, there would be excessive overshoot at every addition step; if it corresponded to more than 500 μl, then the remaining volume in the 1-ml burette would not suffice for reasonable evaluation of the recorder plot.

It is of definite importance [11] that enzyme activities (expressed in U = μmol substrate conversion per min) under given conditions of temperature, pH and basic concentration of the rate-determining substrate, can be determined directly from the recorder plot.

Example

From the plot (Fig. 2) for the determination of a catalase solution, it can be seen that within 5 min (A—B) 0.37 ml of hydrogen peroxide solution (B—C) is consumed to maintain a preset concentration of hydrogen peroxide. With the given value of 5 mg H_2O_2 ml^{-1} for the solution added, the enzyme activity can be calculated from $U = 0.37 \times 5 \times 1000/34.01 \times 5 = 10.88$ μmol min^{-1}. This value is identical with the value reported in the literature

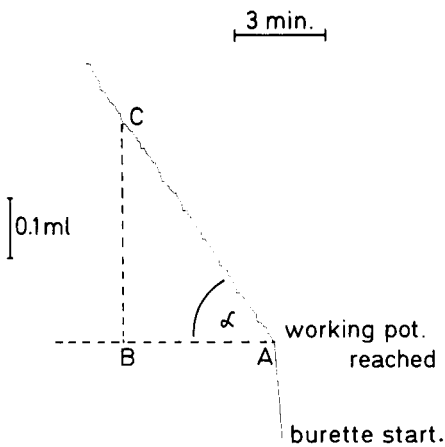

Fig. 2. Recorder plot for the determination of 11 units of catalase in 7.5 ml; 3 mM H_2O_2 as constant concentration.

for closed systems [15] when the same concentration of hydrogen peroxide is used as starting concentration. For lower substrate concentrations, the "stat" value for substrate conversion per unit time is smaller; the difference may be up to two orders of magnitude.

In the examples described here, the basic concentrations of the reactants were chosen to be as similar as possible to those of the standard methods [15], to obtain comparable values for the enzyme activities.

This means that the substrate concentration to be kept constant caused a decrease in transmittance of about 50% or more. This unavoidably diminishes the sensitivity of the determinations but has the advantage of giving the results directly in international units.

Enzyme and substrate solutions

All enzyme solutions were prepared from commercially available products (Boehringer, Mannheim-BRD) by dissolution in a suitable buffer; substrate solutions were prepared, as far as possible, from analytical-grade substances with deionized distilled water.

The enzyme activities of the stock solutions were determined by a suitable standard method [15]; standard and sample solutions were then prepared from these stock solutions by dilution.

CONTROLLED ADDITION OF HYDROGEN PEROXIDE AND DETERMINATION OF CATALASE

Hydrogen peroxide shows a broad absorption band between 200 and 250 nm, thus substances which catalyze the decomposition of hydrogen peroxide can be determined with the aid of the u.v.-absorptiostat. This will be demonstrated by the determination of catalase [15, 16]. The wavelength used was 245 nm; the molar absorptivity was found to be 34 l mol^{-1} cm^{-1} under the very special conditions described here.

Procedure and results

To the quartz cuvette are added: 0.5 ml of sodium phosphate buffer solution (pH 7.0, 0.4, M) and 0.1—1 ml of a catalase (EC 1.11.1.6; 15 U ml^{-1}) for preparing a calibration graph or an equivalent amount of the sample solution. After dilution with twice-distilled water to 7.5 ml, this solution is about 25 mM in buffer. After thermostating for 5 min, the transmittance is adjusted to 100% by varying the slitwidth. Then the automatic addition of hydrogen peroxide (5 mg ml^{-1}) is started, the working potential being selected so as to maintain a constant 8 mM concentration of hydrogen peroxide during the measuring time. This corresponded to 29% transmittance.

The plot of tan α vs. catalase concentration was a straight line going through the origin of the coordinates. Some results for the determination of catalase are given in Table 1.

TABLE 1

Determination of catalase (units/7.5 ml) with 8 mM H_2O_2 as basic concentration

Given	1.51	2.20	4.73	5.98	8.19	11.02	12.91	13.71	14.94	15.00
Found	1.49	2.28	4.57	6.19	8.14	10.92	12.29	14.02	15.43	14.93

CONTROLLED ADDITION OF ASCORBIC ACID AND DETERMINATION OF ASCORBATE OXIDASE

Ascorbic acid shows a well defined absorption band at 265 nm from the enediol group, which disappears on oxidation to dehydroascorbic acid [17]. Ascorbate oxidase can be determined because it catalyzes the oxidation of ascorbic acid by molecular oxygen following the equation:

$$-(OH)C = C(OH)- + O_2 \xrightarrow{\text{asc. oxid.}} -CO-CO- + H_2O_2$$

Procedure and results

To the quartz cuvette are added: 1 ml of sodium phosphate buffer solution (pH 7.0, 0.4 M) and 0.1—1 ml of a solution of ascorbic acid oxidase (EC 1.10.3.3; 0.03 U ml^{-1}) for preparing a calibration graph or an equivalent amount of the sample solution. After dilution with water to 7.5 ml, this solution is about 50 mM in buffer. After thermostating for 5 min, the transmittance is adjusted to 100% and the system is initiated (0.05 mg of ascorbic acid per ml). The working signal is chosen so as to maintain a constant concentration of 12 μM ascorbic acid, corresponding to 45% transmittancy.

Enzyme solution and ascorbic acid were stored at 10°C in the dark.

The molar absorptivity at 265 nm was 14 500 l mol^{-1} cm^{-1} under the conditions used here for ascorbic acid. The plots of tan α vs. catalyst concentration were almost linear and passed through the origin. Table 2 gives some results for the determination of ascorbate oxidase.

Determination of cytochrome c and copper(II). Hydrogen peroxide has a much lower molar absorptivity (ca. 10 l mol^{-1} cm^{-1} at 265 nm) in the 250—270-nm region than ascorbic acid. This may be used to determine a substance which catalyzes the oxidation of ascorbic acid with hydrogen peroxide by selectively following the change in concentration of ascorbic acid in the reaction system. Cytochrome c is such a substance [18]. The determination can be done at 265 nm in sodium acetate buffer solution (pH 3.6, 50 mM in final volume) which is 2 mM in hydrogen peroxide with a constant concentration of 5.2 μM in ascorbic acid. The possible range of determination is 30—300 μg of cytochrome c in 7.5 ml.

TABLE 2

Determination of ascorbate oxidase (milliunits/7.5 ml); 12 μM ascorbic acid as basic concentration

Given	4.74	6.73	7.91	11.08	15.82	17.40	20.57	23.73	28.48	28.48
Found	4.75	7.12	7.63	10.81	14.87	17.72	20.57	24.21	28.17	28.33

As an example of a metallic species which also catalyzes this oxidation, copper(II) can be determined in the range 0.8—8 μg/7.5 ml (50 mM sodium acetate buffer solution pH 4.3; 2 mM in hydrogen peroxide under conditions similar to those for cytochrome c).

CONTROLLED ADDITION OF DIHYDROXYFUMARIC ACID AND DETERMINATION OF PEROXIDASE

Dihydroxyfumaric acid shows a marked enediol absorption band in the u.v. region as does ascorbic acid (λ_{max} = 292 nm [17]). Therefore it can be used to determine suitable catalysts, e.g. peroxidase [17—19]. Under the reaction conditions applied here, the molar absorptivity for dihydroxyfumaric acid at 292 nm was 8500 l mol^{-1} cm^{-1}. The absorption of hydrogen peroxide can be neglected under these conditions.

Procedure and results

To the quartz cuvette are added: 2 ml of sodium acetate buffer solution (pH 4.3, 0.2 M), 2 ml of hydrogen peroxide (10 mg ml^{-1}) and 0.1—1 ml of a solution of peroxidase (EC 1.11.1.7; 0.1 U ml^{-1}) for preparing a calibration graph or an equivalent amount of the sample solution. After dilution with water to 7.5 ml, this solution is 50 mM in buffer and 78 mM in hydrogen peroxide. After thermostating for 5 min, the transmittance is adjusted to 100% and the burette is started (0.15 mg of dihydroxyfumaric acid, as the dihydrate, per ml; the solution is neutralized to pH 5—6 before dilution with water). The working potential is chosen so as to maintain a constant concentration of 40 μM in dihydroxyfumaric acid, corresponding to 21% transmittance. The slight absorption caused by hydrogen peroxide and peroxidase at the wavelength used is included in the blank.

Dihydroxyfumaric acid was stored in the dark at 10°C.

The calibration graph is nearly linear in the given range. Some results for the determination of peroxidase are given in Table 3. The catalytic activity of peroxidase against dihydroxyfumaric acid is only about 1/40th of the activity found against guaiacol [15]. The values given in Table 3 must therefore be multiplied by 40 to give "guaiacol units".

TABLE 3

Determination of peroxidase (milliunits/7.5 ml); 40 μM dihydroxyfumaric acid as basic concentration

Given	19.8	34.6	39.6	49.5	51.9	55.4	59.4	79.2	79.2	99.0
Found	19.8	33.2	41.1	47.5	54.4	55.3	60.4	78.7	78.2	97.0

CONTROLLED ADDITION OF NADH AND DETERMINATION OF SORBITOL DEHYDROGENASE AND LACTATE DEHYDROGENASE

Reduced β-nicotinamide adenine dinucleotide (NADH) shows a marked absorption peak at 340 nm, which can be used for the determination of the activity of NADH-dependent enzymes. This may be shown by the examples of the determination of sorbitol dehydrogenase (SDH) and lactate dehydrogenase (LDH).

Sorbitol dehydrogenase catalyzes the reaction [15]

$$\text{D-Fructose} + \text{NADH} + \text{H}^+ \overset{\text{SDH}}{\rightleftharpoons} \text{D-sorbitol} + \text{NAD}^+$$

This reaction can be used with an excess of fructose for the determination of SDH with NADH.

Lactate dehydrogenase (LDH) catalyzes the reaction [15]:

$$\text{Pyruvate} + \text{NADH} + \text{H}^+ \overset{\text{LDH}}{\rightleftharpoons} \text{lactate} + \text{NAD}^+$$

This reaction can be used with an excess of pyruvate for the determination of LDH again with NADH as substrate added from the burette.

Procedure and results for sorbitol dehydrogenase

To the quartz cuvette are added: 1 ml of sodium phosphate buffer solution (pH 6.1, 0.3 M), 3 ml of D-fructose (40 mg ml^{-1}) and 0.1—1 ml of a solution of SDH (EC 1.1.1.14; 0.15 U ml^{-1}) for preparing a calibration graph or an equivalent amount of the sample solution. After dilution with water to 7.5 ml, this solution is 40 mM in buffer and 89 mM in D-fructose. After thermostating for 5 min, the transmittance is adjusted to 100% and the burette started (1 mg β-$NADHNa_2 \cdot 2H_2O$ ml^{-1} in water). The working potential is selected to maintain a constant concentration of 80 μM in NADH, corresponding to 10% transmittance. As the NADH and SDH solutions are markedly unstable at room temperature, the solutions should be stored at 4°C. The slight absorption of SDH and D-fructose at 340 nm is integrated into the blank.

The molar absorptivity was found to be 6200 l mol^{-1} cm^{-1} for $NADHNa_2 \cdot 2H_2O$ at 340 nm. The plot of tan α vs. SDH concentration was a straight line through the origin. Some results for the determination of SDH are given in Table 4.

Procedure and results for lactate dehydrogenase

To the quartz cuvette are added: 2 ml of sodium phosphate buffer solution (pH 7.5, 0.2 M), 0.5 ml of a solution of pyruvate (2 mg of sodium pyruvate per ml in water) and 0.1—1 ml of a solution of LDH (EC 1.1.1.27; 0.15 U ml^{-1}) for preparing a calibration graph or an equivalent amount of the sample solution. After dilution with water to 7.5 ml, this solution is 50 mM in buffer and 1.2 mM in pyruvate. After thermostating for 5 min, the transmittance was adjusted to 100% and the burette started (1 mg

TABLE 4

Determination of sorbitol or lactate dehydrogenase (milliunits/7.5 ml); 80 μM NADH as basic concentration

Sorbitol dehydrogenase										
Given	15.0	26.2	30.0	60.0	67.5	90.0	97.5	101.2	120.0	150.0
Found	16.5	27.0	31.5	59.3	63.8	90.0	99.0	99.0	121.5	157.5
Lactate dehydrogenase										
Given	18.7	28.1	37.4	56.1	56.2	93.6	112.3	112.3	131.0	149.8
Found	19.6	29.9	33.7	50.5	56.3	92.7	116.0	112.0	127.3	146.0

β-NADH$Na_2 \cdot 2H_2O$ ml^{-1} in water). The working signal was selected so as to maintain a constant concentration of 80 μM in NADH, corresponding to 10% transmittance. The small absorbance of pyruvate is integrated into the blank. NADH and LDH solutions were stored at 4°C.

The plot of tan α vs. LDH concentration gave a straight line going through the origin. Some results for the determination of LDH are given in Table 4.

DETERMINATION OF REACTION RATES AT LOW SUBSTRATE CONCENTRATION

For many kinetic investigations it is desirable to keep the concentration of the substrates as low as possible, but low substrate concentrations cannot be applied in closed systems because the initial rate would often last only a few seconds. Here, the "stat" method is of great advantage, for it is possible to maintain the low substrate reaction conditions.

In order to achieve maximum sensitivity (about 10% lowering of the transmittance for the basic concentration of the substrate, added from the burette), the concentration of the substrate must be kept as low as given in Table 5. Buffer solutions and reaction conditions are the same as described above.

TABLE 5

Determination of enzymes at low substrate concentrations

Enzyme	Substrate A	Conc. in the test vol. (mM)	Substrate B	Conc. in the test vol. (μM)	Solution added from burette (mg ml^{-1})
Catalase	—	—	H_2O_2	800	1
Ascorbate oxidase	—	—	Ascorbic acid	1.5	0.01
Peroxidase	H_2O_2	3.9	Dihydroxy-fum. acid	2.8	0.02
Sorbitol dehydrogenase	D-Fructose	14.8	NADH	3.5	0.1
Lactate dehydrogenase	Pyruvate	1.2	NADH	3.5	0.1

REFERENCES

1 S. Pantel, Anal. Chim. Acta, 104 (1979) 205.
2 J. T. Stock, J. Chem. Educ., 47 (1970) 311.
3 Siemens AG, Halbleiterschaltbeispiele (1970) p. 61.
4 R. Job and S. Freeland, Anal. Biochem., 79 (1977) 575.
5 K. M. Møller, Biochim. Biophys. Acta, 16 (1955) 162.
6 H. V. Malmstadt and E. H. Piepmeier, Anal. Chem., 37 (1965) 34.
7 H. Weisz, D. Klockow and H. Ludwig, Talanta, 16 (1969) 921.
8 D. Klockow, H. Ludwig and M. A. Giraudo, Anal. Chem., 42 (1970) 1682.
9 H. Weisz, K. Rothmaier and H. Ludwig, Anal. Chim. Acta, 73 (1974) 224.
10 H. Weisz and K. Rothmaier, Anal. Chim. Acta, 75 (1975) 119.
11 S. Pantel and H. Weisz, Anal. Chim. Acta, 70 (1974) 391.
12 S. Pantel and H. Weisz, Anal. Chim. Acta, 89 (1977) 47.
13 S. Pantel and H. Weisz, Anal. Chim. Acta, 74 (1975) 275.
14 D. Klockow, G. Karenovics and W. Meiners, Anal. Chim. Acta, 100 (1978) 485.
15 H. U. Bergmeyer, Methoden der Enzymatischen Analyse, 3. Aufl., Verlag Chemie, Weinheim, 1974. Vol. I, pp. 129, 601, 607, 713, 725.
16 Catalase, Worthington Biochem. Corp., Freehold, N. J., 1968.
17 E. Racker, Biochim. Biophys. Acta, 9 (1952) 577.
18 A. L. Kamyshnyi, E. S. Chukhrai and O. M. Poltorak, Zh. Fiz. Khim., 48 (1974) 334; Chem. Abstr., 81 (1974) 132131.
19 E. F. Hartree, Biochem. J., 107 (1968) 581.

Analytica Chimica Acta, 109 (1979) 361—372
© Elsevier Scientific Publishing Company, Amsterdam — Printed in The Netherlands

DESIGN CONSIDERATIONS FOR A TWO-DIMENSIONAL RAPID SCANNING FLUORIMETER

ISIAH M. WARNER*, MICHAEL P. FOGARTY and DENNIS C. SHELLY

Department of Chemistry, Texas A & M University, College Station, Texas 77843 (U.S.A.)

(Received 15th March 1979)

SUMMARY

The design of a two-dimensional rapid scanning fluorimeter which eliminates much unneeded transfer optics is described. The advantages and disadvantages of commercially available optical systems are discussed with regard to preservation of image quality and relative cost. The combination of holographic polychromators and conventional lenses in the recommended design produces spectra as accurate as those obtained on most conventional fluorimeters.

The rapid acquisition of spectral data continues to be an important objective of the spectroscopist, not only for reasons of efficiency but also for enhanced information. For instance, spectral data obtained in a minute is of no kinetic value if the half-life of the monitored reaction is a millisecond. A few years ago, rapid acquisition usually meant the use of mechanical scanning devices such as cam-driven prisms [1]. Rapid data acquisition is now possible by rapid scanning detectors such as vidicons [2], intensified vidicons [3], and self-scanning solid-state detectors [4]. These detectors consist of a two-dimensional array of light-sensing elements (typically 500 × 500) and can easily be scanned in a few tens of milliseconds. In addition to the time and multichannel advantage, the degree of failure for such devices is relatively low. The types [5] and spectroscopic uses [6] of multichannel detectors have been discussed in two excellent reviews.

Many early uses of multichannel detectors [5] involved one-dimensional arrays of scanning elements; this has very considerable advantages of speed over conventional detectors such as photomultiplier tubes. The potential advantages of two-dimensional multichannel detectors have been recently recognized in several investigations. Some of these applications include emission spectroscopy [7], fluorescence spectroscopy [8, 9] and time-resolved spectroscopy [10]. However, none of these studies emphasized the special problems of two-dimensional imaging. Indeed, the real-time correction of two-dimensional images can be a very complex process [11]. Therefore, careful consideration should be given to the minimization of the problems associated with conventional optics. The options for two-dimensional imaging and the increased cost factors for acquiring each option are

discussed in this paper. The results of these considerations are illustrated through an improved two-dimensional rapid scanning fluorimeter. This fluorimeter rapidly acquires fluorescent data in the form of an emission—excitation matrix, M. The elements m_{ij} correspond to the fluorescence intensity monitored at emission wavelength λ_j for excitation of wavelength λ_i. The rapid acquisition of these data in the form of the matrix M produces considerable advantages for the analysis of multicomponent fluorescence data [12, 13].

OPTICAL CONSIDERATIONS

The efficient transfer of electromagnetic radiation is central to the design of any spectrometer. This implies rigorous efforts to maximize throughput as well as preserve image quality and resolution throughout the optical system. The following treatment is therefore separated into discussions of these two distinct problems.

Maximization of throughput

In the design of spectrometers, it is often presumed that simple matching of f numbers will maximize throughput. However, James and Sternberg [14] have delineated the fallacies of such assumptions. They indicated that the quantity of light (luminosity) which passes through a system is governed by the Helmholtz—Lagrange theory. Consider (Fig. 1) an object of height H_0 located at a point P_0. The imaging element E_0 subtends an angle Φ_0 with the point P_0. Given that the optical system is present in a single medium (e.g. air), the Helmholtz—Lagrange invariant requires that the product $\Phi_i H_i$ be a constant, i.e. $\Phi_0 H_0 = \Phi_1 H_1 = \cdots = \Phi_n H_n = \text{Constant}$.

If any optical element is in a different medium, then the index of refraction of each medium must also be included in the product constant. It is useful to note that the Helmholtz—Lagrange invariant must be satisfied in both the X and Y planes. The invariant for each plane is not necessarily the same. In fact, for a spectrometer with a long narrow slit (as is often the case), the invariants will be very different. Computation of the angle Φ_i is simplified if the angle $\Phi_i/2$ is considered. Simple trigonometry provides the relationship

$$\tan(\Phi_i/2) = Y_i/X_i \tag{1}$$

where Y_i is half the height of the imaging element E_i and X_i is the distance of E_i from the image point P_i. It should be noted that the above-mentioned constant (Helmholtz—Lagrange invariant) is likely to be determined by a single focusing element. As an example, the analyzing monochromator in a fluorimeter would determine the constant. By using the diameter of the focusing element and the focal length of the monochromator, the angle Φ_i can be computed from eqn. (1). The product of Φ_i and the height of the entrance slit determines the throughput for the entire optical system. In computing the parameters for the other optical components in the system, the throughput is maximized by keeping all other $\Phi_i H_i$'s greater than or equal

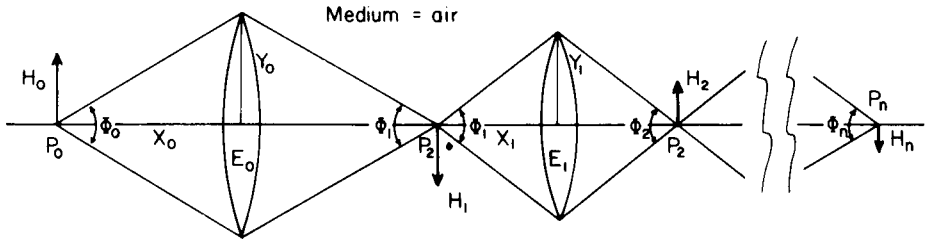

Fig. 1. Optical train (n optical elements) for a typical spectrometer.

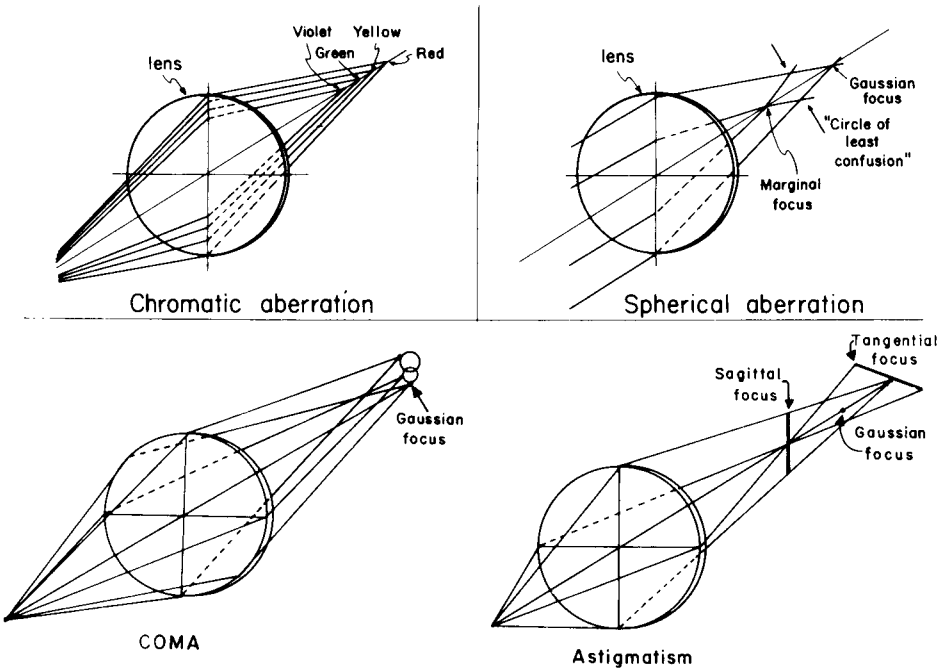

Fig. 2. Common distortions associated with lensing systems.

to the calculated constant while simultaneously satisfying f number requirements.

Preservation of image quality and resolution

In general, all optical components produce some form of image distortion. These distortions are often in the form of spherical aberrations, chromatic aberrations, astigmatism, coma, or some combination of these. Consider the simplified diagrams of Fig. 2, which depict each of these distortions produced by a single "thin" lens. Spherical aberrations arise where parallel light rays on the margin of the lens are brought to a focus. These marginal rays meet on the axis at different points from the normal axial focus which corresponds to the focusing point of the lens computed by using the Gaussian approximation [14]. This approximation for an ideal lens requires that the

bundle of light converge to a point at the "Gaussian focus". For a non-ideal lens system a "circle of least confusion" or "best imaging point" is usually obtained as half way between the Gaussian and marginal focus.

Chromatic aberrations (see Fig. 2) are a consequence of the variation of the index of refraction of a medium with wavelength of light. This aberration causes the image of different wavelengths of light to be formed at various points on the optical axis.

Coma and astigmatism (see Fig. 2) are expected to be the most detrimental of the optical distortions to two-dimensional image quality. Whereas chromatic and spherical aberrations are manifested by differences in the focal points of the light rays focused along the focal axis of the lens, coma is displayed as a convergence of light rays at different points along the focal plane of the lens. The resulting distortion is a "comet-shaped" image of variable intensity composed of many overlapping circles of different diameters. Each of these overlapping circles is a result of focusing pairs of rays from opposite ends of a given annular element of the lens (Fig. 2). If there were no coma effect, all such pairs would meet at a single point. Astigmatism occurs because these pairs may come to a focus before or after the focal plane. This results in the formation of two perpendicular focal planes (sagittal and tangential) separated by the Gaussian foci (Fig. 2).

The preservation of image quality therefore requires careful consideration of conventional alternatives. The advantages and disadvantages of unconventional optical systems are outlined below.

Achromatic lenses. An obvious solution to chromatic and spherical aberrations is the use of achromatic lenses. These are multi-element lenses which have been corrected for these two distortions. Most achromats are doublets but occasionally triplet configurations are used, depending on the degree of correction desired for aberration. Of the doublets, the air-spaced doublets are the most versatile. However, a major disadvantage of achromatic systems is the relatively high cost of acquiring ultraviolet response. Achromats with ultraviolet response can be specially fabricated, but the cost per lens can be 100 times that of conventional u.v. lenses. In addition, corrections for coma and astigmatism are not provided with simple achromats. The additional correction can be acquired with computer-designed higher multiplets. However, such systems employ glass which creates a considerable loss in the useable spectral range. Typically, the cutoff for such lenses is around 400 nm.

Mirrors. Goldstein and Walters [15, 16] recommended preserving the quality of two-dimensional images with symmetric arm mirror pairs. Unlike lenses, mirrors are often free of chromatic or spherical aberrations, largely because of better quality controls and the coating used in their manufacture. However, a major disadvantage of mirrors is that astigmatism and coma are frequently encountered, especially in off-axis applications. These distortions become particularly severe for systems requiring mirrors with small f numbers. It is possible to cancel some of these distortions by using a symmetric arm mirror pair arrangement with very small off-axis angles or a "W" configuration with two such mirror pairs [16]. An additional disadvantage of mirror

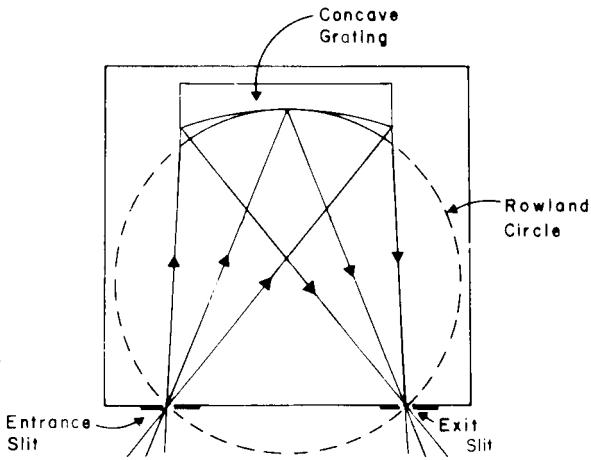

Fig. 3. Conventional concave grating monochromator with image focused onto Rowland circle.

systems is that the cost of specially fabricated systems can be somewhat prohibitive. Depending on the number of elements purchased, this cost can be 5—10 times that of conventional lenses.

Polychromators. Considering the cost and limitations of unconventional lensing systems, the number of lenses required should be minimized. This can be realized through the use of special polychromators. Consider the concave grating monochromator depicted in Fig. 3, which is typical of many monochromator systems. With a concave grating, various wavelengths are focused along a circle (the Rowland circle). Selected wavelengths are brought into focus at the exit slit by mechanically rotating the grating. The exit slit of this monochromator is removed to produce a polychromator. Clearly, such use is not totally adequate because the entire spectral range is not focused at the exit slit plane. However, many rapid scanning spectrometers employ such a polychromatic system [9, 17]. The development of holographically ruled gratings [18] has significantly improved polychromatic systems; these polychromators have a relatively flat spectral response and are capable of displaying 600 nm onto a 1-in. plane. All wavelengths over this 600-nm range are in focus at the exit plane of the polychromator. The exit plane is located 38 mm outside the housing for direct coupling to a multichannel detector. Moreover, the costs of such systems and conventional polychromatic systems are similar.

INSTRUMENT DESIGN

The final configuration of the rapid scanning fluorimeter developed is shown in Fig. 4. The system includes the features of a conventional fluorimeter as well as the two-dimensional capabilities characteristic of the video fluorimeter [8, 9], but subsequent discussion will be confined to the two-dimensional capabilities because conventional fluorimeters are well documented [19].

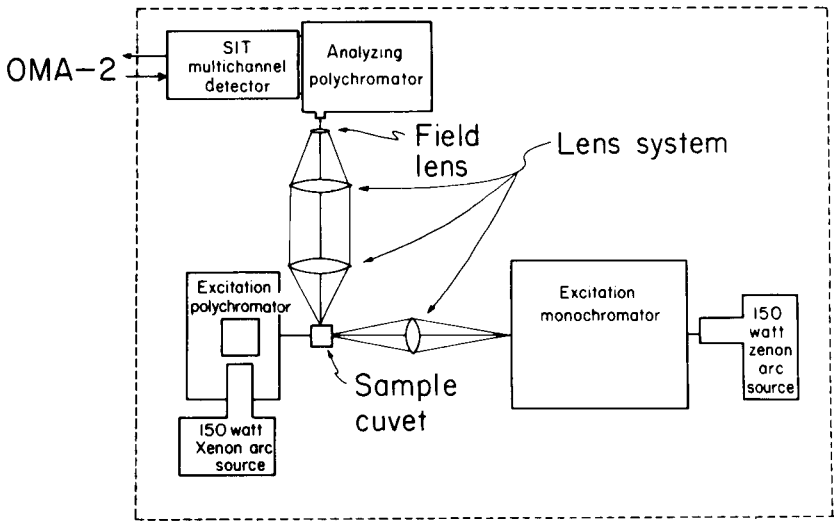

Fig. 4. Optical layout of rapid scanning fluorimeter.

Rapid acquisition of two-dimensional fluorescence data is achieved by placing the excitation monochromator in its usual 90° orientation with respect to the emission monochromator. However, the excitation monochromator is rotated on its side [8] so that the excitation pattern consists of multiple exciting wavelengths spatially dispersed along the long axis of the cuvet. The cuvet image is then a measure of the fluorescence excitation spectrum. In this two-dimensional configuration, the JY UFS 200 polychromator [18] was used. Since the exciting beam is focused 38 mm outside the polychromator, the excitation image plane was focused directly into the center of the cuvet. This configuration totally eliminated the use of additional transfer optics between the excitation polychromator and the sample cuvet. The illumination source, a 150-W xenon arc lamp (Oriel, Model 6111), was mounted above the excitation polychromator because the entrance slit lay at the top in the unusual orientation recommended. The arc was imaged onto the entrance slit of this polychromator by means of a combination of two u.v.-grade fused silica lenses and a right-angle mirror. No efforts were made to eliminate the use of conventional lenses at this point; because of the great intensity of the light source, any slight variation in intensity from non-ideal lens behavior could be neglected.

As the analyzing polychromator, a JY UFS 200 polychromator was again selected. The detector was then mounted directly to the polychromator with the detector surface at the focal plane of the polychromator. Thus, the transfer optics between the analyzing polychromator and the detector were eliminated.

In this configuration, a further problem must be considered: the two-dimensional cuvet image must be effectively imaged onto the entrance slit of the analyzing polychromator. Preservation of this image is critical for perfor-

mance. The several alternatives to conventional lenses outlined above were considered in terms of the preservation of image quality and cost. Cost was an important factor because it was necessary to keep the price of this lensing system below $1000. The high cost of achromatic lenses with ultraviolet response eliminated them from consideration; moreover, the necessary corrections for astigmatism and coma would decrease the usable spectral range of commercially available achromats. A symmetric mirror pair can be purchased for slightly more than $1000, and this has the advantage that mirrors provide the ultraviolet response desired as well as being free of chromatic and spherical aberrations. However, as indicated above, off-axis applications of symmetric mirror pairs requiring low f numbers create severe image distortion by astigmatism. Goldstein and Walters [15] have outlined a formula for the computation of astigmatism in mirror systems. This formula was applied, with the f number of the polychromator used ($f/3$). The minimum distance between the sagittal and tangential image (astigmatism) was calculated as ca. 25 mm, which would give intolerable image distortion. A "W" configuration would reduce the severity of this distortion, but cost would be prohibitive. Accordingly, conventional lens systems were considered.

A single lens would avoid the convolution of aberrations caused by lens combinations and would be satisfactory provided that coma and astigmatism were not too severe. From the Helmholtz—Lagrange invariant (eqn. 1) with the focal ratio ($f/3$) of the analyzing polychromator and the distance of the image from the entrance slit, the required lens was calculated to be 51 mm in diameter with an f number of 1.57. Such a lens would be expected to produce a severe amount of coma, because the thinner the lens, the more nearly ideal is its behavior. Consequently, an ultraviolet lens combination was preferred for transference of the cuvet image onto the entrance slit of the analyzing polychromator. Such lens combinations will involve a convolution of the chromatic and spherical aberration produced by each lens. However, these aberrations should be much less severe than the coma and astigmatism produced by a single lens of $f/1.57$. Figure 4 shows the orientation of the lens combination along with the field lens at the entrance slit of the analyzing polychromator. The field lens is located at the focal length of the preceding lens and is necessary to image the pupil of the preceding lens onto the grating of the analyzing polychromator [14]. It does not alter the f number of the preceding lens combination. This imaging combination and field lens cost only $400.

This compound lens system focuses the spatially resolved cuvet image onto the entrance slit of the analyzing polychromator, which preserves spatial information in the Y-direction and disperses intensity versus wavelength information in the X-direction. Therefore, a two-dimensional image of fluorescence intensity as a function of exciting and emitting wavelength is produced at the exit slit. For n fluorescing components, the mixture matrix, M, has the simple form [12]

$$\mathbf{M} = \sum_{l=1}^{n} \alpha(l)\, \mathbf{X}(l)\, \mathbf{Y}(l) \qquad (2)$$

where M is formed by the outer product of the excitation spectral vector $\mathbf{X}(l)$, the emission spectral vector $\mathbf{Y}(l)$, and $\alpha(l)$, a concentration-dependent term. Previous studies [12, 13, 20] have shown that analysis of multicomponent fluoresence data in the form of the matrix M provides significant advantages.

The two-dimensional image at the exit slit of the polychromator must, of course, be preserved by the detector. A Princeton Applied Research Optical Multichannel Analyzer System (OMA-2) with a silicon-intensified target (SIT) multichannel detector (PAR model 1254) was selected. This detector can be gated for times as short as 40 ns. The entire system is controlled by a dedicated LSI-11 microprocessor (Digital Equipment Corporation) with a single-drive floppy disk for data storage. There are two major advantages to this system: (a) the SIT camera can be controlled in both a single-track (one-dimensional) or multiple-track (two-dimensional) mode; (b) it can be directly coupled to the fluorimeter so that data acquisition is immediate. The system can acquire data to 16-bit accuracy in the single-precision mode and 32-bit accuracy in the double-precision mode.

Figure 5 shows a block diagram of the detection system. A Hewlett Packard 9845 minicomputer (dotted lines) can be coupled through a serial or parallel interface to the microprocessor. The linear algebra and graphics capabilities of this minicomputer make the fluorimeter a versatile system for rapid analysis of fluorescent mixtures.

RESULTS AND DISCUSSION

The ultimate objective in the design of this two-dimensional rapid scanning fluorimeter was to produce an image of quality and accuracy. The degree to which this objective was achieved was assessed for perylene and anthracene. Figure 6(a) shows the excitation spectrum, with three distinct bands, for an ethanolic 10^{-7} M solution of perylene. The emission spectrum is a mirror image of the excitation spectrum. Since the matrix M is the outer product of the excitation and emission vectors, the two-dimensional image corresponding to the dispersed emission band of each excitation band should produce an image with nine peaks. This expectation is realized in Fig. 6(b) although some of the weaker bands do not show up well here; the diagonal pattern in Fig. 6(b) corresponds to scattered exciting radiation.

Figure 7(a) shows the excitation spectrum for an ethanolic 3×10^{-6} M solution of anthracene. The excitation and emission spectra of anthracene show a blue shift compared to the spectra for perylene. The two-dimensional image shows, as expected, sixteen peaks (Fig. 7b).

Figure 8(a) shows the fluorescence excitation—emission matrix of a mixture of perylene and anthracene. The isometric projection shown in Fig. 8(b) was obtained by transferring the acquired data to a larger university computer via an RS232c interface.

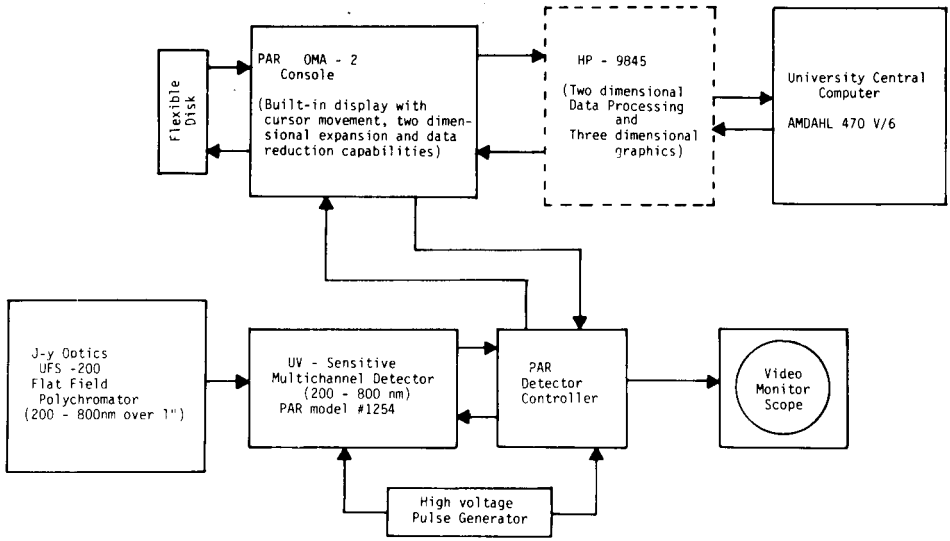

Fig. 5. Block diagram of detection and processing features of system.

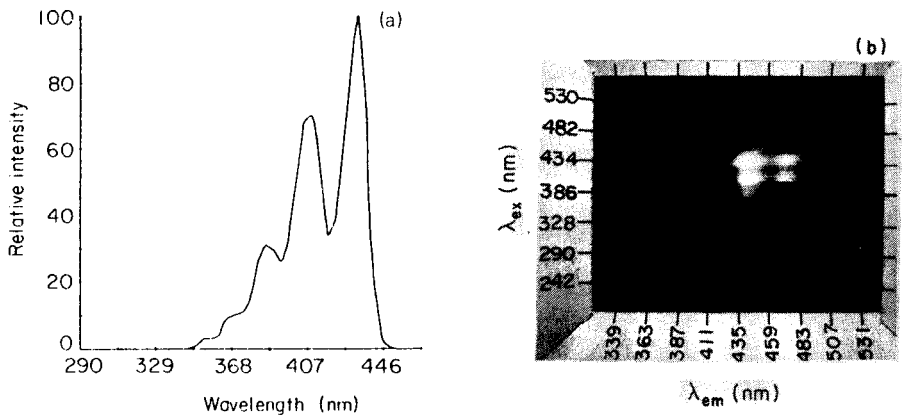

Fig. 6. Production of emission—excitation matrix of perylene. (a) Excitation spectrum of 1×10^{-7} M perylene; (b) photograph of video display of emission—excitation matrix.

In a recent review, Talmi et al. [21] indicated that acquisition of a two-dimensional emission—excitation matrix in the manner described here is less accurate than the more time-consuming mechanical scanning method. To check this aspect, a one-dimensional fluorescence spectrum of perylene (in the same mixture as used for Fig. 8) was obtained by focusing the 150-W lamp onto the entrance slit of a Jarrell-Ash 0.25-m monochromator, so that perylene was selectively excited at 435 nm. The detector was then used in the single-track mode to obtain the emission spectrum (Fig. 9a). Other

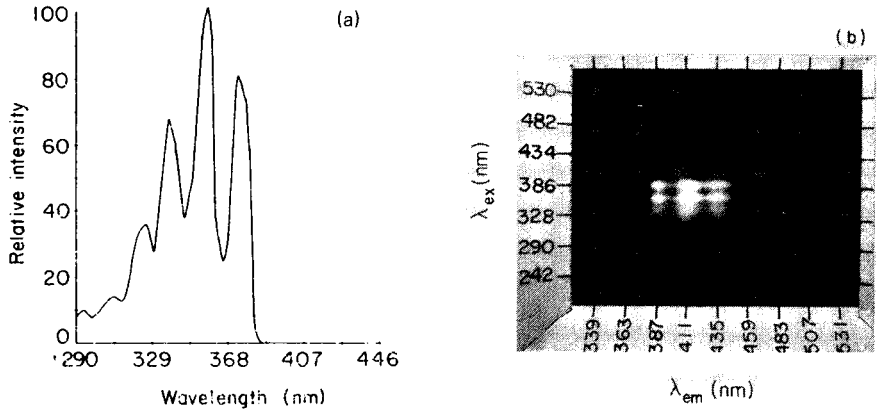

Fig. 7. Production of emission—excitation matrix of anthracene. (a) Excitation spectrum of 3×10^{-6} M anthracene; (b) photograph of video display of emission—excitation matrix.

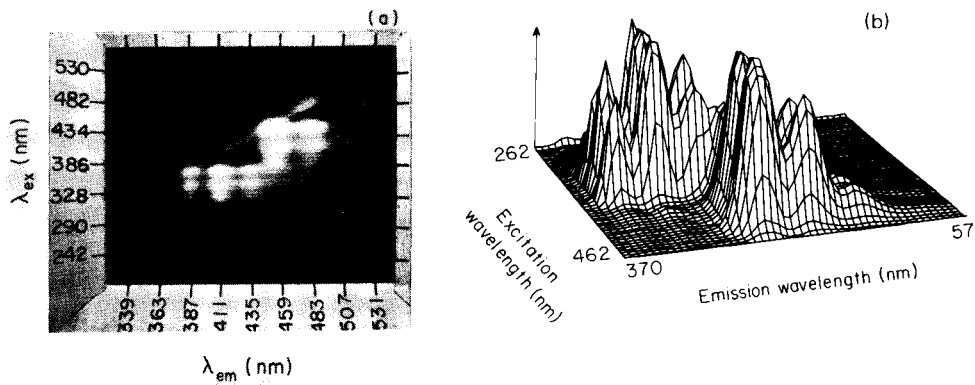

Fig. 8. Emission—excitation matrix of a mixture of perylene and anthracene. (a) Video display; (b) isometric projection.

emission spectra can be obtained by stepping to the desired excitation wavelength and measuring the corresponding emission spectra. Repetition of this process gives an emission—excitation matrix. The single spectrum displayed in Fig. 9(b) was isolated at approximately the 435-nm excitation wavelength from an emission—excitation matrix via the polychromatic illumination method. The quality of this spectrum is as good as that obtained in the one-dimensional mode. The greater noise apparent in Fig. 9(a) can be attributed to the larger number of data points (375) than in Fig. 9(b) (50). Thus, the conclusion of Talmi et al. [21] that spectra obtained in the two-dimensional format of a video fluorimeter are less accurate, is not

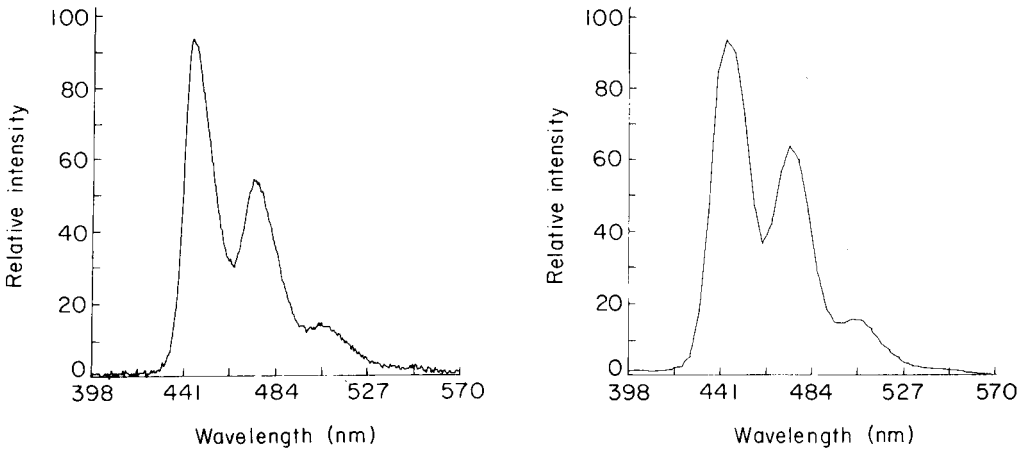

Fig. 9. Comparison of 1D spectrum of perylene (1×10^{-7} M) with single line from 2D spectrum. (a) Emission spectrum obtained by selective excitation of mixture in one-dimensional mode (λ_{ex} = 435 nm); (b) single emission track selected from two-dimensional mixture spectrum ($\lambda_{ex} \approx 435$ nm).

entirely correct. Moreover, the kinetic advantages obtained by acquiring two-dimensional spectra far outweigh any disadvantages.

Finally, the detection limit of the proposed system was compared to that of a conventional fluorimeter. Most conventional fluorimeters have a sensitivity to quinine sulfate — the accepted fluorescence standard — of ca. 10 ng ml^{-1}. When the proposed system was used with 30000-scan integration in the one-dimensional mode for quinine sulfate in 0.05 M sulfuric acid, the sensitivity achieved was about 1 ng ml^{-1}; similar values were obtained when signals were enhanced by using longer scan times and/or target integration. Clearly such limits are adequate for most fluorescence studies, but could be further improved by using other conventional modes of signal enhancement.

Conclusion

By careful considerations of optics and use of holographic gratings, it proved possible to design a two-dimensional rapid scanning system which eliminates much unneeded transfer optics, while remaining comparatively cheap. Expensive specially fabricated optical devices can be avoided, yet high-quality images are still obtained. The fluorimeter described was designed around commercially available optical elements, and produces spectral quality comparable to that of conventional fluorimeters.

The authors thank Dr. Andrew Young of the Department of Physics for useful discussions on optics, and are grateful to the Robert A. Welch Foundation (Grant A-715), the Research Corporation (Grant 55398) and the Texas

A & M University College of Science Seed money program for partial support of this work.

REFERENCES

1 W. Kaye and F. Waska, Anal. Chem., 36 (1964) 2380.
2 M. J. Milano, H. L. Pardue, T. E. Cook, R. E. Santini, D. W. Margerum and J. M. Raycheba, Anal. Chem., 46 (1974) 374.
3 R. P. Cooney, T. Vo-Dinh, G. Walden and J. D. Winefordner, Anal. Chem., 49 (1977) 939.
4 F. A. Sachs and P. E. Howard, Electro-Opt. Systems Design, 9 (1975) 34.
5 Y. Talmi, Anal. Chem., 47 (1975) 697A.
6 Y. Talmi, Anal. Chem., 47 (1975) 658A.
7 D. L. Wood, A. B. Dargis and D. L. Nash, Appl. Spectrosc., 29 (1975) 310.
8 I. M. Warner, J. B. Callis, E. R. Davidson and G. D. Christian, Clin. Chem., 22 (1976) 1483.
9 D. W. Johnson, J. A. Gladden, J. B. Callis and G. D. Christian, Rev. Sci. Instrum., 49 (1978) 54.
10 G. E. Busch and D. M. Rentzepis, Science, 194 (1976) 276.
11 A. A. Sawchuk, IEEE Trans. Comput., C-26 (1977) 34.
12 I. M. Warner, J. B. Callis, G. D. Christian and E. R. Davidson, Anal. Chem., 49 (1977) 564.
13 I. M. Warner, E. R. Davidson and G. D. Christian, Anal. Chem., 49 (1977) 2155.
14 J. F. James and R. S. Sternberg, The Design of Optical Spectrometers, Chapman and Hall, London, 1969.
15 S. A. Goldstein and J. P. Walters, Spectrochim. Acta, Part B, 31 (1976) 201.
16 S. A. Goldstein and J. P. Walters, Spectrochim. Acta, Part B, 31 (1976) 295.
17 G. M. Ridder and D. W. Margerum, Anal. Chem., 49 (1977) 2098.
18 UFS-200 Flat Field Spectrograph, Product of Instruments SA, Inc., Essex Avenue, Metuchen, N.J. 08840.
19 G. G. Guilbault, Practical Fluorescence; Theory, Methods and Techniques, Dekker, New York, 1973.
20 C. N. Ho, G. D. Christian and E. R. Davidson, Anal. Chem., 50 (1978) 1108.
21 Y. Talmi, D. C. Baker, J. R. Jadamec and W. A. Saner, Anal. Chem., 50 (1978) 936A.

Analytica Chimica Acta, 109 (1979) 373—380
© Elsevier Scientific Publishing Company, Amsterdam — Printed in The Netherlands

FURTHER IMPROVEMENTS IN THE 2,4-XYLENOL SPECTROPHOTOMETRIC METHOD FOR NITRATE

GEORGE NORWITZ and PETER N. KELIHER*

Chemistry Department, Villanova University, Villanova, Pa. 19085 (U.S.A.)

(Received 21st January 1979)

SUMMARY

Improvements are described for the 2,4-xylenol spectrophotometric method for nitrate that reduce the elapsed and working time. Diluted (22 + 3) sulfuric acid is added quickly to the sample solution while the flask is immersed in tap water. 2,4-xylenol solution is added, the 6-nitro-2,4-xylenol formed is steam-distilled into a composite ammonia—isopropanol reagent, and the absorbance of the ammonium salt of 6-nitro-2,4-xylenol is measured. Further possible interferences are described. Br_2, I_2, ClO^-, ClO_3^-, BrO_3^-, and IO_4^- cause low results by deactivating or destroying the 2,4-xylenol. Azide, hydrazine, and elemental carbon cause low results by reducing the nitrate in the strong sulfuric acid solution. Se^{4+} causes low results because 2,4-xylenol is consumed in reducing Se^{4+} to the element. Pt^{4+} and Os^{8+} cause high results. Interferences from Br_2, I_2, ClO^-, ClO_3^- IO_3^-, and IO_4^- can be eliminated by reduction to the halide with sulfurous acid and precipitation with silver sulfate. Sulfurous acid reduction also eliminates interferences from V^{5+}. Mn^{7+}, Cr^{6+}, $S_2O_8^{2-}$, and H_2O_2. Interferences from N_3^-, Br_2, I_2, and $S_2O_8^{2-}$ are eliminated merely by boiling a 0.5% sulfuric acid solution for 30 min (and precipitating any residual halide with silver sulfate).

The 2,4-xylenol spectrophotometric method for nitrate with steam distillation is accurate and reproducible; interferences from many inorganic and organic substances can be readily eliminated [1—3]. However, the method is somewhat tedious and time-consuming, since the concentrated sulfuric acid must be added very slowly to the ice-cooled solution.

In this paper, an improved version of the 2,4-xylenol method for nitrate is proposed that reduces the elapsed time and working time considerably, and requires no ice. Inorganic interferences not previously covered and ways of eliminating them are discussed.

EXPERIMENTAL

Apparatus and reagents

The steam distillation apparatus — of the Parnas—Wagner type — was essentially the same as that used previously [1—3], except that the silver condenser was replaced by a regular Liebig condenser (jacket 20 cm in length).

Sulfuric acid (96%), potassium nitrate (dried at 150°C for 1 h), isopro-

panol, ammonia liquor, acetone, sulfurous acid (6%), and other chemicals used were reagent grade, except the sodium hypochlorite solution (4—6% NaClO) which was laboratory grade.

Standard nitrate solution (1 ml = 0.5 mg NO_3^--N). Dissolve 3.6100 g of KNO_3 in water and dilute to 1 l in a volumetric flask.

2,4-Xylenol solution (2.5%). Dilute 5 ml of 2,4-xylenol (Eastman-Kodak) to 200 ml with acetone.

Sulfuric acid (22 + 3). Add 660 ml of sulfuric acid (96%) to 90 ml of water. Cool to room temperature.

Ammonia—isopropanol reagent. Add 825 ml of isopropanol to 825 ml of water, mix, and add 150 ml of ammonia liquor.

Iron(III) solution (4.4%). Dissolve 22 g of $FeNH_4(SO_4)_2 \cdot 12H_2O$ in water containing a few drops of sulfuric acid and dilute to 500 ml with water.

Preparation of calibration curve

Transfer 0.00 (reagent blank), 1.00, 2.00, 3.00, and 4.00 ml of standard nitrate solution to 100-ml volumetric flasks and dilute to the mark. Pipet 10-ml aliquots into 50-ml volumetric flasks. Fill a bucket close to the top with tap water. Immerse each flask in turn so that the top of the flask is about 5 cm above the level of the tap water. Add 25 ml of sulfuric acid (22 + 3) at one stroke from a graduated cylinder and swirl vigorously for about 30 s with the flask immersed. Within 1 h, add 1 ± 0.2 ml of 2,4-xylenol solution and swirl to mix thoroughly. Allow to stand for 10—60 min.

Add 60-ml portions of ammonia—isopropanol reagent to five 100-ml volumetric flasks. Place each flask in turn under the condenser extension tube. Introduce the sample through the entry funnel and wash in with 5—10 ml of water. Steam-distil until the volume in the collection flask is ca. 95 ml. Dilute the solution to the mark and mix. Measure the absorbance at 455 nm against distilled water, deduct the reagent blank, and plot absorbance against mg of NO_3^--N (per 10-ml aliquot).

Procedures

In all the following modifications, unless specified otherwise, an accurately measured portion (up to 75 ml) of the solution or dissolved sample containing up to 2.0 mg of NO_3^--N and up to 250 mg of the interferences is used.

A. In the absence of interferences. Transfer the sample solution to a 100-ml volumetric flask and dilute to the mark. Pipet a 10-ml aliquot into a 50-ml volumetric flask and proceed as described for the calibration curve.

B. In the presence of previously described interferences. Eliminate the interferences as described [2, 3], dilute to 100 ml (or 200 ml) in a volumetric flask, pipet a 10-ml aliquot into a 50-ml volumetric flask, and proceed as described for the calibration curve.

C. In the presence of Br_2, I_2, ClO^-, ClO_3^-, BrO_3^-, IO_3^-, IO_4^-, and V^{5+} by the sulfurous acid reduction method. Transfer the sample solution to a 250-ml beaker, dilute to about 75 ml, and add 5 ml of dilute sulfuric acid (1 + 9) and 25 ml of sulfurous acid (6%). Insert a stirring rod, heat to boiling, and boil for 7 min. Remove from the hot plate and add sufficient aqueous silver sulfate solution (0.44% w/v) from a graduated cylinder, while stirring, to precipitate the halide and provide a moderate excess of silver(I) (this step is not necessary for samples containing only V^{5+}). Theoretically, 1 mg of Br_2, I_2, ClO^-, ClO_3^-, BrO_3^-, IO_3^-, and IO_4^- is equivalent to 0.44, 0.28, 0.69, 0.43, 0.27, 0.20, and 0.19 ml of the silver sulfate solution, respectively. However, provision must be made for the chloride always present in commercial hypochlorites; also a fairly large amount of bromine will volatilize during the heating before the actual reduction occurs, so that much less than the theoretical amount of silver(I) will be required for such samples.

Heat to boiling and boil for 1—2 min. Remove the beaker from the hot plate and test for complete precipitation by adding 1—2 drops of silver sulfate solution (0.44%). If necessary, add more silver sulfate soluton and reboil. Allow to stand for 15 min or more, filter through a Whatman No. 42 paper, and wash with water. (If more than 2.0 mg of iron is present in the sample solution, add 5 ml of hydrogen peroxide (30%) and more iron(III), if necessary to bring the total iron content up to about 5 mg, heat to boiling, boil vigorously for 15 min, wash down the watch glass and sides of the beaker, and boil vigorously for 15 min more.) Cool to room temperature and dilute to 100 or 200 ml in a volumetric flask. Pipet a 10-ml aliquot into a 50-ml volumetric flask and proceed as described for the calibration curve.

D. In the presence of N_3^- (up to 0.5 g), Br_2, I_2, and $S_2O_8^{2-}$ (up to 1 g) by the boiling method. Transfer the sample solution to a 250-ml beaker, dilute to about 110 ml, add 5 ml of dilute sulfuric acid (1 + 9), insert a stirring rod, heat to boiling and boil for 15 min. Wash down the watch glass and sides of the beaker and boil for another 15 min. For samples containing Br_2 and I_2, precipitate any residual halide with silver sulfate solution (0.44%), heat to boiling, boil for 1—2 min, allow to stand for 15 min or more, filter into a 100-ml volumetric flask, and wash with water. Cool to room temperature, dilute to the mark, pipet a 10-ml aliquot into a 50-ml volumetric flask, and proceed as described for the calibration curve.

DISCUSSION AND RESULTS

Improved technique

The use of ice was eliminated by adding 25 ml of sulfuric acid (22 + 3) to the 10-ml aliquot in a 50-ml volumetric flask placed in a bucket of tap water (this gives a solution with a sulfuric acid concentration (1.7 + 1) that is the same as that used previously [1—3]). The solution becomes slightly warm on adding the sulfuric acid but there is no loss of nitrate. Apparently, when the sulfuric acid and the 10-ml aliquot are mixed rapidly in a high-necked flask, there is much less likelihood of losing nitrate than

when concentrated sulfuric acid is added dropwise to the 10-ml aliquot in a beaker while swirling. The sulfuric acid can be added from a graduated cylinder, because the sulfuric acid concentration is not very critical. There is a plateau for maximum color development over the range (1.5 + 1) to (2.0 + 1) sulfuric acid [1]. The only reason why the 17 ml of concentrated sulfuric acid was added dropwise previously [1—3] was to control the temperature. The use of a composite reagent containing ammonia, water, and isopropanol obviously simplifies the procedure. The composite reagent is stable at least for several months.

Further study of interferences

In the study of soluble interfering substances, portions of standard solutions (usually 5 mg ml^{-1}) of the substances were added to 50-ml volumetric flasks containing 2 ml of diluted standard nitrate solution (0.10 mg NO_3^--N). The solution was then diluted with water to 10.0 ml and taken through the procedure. For the study of interference from bromine and iodine, a standard bromine solution (8 ml = 25 mg Br) was prepared by diluting 1.00 ml of bromine (d 3.12) to 1 l with water, and a standard iodine solution by dissolving 0.50 g of iodine in acetone and diluting to exactly 10 ml. Standard solutions of Se^{4+} and Te^{4+} were prepared by boiling SeO_2 and TeO_2 with 70 ml of water and 50 ml of concentrated sulfuric acid and diluting to 250 ml. Standard solutions of gold or platinum were prepared by dissolving 0.125 g of gold or finely divided platinum in aqua regia, adding 20 ml of concentrated sulfuric acid, evaporating to fumes of sulfuric acid, adding 15 ml of concentrated hydrochloric acid to help eliminate residual nitrate, and evaporating to fumes again. The solutions were then evaporated to fumes three more times with intervening washing down of the beaker wall. The solutions were diluted to exactly 25 ml with concentrated sulfuric acid. For the study of the interferences of Se^{4+}, Te^{4+}, Au^{4+}, and Pt^{4+}, the dropwise addition method [2] was used in order to simplify adjustment of the amount of sulfuric acid needed. For the study of the substances insoluble in water, portions were weighed into 50-ml volumetric flasks containing 2.0 ml of the diluted standard nitrate solution and 8.0 ml of water.

The study of the interference of hypochlorite offered special problems, because pure hypochlorites are not available. Laboratory-grade or commercial-grade hypochlorites in solid form or in solution always contain chloride by reason of their method of manufacture [4]. The interference of hypochlorite (added as laboratory-grade sodium hypochlorite solution), therefore, must be reported as the total interference of hypochlorite and chloride.

The 14 additional substances tested that did not interfere with the method are shown in Table 1. Of these substances, red phosphorus, lead dioxide, and carbon were essentially insoluble in the water or sulfuric acid. The non-interference of sodium bismuthate was surprising, since that substance is a powerful oxidant; apparently, when sodium bismuthate is dissolved in sulfuric acid, the unstable Bi^{5+} is converted to Bi^{2+}.

TABLE 1

Additional substances that did not interfere with the 2,4-xylenol method for nitrate (0.10 mg of NO_3^--N) when present in amounts of up to 25 mg

Substance	Added as	Substance	Added as	Substance	Added as
NH_2OH	$(NH_2OH)_2H_2SO_4$	In^{3+}	$In_2(SO_4)_3$	P	P (red)
OCN^-	NaOCN	Ru^{3+}	Ru sulfate[b]	MnO_2	MnO_2
CN_2^{2-}	$CaCN_2$	Nd^{3+}	Nd sulfate[c]	PbO_2	PbO_2
Au^{4+}	Au sulfate[a]	La^{3+}	La sulfate[d]	$NaBiO_3$	$NaBiO_3$
Te^{4+}	TeO_2[a]	Sm^{3+}	Sm sulfate[e]		

[a]See text. [b]Prepared by fuming $K_4Ru(CN)_6 \cdot 3H_2O$ with sulfuric acid. [c]Prepared by fuming $NdCl_3 \cdot 6H_2O$ with sulfuric acid. [d]Prepared by fuming $LaCl_3 \cdot 6H_2O$ with sulfuric acid. [e]Prepared by fuming $SmCl_3 \cdot 6H_2O$ with sulfuric acid.

The additional substances tested that interfered and recoveries in the presence of varying amounts of interference are shown in Table 2. The Br_2, I_2, ClO^-, ClO_3^-, BrO_3^-, IO_3^-, and IO_4^- cause low results by deactivating or destroying the 2,4-xylenol. It would be expected that chlorine, chlorite, and chlorine dioxide would react in the same manner. Azide, hydrazine, and elemental carbon (but not hydroxylamine) cause low results by reducing the nitrate in the strong sulfuric acid solution. Se^{4+} causes low results because 2,4-xylenol is consumed in reducing Se^{4+} to Se; the precipitation occurs a few minutes after addition of 2,4-xylenol. Te^{4+} is reduced to Te but this precipitation does not occur for 30 min, consequently Te^{4+} does not interfere. Larger amounts of Os^{8+} and Pt^{4+} cause high results. In the case of Os^{8+}, the high results are probably due to partial volatilization of OsO_4; a faint yellow color was obtained on distilling osmium solutions without 2,4-xylenol. Corrections for platinum and osmium did not seem feasible.

Recommended permissible limits (per 10-ml aliquot) for the method are: ClO^- (+ Cl^- in the sodium hypochlorite solution), 1 mg; Br_2, ClO_3^-, N_3^-, and N_2H_4, 0.2 mg; I_2, BrO_3^-, IO_3^-, IO_4^-, Pt^{4+}, and Os^{8+}, 10 mg; Se^{4+}, 5 mg; carbon, none.

Elimination of interferences by the sulfurous acid reduction method

Interferences from Br_2, I_2, ClO^-, ClO_3^-, BrO_3^-, IO_3^-, and IO_4^- were eliminated by reduction to the halide ion with sulfurous acid and subsequent treatment with silver sulfate to eliminate the halide ion. Undissolved iodine was quickly brought into solution by the sulfurous acid. The interference of these seven substances cannot be eliminated by the hydrogen peroxide treatment. Evidence for reduction of nitrate in a dilute solution by sulfurous acid was never observed.

The use of 25 ml of sulfurous acid (6%) and boiling for 7 min to complete the reduction and drive off most of the SO_2 are recommended. However, the boiling time is not critical; good results were obtained after boiling for 5 min, even though the solution still smelled of SO_2 (up to 250 mg of SO_3^{2-}

TABLE 2

Further interferences with the 2,4-xylenol method for nitrate (0.10 mg of NO_3^--N)

Interference	Added as	NO_3^--N (mg) recovered in the presence of interference							
		0.1 mg	0.2 mg	0.5 mg	1 mg	2.5 mg	5 mg	10 mg	25 mg
Br_2	Bromine water[a]	0.100	0.100		0.079	0.073	0.070	0.032	0.050
I_2	Iodine sol.[a]						0.100	0.094	0.088
$ClO^-(+Cl^-)$[a]	NaClO sol. (5%)[a]		0.100	0.097	0.100	0.088	0.073	0.038	0.023
ClO_3^-(2)	$KClO_3$	0.102	0.098	0.084			0.062	0.054	
BrO_3^-	$KBrO_3$					0.097	0.107	0.097	0.076
IO_3^-	KIO_3						0.097	0.097	0.063
IO_4^-	KIO_4					0.097	0.104	0.097	0.038
N_3^-	Na_3N	0.104	0.100	0.076	0.045	0.015	0.070	0.048	0.070
N_2H_4	$(NH_4)_2H_2SO_4$	0.100	0.097	0.097	0.079	0.076	0.070	0.085	0.079
Se^{4+}	SeO_2						0.097	0.082	0.082
Pt^{4+}	Pt sulfate[a]						0.097	0.107	0.179
Os^{8+}	OsO_4						0.100	0.104	0.116
C	C							0.066	0.076

[a]See text.

does not interfere with the determination [2]. The recoveries after boiling for 15 min were satisfactory, except in the case of vanadium (for 250 mg of vanadium, the recovery was about 80% on boiling for 15 min). Apparently, prolonged boiling causes some oxidation of V^{4+} to V^{5+}.

The sulfurous acid treatment also eliminates the interference of the oxidants V^{5+}, Mn^{7+}, Cr^{6+}, $S_2O_8^{2-}$, and H_2O_2; the hydrogen peroxide treatment and subsequent boiling will eliminate the interference of all these except V^{5+} [2]. In the sulfurous acid reduction, V^{5+} is reduced to V^{4+}, Mn^{7+} to MnO_2 (which settles out but does not interfere in any case, $S_2O_8^{2-}$ to SO_4^{2-}, and H_2O_2 to water. Because the interference from iron (see below) necessitates additional treatment, it is recommended that the peroxide method [2], rather than the sulfurous acid method be used for the determination of nitrate in the presence of Mn^{7+}, Cr^{6+}, $S_2O_8^{2-}$, and H_2O_2.

The sulfurous acid reduction method cannot be used without modification for samples containing significant amounts of iron, because all the iron present is finally reduced to iron(II), which is a strong interferent with the 2,4-xylenol method; the maximum permissible amount of iron(II) per 10-ml aliquot is 0.2 mg [2]. The interference of up to 100 mg of iron in the sample solution (10 or 5 mg in the 10-ml aliquot, depending on the final dilution) can be eliminated by oxidizing the iron(II) to iron(III) with the hydrogen peroxide after the sulfurous acid reduction and then destroying the excess of peroxide by boiling, the iron acting as a catalyst. However, this treatment does not work in the presence of vanadium, because the V^{4+} formed by the sulfurous acid is oxidized back to the interfering V^{5+} by the peroxide. In the presence of more than 100 mg of iron, the recovery of nitrate after the hydrogen peroxide treatment was low (e.g. for 250 mg of iron, the recovery was about 85%). It is believed that the low results obtained in the presence of the larger amounts of iron are unrelated to the peroxide treatment, but are due to partial reduction of nitrate by the iron(II) during the 7-min boiling time.

TABLE 3

Results for nitrate by the proposed methods for the elimination of interferences

Interference (mg)	NO_3^-–N added (mg)	NO_3^-–N in 10-ml aliquot (mg)	
		Present	Found
Sulfurous acid reduction method[a]			
250 Br_2	0.00	0.000	0.005
	1.50	0.075	0.079
	3.00	0.150	0.154
250 I_2	0.00	0.000	0.005
	1.50	0.075	0.079
	3.00	0.150	0.150
1.5 ml NaClO sol. (5%)	0.00	0.000	0.005
	1.50	0.075	0.082
	3.00	0.150	0.150
1.5 ml NaClO sol. (5%) + 100 Fe(III)	3.00	0.150	0.147
250 ClO_3^-	0.00	0.000	0.000
	1.50	0.075	0.076
	3.00	0.150	0.150
250 ClO_3^- + 100 Fe(III)	1.50	0.075	0.079
	3.00	0.150	0.147
250 BrO_3^-	0.00	0.000	0.000
	1.50	0.075	0.076
	3.00	0.150	0.154
250 BrO_3^- + 100 Fe(III)	3.00	0.150	0.150
250 IO_3	0.00	0.000	0.005
	1.50	0.075	0.073
	3.00	0.150	0.147
250 IO_3^- + 100 Fe(III)	3.00	0.150	0.150
250 IO_4^-	0.00	0.000	0.000
	1.50	0.075	0.079
	3.00	0.150	0.154
250 IO_4^- + 100 Fe(III)	3.00	0.150	0.147
250 V^{5+}	0.00[b]	0.000	0.000
	0.75[b]	0.075	0.073
	1.50[b]	0.150	0.150
Boiling method[b]			
500 N_3^-	0.00	0.000	0.000
	0.75	0.075	0.076
	1.50	0.150	0.154
1000 Br_2	0.00	0.000	0.000
	0.75	0.075	0.082
	1.50	0.150	0.157
1000 I_2	0.00	0.000	0.005
	0.75	0.075	0.073
	1.50	0.150	0.154
1000 $S_2O_8^{2-}$	0.00	0.000	0.000
	0.75	0.075	0.082
	1.50	0.150	0.147

[a]Dilution 200 ml except where specified. [b]Dilution 100 ml.

The interferences of Cl_2, ClO_2 and chlorine dioxide should be eliminated by the sulfurous acid treatment, because these substances are readily reduced by sulfurous acid. The interference of azide is eliminated during the sulfurous acid treatment, because azide decomposes during the boiling (sulfurous acid and azide do not react).

Elimination of interferences by the boiling method

The elimination of interference of azide (hydrazoic acid) in the boiling method is due to its decomposition to N_2 and NH_4^+, while the elimination of $S_2O_8^{2-}$ is due to decomposition to SO_4^{2-} and O_2. Br_2 and I_2 are eliminated in the boiling method mainly by volatilization of the halogens as such. However, provision must be made to remove Br^- and I^- produced by the reaction of Br_2 and I_2 with water; the Br^- and I^- left after the volatilization of 1 g of Br_2 and I_2 required 7 ml and 0.5 ml of the silver sulfate solution, respectively. The boiling method gave high results for nitrate in the presence of hypochlorite for reasons that are unclear; the results were 20% too high in the presence of 1.5 ml of 5% NaClO solution.

Some experiments were conducted on the possible use of the boiling method for elimination of hydrazine, sulfide, thiosulfate, and thiocyanate. These substances seemed to be destroyed during the boiling; however, they reacted with nitrate during the boiling, thus causing low results.

The interference of carbon could be eliminated by filtering the aqueous solution (through a fine filter paper) prior to the aliquoting as was done previously to prevent interference from metals (2).

Results for the elimination of interferences

The results obtained by the proposed methods for synthetic mixtures prepared from standard nitrate solution and solution of the interferences (Table 3) were satisfactory. Analyses of the solutions of interferences without added nitrate showed that the chemicals used did not contain significant amounts of nitrate.

The procedures described should be useful for the determination of nitrate in a variety of materials, including the following: sodium, lithium, and calcium hypochlorite; sodium and potassium chlorate; sodium and potassium bromate; sodium and potassium periodate; bromine; iodine; sodium and ammonium vanadate; ammonium, sodium, and potassium persulfate; sodium azide; hydroxlammonium sulfate; sodium bismuthate, sodium and potassium cyanate; calcium cyanamide. The procedure should also be useful for the determination of nitrate in brines (a pressing problem) and water treated with various chlorine compounds.

REFERENCES

1 G. Norwitz and H. Gordon, Anal. Chim. Acta, 89 (1977) 177.
2 G. Norwitz and P. N. Keliher, Anal. Chim. Acta, 98 (1978) 323.
3 G. Norwitz, J. Farino and P. N. Keliher, Anal. Chim. Acta, 105 (1979) 335.
4 Kirk-Othmer Encyclopedia of Chemical Technology, 2nd edn., Interscience, New York, 1964, Vol. 5, pp. 12—24.

Analytica Chimica Acta, 109 (1979) 381—391
© Elsevier Scientific Publishing Company, Amsterdam — Printed in The Netherlands

OPTIMAL REACTION CONDITIONS FOR THE DIRECT SPECTROPHOTOMETRIC DETERMINATION OF NIOBIUM IN STEELS WITH SULPHOCHLOROPHENOL S

Z. ČÍŽEK

Central Research Institute, Škoda Co., Plzeň (Czechoslovakia)

J. DOLEŽAL*

Department of Analytical Chemistry, Charles University, Prague (Czechoslovakia)

(Received 7th February 1979)

SUMMARY

Optimal reaction conditions for the direct spectrophotometric determination of niobium in steels are described. Conditions for the formation of the niobium—sulphochlorophenol S complex are defined, and the effects of many alloying elements are discussed. Niobium can thus be determined in all types of steels in the range of 0.002—3% Nb.

Sulphochlorophenol S [2,7-di(2-hydroxy-3-sulpho-5-chlorophenylazo)—chromotropic acid; SCPS] forms blue complexes with a number of metal ions under various reaction conditions; these complexes can be used advantageously for the sensitive spectrophotometric determination of several metals, e.g. Sc [1], Zr [2, 3], Mo [4, 5], Al and Ga [6] and In [7]. This work has been summarized [7]. The reactions of sulphochlorophenol S (SCPS) with niobium [7—20] have been studied in greatest detail. The following media have been described as most useful for complex formation: 0.5—3 M HCl [7, 11, 17], 2—4 M HNO_3 [11], 1—6 M HNO_3 and 1—3 M $HClO_4$ [7], 2.32 M $HClO_4$ [10], 1—4 M $HClO_4$ and 1 M HCl [13]. The literature lists conflicting, unexplained interfering effects on the formation of the niobium complexes caused by the presence of sulphate, phosphate, fluoride, oxalate, oxidizing agents (chlorine, nitrogen oxides), reducing agents (ascorbic acid) and other metal ions.

The niobium complex has been used analytically for determining niobium in tungsten, uranium and beryllium [11], in zirconium [9], in nickel alloys [15], and in tantalum after separation of the fluoro complexes on a basic anion exchanger [16]. The direct determination of niobium in alloy steels (> 0.05% Nb) has been described by Savvin et al. [17]; indirect determinations after separation with phytic acid [19] or after extraction of the complex [18, 20] have also been reported.

EXPERIMENTAL

Chemicals and instrumentation

All the chemicals used were of p.a. purity; sulphochlorophenol S (Fluka) was used. The standard niobium solution was prepared by dissolving niobium metal (> 99.9%) in a platinum dish in hydrofluoric acid and nitric acid with evaporation to the appearance of sulphur trioxide fumes after additions of sulphuric acid; the residue was dissolved in 1 M tartaric acid. The stock solutions of niobium in 1 M tartaric acid contained 0.200 mg Nb ml^{-1}. Working solutions containing 0.010 mg Nb ml^{-1} in 0.1 M tartaric acid were prepared immediately before use. The stock solution was stable for at least two months.

Diverse metal ion solutions were prepared from pure salts for Fe, Cr, Co and V, or from the pure metals (> 99.9%) for Ta, Ti, Zr, W, Mo, Al, Mn and Cu.

A Beckman ACTA M 7 spectrophotometer was used for absorbance measurements at 650 nm or for scanning suitable spectral regions. Measurements at elevated temperatures were done with resistance-heated cuvettes.

General procedure for the determination of niobium in steels

The following procedure was adopted on the basis of the detailed study described below. Variations in sample weights, etc., for different niobium contents are summarized in Table 1.

Dissolve a weighed sample in 25 ml of sulphuric acid (1+3) and 1 ml of 85% phosphoric acid, oxidizing with several drops of concentrated nitric acid. Evaporate to sulphur trioxide fumes, rinse the vessel walls with a little water and again evaporate to SO_3 fumes. Allow the residue to cool and dissolve in an appropriate amount of 1 M tartaric acid. Transfer the solution to a suitable volumetric flask (Table 1), dilute to the mark with water and mix well. Pipet a suitable aliquot (Table 1) into a 50-ml volumetric flask, and add 5 ml of hydrochloric acid (1+1) and the required amount of 0.1 M ascorbic acid. After about 10 min, add 10 ml of hydrochloric acid (1+1), dilute with water to about 45 ml and add exactly 2 ml of aqueous 0.5% (w/v) SCPS solution. Dilute the solution with water to the mark and leave to stand at laboratory temperature. Measure the absorbance after 50—60 min in suitable cuvettes at 650 nm against a blank solution prepared in the same way. Determine the niobium content from a calibration curve prepared by using a steel sample with niobium additions or by using standard samples of steel containing niobium.

If an insoluble carbide or oxide residue remains after the sample decomposition, it is solubilized by fusion with 0.5 g of potassium pyrosulphate. If the sample contains interfering elements, the procedure must be modified accordingly (see below).

TABLE 1

Preparation of the samples for analysis

Nb content in sample (%)	Sample weight (g)	Tartaric acid, 1 M (ml)	Volume of stock soln. (ml)	Aliquot (ml)	Ascorbic acid (ml)	Cuvette (mm)
0.002—0.20	0.250	5	100	10	7	20, 50
0.10—3.00	0.200	20	500	5	2	20, 50

RESULTS AND DISCUSSION

Rate of complex formation

The rate of formation of the Nb—SCPS complex in relation to the amount of SCPS and the temperature were studied in 2 M HCl and 2 M $HClO_4$ media. The results are shown in Fig. 1. Clearly, the complex is formed quantitatively at laboratory temperature in ca. 30 min and at 60°C in ca. 5 min. The rates of complex formation in these two acid media are the same, in contrast to literature results. The optimum amount of SCPS is 1 mg. If not stated otherwise, in all further experiments, 1 mg SCPS was used in 50 ml of solution; the complex was developed at laboratory temperature and its absorbance was measured after 50—60 min.

Effect of acids and their anions

The reaction of niobium with SCPS in 0.5—3 M HCl, H_2SO_4, $HClO_4$, HNO_3 and H_3PO_4 solutions was studied by comparison with blanks which contained SCPS and the same amount of the relevant acid. The results are given in Table 2. The optimum medium for complex formation is 1—3 M HCl or $HClO_4$; in less acidic media the interfering effect of other elements increases [7].

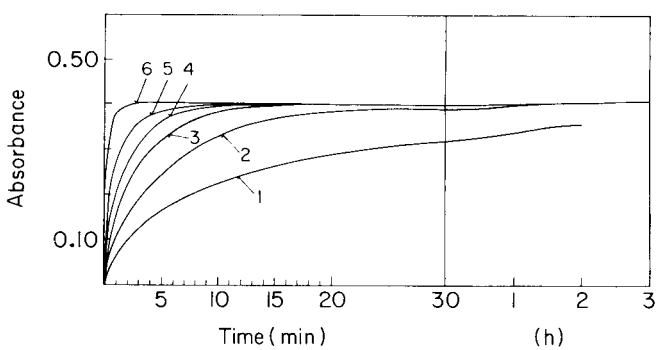

Fig. 1. Rate of complex formation in 2 M HCl or $HClO_4$ (25 μg Nb, 650 nm, 20-mm cells). SCPS added: (1) 0.25 mg; (2) 0.5 mg; (3) 1 mg; (4) 1.5 mg; (5) 2 mg; (6) 1 mg. All measurements were done at 25°C, except curve (6) which was obtained at 60°C.

Sulphuric acid and sulphate have a marked effect on the complex formation; phosphoric acid and phosphate almost completely prevent it. In nitric acid solutions, the reagent and complex are rapidly decomposed by free nitrogen oxides.

Because sulphuric acid, phosphoric acid and potassium pyrosulphate are indispensable in the dissolution of various types of steels, the amounts which must not be exceeded were determined: 0.2 ml H_2SO_4, 0.05 ml H_3PO_4 and 0.25 g $K_2S_2O_7$ in 50 ml. In the presence of larger amounts of potassium pyrosulphate, finely distributed particles of the reagent are precipitated; this effect is caused by the presence of larger amounts of alkali metal.

Effect of some complexing agents

Tartaric acid, ascorbic acid, hydrogen peroxide, fluoride, EDTA, and other complexing agents can be used in the dissolution of various types of steels and in masking some interfering elements; thus their effects were studied in detail. The results indicated that, while EDTA does not affect the formation of the Nb—SCPS complex, the other compounds mentioned may interfere when present in large amounts. Their presence must be limited in the 50-ml reaction mixture to the following maximal amounts: 2 ml of 1 M tartaric acid, 0.5 mg of fluoride and 5 ml of 0.1 M ascorbic acid. Small amounts of hydrogen peroxide interfere by binding niobium in a stable peroxo complex and larger amounts oxidize SCPS.

Interferences by other elements

The interfering effects of all elements found in normal steels were studied qualitatively and quantitatively under the optimal conditions for formation of the Nb—SCPS complex. Thus iron, chromium, nickel, molybdenum, vanadium, titanium, zirconium, tantalum, copper, cobalt, aluminium, silicon and tungsten were tested.

Iron. The effects of iron(III) on the formation of Nb—SCPS complex at various reaction temperatures in 2 M hydrochloric acid are shown in Fig. 2 (cf. Table 3). The effects of iron(II) are shown in Fig. 3. The results indicate

TABLE 2

Effect of acids on the measurement of 25 μg Nb (20-mm cells)

Acid	Absorbance of complex at different molarities					
	0.5	1.0	1.5	2.0	2.5	3.0
HCl	0.42	0.41	0.41	0.41	0.40	0.40
$HClO_4$	0.42	0.42	0.41	0.41	0.41	0.40
HNO_3	Colourless					
H_2SO_4	0.31	0.23	0.18	0.14	—	0.02
H_2SO_4 after 15 h	0.38	0.30	0.21	0.14	—	0.02
H_2SO_4 + 2 ml H_3PO_4	0.01	0.01	0.01	0.00	—	—

that iron(III) reacts with SCPS to form colourless reaction products; thus, even in small amounts, it interferes in the formation of the Nb—SCPS complex. An increase in the reaction temperature increases this interference. Iron(II) forms a weak complex with SCPS, which has an absorbance maximum at ca. 750 nm and does not interfere in the reaction of niobium. The iron(III) interference is best eliminated by adding an equivalent amount of 0.1 M ascorbic acid and then an excess of 1—2 ml. As the interfering effect of ascorbic acid increases with increasing temperature, development should be done at laboratory temperature.

Chromium and nickel. Chromium(III) and nickel(II), which are the principal alloying agents, do not react with SCPS and so do not interfere in the formation of the Nb—SCPS complex even when present in considerable amounts. However, their background absorbances must be borne in mind and eliminated in the determination of niobium (e.g., by measuring and subtracting the background absorbances). The presence of chromate ions causes bleaching of SCPS as a result of oxidation.

Molybdenum. The effect of molybdenum in 1.5 M HCl medium is shown

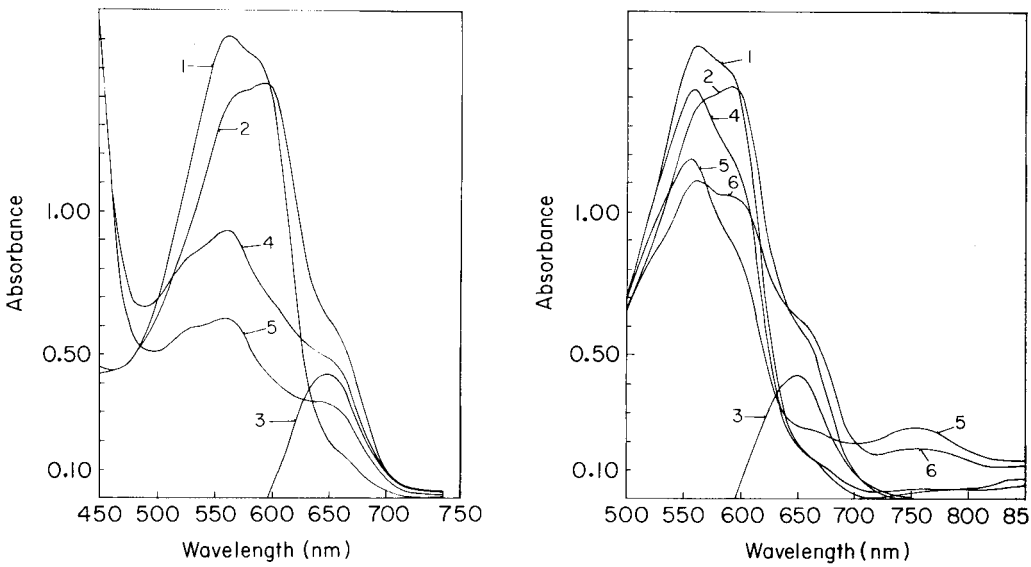

Fig. 2. Effect of iron(III) on absorption spectra (20-mm cells). (1) SCPS, water blank; (2) 25 μg Nb + SCPS, water blank; (3) 25 μg Nb + SCPS, SCPS blank; (4) 25 μg Nb + 50 mg Fe^{3+} + SCPS at 25°C, water blank; (5) 25 μg Nb + 50 mg Fe^{3+} + SCPS at 60°C, water blank.

Fig. 3. Effect of iron(II) on absorption spectra (20-mm cells). (1) SCPS, water blank; (2) 25 μg Nb + SCPS, water blank; (3) 25 μg Nb + SCPS, SCPS blank; (4) 50 mg Fe^{2+} + SCPS, water blank; (5) 100 mg Fe^{2+} + SCPS, water blank; (6) 100 mg Fe^{2+} + 25 μg Nb + SCPS, water blank.

TABLE 3

Effect of iron(III) on the measurement of 25 μg Nb

Fe^{3+} (mg)	Fe^{3+}:Nb	Absorbance (20-mm cells)	
		25°C after 60 min	60°C after 10 min
0	—	0.40	0.40
0.5	20:1	0.39	0.39
1	40:1	0.39	0.38
2	80:1	0.38	0.37
5	200:1	0.37	0.35
10	400:1	0.36	0.31
25	1000:1	0.34	0.22
50	2000:1	0.30	0.12

qualitatively in Fig. 4 and quantitatively in Table 4. The Mo—SCPS complex interferes not only through its absorbace but also through consumption of a considerable amount of the reagent, thus suppressing formation of the niobium complex. It is clear from Table 5, which gives the dependence of the stability of the molybdenum complex on the acidity of the medium, that the effect of molybdenum can be suppressed considerably by using higher acidities, e.g., 3—3.5 M HCl.

Vanadium. The effect of vanadium was evaluated in 2 M HCl; the results are given in Table 6. Obviously, the presence of a small amount of vanadate causes a marked interference by oxidation and bleaching of the reagent. Vanadyl ions do not react with SCPS, but with large vanadium contents the background absorbance must be considered. Ascorbic acid can be used for reduction of vanadate to vanadyl ions, as in the case of iron.

Titanium. The effect of titanium in 2 M HCl is illustrated in Fig. 5. Large amounts of titanium form a weak complex with SCPS with maximum absorbance at ca. 710 nm, which interferes somewhat in the determination of niobium and partly binds SCPS. However, as the interfering effect of titanium appears only at contents greater than 4—5 mg in 50 ml, it can be ignored for practically all types of steel.

Zirconium. Zirconium forms a complex with SCPS under practically the same conditions as niobium and interferes in the determination of niobium. The interfering effect can be readily eliminated by addition of EDTA.

Tantalum. The effects of tantalum in 2 M HCl are indicated in Fig. 6. The presence of tantalum obviously has a marked effect on the determination of niobium at mass ratios greater than Ta : Nb = 1:1. However, as alloying of ferroniobium steels leads to tantalum contents maximally one-tenth that of niobium, the effect of tantalum can be ignored in most cases.

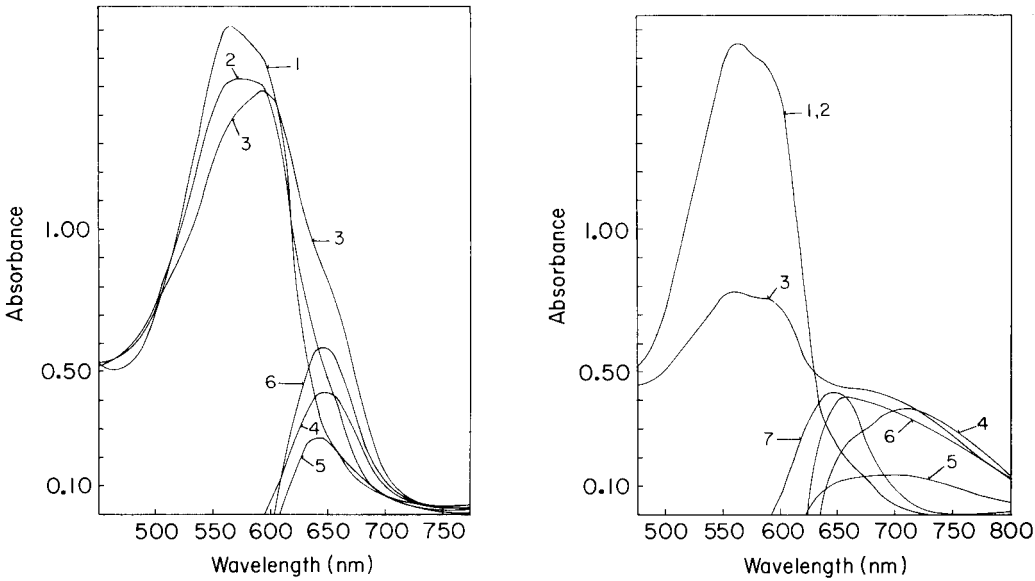

Fig. 4. Effect of molybdenum on absorption spectra (20-mm cells). (1) SCPS, water blank; (2) 0.5 mg Mo + SCPS, water blank; (3) 0.5 mg Mo + 25 μg Nb + SCPS, water blank; (4) 25 μg Nb + SCPS, SCPS blank; (5) 0.5 mg Mo + SCPS, SCPS blank; (6) 0.5 mg Mo + 25 μg Nb + SCPS, SCPS blank.

Fig. 5. Effect of titanium on absorption spectra (20-mm cells). (1) SCPS, water blank; (2) 2.5 mg Ti + SCPS, water blank; (3) 25 mg Ti + SCPS, water blank; (4) 25 mg Ti + SCPS, SCPS blank; (5) 12.5 mg Ti + SCPS, SCPS blank; (6) 25 mg Ti + 25 μg Nb + SCPS, SCPS blank; (7) 25 μg Nb + SCPS, SCPS blank.

TABLE 4

Effect of molybdenum (25-mm cells)

Mo (mg)	Mo:Nb	Absorbance		
		0 μg Nb	25 μg Nb	Difference
0	—	—	0.40	0.40
0.025	1:1	0.03	0.42	0.39
0.050	2:1	0.05	0.43	0.38
0.100	4:1	0.08	0.45	0.37
0.250	10:1	0.18	0.52	0.34
0.500	20:1	0.33	0.62	0.29
1.00	40:1	0.48	0.71	0.23
2.50	100:1	0.57	0.74	0.17
12.5	500:1	0.59	0.63	0.04
25	1000:1	0.59	0.60	0.01

TABLE 5

Dependence of the stability of the Mo—SCPS complex on the acidity of the medium

HCl (M)	Absorbance (650 nm, 20-mm cells)					
	50 μg Mo	50 μg Mo + 10 μg Nb	Diff.	500 μg Mo	500 μg Mo + 10 μg Nb	Diff.
0.5	0.11	0.26	0.15	0.51	0.61	0.10
1.0	0.07	0.23	0.16	0.42	0.53	0.11
1.5	0.04	0.21	0.17	0.33	0.45	0.12
2.0	0.03	0.19	0.16	0.26	0.38	0.12
2.5	0.02	0.18	0.16	0.18	0.31	0.13
3.0	0.02	0.18	0.16	0.11	0.26	0.15
3.5	0.01	0.17	0.16	0.05	0.20	0.15

TABLE 6

Effect of vanadium

V(V) (mg)	Absorbance (650 nm)		VO^{2+} (mg)	Absorbance (650 mm)	
	0 μg Nb	25 μg Nb		25 μg Nb	VO^{2+} [a]
0	—	0.40	0	0.40	
0.025	—0.03	0.40	0.050	0.39	
0.050	—0.08	0.36	0.250	0.40	
0.075	C[b]	0.31	1.0	0.40	
0.100	C	0.27	5.0	0.40	0.03
0.150	C	0.16	25	0.40	0.17
0.200	C	0.06			
0.250	C	C			

[a]Measured against a water blank. [b]Colourless.

Copper, manganese, cobalt and aluminium. No interferences were observed from these elements even when they were present in 1000-fold amounts compared to niobium in 2 M HCl. However, when large copper contents are present, the background absorbance must be compensated.

Silicon and tungsten. The effects of silicon and tungsten were evaluated primarily from the point of view of the high absorbance capacities of silicic acid and tungstic acid, which are formed during the decomposition of steel samples and preparation for measurement. Standard additions of niobium were made to samples of a transformer steel containing 4.3% silicon and a tungsten steel containing 16% tungsten before dissolution; the samples were dissolved in suphuric acid and nitric acid and evaporated to fumes of sulphur trioxide. The residues were dissolved in 1 M tartaric acid and, after filtration

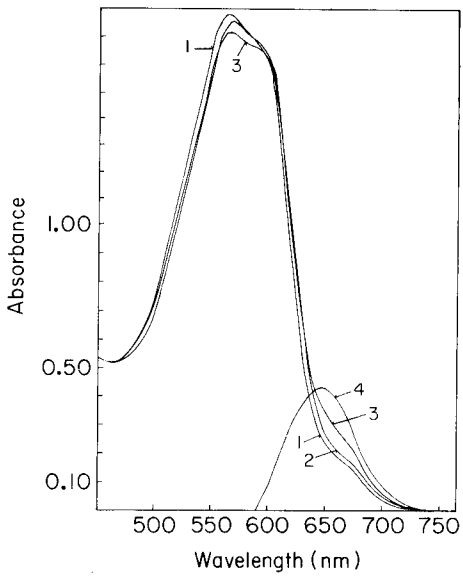

Fig. 6. Effect of tantalum on absorption spectra (20-mm cells). (1) SCPS, water blank; (2) 1 mg Ta + SCPS, water blank; (3) 1 mg Ta + 25 μg Nb + SCPS, water blank; (4) 25 μg Nb + SCPS, SCPS blank.

of the silicic and tungstic acids formed, niobium was determined in the solutions. The results (Table 7) prove that this method of dissolution and sample preparation with precipitation of silicic acid does not involve niobium losses; however, with precipitation of tungstic acid, niobium losses were particularly high because of adsorption on the precipitate.

Thus in the determination of niobium in steels with high tungsten contents, it is necessary to limit the precipitation of tungstic acid by adding a suitable amount of phosphoric acid. In the decomposition of 0.2 g of steel containing 16% tungsten, the tungsten can be maintained in solution by the addition of 5 ml of sulphuric acid and 1 ml of phosphoric acid, and subsequent extraction of the residue with 1 M tartaric acid. In a study of the effect of tungstate ions on the reaction of niobium with SCPS, it was found that 1000-fold amounts of tungsten do not interfere.

Application to steels

The experimental results described above complete and broaden previous observations on the possibilities of analytical application of the niobium complex with sulphochlorophenol S. The data allow procedures to be optimized for the rapid and sensitive direct spectrophotometric determination of small amounts of niobium in various types of steels or in other types of alloys. Table 8 shows the results obtained for niobium in standard samples of British, Czechoslovak and Polish steels by using the recommended procedure with sulphochlorophenol S.

TABLE 7

Effects of silicon and tungsten on the recovery of niobium added to transformer steel and tungsten steel

Nb added (mg)	Nb found after pptn. of $SiO_2.nH_2O$ (mg)	Nb found after pptn. of $WO_3.nH_2O$ (mg)
0.100	0.105	0.000
0.200	0.195	0.080
1.00	0.98	0.45
2.00	2.05	1.00
10.0	9.85	5.75

TABLE 8

Results of analysis of standard samples

Sample	Certified %Nb	Found %Nb	Difference	
			%Nb	% rel.
BCS 261	0.71 (+Ta)	0.693	−0.017	2.4
BCS 432	0.029	0.030	0.001	4.3
ČKD 166 (Czech.)	0.025	0.024	−0.001	5.2
ČKD 167	0.09	0.086		
ČKD 168	0.01	0.007		
ČKD 171	0.035	0.035	−0.000	0.9
Škoda 064	0.64	0.63	−0.01	1.6
4.6.1 (Polish)	0.017	0.019	0.002	8.3
4.6.3	0.059	0.061	0.002	3.3
4.6.4	0.101	0.100	−0.001	1.0
Škoda AR3	1.56	1.54	−0.02	1.3

REFERENCES

1 D. I. Ryabchikov, S. B. Savvin and Yu. M. Dedkov, Zh. Anal. Khim., 19 (1964) 1210.
2 S. B. Savvin and Yu. M. Dedkov, Zavod. Lab., 30 (1964) 645.
3 Yu. M. Dedkov, D. I. Ryabchikov and S. B. Savvin, Zh. Anal. Khim., 20 (1965) 574.
4 S. B. Savvin, V. A. Mineeva, L. A. Okhanova and D. N. Pochadzhanov, Zh. Anal. Khim., 26 (1971) 532.
5 S. V. Elinson, S. B. Savvin and T. I. Nezhnova, Zh. Anal. Khim., 22 (1967) 531.
6 N. Ivanov and N. Todorova, Dokl. Bolg. Akad. Nauk, 29 (1976) 1775.
7 S. B. Savvin, I. P. Alimarin, T. Ya. Belova and L. A. Okhanova, Zh. Anal. Khim., 23 (1968) 1117.
8 I. P. Alimarin, S. B. Savvin and Yu. M. Dedkov, Zh. Anal. Khim., 19 (1964) 328.
9 S. B. Savvin, V. A. Bortsova and E. N. Malkina, Zh. Anal. Khim., 20 (1965) 947.
10 B. Buděšínský and S. B. Savvin, Fresenius Z. Anal. Chem., 214 (1965) 189.
11 S. V. Elinson, S. B. Savvin and N. A. Mirzoyan, Zavod. Lab., 34 (1968) 136.
12 S. V. Elinson, Spektrophotometriya Niobiya i Tantala, Atomizdat, Moscow, 1973.
13 R. Borissova and N. Ivanov, Dokl. Bolg. Akad. Nauk, 29 (1976) 221.

14 E. N. Pashchenko, L. A. Vasilyeva, V. F. Maltsev and N. P. Volkova, Zavod. Lab., 39 (1973) 1297.
15 V. F. Maltsev, N. P. Volkova, E. N. Pashchenko and V. P. Novak, Zavod. Lab., 37 (1971) 1048.
16 H. Hiroshi and A. Takeo, Bunseki Kagaku, 24 (1975) 303.
17 S. B. Savvin, I. D. Pisarenko, E. I. Yurchenko and Yu. M. Dedkov, Zh. Anal. Khim., 21 (1966) 669.
18 S. B. Savvin, P. N. Romanov and Yu. B. Eremin, Zh. Anal. Khim., 21 (1966) 1423.
19 S. Wakamatsu, Jpn. Anal., 18 (1969) 376.
20 N. Ivanov, R. Borissova and E. Veselinova, Fresenius Z. Anal. Chem., 280 (1976) 223.
21 Z. Čížek, Technical Information Report, Škoda Works, Pilsen, 1977.

Analytica Chimica Acta, 109 (1979) 393—399
© Elsevier Scientific Publishing Company, Amsterdam — Printed in The Netherlands

THE DETERMINATION OF SERUM CHOLINESTERASE ACTIVITY BY KINETIC DIRECT INJECTION ENTHALPIMETRY

J. KEITH GRIME*

Department of Chemistry, University of Denver, University Park, Denver, Colorado, 80208 (U.S.A.)

BARRIE TAN

Department of Chemistry, University of Otago, Dunedin (New Zealand)

JOSEPH JORDAN

Department of Chemistry, Pennsylvania State University, University Park, Pennsylvania 16802 (U.S.A.)

(Received 5th February 1979)

SUMMARY

A method is described for the enthalpimetric determination of serum cholinesterase activity. Physiological amounts of cholinesterase (2—5 IU cm^{-3}) in aqueous solutions and reconstituted sera are determined with a precision of 2.5% and 1.4% (r.s.d.), respectively. Typical errors of 1.0% are observed when the enthalpimetric results are compared with a standard colorimetric procedure.

Serum cholinesterase (ChE, E.C.3.1.1.8, acylcholine acylhydrolase), sometimes known as pseudocholinesterase, Type II or butyrylcholinesterase, is present in the liver, pancreas, heart and the white brain matter as well as in serum [1]. Its primary physiological function may be to hydrolyze the various choline esters formed during metabolic processes [2]. ChE catalyzes the hydrolysis of choline esters with a marked increase in activity in its interaction with butyrylcholine compared with acetyl- and benzoylcholine esters [3]. Benzoylcholine and butyrylcholine are considered "specific" substrates for ChE. However, as inhibition has been reported in the presence of an excess of benzoylcholine [3, 4], butyrylcholine iodide was selected as the substrate in the present investigation.

Although not a diagnostic determinant in itself, an abnormal serum ChE activity serves as a sensitive measure of liver function in cases of acute hepatitis, advanced cirrhosis and carcinoma with metastases to the liver [1]. ChE levels may also be monitored in patients for whom Suxemethonium anesthesia is planned or to assess acute or chronic intoxication with phosphorus esters (pesticides), which are potent inhibitors of serum cholinesterase activity [5]. Normal ChE levels in healthy adults range between 2.2 and 5.2 IU cm^{-3} [1]; 1 IU is defined as the amount of enzyme necessary to hydrolyze 1×10^{-6} mol of substrate per min under specified conditions of

pH and temperature. The numerous reports of cholinesterase assay have been reviewed [6—8].

Classical procedures for the assay of cholinesterase activity are generally based on the measurement of the acid produced during the hydrolysis reaction either manometrically or potentiometrically [7, 8]. A simple colorimetric procedure has been reported for the analysis of human serum, involving the formation of an iron(III) hydroxamate with unconsumed acetylcholine [9]. In view of the inconvenient nature of the manometric technique and the likely interferences in pH methods [10], the colorimetric procedure was adapted for the determination of butyrylcholine iodide and used as the correlation method in the work described here.

The prominent feature of the enthalpimetric approach to enzyme assay is the utilization of a ubiquitous property of chemical reactions, the enthalpy of reaction. The primary enzymatic reaction can be monitored without recourse to other enzymatic coupling reactions which are often needed in other methods to provide a measurable entity; propagation of errors associated with this step is therefore obviated. The contribution of calorimetric techniques to clinical and biochemical analysis has been reviewed [11—13]. Calorimetric studies of cholinesterase-catalyzed hydrolyses have been reported. In a study covering several enzyme systems, Monk and Wadso [14] reported the determination of aqueous ChE samples by a flow calorimetric procedure [14]. This work was later extended to examine the inhibition of ChE by organophosphorus pesticides [15]. An enthalpy of reaction for the hydrolysis of butyrylcholine by ChE does not seem to have been reported in the literature, although a value of +1.17 kJ mol^{-1} has been reported for the hydrolysis of acetylcholine by acetylcholinesterase [16]. More recently, cholinesterase activity in human serum has been determined by using classical Tian—Calvet heat conduction calorimetry with acetylcholine as the substrate [17]. This method, capable of assaying two serum samples in 1 h, compared favourably with a spectrophotometric correlation procedure.

In the present report, a serum cholinesterase determination by kinetic direct injection enthalpimetry [18] is described. The reaction investigated is the cholinesterase-catalyzed hydrolysis of butyrylcholine iodide (BuCh) in the presence of Tris buffer at pH 8.0:

$$C_3H_7C(=O)-O(CH_2)_2\overset{+}{N}(CH_3)_3I^- + H_2O \xrightarrow[\text{pH 8.0}]{\text{ChE}} C_3H_7C(=O)-OH + HO(CH_2)_2\overset{+}{N}(CH_3)_3I^- \quad (1)$$

The heat change produced by the enzymatic hydrolysis is amplified by the concurrent protonation of Tris buffer.

The "working equation" for the enthalpimetric determination of enzyme activity (EA) with pseudo zero-order kinetics prevailing is (for an exothermic reaction)

$$EA(IU) = -\Delta H^{-1}\, q_{(t)}\, \Delta t^{-1} \times 10^{-6} \quad (2)$$

where $q_{(t)}\, t^{-1}$ (J min^{-1}) is the overall rate of heat evolution from the concurrent reactions [19, 20]. Clearly, an assignment of the total reaction enthalpy is necessary before this equation can be utilized. Although the enthalpy of protonation of Tris is accurately known, the enthalpy of the enzymatic hydrolysis reaction has not, to our knowledge, been previously reported. Accordingly, the experiments are reported below in two clearly distinct forms. Substrate-limiting experiments (Method 1) are described in which the buffered enzymatic hydrolysis was allowed to go to completion. Measurement of the total caloric output resulted in the assignment of appropriate thermodynamic data. These data were then applied in enzyme-limiting studies (Method 2) in which the coupled reactions were made to proceed at maximal velocity V_{max}, i.e. the substrate concentration greatly exceeded the Michaelis constant, K_m (here $K_m = 1.6 \times 10^{-3}$ mol dm^{-3} [10]). Under these conditions, the Michaelis—Menten equation, $v = V_{max}\,[S]/(K_m + [S])$ (where v is the initial rate of reaction, and [S] is the substrate concentration) simplifies to $v = V_{max}$ and the rate of reaction represented by the rate of heat evolution is proportional to the concentration of the enzyme.

The feasibility of the technique was assessed by its application to the determination of ChE activity in aqueous standards and reconstituted reference sera. The enthalpimetric assay results were compared with those obtained by an adapted colorimetric procedure [9] in which unconsumed BuCh was determined as its iron(III) hydroxamate derivative at 530 nm.

EXPERIMENTAL

Reagents

Doubly distilled water was used throughout. The buffer solution used in all tests was 0.2 mol dm^{-3} Tris [tris(hydroxymethyl)-aminomethane] adjusted to pH 8.0 with hydrochloric acid. Type IV horse serum cholinesterase (E.C.3.1.1.8; nominal activity 15 IU mg^{-1} protein) and 99% butyrylcholine iodide (both from Sigma Chemical Co.) were stored, desiccated, below 0°C.

Elemental microanalysis and Karl Fischer titration showed the BuCh to be essentially anhydrous and at least 99.5% pure. The extent to which aqueous solutions of BuCh undergo non-enzymatic hydrolysis was established by volumetric microtitration of the butyric acid produced by hydrolysis as a function of time; the hydrolysis reached an equilibrium value of 0.5% on dissolution with no apparent increase over a period of 6 h. Aqueous solutions of BuCh stored at 4°C showed no increase in hydrolysis over a period of 6 days. It was also shown by the colorimetric determination of residual BuCh [9] that the same degree of hydrolysis occurred for solutions of BuCh in 0.2 mol dm^{-3} Tris. Appropriate corrections were made to all calculations.

Wellcomtrol II (BC 02) quality-control serum (Lot K1810) was quantitatively diluted to 10.00 cm^{-3} with water.

All reagents used in the colorimetric procedure were identical to those recommended earlier [9] except that barbital buffer was replaced by 0.2 mol dm^{-3} Tris, and 1.0 mol dm^{-3} hydrochloric acid was used instead of 0.5 mol dm^{-3} reagent.

All solutions were prepared freshly before each set of experiments.

Apparatus

The details of the instrumention used have been reported elsewhere [21]. Temperature changes were monitored by measurement of the imbalance potential produced in a d.c. Wheatstone bridge circuit with a 10,000-ohm thermistor as one arm of the bridge. A bridge current of 7.2×10^{-5} A was normally employed. The signal was amplified by a variable-gain, null-detector microvoltmeter (Model 155, Keithley Instrument Co., Cleveland, Ohio) and recorded on a strip-chart potentiometric recorder. Accurate reagent injection was done with gravimetrically calibrated precision syringes (0.5 cm^3) equipped with Chaney adaptors (Model 1750, Hamilton Co.). Substrate and enzyme solutions were thermostated by immersion of the reaction cell and syringe in a water-bath maintained at 25.0 C (±0.002°C short-term stability). Caloric calibration of enthalpograms was achieved in situ by Joule heating of a 0.25-W carbon resistor [21].

A Bausch and Lomb Spectronic 20 spectrophometer was used for absorbance measurements.

Procedures

Method 1. On attainment of thermal equilibrium, as evidenced by an isothermal baseline, about 0.50 cm^3 of enzyme solution (prepared from an aqueous stock solution containing ca. 80 IU cm^{-3} of ChE) was injected into an accurately measured amount of substrate. (For the substrate, ca. 100×10^{-6} mol of BuCh was accurately weighed directly into a carefully dried reaction cell and dissolved in 10 cm^3 of Tris buffer.) The exothermic heat change was monitored as the reaction proceeded to completion. A typical enthalpogram is represented in Fig. 1. After a suitable post-reaction period of

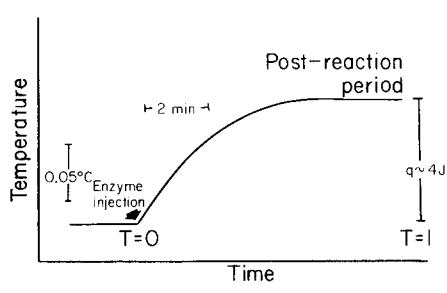

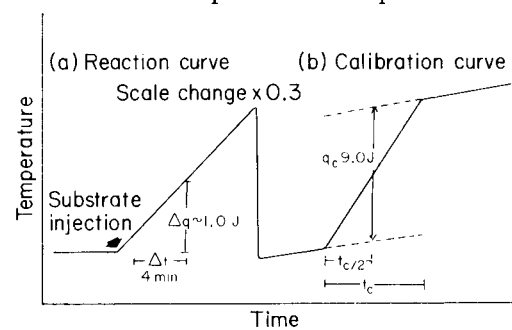

Fig. 1. Typical enthalpogram (Method 1) corrected for heat loss from T = 0.5 to 1.0.

Fig. 2. Typical sequence of enthalpogram and calibration curve (Method 2).

about 2 min, the heat capacity of the cell was determined electrically and the overall reaction enthalpy calculated.

Method 2. Aqueous stock solutions of enzyme were prepared by dissolution of accurately weighed amounts of enzyme in the physiological range (2—5 IU cm^{-3}); enzyme solutions left for 3 h at room temperature showed a decrease in activity of 0.5%. For measurements, 1.00 cm^3 of aqueous enzyme solution or reference serum was transferred quantitatively to the adiabatic cell, and the solution was diluted with 10 cm^3 of Tris buffer. After attainment of thermal equilibrium, 0.5 cm^3 of BuCh solution was injected into the diluted enzyme solution. (In this case, the substrate aqueous stock solution contained ca. 200 × 10^{-6} mol cm^{-3} of BuCh.) The injected substrate solution contained an amount of substrate necessary to maintain a constant maximal rate of reaction throughout the reaction and calibration recording sequence. In practice, a linear reaction trace was recorded for 4 min. After this time, the signal was attenuated (× 0.3) and a calibration curve subsequently recorded by activation of the heating circuitry. A typical enthalpogram and calibration curve is depicted in Fig. 2. EA was calculated by substitution of the appropriate values of Δq, Δt and ΔH into eqn. (2).

RESULTS AND DISCUSSION

Assignment of reaction enthalpy (Method 1)

A preliminary colorimetric study with reagent concentrations similar to those expected for the enthalpimetric procedure (Method 1) established that reaction (1) had reached an equilibrium value of 97.5% completion after 1 min. The reaction was quenched at different intervals of time by the addition of alkaline hydroxylammonium chloride reagent [9]. Reaction enthalpy calculations were adjusted to compensate for this factor.

The total enthalpy change for the combined reactions was −46.1 ± 0.5 kJ mol^{-1} (Table 1). Previous calibration experiments established the enthalpy

TABLE 1

Determination of total reaction enthalpy (Method 1)

Experiment	Amount of BuCh (× 10^{-6} mol)	Amount of heat evolved (J)	ΔH (kJ mol^{-1})
1	91.8	4.22	46.0
2	112.8	5.10	45.2
3	98.6	4.57	46.3
4	102.9	4.80	46.7
5	92.9	4.33	46.6
6	86.3	3.97	46.0
			Av. = 46.1
			R.s.d. % =1.2

of protonation of Tris buffer to be -47.7 ± 0.4 kJ mol^{-1} [21]. Clearly the endothermic enthalpy change associated with the enzymatic reaction alone is small compared to that of the buffer protonation, and cannot be accurately reported since it falls almost within the limits of experimental error.

Determination of enzyme activity (Method 2)

The amount of substrate injected was optimized with respect to the restraints imposed on the Michaelis—Menten equation by the prerequisite of pseudo zero-order kinetics. The substrate concentration must also be minimized to circumvent spurious thermal events induced by dilution.

A series of experiments established that, for solutions containing physiological amounts of enzyme, enzyme activity was invariant for substrate concentrations (in the cell) exceeding 1×10^{-2} mol dm^{-3}, i.e. for injections of at least 1×10^{-4} mol of BuCh. Furthermore, at a fixed substrate concentration of 1×10^{-2} mol dm^{-3} (ca. $6K_m$), the observed enzyme activity increased linearly with increasing amounts of enzyme, up to a maximum of 5 IU. Thus it was concluded that the conditions necessary for the utilization of the zero-order form of the Michaelis—Menten equation had been met.

Although the reaction cell was constructed to maximize adiabaticity, a small but finite heat transfer was observed. Consequently, positive deviations from anticipated reaction curve gradients were observed for concentrated substrate injections producing an initial endothermic dilution pulse. In practice, injections of 1×10^{-4} mol of substrate showed no observable dilution heat effects and this amount of substrate was used for all enthalpimetric assays.

Three series of aqueous enzyme solutions containing ca. 3, 4 and 5 IU cm^{-3} of ChE were assayed simultaneously by colorimetric and enthalpimetric procedures. The same procedure was adopted for samples of Wellcomtrol II reference sera containing "normal" amounts of ChE. The results are listed in Table 2. The accuracy of the enthalpimetric procedure (column 6) is reported with reference to the colorimetric assay. The precision of the enthalpimetric method compares favourably with that of the colorimetric procedure, particularly for the serum assays. The advantages of the enthalpimetric approach, particularly in the area of clinical analysis, are those of convenience in dealing with the biological matrix, e.g. sera, and also the ability to observe the primary enzymatic event by means of a fundamental property instead of empirical standards. The technique allows the determination of two serum samples per hour.

Part of this work was performed at Pennsylvania State University during the research associateship of J.K.G. and was funded during that period by research grant CHE 76-21666 provided by the National Science Foundation.

TABLE 2

Comparison of enthalpimetric and colorimetric results for the determination of cholinesterase activity in aqueous solutions and reference sera

Sample	Colorimetric	Precision R.s.d. (%)[a]	Enthalpimetric	Precision R.s.d. (%)[a]	Error (%)
Aqueous solutions					
ca. 3 IU cm^{-3}	3.34	1.6(7)	3.30	2.5(6)	1.2
ca. 4 IU cm^{-3}	4.07	2.2(7)	4.02	1.5(6)	1.2
ca. 5 IU cm^{-3}	5.61	1.2(6)	5.57	1.9(6)	0.7
Wellcomtrol II reference sera	3.80	2.3(15)	3.84	1.4(9)	1.0

[a]Number of results in parentheses.

REFERENCES

1 J. F. Kachmar, in N. W. Tietz (Ed.), Fundamentals of Clinical Chemistry, W. B. Saunders, Philadelphia, 1970.
2 J. W. Clitherow, N. J. Harper and M. Mitchard, Nature, 199 (1963) 1000.
3 A. M. Beckett, M. Mitchard and J. W. Clitherow, Biochem. Biopharm., 17 (1968) 1601.
4 W. K. Berry, Biochim. Biophys. Acta, 39 (1960) 346.
5 M. Dixon and E. C. Webb, in Enzymes, Longmans, Green and Co., London, 1958.
6 G. G. Guilbault, Enzymatic Methods of Analysis, Pergamon, Oxford, 1970.
7 W. Pilz, in H. U. Bergmeyer (Ed.), Methods of Enzymatic Analysis, 2nd Edn., Vol. 2, Verlag Chemie/Academic Press, New York, 1974.
8 Worthington Enzyme Manual, Worthington Biochemical Corporation, 1977.
9 J. de la Huerga, C. Yesnick and H. Popper, Am. J. Clin. Pathol., 12 (1952) 1126.
10 K. Gibson and G. G. Guilbault, Anal. Chim. Acta, 76 (1975) 245.
11 K. Levin, Clin. Chem., 23 (1977) 929.
12 C. Spink and I. Wadso, In D. Glick (Ed.), Methods of Biochemical Analysis, 23, Interscience, New York, 1976, p. 1.
13 H. D. Brown, Biochemical Microcalorimetry, Academic Press, New York, 1969.
14 P. Monk and I. Wadso, Acta Chem. Scand., 23 (1969) 3.
15 J. Konickova and I. Wadso, Acta Chem. Scand., 25 (1971) 2360.
16 J. M. Sturtevant, J. Biol. Chem., 247 (1972) 968.
17 H. K. O'Farrell, S. K. Chattopadhyay and H. D. Brown, Clin. Chem., 23 (1977) 1853.
18 J. C. Wasilewski, P. T.-S. Pei and J. Jordan, Anal. Chem., 36 (1964) 2131.
19 C. D. McGlothlin and J. Jordan, Anal. Chem., 47 (1975) 1479.
20 C. D. McGlothlin, J. K. Grime and J. Jordan, Enzymatic Enthalpimetry for Clinical Analysis, Symposium of New Approaches to the Routine Determination of Serum Enzymes, Paper No 71, A.C.S., New York, April 1976.
21 J. K. Grime, K. Lockhart and B. Tan, Anal. Chim. Acta, 91 (1977) 243.

Analytica Chimica Acta, 109 (1979) 401—409
© Elsevier Scientific Publishing Company, Amsterdam — Printed in The Netherlands

SEMI-AUTOMATIC CATALYTIC TITRATION OF ETHYLENEDIAMINETETRAACETIC ACID AND METAL IONS WITH THE 1,4-DIHYDROXYPHTHALIMIDE DITHIOSEMICARBAZONE—AERIAL OXYGEN SYSTEM AS INDICATOR REACTION

M. TERNERO and F. PINO

Department of Analytical Chemistry, University of Sevilla (Spain)

D. PEREZ-BENDITO and M. VALCARCEL*

Department of Analytical Chemistry, University of Córdoba (Spain)

(Received 12th March 1979)

SUMMARY

A semi-automatic spectrophotometric method is described for the catalytic titration of ethylenediaminetetraacetic acid, based on its inhibitory effect on the manganese(II)-catalyzed aerial oxidation of 1,4-dihydroxyphthalimide dithiosemicarbazone. Amounts of EDTA in the 750—4000-μg range can be determined with a relative standard deviation of ca. 0.6% (n = 11). Methods are also described for the indirect catalytic titrations of manganese(II) and nickel(II) in the ranges 20—450 μg and 40—1000 μg, respectively, with relative standard deviations (n = 11) of ca. 1%.

The kinetic determination of manganese(II) by its catalytic effect on the autooxidation of 1,4-dihydroxyphthalimide dithiosemicarbazone (OH-PDT) was described earlier [1]. Aminopolycarboxylic acids (e.g. EDTA and EGTA) have an inhibitory effect on this catalytic reaction, and this provides a method of determining these ligands by means of two consecutive reactions: (a) the titration reaction, in which the manganese(II) titrant (catalyst), added to the sample at a constant rate, reacts rapidly and stoichiometrically with the EDTA or EGTA, and (b) the indicator reaction (i.e. the autooxidation of OH-PDT in alkaline medium) which only occurs at a noticeable rate when an excess of manganese(II) is present. As a small excess of titrant at the end-point reacts catalytically, large changes in the rate of the indicator reaction and therefore sharp absorbance changes occur at 600 nm where the oxidation product absorbs.

The semi-automatic determination of aminopolycarboxylic acids and/or metal ion with manganese(II) [2—14] and nickel(II) [15] as catalytic titrants with other indicator reactions has been reported. The reverse determination of manganese and indirect determination of manganese(II) and nickel(II) with the above-mentioned OH-PDT—Mn(II) system is also possible. The determination of EDTA and of metal ions by catalytic end-point detection is described in this paper.

EXPERIMENTAL

Reagents

1,4-Dihydroxyphthalimide dithiosemicarbazone solution. A 0.05% (w/v) solution in dimethylformamide (DMF) was prepared. The reagent was synthesized from 1,4-dihydroxyphthalimidedioxime and thiosemicarbazide [1].

Standard manganese(II) and nickel(II) solution. Solutions were prepared from manganese sulphate (ignited at 500°C) dissolved in hot dilute sulphuric acid, and from nickel sulphate dissolved in distilled water, and standardized by titration with EDTA and by gravimetry with dimethylglyoxime, respectively. Stock solutions (1.000 g l^{-1}) were diluted as required immediately before use.

EDTA and EGTA (0.01 M) solutions. The EDTA solution was prepared from the dihydrated disodium salt dissolved in distilled water, and standardized against standard calcium carbonate solution with murexide as indicator. The EGTA solution was prepared in distilled water, with addition of NaOH to form the disodium salt, and standardized against standard zinc solution with eriochrome black T as indicator. Very dilute solutions (10^{-5} M) were prepared immediately before use.

All solvents and reagents were of analytical-reagent grade.

Apparatus

A Metrohm E1009 photometric titrator with a titration vessel and stirrer was coupled with a Metrohm E536 potentiometric recorder (potentiograph) and a Metrohm E436 automatic constant-rate burette. Other similar devices have been described [2, 13].

Procedures

Preparation of equipment. The autoburette was filled with the appropriate standard manganese(II) solution. The wavelength of the photometric titrator was fixed at 600 nm and the rate of titrant addition at 4 ml min^{-1}. The pH index control was set at 250 mV and the Autocontrol switch at position 10. The chart width was adjusted to 10 mm ml^{-1} or 20 mm ml^{-1} according to the titrant concentration used.

Semi-automatic catalytic titration of EDTA. Samples containing 750—4000 μg of EDTA were added to the 100-ml titration vessel; 2 ml of 0.05% (w/v) OH-PDT solution in DMF and 10 ml of 0.429 M ammonia solution were added, and the sample was diluted to ca. 50 ml with distilled water. The spectrophotometer zero was calibrated with distilled water. When the relative absorbance attained the 0.20—0.25 value, the function switch was turned to Record and the absorbance was monitored on the potentiograph to obtain the titration curve. The end-point was obtained by extrapolating the linear segments on either side of the equivalence point. Standard solutions (50, 70 and 100 ppm) of manganese(II) titrant, depending on the inhibitor present, were used to obtain end-points within the optimal range of titrant volume

(3—7 ml for 10 mm ml^{-1} scale and 1—7 ml for 20 mm ml^{-1}). The recorder has to be calibrated for each titration from the burette readings for best accuracy. The EDTA content was calculated by the proportional method or from calibration curves obtained by plotting the end-volumes against the amount of EDTA.

Semi-automatic indirect catalytic titration of manganese(II) or nickel(II). A back-titration method was used. To a solution containing 20—450 μg of manganese(II) or 40—1000 μg of nickel(II) in a 100-ml titration vessel was added an accurate volume of 1.01×10^{-3} M or 2.02×10^{-3} M standard EDTA solution (depending on the sample concentration); 2 ml of 0.05% (w/v) OH-PDT solution in DMF and 10 ml of 0.429 M ammonia solution were added. After dilution to ca. 50 ml with distilled water the solutions were titrated with standard manganese(II) solutions (50—100 ppm) as described above. The excess of EDTA was calculated by the proportional method or from calibration curves, and hence the metal concentration was easily calculated.

RESULTS AND DISCUSSION

Ions that either react with manganese to form precipitates or strong complexes, or oxidize manganese(II), should be absent.

During the complexiметric titration of manganese with EDTA (or EGTA), the signal (absorbance) changes only slowly until the equivalence point, when the excess of manganese(II) catalyzes the indicator reaction $OH\text{-}PDT_{red} + O_2(aerial) \overset{Mn(II)}{\rightleftharpoons} OH\text{-}PDT_{ox}$. There is a large, sharp change in the absorbance at 600 nm as the colour changes from orange to red-violet.

These titrations are possible because the time (volume of catalytic titrant added) required to start the indicator reaction (pseudo-induction period) is proportional to the amount of inhibitor present. With the apparatus used, the pH index had to be set at the 250-mV position to obtain absorbances in response to the potentiograph. The titrant was added at a constant rate and the Autocontrol switch, which decreases the addition rate towards the end-point, was used to obtain more accurate and reproducible titration curves. An automatic method involving the dead-stop device is also possible but the semi-automatic method gives more satisfactory results.

Effect of variables on the titration curves

The influence of chemical and instrumental variables on the titration curves was studied; the procedure recommended for direct determination of EDTA was used.

Influence of chemical variables. The effect of the reagent concentration was studied in the range 3.11×10^{-5}—12.2×10^{-5} M (1—4 ml of 0.05% OH-PDT solution). The results (Fig. 1) showed that the slopes of the pseudo-induction period and of the catalyzed reaction increased as the reagent concentration increased. The titration curves were more accurate and reproducible when 2—3 ml of the reagent solution was used.

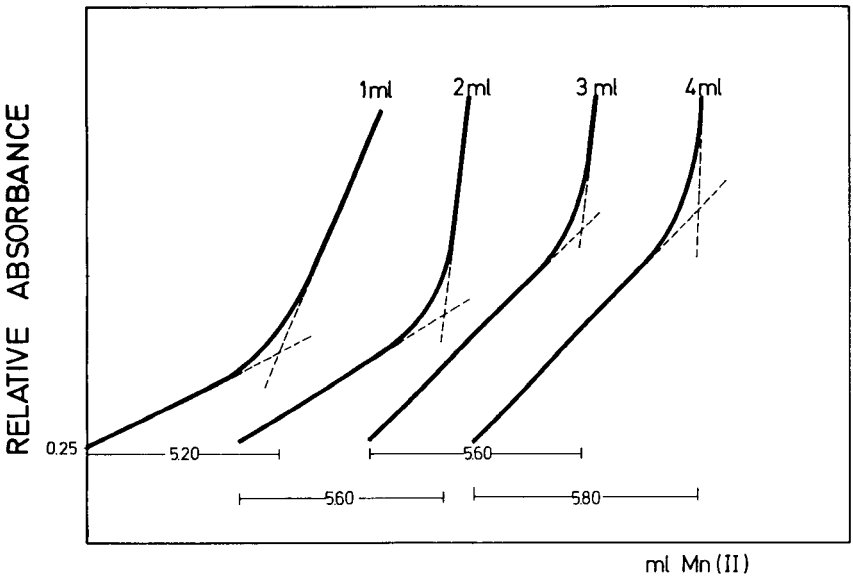

Fig. 1. Influence of OH-PDT concentration on the titration graph (ml of 0.05% OH-PDT solution). Conditions: 5 ml of 1.01×10^{-3} M EDTA solution, 10 ml of 0.429 M ammonia solution, titrated with standard 50-ppm Mn(II) solution. Theoretical end-point, 5.55 ml.

The influence of the ammonia concentration was also important because the indicator reaction rate increased as the ammonia concentration increased; 8—10 ml of 0.429 M ammonia solution (6.86×10^{-2}—8.5×10^{-2} M in a final volume of 50 ml of solution) was selected, because errors below 1% and relative standard deviations around 0.5% were given. Volumes below 8 ml gave appreciable positive errors because the end-point was retarded; above 10 ml, appreciable negative errors (ca. 2%) were observed.

Experiments with different volumes of the solution titrated showed that the most favourable titration curves were obtained when a volume of 40—60 ml was used.

The lowest concentration of manganese(II) catalyst giving accurate, reproducible results was investigated; 4, 5, 7 and 10 ml of 1.01×10^{-3} M EDTA was titrated with standard (30, 50, 70 and 100 ppm) manganese(II) solutions; the 30-ppm standard gave an appreciable positive error (6—13%) and 50 ppm was established as the lowest limit for the standard solution.

Influence of instrumental variables. The titrant addition rate and the Autocontrol system were investigated. The volume of the burette used (20 ml) in connection with the potentiograph gave titrant flows ranging from 0.1 to 4 ml min^{-1}. The influence of the rate of addition of manganese(II) solution (1.33, 2 and 4 ml min^{-1}) was tested. Experiments with the Autocontrol switch were repeated with its use. The results showed that the greater the rate of addition, the smaller the errors, and that the Autocontrol system is the more

favourable. To obtain satisfactory results (average error 0.7%, relative standard deviation 0.5%) a titrant flow rate of 4 ml min^{-1} (maximum attainable with the burette used) and the Autocontrol system are recommended. Higher titrant flow rates were investigated from 8.8 to 13.6 ml min^{-1} by a manual method in which the absorbances and added volumes were read simultaneously. The average error was near zero for 8.8 ml min^{-1} and 5% for 13.6 ml min^{-1}; too fast an addition rate of titrant is not suitable.

The initial relative absorbance, prior to the addition of titrant, was studied; the results showed that the most adequate range was from 0.1 to 0.25 (errors below 1%).

The maximum volume of titrant which can be added without causing dilution errors was determined. The amounts of inhibitor (EDTA) were varied for the same manganese(II) titrant; the results (Fig. 2) showed that 7 ml was the maximum volume (relative standard deviation, 0.5%) possible and that for a total volume of titrant below 3 ml the pseudo-induction period was too short and curved so that extrapolation gave large negative errors.

All these variables were studied with the same chart width of 10 mm ml^{-1} (absolute error of ±0.5 mm equivalent to ±0.05 ml of added titrant). The results for a chart width of 20 mm ml^{-1} were compared with those for 10 mm ml^{-1}. Both scales gave similar errors and relative standard deviations (1.3 and 1.0%, respectively), but the 20 mm ml^{-1} scale gave a lower total

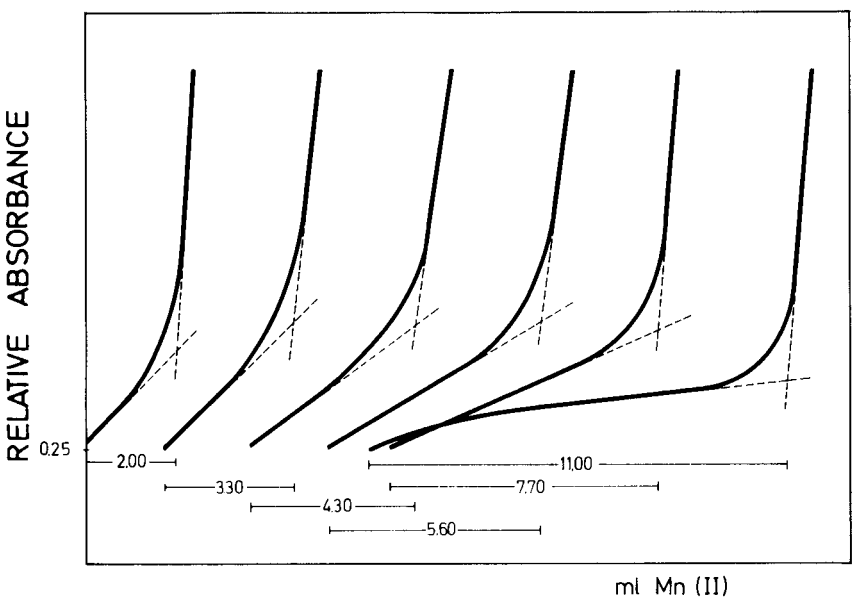

Fig. 2. Titration curves for different final volumes of titrant. Conditions: variable volumes of 1.01×10^{-3} M EDTA solution, 2 ml of 0.05% OH-PDT solution and 10 ml of 0.429 M ammonia solution, titrated with standard 50-ppm Mn(II) solution. Theoretical end-points are 2.22, 3.33, 4.44, 5.55, 7.77 and 11.1 ml, respectively.

minimum volume of titrant (1 ml) and a lower absolute error (±0.025 ml) in the graphical end-point determination.

The stirring rate during the titration also showed some influence. Of the three possible stirrer speeds, the middle one should be chosen.

Direct catalytic titration of EDTA

Direct titrations of EDTA by the catalytic end-point detection method were tested in three concentration ranges, with different standard manganese(II) solutions as follows: 750—2000 μg EDTA (4.03×10^{-5}—10.7×10^{-5} M) with 50 ppm Mn(II); 2000—3000 μg EDTA (1.07×10^{-4}—1.6×10^{-4} M) with 70 ppm Mn(II); 3000—4000 μg EDTA (1.6×10^{-4}—2.15×10^{-4} M) with 100 ppm Mn(II).

The EDTA concentration was obtained by the proportional method (method A) in which the results obtained for the sample were compared with that obtained for a standard EDTA solution; the conditions and the concentration of EDTA must then be as similar as possible in both titrations. The EDTA concentration may also be found (method B) by calibration curves, constructed to read molar concentrations or micrograms of EDTA in the titrated sample. The working plots prepared for each of the three ranges indicated were linear. The results obtained for aqueous EDTA solutions of known concentration by both methods are shown in Table 1.

The methods reported here were investigated in detail for EDTA but are also applicable to EGTA within similar ranges. Other aminopolycarboxylic acids (e.g. NTA) cannot be used, probably because they enhance the catalytic effect of manganese(II) on the indicator reaction and a change in slope of the titration curve is not observed. The use of NTA to enhance the catalytic effect of manganese(II) on the oxidation of malachite green has been reported [16].

The catalyst can also be determined by reverse catalytic titration. A known volume of the EDTA standard solution was titrated with the unknown manganese(II) solution placed in the burette. The results are shown in Table 2.

Back-titration of metal ions

Ions which have no catalytic activity on the indicator reaction can be determined by back-titration if they form a complex with EDTA stronger than that for manganese(II); a known amount of the ligand is added and the excess is back-titrated with a standard manganese(II) solution. Nickel(II) and manganese(II) were titrated in this way; the amounts of manganese determined were lower than in the reversed method. Titration curves for different concentrations of Ni(II) and Mn(II) are shown in Fig. 3. Table 3 shows typical results obtained by the two methods.

In conclusion, the manganese(II)-catalyzed aerial oxidation of OH-PDT gives a rapid, simple, accurate and sensitive way of determining small amounts of some aminopolycarboxylic acids and metal ions.

TABLE 1

Semi-automatic catalytic titration results for aqueous EDTA solution[a]

Mn(II) titrant (M)	EDTA taken (μg)	EDTA found (μg)		% Error and % r.s.d. (n = 11)	
		Method A	Method B	Method A	Method B
9.1×10^{-4}	751	745	755	−0.9	+0.6
	1315	1290	1290	−1.9	−1.9
	1691	1622	1650	−1.7	−2.4
	1879	1866	1850	−0.7 (±0.55)	−1.5 (±0.66)
	2066	2082	2080	+0.8	+0.6
				Av. 1.20	Av. 1.40
1.2×10^{-3}	2066	2062	2085	−0.2	+0.9
	2254	2228	2250	−1.1	−0.2
	2630	2630	2640	0.0 (±0.7)	+0.4 (±0.3)
	2818	2843	2840	+0.9	+0.8
	3006	2996	2990	−0.3	−0.5
				Av. 0.50	Av. 0.56
1.8×10^{-3}	3006	2979	2990	−0.9	−0.5
	3381	3385	3380	+0.1	−0.1
	3569	3589	3585	+0.5 (±0.58)	+0.4 (±0.49)
	3757	3757	3750	0.0	−0.2
	4133	4130	4120	−0.1	−0.3
				Av. 0.32	Av. 0.30

[a]Method A: proportional method. Method B: calibration curve method.

TABLE 2

Determination of manganese(II) by reversed catalytic titration against EDTA[a]
(5 ml of 1.01×10^{-3} M solution, equivalent to 0.277 mg Mn, applied)

Mn(II) taken (mg ml^{-1})	Mn(II) found (mg ml^{-1})		% Error and % r.s.d. (n = 11)	
	Method A	Method B	Method A	Method B
0.039	0.039	0.038	0.0	−2.5
0.049	0.050	0.049	+2.0 (± 1.02)	0.0 (±1.01)
0.059	0.059	0.059	0.0	0.0
0.069	0.070	0.070	+1.2	+1.2
0.079	0.080	0.081	+1.2	+2.5
0.089	0.089	0.090	0.0	+1.1
0.099	0.099	0.099	0.0	0.0
			Av. 1.25	Av. 1.04

[a]Method A: proportional method. Method B: calibration curve method.

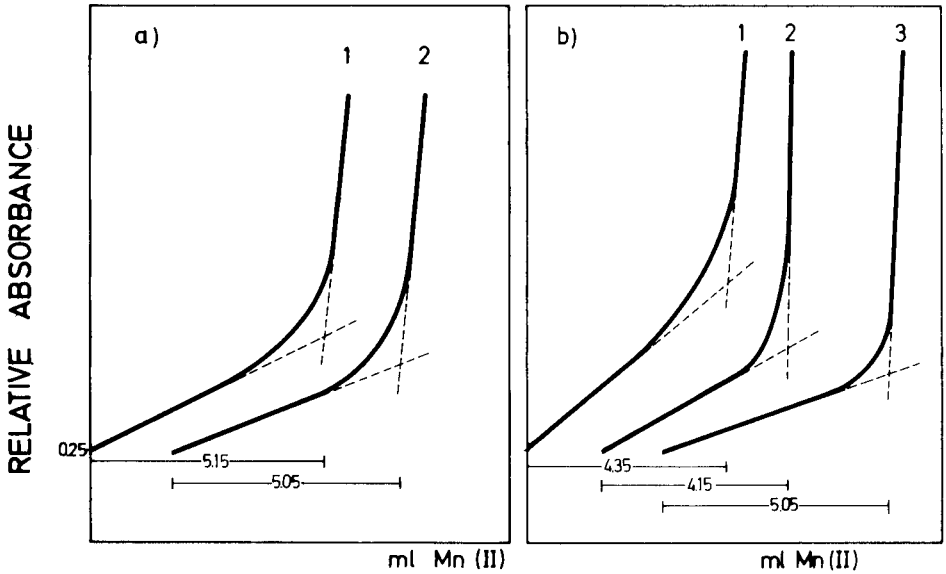

Fig. 3. Recorded curves for the semi-automatic indirect catalytic titration of metal ions. (a) Titration of Mn(II): (1) 20.5 μg of Mn(II) + 5 ml of 1.01×10^{-3} M EDTA standard solution; (2) 300.5 μg of Mn(II) + 10 ml of 1.01×10^{-3} M EDTA standard solution; both titrated with standard 50-ppm Mn(II) solution. Theoretical end-points are 5.13 and 5.09 ml respectively. (b) Titration of Ni(II): (1) 64.5 μg of Ni(II) + 5 ml of 1.01×10^{-3} M EDTA standard solution, titrated with standard 50-ppm Mn(II) solution; (2) 150.5 μg of Ni(II) + 5 ml of 2.02×10^{-3} M EDTA standard solution, titrated with standard 100-ppm Mn(II) solution; (3) 643.0 μg of Ni(II) + 10 ml of 2.02×10^{-3} M EDTA standard solution, titrated with standard 100-ppm Mn(II) solution. Theoretical end-points are 4.34, 4.15 and 5.08 ml, respectively.

TABLE 3

Semi-automatic indirect catalytic titration of manganese(II) and nickel(II) with 9.1×10^{-4} M manganese(II) titrant[a]

EDTA taken (M)	Mn(II) taken (μg)	Mn(II) found (μg)		% Error and % r.s.d. (n = 11)	
		Method A	Method B	Method A	Method B
5 ml 1.01×10^{-3}	20.5	19.9	21.0	−2.9	+2.4
	50.0	49.9	52.0	−0.2	+4.0
	101.5	99.9	101.0	−1.5 (±1.15)	−0.5 (±1.17)
	150.5	147.9	150.0	−1.7	−0.3
	200.5	199.4	201.0	−1.4	+0.2
				Av. −1.54	Av. 1.50
10 ml 1.01×10^{-3}	250.0	253.3	252.0	+2.3	+0.8
	300.5	302.3	302.0	+0.6	+0.5
	350.0	348.9	348.0	−0.3 (±0.35)	−0.6 (±0.40)
	400.0	404.8	403.0	+1.2	+0.7
	450.5	450.2	452.0	−0.1	+0.3
				Av. 0.90	Av. 0.60

TABLE 3 (continued)

EDTA taken (M)	Ni(II) taken (μg)	Ni(II) found (μg)		% Error and % r.s.d. (n = 11)	
		Method A	Method B	Method A	Method B
5 ml 1.01×10^{-3}	43.0	44.0	44.5	+2.3	+3.4
	86.0	85.4	85.0	−0.6	−1.1
	107.5	106.7	106.5	−0.7 (±1.20)	−0.9 (±0.93)
	129.0	130.8	129.5	+1.3	+0.3
	150.5	152.2	151.0	+1.1	+0.3
				Av. 1.20	Av. 1.20
5 ml 2.02×10^{-3}	150.5	149.5	155.0	−0.6	+2.9
	215.6	213.6	215.0	−0.6	0.0
	322.5	325.8	320.0	+1.0 (±1.30)	−0.7 (±0.89)
	376.2	373.9	370.0	−0.6	−1.0
	430.0	427.3	420.0	−0.6	−2.3
				Av. 0.68	Av. 1.38
10 ml 2.02×10^{-3}	430.0	427.2	420.0	−0.6	−2.3
	537.5	544.7	535.0	+1.3	−0.4
	752.5	758.4	760.0	+0.8 (±0.35)	+1.0 (±0.33)
	860.0	849.3	860.0	−1.2	0.0
	967.5	945.5	965.0	−2.2	−0.2
				Av. 1.22	Av. 0.78

[a]Method A: proportional method. Method B: calibration curve method.

REFERENCES

1 D. Pérez Bendito, M. Valcárcel, M. Ternero and F. Pino, Anal. Chim. Acta, 94 (1977) 405.
2 H. A. Mottola, Anal. Chem., 42 (1970) 630.
3 H. Weisz and V. Muschelknautz, Fresenius Z. Anal. Chem., 215(1) (1966) 17.
4 H. Weisz and T. Janjic, Fresenius Z. Anal. Chem., 227(1) (1967) 1.
5 H. Weisz and T. Kiss, Fresenius Z. Anal. Chem., 249(5) (1970) 302.
6 D. Klockow and L. García-Beltran, Fresenius Z. Anal. Chem., 249(5) (1970) 304.
7 T. Kiss, Fresenius Z. Anal. Chem., 252(1) (1970) 12.
8 S. Abe and T. Matsuo, Bunseki Kagaku, 20 (1971) 1168.
9 S. Abe and K. Takahashi, Bunseki Kagaku, 23 (1974) 1326.
10 S. Abe, T. Takahashi and T. Matsuo, Nippon Kagaku Kaishi, (1973) 963.
11 H. Weisz and T. Janjic, Fresenius Z. Anal. Chem., 262(4) (1972) 269.
12 S. Abe and S. Kon, Bunseki Kagaku, 25 (1976) 846.
13 E. A. Piperaki and T. P. Hadjiioannou, Chem. Chron., 6 (1977) 375.
14 T. P. Hadjiioannou, M. A. Koupparis and E. Efstathiou, Anal. Chim. Acta, 88 (1977) 281.
15 A. Gomez Hens, M. Ternero, D. Pérez Bendito and M. Valcárcel, Mikrochim. Acta, in the press.
16 H. Mottola and C. R. Harrison, Talanta, 18 (1971) 683.

Analytica Chimica Acta, 109 (1979) 411—418
©Elsevier Scientific Publishing Company, Amsterdam — Printed in The Netherlands

ETUDE DE LA REACTION $^{14}N(d,n)^{15}O$ A BASSE ENERGIE ET APPLICATION AU DOSAGE DE L'AZOTE DANS LE ZIRCONIUM

A. GIOVAGNOLI, M. VALLADON, C. KOEMMERER, G. BLONDIAUX et J. L. DEBRUN*

C.N.R.S., Groupe Application des Réactions Nucléaires à l'Analyse Chimique, 3A rue de la Ferollerie, 45045 Orléans Cedex (France)

(Reçu le 5 fevrier 1979)

SUMMARY

Study of the $^{14}N(d,n)^{15}O$ reaction at low energy and application to the determination of nitrogen in zirconium

The thick target yield for the $^{14}N(d,n)^{15}O$ reaction was determined between 1 MeV and 5.5 MeV; the "average energy" and the sensitivity of the analysis for nitrogen are calculated. Nitrogen can be determined in zirconium samples at the level of 35 $\mu g\ g^{-1}$, by irradiating at 4 MeV and 5.5 MeV in a deuteron beam from a Van de Graaff accelerator. After irradiation, the samples are subjected to reducing fusion in a graphite crucible, to separate ^{15}O. The results are compared with those obtained by other methods on identical samples; there is a difference of 3—17%.

RESUME

Le rendement en cible épaisse de la réaction $^{14}N(d,n)^{15}O$ a été déterminé entre 1 MeV et 5,5 MeV.La sensibilité pour le dosage de l'azote, ainsi que l' "énergie moyenne", ont été calculés. Nous avons réalisé le dosage de l'azote dans le zirconium au niveau de 35 $\mu g\ g^{-1}$, en irradiant à 4 et 5,5 MeV avec un faisceau de deuterons issus d'un Van de Graaff. Après irradiation, les échantillons subissent une fusion réductrice en creuset de graphite, de façon à séparer ^{15}O. Les résultats obtenus sont comparés à ceux fournis par d'autres méthodes sur des échantillons identiques:il y a une difference de 3—17%.

Le dosage de traces d'azote dans les métaux est généralement réalisé par fusion réductrice ou par la methode de Kjeldahl; dans les deux cas se pose le problème des blancs de l'appareillage et des réactifs. Aux très basses teneurs, la présence d'azote à la surface des échantillons est également un problème. C'est pourquoi plusieurs méthodes d'activation ont déjà été développées, ces méthodes étant exemptes de blancs et de contaminations et étant en outre très sensibles [1—6]. Les réactions suivantes ont déjà été utilisées: $^{14}N(\gamma,n)^{13}N$ [2, 4], $^{14}N(p,\alpha)^{11}C$ [1, 4, 6], $^{14}N(p,n)^{14}O$ [5], et $^{14}N(d,n)^{15}O$ [3]. Les neutrons rapides ont également été proposés [7].

Quelle que soit la méthode classique utilisée, il faut procéder à une séparation de l'azote ou de l'un de ses composés; en activation, des séparations (de C, N ou O) sont nécessaires sauf dans certaines situations privilégiées où une mesure par spectrométrie-γ directe est possible (fortes teneurs ou/et

faible activation de la matrice). Dans le cas du dosage de l' azote dans le zirconium, les méthodes d'activation existantes nécessitent une séparation du radioisotope obtenu et la question se pose, de même que pour les méthodes de fusion réductrice et Kjeldahl, de savoir si l'on mesure finalement un signal qui correspond à la totalité de l'azote contenu dans le métal.

A l'heure actuelle, seule une comparaison des résultats obtenus par différentes méthodes sur des échantillons identiques peut fournir un début de réponse. C'est dans cet esprit que nous avons étudié et réalisé le dosage de l'azote dans le zirconium, en utilisant la réaction $^{14}N(d,n)^{15}O$ suivie de la fusion réductrice pour la séparation de ^{15}O. Les échantillons de zirconium ont été analysés dans le cadre d'une intercomparaison de méthodes organisée par le Bureau Communautaire de Référence, et nos resultats ont ainsi pu être comparés à ceux obtenus par d'autres méthodes.

PARTIE EXPÉRIMENTALE

Irradiations et spectrométrie-γ

Nous avons utilisé le Van de Graaff (7 MeV) du Centre de Recherches Nucléaires du CNRS de Strasbourg en limitant l'énergie maximale à 5,5 MeV. Pour les études d'étalonnage et le tracé de la courbe d'activation $^{14}N(d,n)^{15}O$, les irradiations ont duré une dizaine de secondes et le courant était de l'ordre de 20 nA. Pour les dosages, les irradiations ont duré 3 min et le courant était de l'ordre de 0,5 μA.

Nous avons utilisé un détecteur Ge(Li) (efficacité relative 20%) et un analyseur multicanaux; on détecte les rayons-γ de 511 keV provenant de l'annihilation des positrons émis par ^{15}O. Le détecteur Ge(Li) a été préferé à un détecteur NaI(Tl) bien que le problème de résolution ne soit pas important, car son rapport signal/bruit et sa stabilité sont meilleurs.

Séparation radiochimique de ^{15}O

Nous effectuons la fusion réductrice en creuset de graphite, en ajoutant du palladium pour que la fusion du zirconium soit complète. Les conditions opératoires sont les suivantes: four Heraeus à électrodes, dérivé du VH 9; creusets en graphite (Carbone Lorraine, 28 × 12 mm); gaz porteur, argon à 0,5 l min^{-1}; température, 2500—2800°C, lue avec un pyromètre sur la paroi extérieure du creuset; temps de fusion, 3 min; échantillons, 190 ± 20 mg, plaques de 10 × 10 × 0,3 mm, fondus entre deux plaques de palladium avec un rapport des poids Pd: Zr ≈ 7.

Les gaz extraits rencontrent successivement: un tampon de laine de verre pour arrêter d'éventuelles particules; du CuO puis de la laine d'argent portés à 400°C, pour oxyder CO en CO_2, puis piéger d'éventuels halogènes; du réactif de Schütze pour éventuellement compléter l'oxydation de CO en CO_2; de l'ascarite pour piéger le CO_2. La colonne d'ascarite (1,5 cm diamètre, 4 cm hauteur) se trouve placée entre deux tampons de laine de verre, dans un tube de verre rattaché au circuit du gaz par un rodage sphérique ce qui permet

de défaire rapidement ce tube et de le mettre en place pour la spectrométrie-γ. Une même colonne sert pour une dizaine de fusions.

Le temps nécessaire à la fusion a été déterminé en effectuant un comptage de l'ascarite en multiéchelle, durant le passage des gaz. Nous avons ainsi constaté qu'un temps de 50 s était normalement nécessaire à la récupération de tout le CO_2 dégagé; cependant, cette récupération nécessite parfois (pour des raisons inexpliquées) un temps plus long, de 2,5 min au maximum. C'est pour cette raison que nous avons adopté un temps de fusion de 3 min.

Il faut moins de 5 min entre le moment où l'irradiation se termine et le moment où la spectrométrie-γ commence, y compris le temps nécessaire au décapage.

Etalonnage

L'étalonnage posait plusieurs problèmes : choix d'un étalon azote, différence de géométrie entre cet étalon et l'ascarite, et méthode de calcul des teneurs.

Choix de l'étalon. Après essai de divers nitrures (BN, ZrN, NbN et TaN), nous avons constaté qu'ils contenaient de fortes proportions d'impuretés. Nous avons préféré éliminer tous les nitrures et utiliser des pastilles de $Pb(NO_3)_2$. Il faut alors attendre la décroissance complète de ^{17}F créé par la réaction $^{16}O(d, n)^{17})F$, soit 15 min avant de commencer la mesure de l'activité de ^{15}O dans la pastille de $Pb(NO_3)_2$.

Géométrie de comptage. Le problème de la différence de géométrie entre $Pb(NO_3)_2$ et l'ascarite, et le problème de la quantitativité de l'extraction et de la récupération de ^{15}O, ont été résolus grâce à une même expérience.

(a) L'irradiation du zirconium avec ^3He de 10 MeV durant 2 min à 0,5 μA crée ^{15}O par la réaction $^{16}O(^3He,\alpha)^{15}O$; on mesure plusieurs fois l'activité spécifique de ^{15}O dans les mêmes conditions de géométrie que pour les pastilles de $Pb(NO_3)_2$. Cette activité spécifique est exprimée en nombre d'impulsions par minute de comptage, à la fin de l'irradiation, et par microcoulomb. Rappelons que le zirconium contient 800 ppm d'oxygène et qu'ainsi ^{15}O peut être détecté par spectrométrie-γ directe; il faut cependant compter aussi vite que possible car ^{11}C et ^{18}F interfèrent très vite.

(b) Après irradiation du zirconium dans les mêmes conditions qu'en (a), et fusion dans les mêmes conditions qu'après l'irradition aux deuterons, on mesure plusieurs fois l'activité spécifique de l'ascarite.

Le rapport des activités spécifiques dans les cas (a) et (b) fournit un coefficient global comportant à la fois le coefficient de géométrie et le coefficient (extraction + récupération) de ^{15}O. Ce coefficient global a été trouvé égal à 3,3 avec une estimation de l'écart type égale à 0,3, pour 12 mesures.

Calcul des teneurs

Nous avons utilisé la méthode du pouvoir d'arrêt moyen [8] qui est la plus précise actuellement connue. La formule donnant la teneur x est la suivante: x (μg g^{-1}) = (A_{ec}/A_{et}) (S_{ec}/S_{et}) 10^6 (% N) (C) où A_{ec}, A_{et} sont l'act-

ivité normalisée de l'échantillon et de l'étalon respectivement; S_{ec} , S_{et} sont le pouvoir d'arrêt de l'échantillon et l'étalon respectivement, pour une valeur de l'énergie appelée "énergie moyenne"; %N est le pourcentage d'azote dans l'étalon en poids; et C est le coefficient global comprenant la géométrie et le coefficient (extraction + récupération).

L'énergie moyenne E_m a été calculée [9] à partir de la courbe d'activation intégrée de la réaction $^{14}N(d,n)^{15}O$ obtenue par irradiation de pastilles de NH_4Br. Pour les valeurs des pouvoirs d'arrêt, nous avons utilisé les données récentes de Andersen et Ziegler [10].

Echantillons

Pour la réalisation des dosages nous avons utilisé du zirconium fourni par le Bureau Communautaire de Référence. Ces échantillons se présentaient initialement sous la forme de disques (diamètre 17 mm, épaisseur 1 mm). Nous avons laminé ces disques de façon à obtenir les plaquettes décrites dans le paragraphe relatif à la séparation de ^{15}O. Après laminage, les échantillons ont été dégraissés, puis décapés dans le mélange $HF—H_2O$ (1 + 40) à température ambiante. Nous avons ensuite procédé à un polissage léger à l'alumine.

Avant et parfois après irradiation, les échantillons sont à nouveau décapés dans le bain indiqué ci-dessus, deux fois durant 10 s. Ceci élimine environ 3,5 μm, ainsi que nous l'avons mesuré grâce à un système déjà décrit par ailleurs [11]. Pour tenir compte du décapage après irradiation qui a été effectué dans certaines expériences, nous avons utilisé la courbe d'activation intégrée de la réaction $^{14}N(d,n)^{15}O$ et les relations parcours-énergie calculées par Williamson et al. [12].

RESULTATS ET DISCUSSIONS

La Fig. 1 représente la variation en fonction de l'énergie des deuterons incidents, de l'activité spécifique pour la réaction $^{14}N(d,n)^{15}O$. L'activité spécifique correspond ici aux conditions suivantes: cible épaisse de NH_4Br; nombre gammas de 511-keV par seconde de comptage, pour une irradiation d'une seconde et une intensité de courant de 10^{-9} A, mesure effectuée juste à la fin de l'irradiation; l'échantillon, enveloppé dans une feuille d'aluminium de 16 μm, est placé directement avec la face irradiée sur le capot du détecteur Ge(Li).

Nous constatons qu'entre 2 MeV et 5,5 MeV, l'activité spécifique est fonction fortement croissante de l'énergie. Il conviendrait peut-être d'irradier à plus forte énergie, de façon à atteindre une zone moins sensible aux fluctuations en énergie: l'incidence d'une éventuelle erreur de décapage serait ainsi minimisée. Une augmentation de l'énergie entrainerait aussi un accroissement de sensibilité mais il convient de rester en dessous du seuil de la réaction d'interférence sur l'oxygène: $^{16}O(d,^3H)^{15}O$, seuil = 10,6 MeV. Les échantillons contiennent environ 800 ppm d'oxygène.

Si l'on reste en dessous de 10,6 MeV, la réaction $^{14}N(d,n)^{15}O$ est totale-

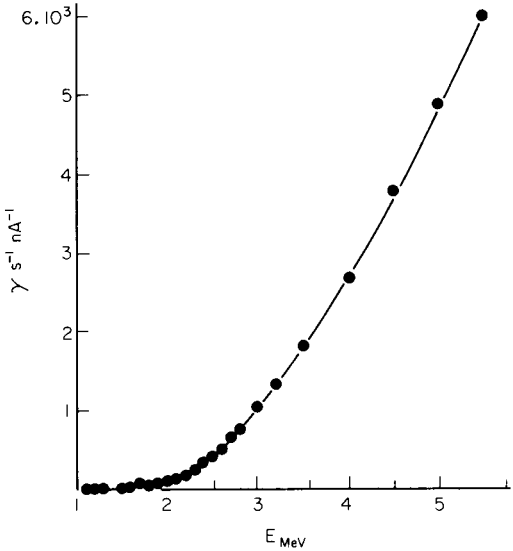

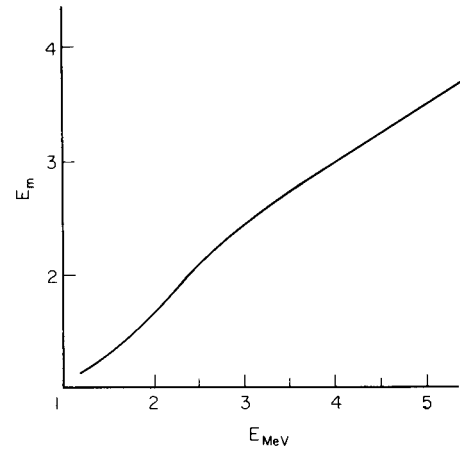

Fig. 1. Courbe d'activation intégrée de la reaction ^{14}N (d,n)^{15}O; cible: NH_4Br.

Fig. 2. Variation de l'énergie moyenne E_m, en fonction de l'énergie incidente.

ment exempte d'interférences. Notons que l'activité induite dans l'échantillon par les deuterons est environ de 50 mRad h^{-1} après une irradiation de 3 min à 0,5 μA et à 5 MeV; des irradiations à plus forte énergie conduiraient à des activités plus importantes et qui pourraient se révéler gênantes pour les manipulations. La Fig. 2 représente la variation de l'énergie moyenne (E_m) pour la réaction $^{14}N(d,n)^{15}O$, en fonction de l'énergie des deuterons incidents; l'énergie moyenne est calculée à partir de la courbe de la Fig. 1, suivant une méthode déjà décrite [9].

La Fig. 3 représente la variation de la sensibilité du dosage de l'azote par la réaction $^{14}N(d,n)^{15}O$. Cette sensibilité correspond aux conditions suivantes: la plus petite activité détectable est égale à 3 fois la racine carrée du bruit de fond dans la bande d'énergie contenant le pic à 511 keV; le temps d'attente après l'irradiation est nul; l'activité spécifique utilisée pour le calcul correspond à une cible de zirconium n'ayant pas subi de fusion, ayant été irradiée durant une fois la période de ^{15}O, à 1 μA, et ayant été comptée durant 1,8 fois la période de ^{15}O.

La sensibilité pratique est environ 20 fois moins bonne que la sensibilité calculée (Fig. 3), compte tenu du facteur de géométrie (3,3) et du temps nécessaire à la récupération de l'échantillon, au décapage et à la fusion (5 min). Dans le Tableau 1, nous présentons les résultats que nous avons obtenus, ainsi que ceux qui ont été obtenus par d'autres laboratoires et d'autres méthodes sur des échantillons identiques. L'accord général n'est pas très bon puisqu'il y a une difference de 17% entre la valeur la plus basse et la valeur la plus haute. La reproductibilité indiquée ici pour les méthodes

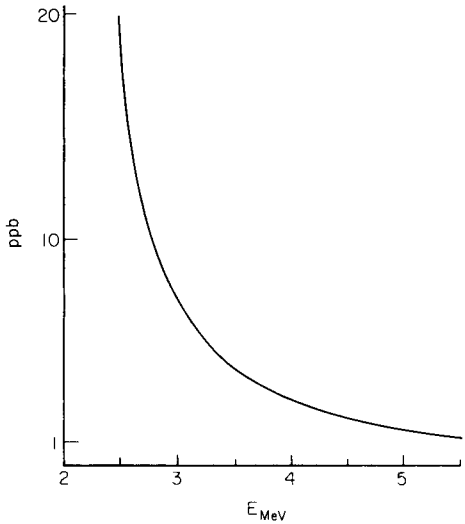

Fig. 3. Sensibilité calculée, pour le dosage de l'azote par la réaction ^{14}N (d,n)^{15}O.

TABLEAU 1

Resultats comparatifs pour le dosage de l'azote dans le zirconium

Méthode	Nombre de valeurs	Valeur moyenne ($\mu g\ g^{-1}$)	Ecart type ou estimation de l'écart type ($\mu g\ g^{-1}$)
Fusion réductrice sous vide (four Balzers EAN-202)	16	30	2
Fusion reductrice gaz porteur (four Ströhlein)	36	31	2
Fusion réductrice gaz porteur (four LECO TN 14)	8	32	2
Micro-Kjeldahl [14]	9	32	1
Fusion oxydante activation $^{14}N(\gamma,n)^{13}N$	9	32	2
Fusion oxydante activation $^{14}N(p,\alpha)^{11}C$	14	34	1
$^{14}N(d,n)^{15}O^a$	13	34,6	4
$^{14}N(d,n)^{15}O^b$	13	35	3,8
$^{14}N(d,n)^{15}O^c$	8	35	4,6

[a]Sans décapage après irradiation à 5,5 MeV. [b]Sans décapage après irradiation à 4 MeV. [c] Décapage après irradiation à 4 MeV.

autre que la notre est bonne, 3—6%, mais il faut signaler qu'il s'agit — sauf pour la méthode "Ströhlein" et la notre — de résultats obtenus après la première intercomparaison.

La reproductibilité est naturellement moins bonne lorsque l'on décape. Nous remarquons que les valeurs moyennes obtenues pour les trois conditions expérimentales différentes que nous avons utilisées, ne sont pas significativement différentes. Ceci nous permet d'affirmer qu'au niveau de 30 $\mu g\ g^{-1}$, il n'est pas nécessaire de décaper le zirconium après irradiation. Des mesures de surface ont d'ailleurs montré que la teneur superficielle en azote du zirconium, tel que nous le préparons avant irradiation, est inférieure ou égale à 0,05 $\mu g\ cm^{-2}$ [13]. Ceci conduit à une erreur inférieure à 1 $\mu g\ g^{-1}$ dans nos conditions opératoires.

Notre reproductibilité est surtout fonction de la fusion du zirconium; en effet nous avons obtenu les reproductibilités suivantes: étalons $Pb(NO_3)_2$, s = 1,5% (10 essais); mesure de ^{15}O sur Zr irradié avec ^{3}He, sans fusion, s = 2,5% (10 essais); mesure de ^{15}O sur Zr irradié avec ^{3}He, avec fusion, s = 11% (10 essais).

De même, pour la mesure de ^{15}O sur zirconium irradié avec les deuterons et fusion, la reproductibilité est de 11% sans décapage. Selon nous, le problème vient de la fusion, bien qu'elle soit effectuée dans des conditions considérées comme adéquates. La valeur moyenne obtenue ne devrait pas être faussée par des incertitudes sur la fusion puisque ces incertitudes sont reflétées à la fois sur les échantillons analysés et sur les échantillons servant à mesurer le coefficient (extraction + géométrie). Par ailleurs, l'erreur provenant de la méthode de calcul des teneurs est négligeable [8], et les erreurs provenant des incertitudes sur les pouvoirs d'arrêt sont faibles [10] par rapport à la dispersion des résultats.

CONCLUSIONS

Ces travaux montrent que la méthode de dosage de l'azote dans le zirconium, faisant appel à la réaction $^{14}N(d,n)^{15}O$ suivie de fusion réductrice, fournit des résultats comparables à ceux obtenus par les méthodes classiques de fusion réductrice sous vide ou sous gaz porteur. A des niveaux assez élevés, tel celui de 35 $\mu g\ g^{-1}$, le seul intérêt de cette méthode semble tout simplement d'être une méthode indépendante utilisable au cours de travaux de certification de matériaux de référence. Par contre, cette méthode est certainement intéressante pour l'analyse d'échantillons plus purs ($\leqslant$ 1 $\mu g\ N\ g^{-1}$), pour lesquels les méthodes classiques sont souvent inopérantes.

A notre sens, les méthodes d'activation avec les particules chargées peuvent quand même être utiles à haut niveau de concentration, pourvu qu'elles soient non-destructives. En effet, il apparaît clairement que les méthodes de fusion réductrice sous vide ou sous gaz porteur, ne permettent pas d'obtenir dans tous les cas une bonne précision (cf. Tableau 1). Avec les méthodes non-destructives, la fusion est supprimée [5, 6], encore faut-il trouver des réactions nucléaires bien adaptées. En ce sens, les réactions avec des ions lourds bore, carbone, azote, oxygène, etc., sont à priori attractives; en effet, l'activation des éléments légers est ici très favorisée par rapport à celle

des éléments lourds, du fait de la barrière coulombienne. Le problème à résoudre est alors celui des données (pouvoirs d'arrêt des ions lourds); ce problème peut être contourné en utilisant la méthode de la double réaction nucléaire [15].

Nous remercions vivement la direction du Centre de Recherches Nucléaires du CNRS à Strasbourg (Cronenbourg) de nous avoir permis d'utiliser le Van de Graaff, et les responsables et les opérateurs pour leur aide efficace. Ces travaux ont été en partie financés par le Bureau Communautaire de Référence (Contrats 093-75-9 BCRF et 093-1.75-11 BCRF), que nous remercions pour son aide et pour la permission qu'il nous accorde de publier les résultats de l'intercomparaison.

BIBLIOGRAPHIE

1 T. Nozaki, T. Okuo, H. Akutsu et M. Furukawa, Bull. Chem. Soc. Jpn., 39 (1966) 2685.
2 A. Marschal, J. Gosset et Ch. Engelmann, J. Radioanal. Chem., 8 (1971) 243.
3 F. Mayolet, P. Reimers et Ch. Engelmann, J. Radioanal. Chem., 12 (1972) 115.
4 Ch. Engelmann, J. Gosset et C. Grumet, J. Radioanal. Chem., 28 (1975) 185.
5 K. Strijckmans, C. Vandecasteele et J. Hoste, Anal. Chim. Acta, 89 (1977) 255.
6 K. Strijckmans, C. Vandecasteele et J. Hoste, Anal. Chim. Acta, 96 (1978) 195.
7 P. Guazzoni, Thèse, Université de Grenoble (1970).
8 K. Ishii, M. Valladon et J. L. Debrun, Nucl. Instrum. Methods, 150 (1978) 213.
9 K. Ishii, M. Valladon, C. S. Sastri et J. L. Debrun, Nucl. Instrum. Methods, 153 (1978) 503.
10 H. H. Andersen et J. F. Ziegler, Hydrogen stopping powers and ranges in all elements, Pergamon, Oxford, 1977.
11 M. Valladon et J. L. Debrun, J. Radioanal. Chem., 39 (1977) 385.
12 C. S. Williamson, J. P. Bougeot et J. Picard, Rapport CEA-R 3042, 1966, France.
13 L. Quaglia, G. Weber, D. David, J. Van Audenhove et J. Pauwels, Rapport du Bureau Eurisotop No. 90, 1976.
14 W. Werner et G. Tölg, Fresenius Z. Anal. Chem., 276 (1975) 103.
15 K. Ishii, C. S. Sastri, M. Valladon, B. Borderie et J. L. Debrun, Nucl. Instrum. Methods, 153 (1978) 507.

Analytica Chimica Acta, 109 (1979) 419—423
© Elsevier Scientific Publishing Company, Amsterdam — Printed in The Netherlands

Short Communication

THE DETERMINATION OF ZINC, COPPER, LEAD AND MANGANESE IN PHOSPHATE-CONTAINING MATRICES BY COPRECIPITATION ON IRON(III) HYDROXIDE AND X-RAY FLUORESCENCE SPECTROMETRY

E. BRUNINX*, A. VAN EENBERGEN and A. SCHOUTEN

Philips Research Laboratories, Eindhoven (The Netherlands)

(Received 23rd February 1979)

Summary. Trace amounts of zinc, copper, lead and manganese (10—75 μg) are coprecipitated on iron(III) hydroxide at pH 8.5 after masking of phosphate by calcium. Reliable results are obtained for mixtures with widely different concentrations. The limit of detection is about 1 μg.

A method for the determination of iron, zinc and lead in surface waters by coprecipitation on iron(III) hydroxide has already been described [1]. In this communication, a study of the coprecipitation of four elements (zinc, copper, lead and manganese) with widely varying concentrations in a phosphate-containing matrix is reported. There were three reasons for undertaking this work. First, it was necessary to test whether some of the weakly coprecipitated ions (e.g., manganese) might be desorbed by the more strongly coprecipitated elements (e.g., lead). Secondly, some organic matrices contain appreciable amounts of phosphorus; after the destruction step, the phosphate formed can inhibit the formation of the iron(III) hydroxide precipitate. This difficulty can be circumvented by complexing the excess of phosphate with calcium, but the medium is then different from that used previously [1] and therefore necessitated closer study. Thirdly, the high degree of loading of the precipitate — resulting in considerably thicker samples — required a re-examination of the calibration line construction and the background correction.

Method of analysis

Influence of phosphate. Precipitation at pH 8.5 of a fixed amount of iron (1 mg) in the presence of increasing quantities of phosphate gave the curve shown in Fig. 1. The small quantity of precipitate formed for molar ratios of Fe : P < 1.7 (i.e., in an excess of phosphate) consists mainly of iron phosphate and is not sufficient to coprecipitate the trace elements in solution. When increasing quantities of calcium were added (e.g., at point A in Fig. 1 where Fe : P = 0.45), it was found that all iron precipitates completely for Ca : P molar ratios in the range 0.13—0.3.

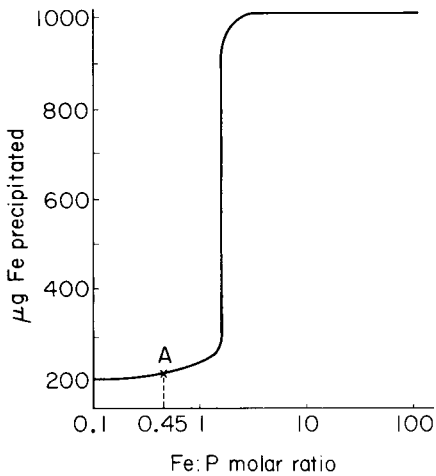

Fig. 1. Precipitation of 1 mg Fe^{3+} as a function of Fe : P ratio in 100 ml of 10^{-2} M KNO_3 at pH 8.5.

It is somewhat unfortunate that the equilibrium constants for the formation of the calcium phosphate complexes are rather small [2], but it is an advantage that calcium does not coprecipitate well with iron(III) hydroxide [3]. In all experiments, therefore, the Ca:P molar ratio was maintained at 0.24. Analysis of a precipitate formed from a solution which contained Fe:Ca:P = 2:1:4 (molar ratio), indicated the presence of $Ca_{10}(OH)_2(PO_4)_6$ together with a mixture of iron(III) hydroxide and iron(III) phosphate. For these tests, iron and calcium were determined by atomic absorption spectrometry and phosphorus by spectrophotometry.

Validity of the thin-layer model. The intensity from an element i in a thin film having a thickness t, is given [4] by

$$I_i = (K\rho_i I^0/\bar{\mu}\rho)\,(1 - \exp(-\bar{\mu}\rho t)) \qquad (1)$$

where I_i = secondary analyte-line intensity from metal i; K = constant factor; ρ_i = density of metal i (g cm^{-3}); I^0 = incident primary intensity; $\bar{\mu}$ = mass absorption coefficient of the specimen (cm^2 g^{-1}) including the terms for primary and secondary radiation absorption in the sample; ρ = density of the specimen (g cm^{-3}); and t = thickness of the sample (cm).

Since the precipitate used in the preparation of the calibration line consists of an almost fixed amount of iron and variable quantities of metal (zinc, copper, lead or manganese), eqn. (1) can be employed for both the metal and the iron. The ratio of the metal/iron intensity can then be expressed by

$$\frac{I_{Me}}{I_{Fe}} = \frac{K_{Me} I^0_{Me}[1 - \exp(-\bar{\mu}_{Me}\rho t)]\, \rho_{Me}\bar{\mu}_{Fe}}{K_{Fe} I^0_{Fe}[1 - \exp(-\bar{\mu}_{Fe}\rho t)]\, \rho_{Fe}\bar{\mu}_{Me}} \quad (2)$$

In practice, this means that the calibration line (1 mg of iron(III) and increasing quantities of metal up to 100 μg) is prepared by measuring the intensity ratio (metal/iron) as a function of the mass ratio:

$$I_{Me}/I_{Fe} = a\, m_{Me}/m_{Fe} \quad (3)$$

In the present experiments, however, four different metals — up to 75 μg each or 300 μg in total — were used with 1 mg or iron, and so the calibration line had to be checked.

Calculation by means of eqn. (2) showed that the errors caused by increasing thickness t (or by a higher degree of trace element loading) were within the uncertainty of the analytical procedure. Therefore the calibration line prepared for the single element could also be used for the thicker multi-element samples (see below).

The background intensity was taken as the average of the intensities to the left and right of the peak (or the intensity on the left multiplied by a calculated factor). The data treatment was identical to that described earlier [1].

Experimental

All experiments were done with 100 ml of 10^{-2} M KNO_3 acidified to pH 1.5—2 with HCl, to which were added the required quantities of iron (1 mg), phosphate, calcium (Ca:P = 0.24), and trace metals. The precipitation step at pH 8.5 was identical with that described earlier [1].

The instrumental settings for the x-ray fluorescence spectrometer were: Philips PW 1220; W-tube; 50 kV; 20 mA; fine collimator, scintillation counter and an automatic pulse-height selector; LiF (200); air path. At least 10^4 counts were collected; background intensities were counted for 400 s.

Results and discussion

Table 1 summarizes all the data obtained in the analysis of the various solutions. The results for samples 1—5, with equal and increasing amounts of zinc, copper, lead and manganese, show that there is no overloading of the iron hydroxide precipitate; for the highest quantity added (75 μg each), however, the results tend to be somewhat low.

Zinc and lead are known to be strongly coprecipitated while copper and manganese are less so [3, 5]. Samples 6—10, where alternately the zinc/lead and copper/manganese are in high concentration, do not show any irregular behaviour. This is also true for samples containing one element at a high concentration with the others in small amounts (samples 10—13). Similarly, with three elements at high concentrations and one at low concentration (samples 14—17), and with only two elements present (samples

TABLE 1

Coprecipitation of trace elements in a wide concentration range (100 ml of 10^{-2} M KNO_3; 1 mg Fe^{3+}; 5 mg PO_4^{3-}; 0.5 mg Ca^{2+}; pH 8.5. The quoted standard deviations are the values for 1 *s*.)

No.	Fe found (μg)	Zn (μg)		Cu (μg)		Pb (μg)		Mn (μg)	
		Added	Found	Added	Found	Added	Found	Added	Found
1	1019 ± 34	10	9 ± 1	10	6 ± 1	10	11 ± 1	10	12 ± 2
2	961 ± 33	50	47 ± 2	50	46 ± 2	50	48 ± 2	50	47 ± 2
3	998 ± 33	50	49 ± 2	50	48 ± 2	50	50 ± 2	50	49 ± 2
4	945 ± 33	75	71 ± 3	75	70 ± 3	75	75 ± 3	75	67 ± 3
5	931 ± 33	75	69 ± 3	75	67 ± 2	75	73 ± 3	75	69 ± 3
6	931 ± 33	75	69 ± 3	10	8 ± 1	75	72 ± 3	10	10 ± 2
7	949 ± 33	75	71 ± 3	10	8 ± 1	75	75 ± 3	10	10 ± 2
8	1031 ± 34	10	8 ± 1	75	74 ± 3	10	7 ± 1	75	75 ± 3
9	1023 ± 34	10	8 ± 1	75	74 ± 1	10	7 ± 1	75	75 ± 3
10	980 ± 33	10	8 ± 1	10	10 ± 3	75	76 ± 3	10	10 ± 2
11	1061 ± 34	10	9 ± 1	10	10 ± 1	75	79 ± 3	10	10 ± 2
12	1025 ± 34	10	9 ± 1	10	10 ± 1	10	8 ± 1	75	76 ± 3
13	1006 ± 34	10	9 ± 1	10	9 ± 1	10	7 ± 1	75	74 ± 3
14	960 ± 33	75	70 ± 3	75	69 ± 3	75	74 ± 3	10	10 ± 2
15	951 ± 33	75	71 ± 3	75	70 ± 3	75	74 ± 3	10	9 ± 2
16	972 ± 33	75	70 ± 3	10	9 ± 1	75	72 ± 3	75	73 ± 3
17	950 ± 33	75	69 ± 3	10	9 ± 1	75	74 ± 3	75	70 ± 3
18	1015 ± 34	10	10 ± 1					10	12 ± 2
19	1056 ± 34			10	11 ± 1	10	11 ± 1		
20	982 ± 33			10	10 ± 1			10	11 ± 2
21	1013 ± 34					10	11 ± 1	10	10 ± 2

18—21), there are no significant deviations.

All the results in Table 1 were tested by calculating (by a least-squares method) the value of K in the equation: m (found) = K m (added), where m is the mass of the element. The results are given in Table 2 together with the uncertainty of K (as 1 s) and the correlation factor r. The standard deviations quoted for K are probably too low, because the standard deviations of the individual results were not included in the equation (i.e., unweighted least-squares analysis was used).

The K values indicate that the precipitation of iron is quantitative, but that the results for the four trace elements tend to be low, the largest deviations being observed for copper.

The technique is reproducible as can be seen from the excellent correlation coefficients for all elements. It is clear that no absorption-enhancement corrections are necessary and that eqn. (3) is applicable over a wide concentration range.

From the above data obtained with phosphate present and from the earlier data [1], it can be safely concluded that the coprecipitation of

TABLE 2

Correlation between measured and true contents

Element	No. of observations	K	r
Fe	21	0.99 ± 0.04	0.999
Zn, Cu, Pb, Mn	76	0.96 ± 0.01	0.997
Zn	18	0.94 ± 0.01	0.999
Cu	19	0.94 ± 0.01	0.998
Pb	19	0.99 ± 0.01	0.998
Mn	20	0.97 ± 0.01	0.997

mixtures of trace elements in widely varying concentrations is reliable. The accuracy and reproducibility are similar to those observed for analogous trace element analyses [6]. The limits of detection are somewhat lower than in the previous work [1], owing to a better spectrometer; for all the elements tested they lie around 1 μg for a precipitate of 1 mg of iron.

REFERENCES

1 E. Bruninx and E. v. Meijl, Anal. Chim. Acta, 80 (1975) 85.
2 L. Sillén and A. E. Martell, Stability constants of metal ion complexes, Suppl. No. 1, The Chemical Society, 1971.
3 E. Bruninx, Phil. J. Res., 33 (1978) 268.
4 E. P. Bertin, Principles and Practice of X-ray Spectrometric Analysis, Plenum Press, New York, 1970, p. 417.
5 E. Bruninx, Philips Res. Repts., 30 (1975) 177.
6 R. Dybczynski, A. Tugsavul and O. Suschny, Analyst, 103 (1978) 733.

Analytica Chimica Acta, 109 (1979) 425—430
© Elsevier Scientific Publishing Company, Amsterdam — Printed in The Netherlands

Short Communication

APPLICATION OF A RAPID SCANNING PHOTODIODE-ARRAY SPECTROPHOTOMETER TO THE CONTINUOUS DETERMINATION OF NICKEL AND COBALT

LEIF ANDERSON, TORBJÖRN ANFÄLT,** ANDERS GRANÉLI* and MATS STRANDBERG***

Department of Analytical Chemistry, Chalmers University of Technology and University of Gothenburg, S-412 96 Göteborg (Sweden)

(Received 27th February 1979)

Summary. A computer-processed linear photodiode-array spectrophotometer is used for the continuous and simultaneous determination of nickel and cobalt in the process water of a storage battery. Disodium ethyl-bis(5-tetrazolylazo) acetate is used as the pnotometric reagent. The interference of copper(II) is eliminated by reduction and complexation of copper(I).

Image-sensing devices, such as vidicon tubes and photodiode arrays, have been successfully applied to spectrophotometric measurements. Linear photodiode arrays have proved to be of particular value as multichannel detectors in rapid scanning spectrophotometers. These have been used for the simultaneous determination of several elements in atomic emission and absorption spectrometry [1] and as u.v.—visible detectors in liquid chromatography [2—4]. A general evaluation of a rapid scanning diode array spectrophotometer has also been reported [5]. However, no effort has been directed towards the use of such instruments for the simultaneous determination of

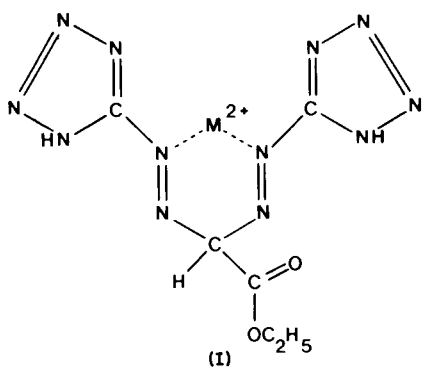

(I)

**Present address: Bifok AB, box 7004, S-19107 Sollentuna, Sweden.
***Present address: Astra Pharmaceuticals AB, S-15185 Södertälje, Sweden.

TABLE 1

The chemistry of disodium ethyl-bis(5-tetrazolylazo) acetate as determined by Frumina et al. [7]

Metal	Stoichiometry metal: reagent	Optimum pH for complexation	λ_{max} (nm)	Molar absorptivity (l mol^{-1} cm^{-1})	Stability constant
Co^{2+}	1:2	4—13	583	1.21×10^4	2.82×10^{-24}
Co^{2+}	1:3	2—3	583	—	—
Ni^{2+}	1:2	6—9	505	2.74×10^4	0.54×10^{-24}
Cu^{2+}	1:1	3—9	535	1.45×10^4	1.24×10^{-18}
Fe^{2+}	1:2	3	520	7.84×10^3	0.60×10^{-25}
Fe^{3+}	1:3	3	632	7.31×10^3	3.54×10^{-38}
Pb^{2+}	1:2	5—10	600	9.6×10^3	1.09×10^{-24}

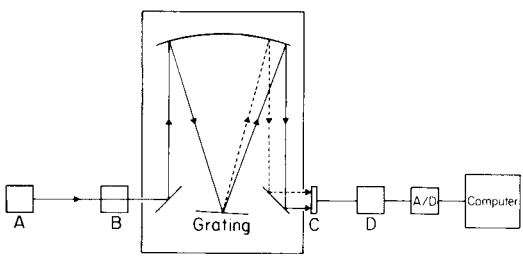

Fig. 1. Schematic diagram of rapid scanning photodiode-array spectrophotometer showing xenon arc lamp (A), cuvette (B), linear diode array (C) and sample and hold amplifier and clock pulse generator for the sampling of the photocurrents (D).

several elements by molecular absorption spectrometry. This may be due to the difficulty in finding reagents which form complexes with several elements with sufficiently different absorption spectra that they can be resolved in mixtures. A reagent with such possibilities is disodium ethyl-bis(5-tetrazolylazo) acetate (I) [6]. The chemistry of this reagent has been investigated by Frumina et al. [7] (Table 1). From the stability constants, absorptivities and wavelengths of maximum absorption of the metal indicator complexes, the indicator seems suitable for the spectrophotometric determination of Ni^{2+}, Co^{2+} and Cu^{2+}. This communication describes the simultaneous determination of nickel and cobalt in the process water of a storage battery factory (Jungner AB, Sweden) with disodium ethyl-bis(5-tetrazolylazo) acetate and a diode-array spectrophometer.

Experimental

Apparatus. A schematic diagram of the apparatus is shown in Fig. 1. The radiation from the lamp (150-W xenon arc, Oriel Corp.) is dispersed by an Ebert grating monochromator (147.5 grooves/mm, Jarrell-Ash) onto a 256-element linear photodiode array (Reticon Corp.). The spectral range focussed on the diode array is 350 nm wide. The photocurrents produced by each diode element discharge a capacitance and the excess charge, proportional

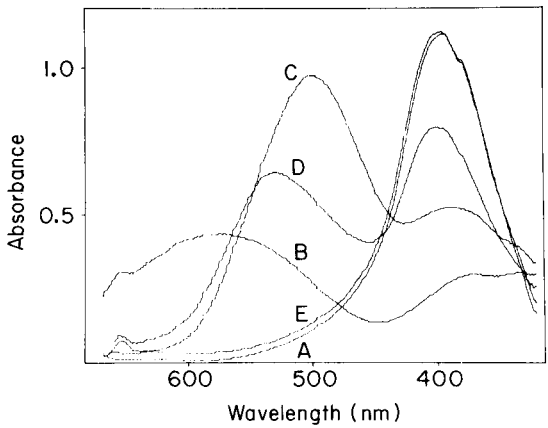

Fig. 2. Absorption spectra of 0.1 mM disodium ethyl-bis(5-tetrazolylazo) acetate at pH 4.5 (A) and with 0.05 mM Co^{2+} (B), Ni^{2+} (C) and Cu^{2+} (D), respectively, in 0.1 mM reagent. Curve E is the same as D after reduction and masking of Cu^{2+}.

to the illumination, is measured by a 12-bit A/D converter. Each time a diode is sampled, its capacitance is recharged. This means that the photocurrents are integrated during the interval between two successive measurements. The sampling rate can be chosen from 1 to 13 kHz which means that a maximum of approximately 40 complete spectra per second may be recorded. The spectrophotometric data are processed by a CAI ALPHA LSI-2/20G minicomputer, which calculates the absorbances from the photocurrents and performs matrix operations.

Reagents. A 1 mM solution of disodium ethyl-bis(5-tetrazolylazo) acetate (B.D.H. Ltd.) was prepared by dissolution in 1 M acetate buffer at pH 4.5. A 0.1 M ascorbic acid solution and a 0.1 M sodium thiosulfate solution were also prepared. Stock solutions (1000 ppm) of Ni^{2+}, Cu^{2+} and Co^{2+} were prepared from ampoules (Merck).

Procedures. Absorption spectra covering the region 320—670 nm were recorded (Fig. 2) for 0.1 mM reagent solution and for mixtures of 0.05 mM Ni^{2+}, Cu^{2+} or Co^{2+} in 0.1 mM reagent. The diodes corresponding to the wavelengths of maximum absorption were selected from these spectra. The molar absorptivity of each species at these wavelengths was calculated from the absorbance, the concentrations of metal and reagent, and the stoichiometry.

Spectra were also recorded for standard solutions of nickel and cobalt (0.5—2 ppm) as well as for mixtures of the two ions in 0.1 mM reagent solution. The total absorbance at wavelength j is

$$A_j = \sum_{i=1}^{N} \epsilon_{ij} \cdot c_i \qquad (1)$$

where ϵ_{ij} is the molar absorptivity of the ith species of concentration c_i. The concentration c_i was calculated from j such linear equations by matrix operations.

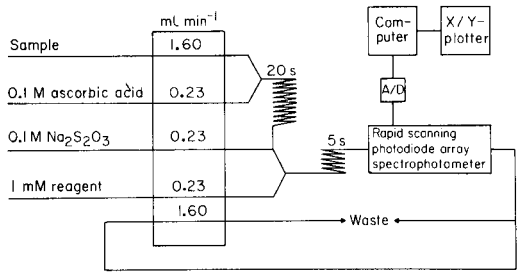

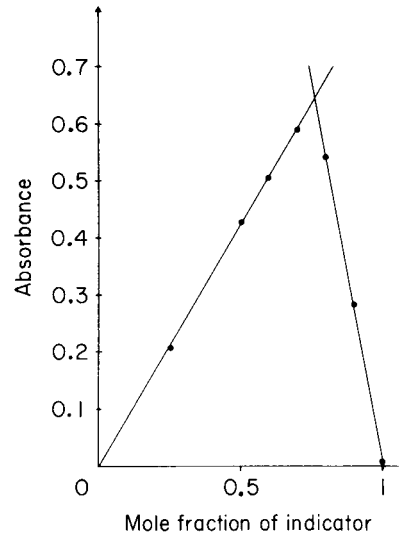

Fig. 3. Schematic diagram of continuous flow apparatus for the monitoring of nickel(II) and cobalt(II), showing reagents, flow rates and coil delay times.

Fig. 4. Continuous variations curve for cobalt(II) and disodium ethyl-bis(5-tetrazolyl-azo) acetate at 580 nm and pH 4.5.

Samples from the storage battery factory were analysed in this way and by atomic absorption spectrometry for comparison. Because the analysis was intended for continuous monitoring of nickel and cobalt, it was adapted to a continuous flow system as shown in Fig. 3.

Results and discussion

The absorption spectra recorded for calibration are shown in Fig. 2. Cobalt clearly reduces the reagent peak at 400 nm more than nickel does, which indicates differences in stoichiometry. An investigation by the method of continuous variations (Fig. 4) showed that the stoichiometry of the cobalt complex is 1:3 even at pH values greater than 3, and not 1:2 as suggested earlier [6, 7]. As may also be seen from curve D (Fig. 2), copper(II) would interfere considerably with determinations of both nickel and cobalt. In order to eliminate this interference, copper(II) was reduced with ascorbic acid and the copper(I) produced was masked with thiosulfate which forms strong complexes with copper(I) ($\log \beta_2 = 12$). Curve E (Fig. 2) shows that the interference from copper(II) was almost completely eliminated in this way. Since copper(II) is reduced by thiosulfate, it might be possible to eliminate the ascorbic acid.

Since the analysis was intended for continuous monitoring of nickel and cobalt a continuous flow system was employed. The molar absorptivities ϵ_{ij} determined from the injection of a mixture containing 2.55×10^{-5} M Ni^{2+} and Co^{2+} into 1 mM reagent solution are shown in Table 2. The stoichiometries used in the calculations were NiR_2 and CoR_3, respectively.

TABLE 2

Molar absorptivities ϵ_{ij} of reagent (R), NiR_2 and CoR_3 in 0.1 M acetate buffer at pH 4.5

Diode no.	Wavelength (nm)	Molar absorptivity ($\times 10^3$ l mol^{-1} cm^{-1})		
		R	NiR_2	CoR_3
55	598[a]	0.1	5.5	12.5
125	500	1.5	31.1	8.8
195	401	12.9	12.4	13.8

[a]A wavelength of 598 nm was chosen instead of 583 nm in order to decrease the influence of the nickel complex.

TABLE 3

Results from analysis of mixtures of nickel and cobalt and of process water sample

Taken (ppm)		Found (ppm)		Taken (ppm)		Found (ppm)	
Ni	Co	Ni	Co	Ni	Co	Ni	Co
0.50	0	0.52	0.06	0.50	0.50	0.50	0.52
1.00	0	1.03	0.05	1.00	0.50	0.96	0.40
1.50	0	1.50	0.00	0.50	1.00	0.48	0.96
2.00	0	2.07	0.00	1.50	1.50	1.34	1.28
0	0.50	0.03	0.58	Process water sample		1.42	0.11
0	1.00	0.01	1.09	Same sample analyzed		1.70	0.13
0	1.50	0.00	1.50	by a.a.s.			
0	2.00	0.00	1.93				

The results of analyses of standard solutions and of a process water sample based on eqn. (1) are shown in Table 3; results obtained by atomic absorption spectrometry are also given. The somewhat poor accuracy of the proposed technique, which is sufficient for the purpose, is due to the fact that only one calibration point was used for each species. The precision of the method was determined from nine consecutive measurements on the process water. The coefficients of variation for nickel and cobalt were 0.3% and 9%, respectively, the mean values being 1.42 ppm for nickel and 0.11 ppm for cobalt.

The results obtained by atomic absorption spectrometry revealed that the process water also contained 0.3 ppm copper; this was masked in the continuous flow analysis. The amount of copper may, however, be determined from the difference in absorbance at 500 nm between two successive determinations with and without reduction and masking.

The authors are greatly indebted to Professor David Dyrssen for general discussions.

REFERENCES

1 G. Horlick and E. Codding, Anal. Chem., 45 (1973) 1490; Spectrosc. Lett., 7 (1974) 33; Appl. Spectrosc., 29 (1975) 167.
2 R. Dessy, W. Nunn and C. Titus, J. Chromatogr. Sci., 14 (1976) 195.
3 R. Dessy, W. Reynolds, W. Nunn, C. Titus and G. Moler, J. Chromatogr., 126 (1976) 347.
4 M. Milano, S. Law and E. Grushka, J. Chromatogr., 125 (1976) 315.
5 B. Yates and T. Kuwana, Anal. Chem., 48 (1973) 510.
6 H. Jonassen, V. Chamblin, V. Wagner and R. Henry, Anal. Chem., 30 (1958) 1661.
7 N. Frumina, N. Goryunova and I. Mustafin, Primen. Org. Reaktivov Anal., (1968) 22.

Analytica Chimica Acta, 109 (1979) 431—436
© Elsevier Scientific Publishing Company, Amsterdam — Printed in The Netherlands

Short Communication

SULPHURIC—PERCHLORIC ACID DIGESTION OF PLANT MATERIAL FOR THE DETERMINATION OF NITROGEN, PHOSPHORUS, POTASSIUM, CALCIUM AND MAGNESIUM

M. S. CRESSER* and J. W. PARSONS

Soil Science Department, University of Aberdeen, Aberdeen AB9 2UE (Gt. Britain)

(Received 6th April 1979)

Summary. Modifications of an earlier procedure to improve reliability in routine use are described. Contamination from glass beads and new digestion flasks may be significant. Other possible sources of error are discussed.

In 1974 a procedure was described for the determination of plant nitrogen based on rapid digestion with sulphuric and perchloric acids [1], and it was suggested that the same digest should be suitable for the determination of other major nutrient elements. The procedure has now been used for the analysis of many thousands of samples for nitrogen, phosphorus, potassium, sodium, calcium and magnesium in this laboratory. This communication reports possible sources of error or poor precision in the determination of the major nutrient elements, and minor modifications to the procedure which extend its range of application.

Experimental procedures

Weigh (to ±0.1 mg) approximately 200 mg of oven-dried plant material, ground to pass a 1-mm sieve, into a clean dry 100-ml Kjeldahl flask. Add 5 ml of concentrated sulphuric acid (reagent grade) and 2—3 grains of acid-washed quartz sand, swirl the flask and leave to stand for 20 min. Heat to boiling over 5 min, avoiding excessive frothing. Boil gently for a further 30 min. Stop heating momentarily and add 1 ml of a 4% (v/v) solution of perchloric acid (62%) in concentrated sulphuric acid to the digest. Heat gently for a further 10 min: the digest should clear within 5 min. Cool, transfer the digest quantitatively to a 50-ml volumetric flask, and dilute to mark with distilled water. Put replicate blanks through the entire digestion procedure with each batch of digestions.

Determine nitrogen on replicate 10-ml aliquots of digest by conventional distillation/titration techniques [1]. Determine magnesium and calcium by atomic absorption spectrometry, using lanthanum at a final concentration of 5 mg ml^{-1} as a releasing agent in the air—acetylene flame. Determine potassium by flame emission spectrometry, and phosphorus by solution spectrophotometry [2].

Results and discussion

Modifications to digestion procedure. If the digestion procedure originally proposed [1] is employed, the phosphorus levels of the resulting digests may be too low for precise analysis. The sample mass taken was therefore doubled to 200 mg, and the final volume halved to 50 ml. The sample mass cannot be increased to 300 mg because digests then require additional perchloric acid to clear. More than 2 ml of the 4% perchloric acid causes significant losses of nitrogen.

A change from coal gas to natural gas in this laboratory made it difficult to obtain clear digests. This was eventually attributed to an inadequate rate of heating in the preliminary stage. Triplicate subsamples of standard kale were digested for total heating periods of 45 min but with initial periods of 5, 10 and 15 min to heat the digest to boiling; the mean results were 4.30, 4.30 and 4.17%, respectively (certified value, 4.32%). For triplicate subsamples of *Pinus sylvestris* needles, the corresponding mean results were 1.27, 1.25 and 1.22%. At the slowest initial heating rate, many digests did not clear. Subsequently, all samples were brought to boiling over 5 min, rather than over the 15 min initially proposed [1].

Contamination from glass beads. For the determination of nitrogen alone, the addition of 2—3 glass beads was recommended to promote smooth boiling [1]. The modified procedure was applied to 12 samples previously used in an interlaboratory comparison [3], with beads or acid-washed quartz sand grains to minimize bumping. Reasonable agreement with published values was obtained for calcium, potassium and phosphorus (Table 1) but for magnesium a serious positive systematic error was observed when beads were used rather than sand: the precision was conspicuously poor and the blanks variable. To eliminate the possibility of poor accuracy of the quoted mean values for magnesium, 6 of the 12 samples were also analysed in duplicate after overnight ashing at 450°C and dissolution of the residues in hydrochloric acid. The results, included in Table 1, show good agreement with the quoted mean values [3]. Two series of 12 blank digestions were measured, one with and one without the addition of 3 beads per flask. Magnesium was detected only in the blanks from flasks containing beads. The results, expressed in terms of the % errors which would be caused by contamination from the beads for a 200-mg plant sample containing 0.25% magnesium, varied from 0.0%, for 5 of the flasks, to 16.4% at the highest level of contamination.

Duplicate 5-g samples from the beads used (British Drug Houses, glass balls, unknown age), from a new bottle of beads from the same supplier, and from an old bottle of beads from an unknown source were digested. The mean values for extracted magnesium per bead were found to be 14.5 μg, 1.2 μg and 0.04 μg, respectively, for the three bottles of beads. Apart from the obvious undesirability of high blanks, the major problem in the present analysis was due to the variability between beads. This may have been due to the decrease in extractable magnesium in some of the beads after prolonged

TABLE 1

Analysis of samples provided by IUFRO for interlaboratory comparison [3]

Sample	% Ca		% Mg				% K		% P		
	A[a]	B[b]	A	B	C[c]	D[d]	A	B	A	B	E[e]
22043	0.64	0.66	0.092	0.090	0.097	—	0.57	0.60	0.092	0.097	0.11
22044	0.44	0.44	0.148	0.143	0.153	0.145	0.70	0.68	0.111	0.117	0.12
22045	1.92	1.86	0.252	0.254	0.273	—	1.28	1.26	0.231	0.236	0.22
22046	1.23	1.18	0.300	0.299	0.318	0.294	2.08	2.06	0.272	0.294	0.29
22047	0.28	0.28	0.058	0.056	0.064	0.058	0.51	0.51	0.119	0.117	0.12
22048	0.66	0.67	0.092	0.090	0.098	—	0.58	0.58	0.093	0.098	0.10
22049	0.28	0.28	0.054	0.054	0.058	0.055	0.52	0.52	0.112	0.118	0.11
22050	0.67	0.67	0.090	0.092	0.097	0.090	0.60	0.59	0.094	0.096	0.10
22051	1.18	1.20	0.300	0.294	0.310	0.299	2.12	2.10	0.285	0.293	0.29
22052	0.63	0.67	0.091	0.090	0.094	0.090	0.59	0.56	0.092	0.098	0.09
22053	1.84	1.86	0.255	0.252	0.265	—	1.30	1.26	0.214	0.229	0.24
22054	0.44	0.43	0.145	0.145	0.155	—	0.70	0.68	0.105	0.121	0.12

[a]Proposed procedure. [b]Mean of IUFRO values [3]. [c]Proposed procedure, with glass beads in place of sand. [d]Ashing at 450° C/Hydrochloric acid dissolution. [e]Ashing in presence of magnesium acetate/hydrochloric acid dissolution.

usage. When six sequential digestions were performed on the same 5-g samples of beads, the amount of magnesium extracted decreased steadily.

To see if this contamination also affected the determination of other elements in the digest, the calcium, potassium, sodium, manganese and iron contents of the initial bead digests were also determined. The results (Table 2) show that significant problems are likely to be encountered only for magnesium, sodium and iron. They could be particularly severe for iron, especially for iron-deficient samples, because the blanks would be relatively very high and variable.

As a replacement for the glass beads, colourless grains of sharp quartz sand, 2—4 mm across were selected. These were boiled three times for 30 min in a substantial excess of concentrated sulphuric acid, carefully washed with distilled water and dried prior to use. The blanks obtained from the sand were very much lower than those from the beads.

Although manganese and iron were of less interest than the other nutrients in the present work, the levels were determined in six digests selected at random, without replication. The results (Table 3) show that the digest may also be used for these elements. Sodium may also be determined, but the results are not included here because of the gross variability of the values quoted in the interlaboratory study [3].

Contamination from flasks. Because of the ease with which certain elements

TABLE 2

Contamination from glass beads (μg per bead)

	Ca	Na	K	Mn	Fe	Mg
Old B.D.H. beads	1.4	7.1	4.3	<0.03	0.8	13.9
	1.0	7.1	4.3	<0.03	1.1	15.0
New B.D.H. beads	<0.2	2.5	2.3	<0.02	0.5	1.2
	<0.2	5.7	3.0	<0.02	0.4	1.1
Beads of unknown	<0.2	3.3	2.6	<0.02	0.3	0.03
source	<0.2	3.3	3.2	<0.02	0.3	0.04

TABLE 3

Determination of iron and manganese

Sample	Fe (μg g^{-1})		Mn (μg g^{-1})	
	A[a]	B[b]	A	B
22044	120	108	37	39
22045	141	137	87	90
22046	104	115	400	399
22048	121	122	93	86
22049	90	97	512	529
22052	122	117	94	88

[a]Proposed procedure. [b]Mean of IUFRO values [3].

could be extracted from glass beads, possible contamination from new Kjeldahl flasks was also studied. Six new flasks and six old flasks were cleaned by soaking overnight in detergent solution and rinsing thoroughly with hot water and deionized water. Six blank digestions were then carried out sequentially in each flask, and the digests analysed. No significant amounts of magnesium, calcium, potassium, manganese or iron were found. The sodium blanks from new flasks were initially 47—86 μg higher than those from old flasks: after six digestions the difference became negligible. Clearly to avoid systematic errors in sodium determinations, pretreatment of new flasks with boiling acid is essential.

Possible precipitation losses. Possible losses of calcium and potassium by precipitation as the sulphate and perchlorate, respectively, in the diluted digests were checked. Potassium (1—5 mg) and calcium (1—5 mg) salts were digested with various mixtures comprising 6.0—3.5 ml of concentrated sulphuric acid and 0—2.5 ml of the 4% perchloric acid in sulphuric acid as in the recommended procedure. The diluted solutions were measured immediately and again after standing for six days without shaking. No significant losses of potassium or calcium were observed.

Effects of acid concentrations. Sets of standards were prepared for calcium, magnesium and potassium containing appropriate amounts of sulphuric acid alone, and of sulphuric acid and sulphuric—perchloric acid mixture: the perchloric acid had no effect on the calibration graphs.

The acidity of 20 plant digests was measured by conventional acid—base titration. On average, only 18% of the sulphuric acid was neutralized or lost during digestion. This figure remained constant even when the flasks were deliberately heated more strongly than normal. Reductions in acidity of up to 25% caused changes of less than 1% in the signals for magnesium, calcium or potassium at the levels of interest over a wide range of flame conditions and burner heights. All standards for flame spectrometry were therefore prepared containing 5 ml of concentrated sulphuric acid and 1 ml of the concentrated sulphuric—perchloric acid mixture per 50 ml of digest. Weighing of flasks to give a constant mass of acid [1] was unnecessary.

Spectrophotometric phosphorus determination. The effect of the final concentration of sulphuric acid on the absorbance and development of the blue phosphate complex was studied in detail. A well defined plateau occurred over the range 0.15—0.30 M sulphuric acid (final acid concentration). The mixed reagent (ammonium molybdate, potassium antimonyl tartrate, ascorbic acid and sulphuric acid) requires an acid molarity of 1 M or more to prevent the spontaneous formation of a blue complex in the absence of phosphate. The mean sulphuric acid molarity of 20 diluted (50 ml) digests of *Pinus sylvestris* needles was found to be 1.76 M. If 10 ml of mixed reagent in 1 M sulphuric acid is used, in a final volume of 50 ml, any volume of sample up to 2.8 ml may be taken for analysis; a 2-ml aliquot is normally adequate. A 6-fold amount (by weight) of silicon as silicate caused no interference in the determination of 5 μg of phosphorus under these conditions; in any case silicates would be largely converted to insoluble silica during the digestion. The presence of perchloric acid at concentrations double those which could conceivably be encountered in digests also caused no interference.

Conclusions

The simple, safe and rapid sulphuric—perchloric acid digestion procedure proposed yields solutions suitable for the determination of nitrogen, phosphorus, potassium, calcium and magnesium, as well as iron, manganese and sodium if required. Contamination from magnesium, iron and sodium in glass beads and sodium in new Kjeldahl flasks must be removed. Adjusting the sulphuric acid contents of digests to constant mass is unnecessary, because changes in the molarity of acid in digests do not have significant effects.

The authors are indebted to Mrs. E. Haw, Mrs. F. Mitchell and Mr. K. Hadden for experimental assistance.

REFERENCES

1 T. Batey, M. S. Cresser and I. R. Willett, Anal. Chim. Acta, 69 (1974) 484.
2 J. Murphy, and J. P. Riley, Anal. Chim. Acta, 27 (1962) 31.
3 International Methods for Chemical Analysis, Report on activities 1971—1973, IUFRO Subject Group S1.02 Working Party 3 (1973).

Analytica Chimica Acta, 109 (1979) 437
© Elsevier Scientific Publishing Company, Amsterdam — Printed in The Netherlands

Errata

S. G. Schulman and W. J. Underberg, pH-Dependence of the Fluorescence of Acridone in Aqueous Mineral Acid Solutions. *Anal. Chim. Acta*, 107 (1979) 411—414.

Page 412: lines 1 and 6 beneath eqn. (1), for K^*_{CN} read K^*_a.
Page 413: lines 4 and 8 beneath eqn. (4), for K^*_{CN} read K^*_a.
Eqn. (5), for k^*_a read K^*_a.
Line 4 beneath eqn. (4) and lines 1, 4 and 8 beneath eqn. (6), for $mol^{-1}\ s^{-1}$ read $l\ mol^{-1}\ s^{-1}$.

ANALYTICA CHIMICA ACTA, Vol. 109 (1979)

AUTHOR INDEX

journal of MEMBRANE SCIENCE

a focal point for "membranologists" and a vehicle for the dissemination of information dealing with the science and technology of membrane processes and phenomena

A selection of papers published in the first four volumes

Diffusional release of a solute from a polymer matrix, *D. R. Paul and S. K. McSpadden (Austin, TX).* Production of energy from concentrated brines by pressure-retarded osmosis. I. Preliminary technical and economic correlations. *S. Loeb (Beer Sheva).* Ultrathin silicone/polycarbonate membranes for gas separation processes, *W. J. Ward III, W. R. Browall and R. M. Salemme (Schenectady, NY).* Separations of organic compounds by liquid membrane processes, *R. P. Cahn and N. N. Li (Linden, NJ).* Dual sorption theory *(Review paper), W. R. Vieth, J. M. Howell and J. H. Hsieh (New Brunswick, NJ).* Electron and ion transport in membranes, *D. Walz and O. Kedem (Basel).* Electric relaxation studies of synthetic membrane cells: Oscillations in the $NaCl/NH_4Cl_4$ system, *J. E. Anderson and W. Pusch (Frankfurt am Main).* Coupled transport membranes, I. Copper separations, *R. W. Baker et al. (Bend, OR).* Diffusive and hydraulic permeabilities of commercially available cellulosic hemodialysis films and hollow fibres, *E. Klein et al. (New Orleans, LA).* Simultaneous diffusion of ions and ion pairs across liquid membranes, *M. E. Duffrey, D. F. Evans and E. L. Cussler (Pittsburgh, PA).* The use of membranes in studies of reaction kinetics: arsenite catalysis of CO_2 hydration, *R. J. Lander and J. A. Quinn (Philadelphia, PA).* Application of bipolar membrane technology: a novel process for control of sulfur dioxide from flue gases *(K.-J. Liu, F. P. Chlanda and K. Nagasubramanian (Morristown, NJ).* Therapeutic systems and controlled drug delivery, *S. K. Chandrasekaran, R. Capozza and P. S. L. Wong (Palo Alto, CA).* Synthetic and biological membranes: Common phenomena, *J. L. Gainer and J. C. Ludlow (Charlottesville, VA).* Determination of human erythrocyte membrane hydraulic conductivity, *W. R. Galey (Albuquerque, NM).* Hybrid bacterial and enxyme membrane electrode with nicotinamide adenine dinucleotide response, *T. L. Reichel and G. A. Rechnitz (Newark, DW).* Energy-transducing membrane. I. Photo-response of a chlorophyll-liquid crystal membrane, *M. Aizawa, M. Hirano and S. Suzuki (Yokohama).* Enzyme immunosensor. II. Electrochemical determination of IgG with an antibody-bound membrane, *M. Aizawa, A. Morioka and S. Suzuki (Yokohama).* Ion transport in free and supported nitrobenzene aliquat nitrate liquid membrane ion selective electrodes. II. Interfacial kinetics and time-dependent phenomena, *D. E. Mathis, F. S. Stover and R. P. Buck (Chapel Hill, NC).* Water-dissolved-oxygen permeability coefficients of hydrogel contact lenses and boundary layer effects, *M. F. Refojo and F.-H. Leong (Boston, MA).*

Subscription Information

1979: Volumes 4 and 5 (in six issues)
Subscription Price: US $170.75/Dfl. 350.00 including postage

A free specimen copy of the journal is available on request.

ELSEVIER

P.O. Box 211,
1000 AE Amsterdam
The Netherlands

52 Vanderbilt Ave
New York, N.Y. 10017

The Dutch guilder price is definitive. US $ prices are subject to exchange rate fluctuations.

8133

Electrochemical Reactor Design

2nd edition

by David J. Pickett, *Department of Chemical Engineering, The University of Manchester Institute of Science and Technology.*

1977 2nd edition 1979 US $75.50/Dfl. 155.00 ISBN: 0-444-41814-8

This book, first published in 1977, sets out general design procedures for electro-chemical reactors in an analogous way to those used for chemical reactors and other process equipment.

The first edition met with such favourable response that this second edition was prepared. An important feature of this is the incorporation of forty detailed calculations as worked examples. Many of these calculations have been used as tutorial problems for final year chemical engineering students and cover the basic points made in each of the seven chapters. The numbering of the calculations indicates the relevant chapter and each problem is cross-referenced to the appropriate pages in the text.

As the book is suitable for self-instruction for industrial practitioners in process engineering and applied electro-chemistry, the basic methods are exemplified for the more common types of reactor employed. Sections are also devoted to the acquisition of design data and many references are given to existing theoretical and experimental work in the field; also, the worked examples will prove a valuable aid to those people involved in design calculation.

ELSEVIER

P.O. Box 211,
1000 AE Amsterdam
The Netherlands

52 Vanderbilt Ave
New York, N.Y. 10017

The Dutch guilder price is definitive. US $ prices are subject to exchange rate fluctuations.

8144

(continued from outside of cover)

Short Communications

© Elsevier Scientific Publishing Company, 1979.
All rights reserved. No part of this publication may be reproduced, stored in a retrieval system or transmitted in any form or by any means, electronic, mechanical, photocopying, recording or otherwise, without the prior written permission of the publisher, Elsevier Scientific Publishing Company, P.O. Box 330, 1000 AH Amsterdam, The Netherlands.

Submission of an article for publication implies the transfer of the copyright from the author to the publisher and is also understood to imply that the article is not being considered for publication elsewhere.

Submission to this journal of a paper entails the author's irrevocable and exclusive authorization of the publisher to collect any sums or considerations for copying or reproduction payable by third parties (as mentioned in article 17 paragraph 2 of the Dutch Copyright Act of 1912 and in the Royal Decree of June 20, 1974 (S.'351) pursuant to article 16 b of the Dutch Copyright Act of 1912) and/or to act in or out of Court in connection therewith.

Printed in The Netherlands.

CONTENTS

(continued on inside page of cover)